APPLICATIONS OF COMPUTATIONAL INTELLIGENCE TECHNIQUES FOR SOLVING THE OPTIMAL POWER FLOW PROBLEM IN MODERN POWER SYSTEMS

Thesis Submitted

In Partial Fulfillment of the Requirements for the

Degree of

DOCTOR OF PHILOSOPHY

in

Electrical Engineering

by

UDIT MITTAL

(Roll No. 2K17/PhD/EE/15)

Under the Joint Supervision of

Prof. Uma Nangia

Prof. Narender Kumar Jain



Department of Electrical Engineering DELHI TECHNOLOGICAL UNIVERSITY

(Formerly Delhi College of Engineering)
Shahbad Daulatpur, Main Bawana Road, Delhi-110042, India
August, 2025

ACKNOWLEDGEMENT

First and foremost, I would like to express my deepest gratitude to my supervisors, Prof. Uma Nangia and Prof. N. K. Jain, for their invaluable guidance, unwavering support, and constant motivation throughout the course of this research work. Their mentorship has been exceptional, and working under their supervision has been an enriching and remarkable experience. The countless hours of insightful discussions with them have undoubtedly shaped my thoughts and steered my research in the right direction toward achieving the desired objectives. It has been a proud privilege to work with such dedicated mentors who are always willing to lend a helping hand. I am profoundly thankful to them for their wise counsel, inspiring thoughts, and continuous encouragement, which have been instrumental in the completion of this work.

I would like to express my deepest gratitude to my colleague and co-author, Dr. Saket Gupta. His unwavering support and encouragement have been a constant source of strength. His work in this field has deeply influenced mine, and I am incredibly grateful for his expertise and insightful guidance throughout this journey.

I would like to extend my heartfelt thanks to the SRC members for their valuable feedback and suggestions during the course of my research.

I extend my heartfelt thanks to my friends and colleagues, especially Dr. Amit Kumar Roy, Dr. Subhash Yadav, and Ms. Vaishnavi Bansal, for their constant motivation and gentle reminders to stay focused and complete my work on time. Their encouragement has been invaluable throughout this journey.

I am deeply grateful to my parents for their unwavering faith, endless sacrifices, and

constant blessings. Their patience in waiting for the completion of my Ph.D. and their steadfast

encouragement have been the pillars of my journey. Everything I have achieved stands on the

foundation they have built for me.

I also extend my heartfelt thanks to my sister, Karishma, for being a constant source of

encouragement and support throughout this journey. Her faith in me never wavered, and her

belief became my strength during the toughest and most rewarding times alike.

I owe heartfelt thanks to my wife, Sonam, whose unwavering support and

encouragement have been my greatest strength. As my core support system, she has been my

pillar of strength, and words alone cannot express my admiration and appreciation for her

enduring love and sacrifices. I would also like to express my heartfelt appreciation to my sons

Anubhav and Udbhav whose smiles, innocence, and boundless energy have been a source of

joy and motivation for me.

Finally, I bow in gratitude to Almighty God, whose grace and blessings have made

this work possible.

Place: Delhi

(UDIT MITTAL)

Date: 14/08/2025

ii

DECLARATION

I, Udit Mittal, a Ph.D. student, hereby declare that the thesis titled "Applications of

Computational Intelligence Techniques for Solving the Optimal Power Flow Problem in

Modern Power Systems", submitted by me to the Department of Electrical Engineering, Delhi

Technological University, Delhi, in partial fulfillment of the requirements for the award of the

degree of Doctor of Philosophy, has not previously been submitted for the award of any degree,

diploma, associateship, fellowship, or any other similar title or recognition.

Place: Delhi

(UDIT MITTAL)

Date: 14/08/2025

iii

CERTIFICATE

On the basis of the declaration submitted by Mr. Udit Mittal, student of Ph.D., I hereby

certify that the thesis titled Applications of Computational Intelligence Techniques for

Solving the Optimal Power Flow Problem in Modern Power Systems which is submitted

to the Department of Electrical Engineering, Delhi Technological University, Delhi in partial

fulfillment of the requirement for the award of the degree of Doctor of Philosophy is an

original contribution with existing knowledge and faithful record of research carried out by

him under my guidance and supervision.

To the best of my knowledge this work has not been submitted in part or full for any

Degree or Diploma to this University or elsewhere.

Date: 14/08/2025

(Prof. Uma Nangia)

Professor

Supervisor

Department of Electrical Engineering

Delhi Technological University

Delhi, India

(Prof. N. K. Jain)

Supervisor

Professor

Department of Electrical Engineering

Delhi Technological University

Delhi, India

iv

ABSTRACT

The growing demand for electricity, rising greenhouse gas emissions, and the global emphasis on sustainability have led to the integration of intelligent optimization techniques in modern power systems to ensure efficient, stable, and sustainable gird operations. This thesis addresses the Optimal Power Flow (OPF) problem, focusing on single-objective and multi-objective formulations to optimize economic, technical, and environmental parameters in modern power systems. Key objectives include fuel cost minimization, power loss reduction, voltage stability improvement, voltage deviation minimization, and emission reduction.

The OPF problem is inherently complex, characterized by its nonlinear, nonconvex, and high-dimensional nature. The nonlinear, high-dimensional nature of the OPF problem is tackled using state-of-the-art metaheuristic algorithms, including the Learning-based Sine Cosine Algorithm (L-SCA), Hybrid Rao-2 Sine Cosine Algorithm (HRSCA), Coot Optimization Algorithm (COOT), and Electric Eel Foraging Optimizer (EEFO). Extensive testing has been conducted on standard IEEE networks, including the IEEE 30-bus, 57-bus, 118-bus systems, and the Algerian 59-bus network, to validate the scalability and robustness of these algorithms under varying operational scenarios.

Single-objective and multi-objective formulations are analyzed to optimize control variables such as generator outputs, bus voltages, transformer tap settings, and reactive power compensation. Additionally, the integration of Distributed Generation (DG) units as constant power sources is investigated to assess the impact of renewable energy integration on system performance. The findings highlight significant improvements in system efficiency, reduced operational costs, enhanced stability, and reduced environmental impact.

The proposed methodologies demonstrate rapid convergence, high-quality solutions, and computational efficiency, showcasing their applicability to real-world power systems. By addressing critical challenges such as fuel cost minimization, handling load growth scenarios, voltage collapse prevention, and emission reduction, this work contributes significantly to the development of sustainable and reliable energy systems. Future studies could explore the integration of advanced hybrid optimization techniques and real-time dynamic control systems to further enhance the efficiency and scalability of the proposed methodologies, particularly for large-scale, decentralized power systems with renewable energy integration.

Table of Contents

ACKNOWLEDGEMENT	i
DECLARATION	iii
CERTIFICATE	iv
ABSTRACT	V
TABLE OF CONTENTS	vi
LIST OF FIGURES	xii
LIST OF TABLES	xiv
LIST OF SYMBOLS, ABBREVIATION AND NOMENCLATURE	xvi
List of Symbols	xvi
List of Abbreviations	.xvii
List of Nomenclature	xix
CHAPTER-1	
INTRODUCTION	1-8
1.1 Introduction	1
1.2 Historical Context	1
1.3 Motivation	2
1.4 Challenges in Power System Stability and Optimization	3
1.4.1 Economic Pressures on Grid Operation	3
1.4.2 Voltage Instability	3
1.4.3 Reliance on Load Shedding for Stability	4
1.4.4 Environmental Sustainability Challenges	4
1.5 Objectives of OPF in Modern Power Systems	4
1.5.1 Techno-Economic Objectives	4
1.5.2 Environmental Objectives	6
1.6 Problem Statement	7
1.7 Outline of Thesis	7
CHAPTER-2	
LITERATURE REVIEW	9-31

2.1	Introd	luction	9
2.2	Tradi	tional Approaches	9
2.3	Popul	ation-based metaheuristic algorithms	10
	2.3.1	Evolutionary algorithms for OPF solution	11
	2.3.2	Swarm intelligence-based algorithms for OPF solution	12
	2.3.3	Hybrid and Advanced Techniques	23
2.4	Gaps	in Current Research and Opportunities for Further Study	29
2.5	Resea	arch Objectives	31
CF	IAPT	ER-3	
OF	TIM	AL POWER FLOW: FUNDAMENTALS & VARIOUS	S TEST
SY	STE	MS	32-42
3.1	Gener	ral Structure of OPF	32
	3.1.1	Single-Objective OPF	32
	3.1.2	Multi-Objective OPF	32
3.2	Const	raints	33
	3.2.1	Equality constraints	33
	3.2.2	Inequality constraints	33
3.3	Objec	etive Functions	34
	3.3.1	Fuel cost minimization (FCM)/Total fuel cost minimization (TFCM)	34
	3.3.2	Voltage deviation minimization (VDM) considering QFC	35
	3.3.3	Voltage security index (VSI)	36
	3.3.4	Voltage Stability Improvement (VSI) considering QFC	36
	3.3.5	Active power loss minimization (APLM)	37
	3.3.6	Reactive power loss minimization (RPLM)	37
	3.3.7	Emission minimization (EM)/Emission cost minimization (ECM)	38
3.4	Const	raints Handling	38
3.5	Stand	ard Test Systems for OPF Analysis	39
	3.5.1	IEEE 9-bus system	39
	3.5.2	IEEE 14-bus system	39
	3.5.3	IEEE 26-bus system	39
	3.5.4	IEEE 30-bus system	40
	3.5.5	IEEE 57-bus system	40

	3.5.6	IEEE 118-bus system	40
	3.5.7	IEEE 300-bus system	40
	3.5.8	Indian 75-bus system	41
	3.5.9	Algerian 59-bus system	41
3.6	Other	Test Systems in OPF literature	41
	3.6.1	Large-Scale Systems	41
	3.6.2	Regional and Custom Configurations	41
	3.6.3	Specialized Test Networks	41
3.7	Concl	lusion	42
CE	IAPT	ER-4	
LE	ARN	ING-BASED SINE-COSINE ALGORITHM (L-SCA) FO	R OPF
SO	LUT	IONS	43-67
4.1	Motiv	vation for developing L-SCA	43
4.2	Introd	luction to the Proposed Algorithm	43
	4.2.1	Overview of SCA	43
	4.2.2	Proposed Learning-based SCA (L-SCA)	44
4.3	Comp	outational Steps of the Proposed L-SCA for OPF	45
4.4	Case S	Studies using the Proposed L-SCA for OPF	48
4.5	Simul	lation Results and Analysis	49
	4.5.1	Results for IEEE 57-Bus System	49
	4.5.2	Results for Algerian 59-bus system	55
	4.5.3	Results for IEEE 118-Bus System	61
4.6	Discu	ssion of Findings	66
4.7	Concl	lusion	66
CE	IAPT	TER-5	
Н	BRII	D RAO-2 SINE COSINE ALGORITHM FOR OPTIMAL P	OWER
FL	ow s	SOLUTIONS	.68-103
5.1	Introd	luction	68
5.2	Mathe	ematical Formulation of the OPF Problem	70
	5.2.1	Objective Functions	70

	5.2.2	Constraints	72
5.3	Propos	sed HRSCA Methodology	74
	5.3.1	Overview of Sine Cosine Algorithm (SCA)	.74
	5.3.2	Overview of Rao-2 Algorithm	.76
	5.3.3	Hybridization of SCA and Rao-2	77
	5.3.4	Computation Steps for HRSCA and Flowchart	78
5.4	Simul	ation Results and Analysis	82
	5.4.1	Performance on IEEE 30-Bus Test System	83
	5.4.2	Performance on IEEE 118-Bus Test System	95
5.5	Discus	ssion of Findings	102
5.6	Concl	usion	103
CF	IAPT]	ER-6	
		CATION OF THE COOT OPTIMIZATION ALGORITHM (CC PF	
6.1	Introd	duction	104
6.2	Proble	em Formulation for OPF	104
	6.2.1	Objectives of OPF	105
	6.2.2	Constraints in OPF	106
	6.2.3	OPF Problem Formulation for COA	106
6.3	Imple	ementation of the Coot Optimization Algorithm	106
	6.3.1	Overview of COA	106
	6.3.2	Steps in COA for OPF	107
	6.3.3	Simulation Setup and Test System	109
6.4	Case S	Studies, Results, and Discussion	.111
	6.4.1	Case 1 - OPF for FCM	.111
	6.4.2	Case 2 - OPF for EM	.112
	6.4.3	Case 3 - OPF for PLM	113

CHAPTER-7

OP	F WITH DISTRIBUTED GENERATION: APPLICA	TION OF THE
EE	FO ALGORITHM	116-132
7.1	Introduction	116
7.2	Problem Formulation	117
	7.2.1 General Structure of OPF	117
	7.2.2 OPF Objective Functions	118
	7.2.3 Constraints	119
7.3	Overview of Electric Eel Foraging Optimization (EEFO) Algorithm	119
	7.3.1 Inspiration	119
	7.3.2 Interacting Behaviour in EEFO	120
	7.3.3 Resting Behaviour in EEFO	121
	7.3.4 Hunting Behaviour in EEFO	121
	7.3.5 Migration Behaviour in EEFO	122
	7.3.6 Transition from Exploration to Exploitation	123
7.4	Simulation Results and Analysis	125
	7.4.1 Test System: IEEE 30-Bus	126
	7.4.2 Case Studies	127
7.5	Conclusion	132
СН	IAPTER-8	
CC	ONCLUSION, FUTURE SCOPE AND SOCIAL IMPAC	T133-138
8.1	Conclusion	133
8.2	Future Scope	134
	8.2.1 Incorporation of Renewable Energy Sources (RES)	134
	8.2.2 Real-time Applications	135
	8.2.3 Multi-Objective Optimization	135
	8.2.4 Hybrid Approaches	135
	8.2.5 Advanced Power System Models	136

	8.2.6	Exploration of Novel Objective Functions	136
8.3	Social	Impact	137
	8.3.1	Economic Impact	137
	8.3.2	Environmental Sustainability	137
	8.3.3	Grid Stability and Resilience	137
	8.3.4	Advancing Smart Grids	137
	8.3.5	Global Energy Transition	138
References 1			139
Ap	pendix	X	152
Lis	t of Pu	ublications	154
Pla	giaris	m Verification	155
Pla	giaris	m Report	156
Bri	ef Pro	ofile	157

LIST OF FIGURES

Fig. 2.1	Schematic overview depicting categorization of OPF algorithms	11
Fig. 2.2	OPF Algorithm Distribution	29
Fig. 4.1	Flowchart of the proposed L-SCA to solve OPF problem	47
Fig. 4.2	Graphical framework for L-SCA based OPF implementation	49
Fig. 4.3	Fuel cost convergence characteristics for Case 1	50
Fig. 4.4	Load bus voltage profile for Case 2	53
Fig. 4.5	Active power loss convergence characteristics for Case 4	55
Fig. 4.6	Fuel cost convergence characteristics for Case 5	57
Fig. 4.7	Load bus voltage profile for Case 6	58
Fig. 4.8	Active power loss convergence characteristics for Case 4	59
Fig. 4.9	Emission cost convergence characteristics for Case 9	60
Fig. 4.10	Fuel cost convergence characteristics for Case 10	63
Fig. 4.11	Load bus voltage profile for Case 11	64
Fig. 4.12	Active power loss convergence characteristics for Case 12	65
Fig. 5.1	Graphical framework for HRSCA based OPF scheme for diverse scenarios	78
Fig. 5.2	Proposed HRSCA algorithm flow chart	81
Fig. 5.3	Convergence curves in Case 1 with HRSCA, Rao-2, and SCA	86
Fig. 5.4	Comparison of voltage profiles in Case 2 using HRSCA and Rao-2 algorithms	87
Fig. 5.5	Convergence curve in Case 4 (a) with HRSCA, Rao-2 and SCA algorithms	88
Fig. 5.6	Convergence curves for Case 5 comparing HRSCA, Rao-2, and SCA	90
Fig. 5.7	Convergence curve in Case 9 with HRSCA, Rao-2 and SCA	98
Fig. 5.8(a)	Comparison of voltage profiles in Case 10 using HRSCA, Rao-2, and base case	99
Fig. 5.8(b)	Convergence curves for Case 10 comparing HRSCA, Rao-2, and SCA	99
Fig. 5.9	Convergence curves for Case 11 comparing HRSCA, Rao-2, and SCA	100
Fig. 6.1	Coots gliding in a synchronized manner across the water surface	107
Fig. 6.2	Flowchart of the Coot Optimization Algorithm for OPF	110
Fig. 6.3	Convergence characteristics comparison of Case 1 using COA and other recent	112

Fig. 6.4	algorithms	113
Fig. 6.5	Convergence characteristics comparison of Case 3 with COA and other recent algorithms	115
Fig. 7.1	Electric Eels: Utilizing Electric Pulses for Prey Capture	123
Fig. 7.2	Flowchart of the Electric Eel Foraging Optimizer for OPF	125
Fig. 7.3	Convergence characteristics comparison of Case 1 using the EEFO	129
Fig. 7.4	Voltage profile for Case 1 - without DG and with DG scenarios	130
Fig. 7.5	Convergence characteristics comparison of Case 1 using the EEFO	131
Fig. 7.6	Voltage profile for Case 2 - without DG and with DG scenarios	132

LIST OF TABLES

Table 2.1	Summary of hybrid approaches for OPF in the last decade	27
Table 4.1	Various cases examined in the present work using L-SCA	48
Table 4.2	Comparison of L-SCA with other popular algorithms reported in literature for Case 1	50
Table 4.3	Optimal settings of control variables	51
Table 4.4	Comparison of L-SCA with other popular algorithms reported in literature for Case 2	52
Table 4.5	Comparison of L-SCA with other popular algorithms reported in literature for Case 3	53
Table 4.6	Comparison of L-SCA with other popular algorithms reported in literature for Case 4	54
Table 4.7	Optimal settings of control variables	56
Table 4.8	Comparison of L-SCA with other popular algorithms reported in literature for Case 5	56
Table 4.9	Comparison of L-SCA with other popular algorithms reported in literature for Case 6	57
Table 4.10	Comparison of L-SCA with other popular algorithms reported in literature for Case 7	58
Table 4.11	Comparison of L-SCA with other popular algorithms reported in literature for Case 9	60
Table 4.12	Optimal settings of control variables	61
Table 4.13	Comparison of L-SCA and other popular algorithms for Case 10	63
Table 4.14	Comparison of L-SCA and other reported algorithms for Case 11	64
Table 4.15	Comparison of L-SCA and other popular algorithms for Case 12	65
Table 4.16	Statistical analysis of Cases 1, 4, 5, 7, 10 and 12 using the L-SCA and SCA algorithms	66
Table 5.1	Steps in HRSCA	78
Table 5.2	Parameter settings for HRSCA in the current study	82
Table 5.3	Allowable generator unit parameters and fuel cost coefficients for IEEE 30-bus test system	83
Table 5.4	Optimized control variables obtained by HRSCA for IEEE 30-bus test system	85
Table 5.5	Optimized control variables obtained for Case 6	91
Table 5.6	Optimized control variables for Case 7 and Case 8 for IEEE 30-bus test system (Scenario-3)	93
Table 5.7	Optimized control variables obtained by HRSCA for IEEE 118-bus test system	96
Table 5.8	Comparison of HRSCA, Rao-2, SCA, and other algorithms for FCM in Case 9	97
Table 5.9	Comparing HRSCA with Rao-2 and other leading algorithms for PLM in Case 11	100

Table 5.10	Optimized control variables in Case 12 with PLM Objective at LF = 1.658 p.u	101
Table 6.1	Algorithm Parameters assigned for COOT Algorithm on IEEE 30-bus System	111
Table 6.2	Comparison of the outcomes achieved through various optimization algorithms for Case 1	111
Table 6.3	Comparison of the outcomes achieved through various optimization algorithms for Case 2	113
Table 6.4	Comparison of the outcomes achieved through various optimization algorithms for Case 3	114
Table 7.1	Allowable generator unit parameters and fuel cost coefficients for IEEE 30-bus test system	126
Table 7.2	Algorithm Parameters	127
Table 7.3	OPF solution with optimal CV settings for IEEE 30-bus test system (Cases 1 & 2)	128
Table A.1	Summary of systems under study	152
Table A.2	Branch power flow in Case 6 with $P_D = 421.6014 \text{ MW}$	152
Table A.3	Allowable generator unit parameters and fuel cost coefficients for IEEE 118-bus system	153

LIST OF SYMBOLS, ABBREVIATION AND NOMENCLATURE

List of Symbols

$Z_{\min}(x,u)$	Objective function
x, u	State variables, Control variables
g , h	Equality and inequality constraints respectively
P_{losses} , Q_{losses}	Total active and reactive power losses respectively
P_{G_i}, Q_{G_i}	Active and reactive power of i^{th} generator
P_{D_i} , Q_{D_i}	Active and reactive power demands at i^{th} bus
S_{line} , S_{line}^{max}	Line flow limit in MVA, upper limit of i^{th} line
NB	Number of buses
NG, NPQ	Number of generators, Load buses
NL	Number of transmission lines
P_{G_1}	Power generated at slack bus
$P_{G_i}^{ ext{min}},\ P_{G_i}^{ ext{max}}, \ Q_{G_i}^{ ext{min}},\ Q_{G_i}^{ ext{max}}$	Limits of active and reactive powers of i^{th} generator respectively
$V_{G_i}^{\min}, V_{G_i}^{\max}$	i^{th} generator voltage limits
$V_{L_i}^{\min}$, $V_{L_i}^{\max}$	Load bus voltage limits at i^{th} bus
T, NT	Regulating transformer tap setting, Count of T
T_i^{\min} , T_i^{\max}	Limits for discrete tap settings for i^{th} transformer
Q_{C} , NC	Shunt VAR compensation, count of Q_C devices
$Q_{c_i}^{\min} Q_{c_i}^{\max}$	Limits on output of shunt VAR compensators at i^{th} bus
a_i, b_i, c_i	Fuel cost coefficients of i^{th} generator
Y_{jj}	Sum of admittances connected to j th load bus
L_{j}	L-index of any j^{th} load bus
Y_{ji}	Mutual admittance of line between j^{th} and i^{th} bus
W	Matrix obtained by partial inversion of bus admittance matrix
$G_{L_{i-j}}$	Conductance of line L between i^{th} and the j^{th} bus
δ_{ij}	Difference in phase angle between i^{th} and the j^{th} bus voltages
$\alpha_i, \beta_i, \gamma_i, \omega_i, \mu_i$	Emission coefficients for i^{th} generator unit
$oldsymbol{x}_i^t$, $P_{best_i}^{t}$	Position of current solution and best solution (target point) respectively at t^{th} iteration in i^{th} dimension

t, t_{max} Current iteration number and maximum number of

iterations respectively
User defined constant

 N_{POP} Population size in the optimization algorithm N_{Leader} Number of leaders in the Coot algorithm N_{Coot} Number of followers in the Coot algorithm

DDimension of the problemCP(i)The coot position of i^{th} coot g_{best} The global best position

 η Curling factor

List of Abbreviations

OPF Optimal Power Flow

SOOPF Single-Objective Optimal Power Flow MOOPF Multi-Objective Optimal Power Flow

MOO Multi-Objective Optimization
OPFS Optimized Power Flow Scheme

FCM Fuel Cost Minimization

RPLM Reactive Power Loss Minimization

EM Emission Minimization

PLM/APLM Real Power Loss Minimization/Active Power Loss

Minimization

PLMFC Real Power Loss along with Fuel Cost Minimization

VDM Voltage Deviation Minimization

VSI Voltage Security Index LMS Load Margin Stability

LF Loading Factor

CI Computational Intelligence

ML Machine Learning SCA Sine-Cosine Algorithm

HRSCA Hybrid Rao-2 Sine-Cosine Algorithm

MGOA Modified Grasshopper Optimization Algorithm

DSA Differential Search Algorithm

MOMICA Multi-Objective Modified Imperialist Competitive

Algorithm

NKEA Neighborhood Knowledge-based Evolutionary Algorithm
ESDE-MC Enhanced Self-adaptive Differential Evolution with Mixed

Crossover

BHBO Black-hole-based Optimization ACO Ant Colony Optimization

LCA League Championship Algorithm

PGA Parallel GA

FSLP Fast Successive Linear Programming

GWO Grey Wolf Optimizer

FPA Flower Pollination Algorithm

ICBO Improved Colliding Bodies Optimization

PSO Particle Swarm Optimization

GA Genetic Algorithm

TLBO Teaching-Learning-Based Optimization

BFO Bacterial Foraging Optimization

SSA Salp Swarm Algorithm

FACTS Flexible AC Transmission Systems
BSA Backtracking Search Algorithm
GSA Gravitational Search Algorithm
SPSA Sparrow Search Algorithm
HSA Harmony Search Algorithm

BAAMO Boundary Assigned Animal Migration Optimization
ARCBBO Adaptive Real-Coded Biogeography-Based Optimization

FHSA Fuzzy-based Harmony Search Algorithm
IPSO Improved Particle Swarm Optimization

DE Differential Evolution

NSGA-II Non-dominated Sorting Genetic Algorithm II

ABC Artificial Bee Colony
MFO Moth Flame Optimization
WOA Whale Optimization Algorithm

GOA Grasshopper Optimization Algorithm

SSA Salp Swarm Algorithm

BFO Bacterial Foraging Optimization

KHA Krill Herd Algorithm

GSO Group Search Optimization

ALO Ant Lion Optimizer

IGA Improved Genetic Algorithm
EGA Enhanced Genetic Algorithm

PSOPC Particle Swarm Optimization with Passive Congregation

MABC Modified Artificial Bee Colony

NSMOOGSA Non-dominated Sorting Multi Objective Opposition-based

GSA

HSA Harmony Search Algorithm

IHSA Improved Harmony Search Algorithm

DHSA Differential-based Harmony Search Algorithm
MTLBO Modified Teaching-Learning Based Optimization
LTLBO Lévy Mutation Teaching-Learning Based Optimization

IBF Improved Bacterial Foraging
CKH Chaotic Krill Herd Algorithm
SKHA Stud Krill Herd Algorithm

MFO Moth Flame Optimization

IMFO Improved Moth Flame OptimizationMSA Multi-Objective Search Algorithm

EMSA Enhanced Multi-Objective Search Algorithm

MSCA Modified Sine-Cosine Algorithm
MJAYA Modified JAYA Algorithm

AMTPG-Jaya Adaptive Multi-Team Perturbation-Guiding JAYA

Rao-2 Rao-2 Algorithm

MRao-2 Modified Rao-2 Algorithm

ISSA Improved Salp Swarm Algorithm
COA Coot Optimization Algorithm

ICOA Improved Coot Optimization Algorithm

EEFO Electric Eel Foraging Optimizer

DG Distributed Generation
RES Renewable Energy Sources

VPL Valve-Point Loading

List of Nomenclature

Slack Bus A reference bus in a power network with fixed

voltage magnitude and angle

Shunt VAR Reactive power compensation provided by shunt

devices

Tap changing A device used to regulate the voltage levels in

transformer power systems

Control variables Adjustable parameters in the power system used to

influence its operation

Equality constraints Conditions that must be exactly satisfied in the

optimization problem

Inequality constraints Conditions that set boundaries (upper or lower

limits) in the optimization problem

Shunt VAR Reactive power compensation provided by shunt

compensation devices to improve voltage stability

VPL Effect Represents the non-linear ripple effects in the fuel

cost curve due to generator valve-point effects.

Convergence The process of approaching a solution or a fixed

value in an optimization context

CHAPTER 1

INTRODUCTION

1.1 Introduction

The secure and efficient operation of power systems is increasingly critical, particularly as global energy demand rises and as renewable energy sources (RES) and power electronic appliances become integral to modern, interconnected power grids. Effective management, planning, and control are essential to support this demand, along with ensuring the stability and economic operation of both existing and future electrical grids. Achieving these objectives is often facilitated by the **Optimal Power Flow (OPF)** framework, which provides essential results for economic operation, planning, and control. The purpose of the OPF is to optimize a chosen objective function by optimal setting of the power system control variables within specified *equality* and *inequality* constraints.

The objectives of OPF can be broadly categorized into *techno-economic* and *environmental* aspects, each crucial to modern power systems. Techno-economic objectives primarily include fuel cost minimization (FCM) and real or active power loss minimization (RPLM/APLM). FCM is frequently prioritized for its direct impact on reducing generation costs, which is vital for efficient economic operation. RPLM further helps in reducing overall power production requirements by minimizing system losses. Additionally, technical objectives encompass voltage stability enhancement (VSE) to ensure system resilience and voltage profile improvement (VPI) to maintain optimal voltage levels across the network.

As thermal power plants continue to play a significant role in meeting the increasing demand, environmental objectives such as emission cost minimization (ECM) have become essential to address the environmental impacts of power generation. By balancing these technoeconomic and environmental objectives, OPF methodologies enable a more robust, sustainable, and cost-effective power system.

1.2 Historical Context

Since the term "Optimal Power Flow" was first introduced by Carpentier in the early 1960s (Carpentier, 1962) and subsequently formulated by Dommel and Tinney (1968), OPF has been extensively studied to enhance power system reliability, control, economic scheduling, and planning (Hazra & Sinha, 2011). Initially, power systems were designed with a focus on reliable and centralized electricity generation, with economic load dispatch being the primary

optimization objective. Classic optimization methods, such as linear programming and mixed-integer programming, were used to handle these early systems, focusing on balancing generation and demand with minimal operational cost.

The 21st century brought about a paradigm shift with the integration of RES. The intermittent nature of these sources, such as wind and solar power, introduced variability and uncertainty into the grid. This necessitates more sophisticated optimization techniques to ensure reliable and efficient power system operation.

Recent advancements in computational power and computational intelligence have accelerated the development of hybrid and adaptive optimization methods. These modern approaches are designed to address both single and multi-objective optimization needs, balancing technical, economic, and environmental goals. This ongoing progress in optimization techniques highlights how the field is adapting to the growing complexity and demands of modern power systems.

1.3 Motivation

The increasing complexity of power systems presents a pressing need for advanced optimization methods. Modern optimization techniques have evolved in response to the increasing complexities of power systems. Classical deterministic methods are now frequently supplemented or replaced by metaheuristic algorithms, such as particle swarm optimization (PSO), genetic algorithm (GA), and newer hybrid approaches. These metaheuristic techniques offer robust global search capabilities, enabling researchers to navigate the non-linear, multi-objective, and high-dimensional challenges of modern power systems more effectively than traditional methods, which often become trapped in local optima. Recent advancements in computational intelligence have further empowered researchers to explore innovative global optimization approaches, enabling the discovery of optimal solutions for complex power system problems.

This research work is motivated by the need to develop and apply optimization techniques that can address these challenges effectively. By employing advanced metaheuristic (modified or improved version) and hybrid optimization methods, this research study aims to contribute to the development of stable, efficient, and sustainable power systems that meet the demands of modern grids, while considering economic and environmental objectives.

However, the stochastic nature of population-based metaheuristics makes performance evaluation for OPF a challenging task. The "No Free Lunch" theorem by Wolpert and

Macready (1997) highlights this complexity, demonstrating that no single optimization algorithm can universally solve all types of engineering and complex optimization problems. This insight highlights the importance of refining existing algorithms and developing new ones to address specific needs in diverse contexts. Consequently, this thesis is motivated by the objective of creating a highly efficient optimization method tailored to solve the OPF problem effectively, offering robust solutions for stable and sustainable power system operations.

1.4 Challenges in Power System Stability and Optimization

The secure and reliable transmission of electricity is essential for modern power networks, especially given the continuous growth in electrical demand. Long transmission distances, economic constraints, environmental concerns related to grid expansion, and rising load demands can all lead to stressed power systems that are more vulnerable to outages (Shiraki et al. 2016). With the increasing integration of renewable energy sources (RES), the power grid faces new *challenges*, particularly the overloading of transmission lines, which can result in voltage drops and even system collapse during high-stress conditions (Athari and Wang 2018; Liang et al. 2022).

Below are the main challenges that grid operators and researchers face as they seek to ensure stable, efficient, and sustainable power delivery:

1.4.1 Economic Pressures on Grid Operation

Economic pressures influence how grids are operated, with operators often running systems close to maximum capacity to improve loadability and reduce costs. However, this approach heightens the risk of voltage collapse, particularly when the system approaches critical load conditions. In cases of voltage collapse, cascading outages or blackouts can follow (Laghari et al. 2013; Samuel et al. 2014). Therefore, it is critical for system operators to assess the stability margins accurately and determine how much additional load capacity the system can handle before reaching an unstable state. This tension between economic efficiency and system reliability presents a significant operational challenge, underscoring the need for solutions that minimize operational costs without compromising stability.

1.4.2 Voltage Instability

Overloaded transmission lines and network topology changes frequently lead to voltage instability, a major cause of global blackouts. Accurate assessments of stability margins are crucial to prevent cascading failures and ensure secure power system operation, especially

under contingency conditions. This technical challenge underscores the importance of maintaining a stable voltage profile to support continuous and reliable power delivery.

1.4.3 Reliance on Load Shedding for Stability

During emergencies, operators often rely on load shedding to prevent system collapse. This approach addresses immediate threats but indicates a reactive, rather than proactive, management of stability, which may impact both economic and technical objectives by causing interruptions and operational inefficiencies. This reliance highlights the need for improved stability management strategies that reduce the necessity of disruptive, last-resort measures to maintain system security.

1.4.4 Environmental Sustainability Challenges

The need to reduce emissions and fuel consumption adds environmental considerations, requiring optimization techniques that support emission minimization while enhancing operational efficiency.

Addressing the above challenges requires optimization techniques that balance competing objectives across technical, economic, and environmental domains. These techniques should aim to minimize fuel and emission costs, reduce power losses, and enhance voltage stability, thereby promoting efficient and sustainable power system operations.

1.5 Objectives of OPF in Modern Power Systems

The objectives of OPF can be broadly categorized into *techno-economic* and *environmental* aspects. Each of these objectives plays a critical role in enhancing the operational efficiency, reliability, and sustainability of modern power systems.

1.5.1 Techno-Economic Objectives

The techno-economic objectives are pivotal for the economic efficiency and operational reliability of power systems. Key objectives within this category include:

a) Fuel Cost Minimization (FCM)

Minimizing fuel costs is often a primary objective in OPF as it directly impacts the overall generation costs. By optimizing the fuel usage across generators, FCM reduces operational expenses, thereby enabling economically efficient system operation and benefiting both utility providers and consumers. To address complex real-world conditions, FCM is often divided into the following sub-objectives:

Fuel Cost Minimization with Valve-Point Loadings (FCM-VPL)

This objective accounts for the non-linearities introduced by valve-point effects in generation units. Incorporating valve-point loadings enables a more accurate fuel cost model by considering the ripple effect in the cost curve, which leads to better optimization under real operational conditions.

Fuel Cost Minimization with Prohibited Operating Zones (FCM-POZ)

Certain operational zones within generators may be restricted due to physical or safety limitations. This objective ensures that the OPF solution respects these zones, leading to feasible and safe operation while still optimizing fuel costs.

Fuel Cost Minimization Considering Multiple Fuel Sources (FCM-MFS)

Thermal generating units can be powered by multiple fuel sources, including oil, coal, and natural gas. By incorporating fuel selection into OPF, the optimal fuel mix can be determined, considering factors like fuel availability and price fluctuations to minimize overall costs.

b) Real Power Loss Minimization (PLM)

PLM aims to reduce the total active power losses in the system, thus decreasing the amount of power that must be generated to meet demand. Lower system losses lead to reduced generation requirements, which further supports cost savings and contributes to system efficiency.

c) Reactive power loss minimization (RPLM)

This objective focuses on minimizing reactive power losses within the system. Reactive power losses primarily arise due to the reactance of transmission lines, and they significantly impact both system stability and voltage regulation. By reducing reactive power losses, the system can operate more efficiently, as lower reactive losses enhance voltage stability and improve overall power quality.

d) Voltage Stability Enhancement (VSE)

Voltage stability is essential for ensuring the system's resilience to disturbances. Enhancing voltage stability through OPF helps prevent voltage collapse, which can lead to large-scale blackouts, and ensures the system remains robust under various operating conditions. The L-index serves as an indicator, showing how close a bus is to a potential voltage collapse, allowing for proactive stability management. Additionally, the objective

of VSE in contingency conditions like line outages or generator failures, etc., is also frequently explored and addressed in OPF literature.

e) Severity Index (SI) Minimization

The Severity Index (SI) quantifies the severity of line overloads within the power system. Contingencies are ranked based on this index, with higher values indicating greater severity. System operators can leverage the SI to prioritize actions and address critical issues, thereby enhancing system stability and mitigating the risk of failures.

Unlike the SI, which solely considers line overloads, the *Severity Value Minimization* (SVM) function provides a more holistic approach. SVM aims to minimize the overall severity of violations in the power system by accounting for both line power flows (overloading) and bus voltage deviations.

f) Voltage Profile Improvement (VPI)/ Voltage Deviation Minimization (VDM)

Maintaining optimal voltage levels across the network is necessary for system reliability and safety. VPI ensures that voltage levels are within desired limits throughout the system, which not only supports the performance of equipment but also reduces the risk of voltage-related issues. Improving the voltage profile involves minimizing voltage deviations at all load buses, from the reference value (VD) of 1.0 p.u.

g) Voltage Security Index (VSI)

VSI serves as a performance index to evaluate a power system's ability to maintain voltage levels within a predefined acceptable range, thereby indicating the system's stability and security. Minimizing VSI indicates that the voltages across the system are closer to the average voltage, implying less fluctuation and greater stability.

1.5.2 Environmental Objectives

In addition to techno-economic goals, OPF increasingly integrates environmental objectives to align with **sustainability goals**. Common objectives include:

a) Emission Minimization (EM)

In the context of OPF, the emissions minimization objective focuses on reducing harmful pollutants produced by power generation by thermal units. This objective considers various emissions, such as sulfur oxides (SOx), nitrogen oxides (NOx), and thermal emissions. By minimizing these emissions, OPF contributes to cleaner energy production and aligns with environmental standards. This approach not only addresses the ecological impacts of power

systems but also supports sustainable power generation by integrating cleaner technologies and optimizing power generation strategies to reduce overall emissions.

b) Renewable Energy Integration

With the rising emphasis on clean energy, OPF also considers the optimal integration of renewable resources. This helps in balancing conventional and renewable sources, thus fostering a more sustainable power system.

1.6 Problem Statement

The rapid growth in energy demand, coupled with the integration of RES, has introduced significant complexity into modern power systems. Traditional optimization techniques, such as linear and non-linear programming, are increasingly inadequate for addressing the non-linear, multi-objective, and high-dimensional challenges of today's power systems. As a result, power grids face heightened risks of instability, economic inefficiency, and environmental impact, particularly in scenarios involving high renewable penetration and fluctuating power generation.

This research work presented in this thesis aims to address these challenges by developing and applying advanced optimization techniques. The primary focus is on reducing fuel costs, lowering emissions, enhancing voltage stability, and minimizing power losses, while addressing both individual and simultaneous objectives. By focusing on single and multi-objective optimization through both modified (improved/enhanced) and hybrid approaches, this study seeks to help build power systems that are resilient, efficient, and sustainable, meeting the complex needs of today's energy networks.

1.7 Outline of Thesis

This thesis comprises eight chapters, beginning with an introduction to the critical role of OPF in modern power systems and a review of its evolving methodologies. Subsequent chapters explore advanced optimization algorithms, including L-SCA, HRSCA, COA, and EEFO, demonstrating their applications and effectiveness in addressing OPF challenges. The thesis concludes with future research directions, followed by references.

Chapter 1: This chapter introduces the critical role of OPF in ensuring the secure, efficient, and sustainable operation of modern power systems. It emphasizes the growing importance of OPF in the face of increasing energy demand and the integration of renewable energy sources (RES). The chapter discusses the evolution of OPF methodologies, from traditional approaches to more advanced metaheuristic techniques, and highlights the need for developing

sophisticated optimization algorithms to address the complex challenges facing today's power grids.

Chapter 2: This chapter provides a comprehensive review of the evolution of OPF methodologies. It focuses on the transition from classical optimization techniques to more modern metaheuristic algorithms. It highlights the strengths, limitations, and advancements in heuristic and hybrid approaches for addressing multi-objective and constrained OPF problems. Recent developments and comparisons of these techniques are also covered.

Chapter 3: This chapter provides a comprehensive overview of the OPF framework, including its structure, objectives, and constraints. Detailed descriptions and mathematical formulations of various OPF objectives are discussed. It outlines the single- and multi-objective formulations and describes the standard test systems used for validating optimization techniques.

Chapter 4: This chapter introduces the L-SCA, a modified optimization algorithm that enhances the performance of the standard SCA by incorporating a learning phase inspired by teaching-learning mechanisms. The algorithm's ability to balance exploration and exploitation is demonstrated through case studies on standard power systems.

Chapter 5: This chapter presents the HRSCA, a novel hybrid optimization algorithm designed to address OPF challenges under high loading and generator outages. Combining the strengths of SCA and Rao-2, HRSCA achieves superior results in single- and multi-objective scenarios across various test systems, focusing on cost reduction and stability enhancement.

Chapter 6: This chapter explores the COA, inspired by the foraging behavior of coot birds, for solving OPF problems. The algorithm's efficiency in balancing global search and local refinement is validated through its application to fuel cost, emission, and power loss minimization.

Chapter 7: This chapter applies EEFO algorithm to OPF problems involving distributed generation. The EEFO algorithm's unique ability to address challenges posed by renewable energy integration is demonstrated through its robust performance in achieving cost-effective and stable grid operations.

Chapter 8: This chapter concludes the thesis by summarizing the effectiveness of the proposed algorithms in addressing OPF challenges. It highlights the potential for integrating RES, real-time applications, and multi-objective optimization in future research.

CHAPTER 2

LITERATURE REVIEW

2.1 Introduction

Over the past two decades, there has been a significant shift among researchers toward using population-based metaheuristic algorithms to address power system challenges. Pandya (2008) presented a review of various classical optimization methods as well as some AI techniques for OPF solutions. Following this, AlRashidi and El-Hawary (2009) provided an extensive coverage of population-based CI tools applied to OPF up to 2008. A two-part survey by Frank et al. (2012a; 2012b) further extended the discussion, with the first part focusing on classical and stochastic optimization methods for OPF, and the second highlighting the growing interest in non-deterministic and hybrid techniques, analyzing their strengths, limitations, and computational performance. Niu et al. (2014) presented a detailed survey of OPF related research work from 2000 to 2014, covering popular heuristic optimization algorithms (HOAs) such as evolutionary programming (EP), genetic algorithm (GA), differential evolution (DE), and particle swarm optimization (PSO), along with some hybrid methods. Maskar et al. (2017) followed with a review that encompassed both conventional and AI-driven techniques for OPF, summarizing research developments up to 2016. Later, Mittal et al. (2022) presented a more comprehensive review and comparison of OPF solution methods, focusing on widely adopted metaheuristics and extending literature coverage to 2020. In a subsequent and more in-depth examination, Mittal et al. (2024) analysed the application of various population-based AI techniques that have gained significant traction in recent years (2012–2022) for addressing OPF problems.

2.2 Traditional Approaches

The OPF problem is a non-linear, high-dimensional, non-differentiable, multi-modal, and non-convex optimization challenge that involves both *discrete* and *continuous control variables*. Initially, OPF challenges were addressed primarily through conventional/classical optimization techniques (COTs). The Gradient based method (Lee et al. 1985), Newton's method (Tinney and Hart 1967; Sun et al. 1984), quadratic programming (QP) (Reid and Hasdorff 1973), nonlinear programming (NLP) (Dommel and Tinney 1968), interior point (Wei et al. 1998), and linear programming (LP) (Zehar and Sayah 2008) are some popular mathematical programming-based deterministic methods that fall under the umbrella of these

COTs and typically applied in OPF problem solution. However, these conventional approaches are constrained by the requirement that the objective function be continuous and differentiable, even though some of them typically guarantee convergence. Newton methods and gradient-based methods have trouble handling inequality constraints and are more likely to get stuck in local optima. Their performance is highly sensitive to initial conditions, especially in high-dimensional control parameter spaces, which can result in insecure convergence characteristics, as discussed by Nocedal & Wright (2006). Additionally, these methods lack the flexibility to accurately model discrete control variables, such as voltage regulator transformer taps and shunt compensator switching, both essential in OPF applications.

Because of these serious issues, these COTs are incapable of solving real-world OPF problems with non-smooth, non-differentiable, and multi-modal objective functions. Therefore, the limitations of COTs in handling non-linearities and high computational costs necessitate exploring alternative approaches. Momoh et al. (1999a; 1999b) and Frank et al. (2012a) have conducted an extensive survey, covering various conservative and conventional approaches implemented on OPF solution studies.

2.3 Population-based metaheuristic algorithms

Over the last few years, the rapid progress in computational intelligence (CI) has led to the development of population-based metaheuristic algorithms. The use of metaheuristics, under the umbrella of computational intelligence, has revolutionized power system optimization in the past two decades. Several standard versions of these algorithms have been applied to OPF problems, producing incredibly promising results. These algorithms present a promising approach to solve complex constrained optimization problems and mitigate the limitations of classical optimization techniques (Wang et al. 2023). Recognizing this potential, researchers have introduced various metaheuristic techniques to tackle complex OPF problems efficiently, minimizing execution time.

Despite their advantages, standard implementations of these metaheuristics can encounter issues with local optima or premature convergence in particularly complex problem spaces. To address these limitations, researchers have developed *enhanced*, *modified*, or *hybridized* versions of metaheuristics, which now serve as competitive alternatives to traditional methods. These advanced approaches provide higher accuracy and reliability for real-world OPF problems. Comprehensive studies by Frank et al. (2012b) and Mittal et al. (2024) have explored a wide range of CI-based OPF methods, showcasing the effectiveness of non-deterministic algorithms, including their improved and hybridized versions, in addressing modern power

system optimization challenges. Figure 2.1 provides a visual representation of the evolution of population-based optimization techniques used for OPF problems. It categorizes these algorithms based on their underlying principles and historical development.

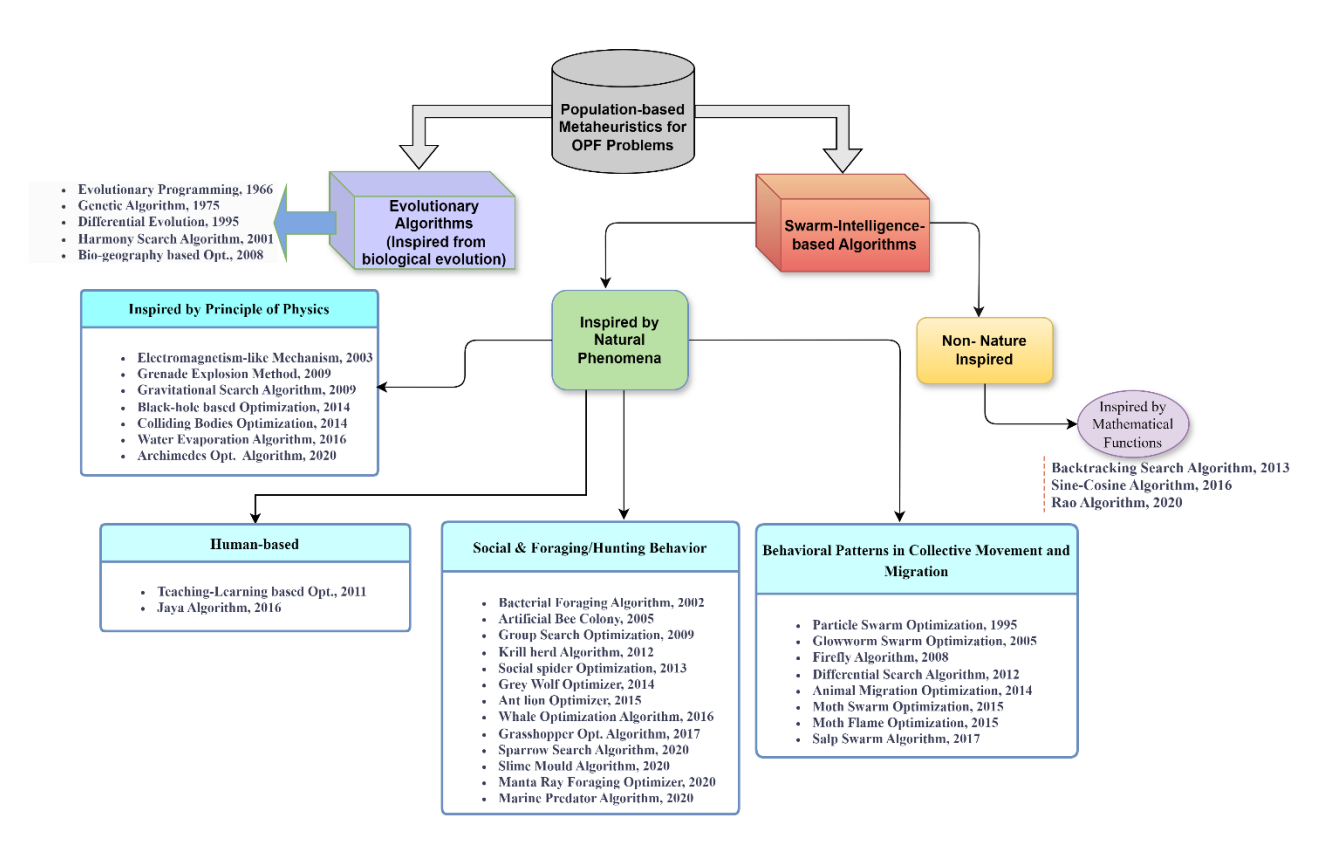


Fig. 2.1 Schematic overview depicting categorization of OPF algorithms and their inception over time

2.3.1 Evolutionary algorithms for OPF solution

Evolutionary Algorithms (EAs) are among the earliest AI-based approaches applied to power system optimization problems (PSOPs) and are inspired by biological evolution. The Evolutionary Programming (EP) approach is a subset of EAs. Yuryevich and Wong (1999) were pioneers in developing an EP-based algorithm for OPF, enhancing it with gradient information to accelerate convergence and improve performance, especially on large-scale systems. Later, Kahourzade et al. (2015) conducted a comparative analysis of PSO, EP, and GA to assess their effectiveness in solving the OPF problem. Using the IEEE 30-bus test system, they evaluated these algorithms across various single and multi-objective functions.

GA has been one of the most popular and widely used evolutionary tools inspired from biological evolution to find optimal solutions to search problems. Bakirtzis et al. (2002) introduced an Enhanced GA to solve complex OPF problems with both continuous and discrete control variables. By incorporating problem-specific operators, the EGA achieved

improvements in convergence speed and solution quality. This method was validated on an IEEE 30-bus test system and an IEEE RT-96 three-area 73-bus system. Later, Attia et al. (2012) employed an Adapted Genetic Algorithm (AGA) with a variable population size, adjusted based on different fitness functions, to solve the OPF problem on the IEEE 30-bus system. However, despite these advancements, the popularity of GA in OPF has declined due to challenges such as premature convergence, high computational costs, and sensitivity to hyperparameters, along with the development of more efficient problem-specific algorithms and advancements in AI techniques.

The Differential Evolution Algorithm (DEA), inspired by biological evolution, has seen significant applications in power system optimization. El-Fergany and Hasanien (2015) applied DEA to the IEEE 30-bus test system for various techno-economic objectives and extended it to multi-objective OPF (MOOPF) using a fuzzy-based Pareto front. Shaheen et al. (2016) introduced a forced initialization multi-objective DEA (MODEA) with an epsilon-constraint approach, followed by their 2017 work on a multi-objective DE (MDE) algorithm for IEEE 57- and 118-bus systems. Reddy (2018) further advanced DEA with a multi-objective approach for mixed control variables, demonstrating its effectiveness on IEEE 30- and 300-bus networks.

The Biogeography-Based Optimization (BBO) algorithm was initially applied by Bhattacharya and Chattopadhyay (2009) to address economic load dispatch challenges. Building on this, Kumar and Premalatha (2015) proposed an Adaptive Real-Coded BBO (ARCBBO) technique designed to enhance population diversity and exploration abilities in the OPF problem by integrating adaptive Gaussian mutation. The effectiveness of ARCBBO was demonstrated on IEEE 30-bus and 57-bus systems, addressing both techno-economic and environmental optimization objectives.

2.3.2 Swarm intelligence-based algorithms for OPF solution

Nature-inspired algorithms for OPF

OPF algorithms based on movement patterns & collective behavior in migration

Swarm intelligence-based optimization techniques have proven effective in addressing OPF problems by emulating the cooperative and adaptive behavior observed in natural swarms. Among these, PSO algorithm has been widely applied. Abido (2002) introduced PSO for OPF, testing it on the IEEE 30-bus standard system. To improve the search performance of standard PSO, Vlachogiannis and Lee (2006) proposed PSO with Passive

Congregation (PSOPC) and enhanced it with the constriction factor approach to solve the OPF on IEEE 30 and 118-bus test systems. Later, Niknam et al. (2012a) introduced an improved PSO (IPSO) for single- and multi-objective OPF, using chaos theory and a selfadaptive mechanism to fine-tune parameters, validated on the IEEE 30-bus test system. Despite PSO's minimal parameter tuning requirements, it can suffer from premature convergence in high-dimensional, complex problems, sometimes failing to reach the global optimum. Another swarm intelligence method, Glowworm Swarm Optimization (GSO), was applied by Reddy and Rathnam (2016) to solve single-objective OPF (SOOPF) and MOOPF problems. GSO was evaluated for its effectiveness in minimizing generation cost in an SOOPF problem on both the IEEE 30-bus test system and a practical 75-bus Indian grid system, with performance compared to PSO. In a later study, Alghamdi (2022) applied the Firefly Algorithm (FA) to the OPF problem, proposing the Gaussian-Based Bare Bones Lévy Flight Firefly Algorithm (GBLFA) and a modified version, the Modified GBLFA (MGBLFA). These approaches incorporated both thermal units and RES, such as wind and solar, and addressed various techno-economic and environmental objectives on the IEEE 30-bus network. Bouchekara and Abido (2014) applied the Differential Search Algorithm (DSA) to solve the SOOPF problem, targeting techno-economic objectives under contingency conditions, and validated their approach on IEEE 30- and 118-bus networks. Abaci and Yamacli (2016) further applied DSA to both SOOPF and MOOPF objectives, using IEEE 9-, 30-, and 57-bus test systems to address techno-economic and environmental objectives. Dash et al. (2022) proposed Boundary Assigned Animal Migration Optimization (BAAMO) to address OPF problems. BAAMO was evaluated on IEEE 30, 57, and 118-bus systems, considering techno-economic and technical objectives. BAAMO demonstrated superior performance compared to PSO, GA, DE, ABC, and GSA in terms of fuel cost reduction and improved system performance. However, the algorithm's computational time was relatively high due to its iterative update process. Mirjalili (2015) introduced Moth-Flame Optimization (MFO) algorithm inspired by the natural navigation strategy known as "transverse orientation," used by moths. Buch et al. (2017) applied MFO algorithm to a standard IEEE 30-bus system, focusing on techno-economic and environmental objectives. Compared to other algorithms like PSO, GWO, and ABC, the proposed MFO consistently delivered high-quality solutions for OPF problems. Taher et al. (2019a) proposed an improved MFO (IMFO) algorithm that incorporates modified spiral paths for moths as they converge around flames. The IMFO algorithm was validated on IEEE test networks with 30, 57, and 118 buses, addressing both SOOPF and MOOPF problems with fifteen different

objective functions. Comparative results with established optimization algorithms, including basic MFO, GA, PSO, and TLBO, demonstrated that IMFO achieved accurate, high-quality OPF solutions with faster convergence rates. Buch and Trivedi (2019) introduced an enhanced MFO, namely adaptive MFO (AMFO), to address large-scale OPF problems. AMFO incorporated an adaptive mechanism to improve the optimization process. The algorithm was tested on the IEEE 118-bus system, considering various technoeconomic and environmental single-objective functions. AMFO outperformed other algorithms like basic MFO, GWO, and the SCA in terms of solution quality and convergence speed, demonstrating its effectiveness in solving large-scale OPF problems.

Mohamed et al. (2017) introduced the Moth Swarm Algorithm (MSA), building on the conventional MFO algorithm to enhance its optimization performance. MSA integrates new optimization operators inspired by moth behaviour to strengthen both exploration and exploitation capabilities. The algorithm was applied to IEEE 30-, 57-, and 118-bus systems, addressing various techno-economic and environmental objectives. MSA outperformed other algorithms, including modified PSO, modified DE, and MFO, in terms of solution quality and convergence speed. Bentouati et al. (2021) proposed an enhanced version of the Moth Swarm Algorithm (EMSA) to address limitations of the basic MSA, such as premature convergence and lack of diversity. EMSA was tested on IEEE 30-, 37-, and 118-bus systems for both single and multi-objective formulations, addressing technical, economic, and emission objectives, and demonstrated superior performance over the basic MSA.

El-Fergany and Hasanien (2020) applied the Salp Swarm Algorithm (SSA) to the OPF problem, targeting various technical, economic, and environmental objectives. Initially, each objective was addressed individually, then jointly optimized through SSA. The study included voltage stability analysis, using eigenvalues of a reduced Jacobian matrix to assess proximity to voltage instability. Generator output power, voltage levels, transformer tap settings, and capacitor placements formed the search space, and the SSA's performance was evaluated on IEEE 57- and 118-bus systems. Comparisons with other optimization methods, supported by parametric and non-parametric statistical tests, highlighted SSA's competitiveness in effectively solving OPF challenges. Abd El-sattar et al. (2021) proposed an improved Salp Swarm Algorithm (ISSA) to enhance exploration and exploitation capabilities for addressing the OPF problem. The ISSA was designed to optimize various cost-based objective functions. ISSA was tested on IEEE 30-, 57-, and 118-bus networks, demonstrating superior convergence compared to SSA, MFO, and GA.

Amjady et al. (2012) proposed an improved Bacterial Foraging Optimization (IBFO) algorithm to enhance the performance of the basic BFO algorithm in addressing OPF and OPF-SC problems. The IBF algorithm incorporated innovative search mechanisms and solution strategies to improve exploration, exploitation, and convergence. The algorithm was evaluated on 26-bus, 30-bus, and 118-bus IEEE test systems, demonstrating superior performance compared to other optimization algorithms like basic BFO, EP, and PSO.

Adaryani and Karami (2013) proposed an Artificial Bee Colony (ABC) algorithm inspired by the foraging behavior of honeybees. The ABC algorithm was applied to the MOOPF problem, considering various techno-economic and environmental objectives. The algorithm was tested on IEEE 9, 30, and 57-bus systems, demonstrating competitive performance compared to other optimization algorithms like PSO and GSA. Further Khorsandi et al. (2013) developed a fuzzy-logic-based modified ABC (MABC) algorithm for OPF, designed to handle both discrete and continuous variables for optimizing key techno-economic and environmental objectives. The MABC algorithm was tested on IEEE 30- and 118-bus networks, addressing both SOOPF and MOOPF problems, and demonstrated superior performance over other optimization algorithms in terms of solution quality and convergence speed. Chen et al. (2014) proposed a multi-hive multi-objective bee algorithm (M2OBA) to solve MOOPF problems. M2OBA incorporates a multi-hive structure and multi-objective strategies to enhance the efficiency of the bee foraging process. The algorithm was tested on a 30-bus IEEE system, demonstrating superior performance compared to NSGA, MOPSO, and multi-objective ABC. He et al. (2015) proposed an improved ABC (IABC) algorithm to solve fuzzy MOOPF problems, considering technoeconomic and environmental objectives. IABC incorporates DE operators to enhance exploration and generate novel solutions. The algorithm was tested on 30, 57, and 300-bus IEEE systems, demonstrating superior performance compared to ABC, GA, and PSO. Jadhav and Bamane (2016) proposed a g-best guided ABC (GABC) algorithm to address both standard and temperature-dependent OPF problems. The GABC algorithm was evaluated on IEEE 30-bus and 57-bus systems with a focus on economic objectives, showing improved performance compared to the standard ABC algorithm. The 30-bus system was also used to assess the impact of temperature on fuel cost as well as power loss. Bai et al. (2017) proposed an improved ABC (IABC) algorithm to solve OPF problems. IABC incorporated orthogonal learning to improve its performance. The algorithm was tested on IEEE 30 and 118 bus systems, demonstrating superior performance compared to basic ABC, enhanced GA, MDE, and others in terms of convergence speed and fuel cost reduction.

Basu (2016) implemented the Group Search Optimization (GSO) algorithm, inspired by the producer-scrounger behavior in animals, and tested it on IEEE 30, 57, and 118 bus systems. The evaluation focused on techno-economic and environmental objectives, formulating four single-objective OPF problems and two compound-objective ones. Simulation results validated the effectiveness of GSO, demonstrating promising solutions with faster convergence. Daryani et al. (2016) proposed an adaptive GSO (AGSO) algorithm to address MOOPF problems, considering environmental and security aspects. AGSO was tested on benchmark cases and IEEE 30- and 57-bus networks, demonstrating superior performance compared to standard GSO.

Mukherji and Mukherjee (2015) enhanced the Krill Herd Algorithm (KHA) for OPF by incorporating chaos theory, drawing inspiration from krill swarm behavior to boost computational speed and convergence rates. This chaotic KHA was validated on both a 26-bus system and the IEEE 57-bus test network, showing superior performance over other computational intelligence techniques. The algorithm effectively addressed key economic and technical objectives, achieving faster convergence and identifying optimal solutions across diverse operational scenarios. Roy and Paul (2015) developed an enhanced KH algorithm for OPF by incorporating genetic operators (crossover and mutation) to address key techno-economic objectives, such as fuel cost minimization and power loss reduction. The algorithm was tested on IEEE 30-, 57-, and 118-bus systems. The integration of crossover and mutation operators improved the balance between local and global search, resulting in high-quality solutions, faster convergence, and greater computational efficiency compared to other algorithms documented in the OPF literature.

Nguyen (2019) introduced the Novel Improved Social Spider Optimization (NISSO) algorithm to tackle the OPF problem. NISSO included several enhancements to the original SSO algorithm, resulting in improved convergence speed and solution quality. The algorithm was tested on IEEE 30, 57, and 118-bus systems, focusing on technical, economic, and environmental objectives. NISSO demonstrated superior performance compared to the original SSO algorithm and other state-of-the-art optimization methods.

El-Fergany and Hasanien (2015) applied the Grey Wolf Optimizer (GWO) to OPF on IEEE 30- and 118-bus systems, addressing both technical and economic objectives, though the algorithm showed lower computational efficiency on larger systems. Meng et al. (2021) introduced an enhanced version, the Crisscross Search-based GWO (CS-GWO), with a single controllable parameter for improved adaptability. By incorporating crossover operators (horizontal and vertical), CS-GWO increased population diversity and minimized the risk of getting trapped in local optima. Tested on IEEE 30- and 118-bus networks for both SOOPF and MOOPF scenarios (MOOPF on 30-bus only), CS-GWO outperformed other algorithms such as PSO, ABC, BSA, and GSA, particularly in terms of solution quality and convergence speed for larger systems.

Mahdad (2020) proposed a Partitioned Ant Lion Optimizer (PALO) algorithm to improve the performance of the ALO algorithm (proposed by Seyedali Mirjalili in 2015) in solving OPF problems. PALO was tested on IEEE 30-bus and large-scale Polish power systems, considering technical and economic objectives. The algorithm demonstrated effectiveness in solving large-scale security OPF problems with diverse FACTS devices, outperforming other contemporary metaheuristic techniques.

El-Dabah et al. (2022) introduced a non-dominated sorting Whale Optimization Algorithm (NSWOA) for both SOOPF and MOOPF formulations, focusing on cost-based and various technical objectives on the IEEE 30-bus test network. The optimal compromise solution was selected based on the minimal Euclidean distance from the non-dominated solution set. The proposed NSWOA outperformed established methods like PSO, SCA, and SSA, particularly in reducing fuel cost and power loss in multi-objective scenarios.

Taher et al. (2019b) proposed a modified Grasshopper Optimization Algorithm (MGOA) to enhance the performance of the original GOA (introduced by Mirjalili in 2017). MGOA incorporated a modified mutation process to improve global exploration and avoid local optima. The algorithm was tested on IEEE 30-, 57-, and 118-bus systems, addressing various techno-economic and environmental objectives across 13 distinct case studies in both SOOPF and MOOPF formulations. MGOA outperformed GOA, GA, PSO, and TLBO, demonstrating superior performance.

Khunkitti et al. (2021) introduced the Slime Mould Algorithm (SMA) for SOOPF and MOOPF problems, applying it to IEEE 30-, 57-, and 118-bus systems with technical, economic, and environmental objectives. SMA demonstrated competitive computational

times and outperformed other algorithms in solution quality, especially on the 57- and 118-bus systems, delivering superior Pareto fronts compared to PSO across all test cases. Al-Kaabi et al. (2022) developed a multi-objective slime mould algorithm (MOSMA) to address MOOPF problems on IEEE 30- and 57-bus systems, as well as a practical Iraqi Super Grid. Across 29 case studies, they tackled various technical, economic, and environmental objectives in two- to five-objective formulations. Using Pareto theory and fuzzy set theory, the authors identified optimal and favorable solutions. MOSMA demonstrated strong convergence, effectiveness, and well-distributed solutions on the Pareto front, outperforming other recent optimization algorithms.

Islam et al. (2021) applied the Marine Predator Algorithm (MPA) to solve the SOOPF problem, focusing on technical and economic objectives. The method was tested on the IEEE 30-bus network and compared to popular optimization algorithms such as SCA, PSO, and GSA. The MPA approach demonstrated competitive performance, yielding results comparable to those of SCA, GWO, PSO, and other algorithms in terms of fuel cost and efficiency.

Jebaraj and Sakthivel (2022) introduced the Sparrow Search Algorithm (SPSA) for OPF optimization on IEEE 30-, 57-, and 118-bus systems, addressing 33 economic and technical objectives across single, bi-, tri-, and quad-objective formulations, including scenarios with single-line outage contingencies. Comparative analysis indicated that SPSA consistently outperformed existing algorithms such as MFO, MPSO, MSA, and ABC, highlighting its robustness and effectiveness in handling multi-objective OPF scenarios.

The Manta Ray Foraging Optimizer (MRFO) is based on the survival strategies of manta rays. Kahraman et al. (2022) introduced an improved multi-objective Manta Ray Foraging Optimizer (IMOMRFO) to tackle the MOOPF problem. The authors improved its exploration and exploitation capabilities by incorporating a crowding distance-based Pareto archival process. IMOMRFO was tested on IEEE 30- and 57-bus systems, successfully optimizing various technical, economic, and environmental objectives simultaneously.

OPF algorithms inspired by principle of physics

The Electromagnetism-like mechanism is based on the principle of attraction and repulsion between electrically charged particles distributed in the search space. The particle with the highest charge, known as the optimal particle, strongly attracts particles with higher fitness values while repelling those with lower fitness. El-Hana et al. (2016) introduced an

improved Electromagnetism-like mechanism (IEM) to optimize control variables for achieving optimal OPF solutions across seven single-objective cases with various constraints. Tested on IEEE 30- and 57-bus networks, IEM demonstrated superior performance in solution accuracy, convergence speed, and computational efficiency, outperforming well-known algorithms like BBO, DE, and PSO.

Bouchekara et al. (2016a) utilized the Grenade Explosion Method (GEM), inspired by the dynamics of a grenade explosion, to address both SOOPF and MOOPF problems, focusing on six techno-economic objectives. The approach incorporated a fuzzy decision-making method, transforming objective functions into fuzzy membership functions for optimization. Tested on an IEEE 30-bus system, GEM demonstrated superior performance in optimizing both single and multiple objectives.

Duman et al. (2012) introduced the Gravitational Search Algorithm (GSA) to address the OPF problem. GSA was tested on IEEE 30- and 57-bus systems under normal and contingency conditions, considering various economic and technical objectives. GSA outperformed other algorithms in SOOPF scenarios, demonstrating its effectiveness in achieving optimal solutions, especially for economic objectives. The algorithm also exhibited strong scalability in larger systems. Bhattacharya and Roy (2012) applied GSA to solve three single-objective (SOOPF) and three multi-objective (MOOPF) cases. The algorithm was tested on both a standard 26-bus system and a large-scale 118-bus IEEE system, addressing identical single, bi-objective, and tri-objective cases across both systems. The results demonstrated that the GSA-based approach effectively determined optimal solutions, with performance comparable to previously established algorithms.

Bouchekara (2014b) implemented the Black Hole-based Optimization (BHBO) algorithm, which mimics the behavior of black holes by drawing candidate solutions (stars) towards an optimal solution. The parameter-less algorithm was applied to solve various OPF problems, optimizing control variables on IEEE 30-bus and Algerian 59-bus networks while considering different objective functions. However, its effectiveness for MOOPF problems was not explored.

The Colliding Bodies Optimization (CBO) algorithm, developed by Kaveh and Mahdavi (2014), uses conservation of momentum principles to navigate search spaces. An Enhanced CBO (ECBO) introduced by Kaveh and Ghazaan (2014) incorporated a regeneration mechanism to circumvent local optima. Further enhancements by Bouchekara et al. (2016b)

led to the development of an Improved CBO (ICBO), which utilized three colliding bodies to enhance performance. ICBO was applied to IEEE test systems of 30, 57, and 118 buses, effectively addressing OPF challenges across technical, economic, and reliability objectives in both normal and contingency scenarios. Its robustness and adherence to constraints showcased its potential, indicating the feasibility of developing a multi-objective CBO to tackle broader MOOPF problems.

Saha et al. (2017) applied the Water Evaporation Algorithm (WEA), inspired by evaporation dynamics, to solve the OPF problem. Tested on IEEE 30- and 118-bus systems, WEA addressed various technical and economic objectives, including operational efficiency and system stability. In multi-objective scenarios on the 30-bus system, WEA outperformed methods like HSA, NSGA-II, and TLBO, showing strong optimization performance.

Akdag (2022) proposed an Improved Arithmetic Optimization Algorithm (IAOA) to enhance the exploration capabilities of the original AOA. IAOA was tested on IEEE 30- and 57-bus networks and the 16-bus South Marmara system, addressing technical and economic objectives. The algorithm demonstrated superior performance compared to TLBO, SCA, DSA, and other methods in both single and multi-objective settings.

OPF Algorithms Inspired by human natural behavior

The Teaching-Learning-Based Optimization (TLBO) algorithm, developed by Rao et al. (2011), is a parameter-free, population-based method inspired by the teaching and learning process in classrooms. This approach simulates the transfer and collaborative exchange of knowledge among learners, enhancing solution quality. Bouchekara et al. (2014a) applied TLBO to solve SOOPF problem across various technical and economic objectives on IEEE 30 and 118-bus networks. Specifically, the algorithm was tested for its scalability with a single objective on the 118-bus network. The results showed that TLBO provided better or comparable outcomes to other documented methods, affirming its effectiveness and scalability. Shabanpour-Haghighi et al. (2014) enhanced the Teaching-Learning-Based Optimization (TLBO) algorithm by incorporating a self-adapting wavelet mutation (SAWM) to address MOOPF problems, particularly focusing on economic and environmental objectives. This modification aimed to expand the search capabilities and efficiency of the algorithm. Tested on IEEE 30 and 57-bus systems, the modified TLBO demonstrated improved performance, achieving faster convergence and greater precision in fewer iterations compared to the standard TLBO. Ghasemi et al. (2015) enhanced the TLBO

algorithm by incorporating a Lévy mutation strategy, creating the Lévy mutation-based TLBO (LTLBO). This modification improved the algorithm's exploration abilities and increased population diversity, enhancing its effectiveness for OPF problems. The LTLBO algorithm was tested on IEEE 30-bus system, focusing on objectives such as cost minimization, voltage profile improvement, and emission reduction, and on IEEE 57-bus system with a cost minimization objective. LTLBO demonstrated superior performance compared to basic TLBO, ABC, GSA, and other algorithms. Akbari et al. (2022) introduced the Teaching–Learning-Studying-Based Optimization (TLSBO) algorithm, an enhancement of TLBO that incorporates a studying strategy. TLSBO was tested on the IEEE 30-bus system, addressing SOOPF and MOOPF problems with economic, technical, and environmental objectives. TLSBO outperformed the original TLBO in terms of solution quality and convergence speed.

El-Sattar et al. (2019) developed multiple Jaya-based optimization frameworks for addressing both SOOPF and MOOPF problems. These frameworks were designed to tackle a range of technical, economic, and environmental objectives, applying them across 23 case studies on IEEE 30 and 57-bus systems. Upon evaluation, these Jaya-based methods demonstrated robust and effective performance, showcasing superior convergence and overall robustness when compared to other existing optimization strategies. Elattar and ElSayed (2019) introduced a modified version of Jaya (MJAYA) to overcome the problem of premature convergence of the original Jaya. The authors applied MJAYA algorithm to solve OPF problem including RES and examined their effects on objective functions considering objectives such as technical (enhancing system stability), economic (reducing operational costs), and environmental (minimizing emissions). By using pricing and weighting parameters, they converted the multi-objective problem into a single-objective framework for more straightforward optimization. Tested on IEEE 30 and 118-bus systems, MJAYA showed improved performance over existing methods. Warid (2020) introduced the adaptive multiple teams perturbation-guiding Jaya (AMTPG-Jaya) algorithm for the first time to solve the OPF problem, using dynamic "teams" to find optimal solutions. Tested on IEEE 30 and 118-bus systems, AMTPG-Jaya targeted economic and technical objectives, demonstrating superior performance over the basic TLBO and other stochastic methods. The algorithm excelled in terms of solution quality, feasibility, and computational efficiency, especially for large-scale power systems.

Non-nature inspired algorithms for OPF

Non-nature-inspired algorithms, in contrast to metaheuristic algorithms that mimic natural phenomena, are grounded in social and mathematical principles rather than biological or environmental analogies.

Kılıç (2015) pioneered the application of the Backtracking Search Algorithm (BSA) to SOOPF problems, incorporating diverse cost functions with valve point loading and power system constraints. The BSA was tested on the IEEE 30-bus test system and demonstrated superior performance in terms of generation cost and convergence speed compared to other algorithms like GA, EP, DE, modified DE, ABC, and others. While the results affirmed BSA's effectiveness on this scale, further studies were suggested to explore its performance on larger systems.

Chaib et al. (2016) applied the BSA to address OPF problems with complex objectives involving discontinuities. The method was evaluated on IEEE 30-bus, 57-bus, and 118-bus systems through 16 case studies. BSA showed superior performance and robustness over other established algorithms like DE, PSO, ABC, GA, and BBO, especially in large-scale network settings. Further research was recommended to extend its application to MOOPF problems using Pareto-optimal solutions. In their study, Daqaq et al. (2021) developed a multi-objective BSA (MOBSA) for solving OPF problems in power systems, targeting both technical and economic objectives. Tested on IEEE 30, 57, and 118-bus networks, MOBSA successfully generated well-distributed Pareto optimal solutions, which were further analyzed using fuzzy membership techniques to identify optimal trade-offs. Comparative evaluations with other multi-objective algorithms underscored MOBSA's robustness and effectiveness, highlighting its contribution to OPF methodologies.

Mirjalili (2016) introduced the Sine Cosine Algorithm (SCA), which uses mathematical principles to efficiently search for optimal solutions. Attia et al. (2018) later developed a modified version, MSCA, enhancing SCA with Lévy flights and adaptive population tuning to improve convergence speed and avoid local optima. Tested on IEEE 30- and 118-bus networks, MSCA demonstrated its effectiveness in optimizing cost-based and technical objectives. By adjusting control variables in fewer iterations, MSCA proved particularly advantageous for large-scale OPF problems, outperforming other previously documented optimization algorithms. Karimulla and Ravi (2021) enhanced the Sine Cosine Algorithm (ESCA) by incorporating Lévy flights to address MOOPF challenges on a 30-bus IEEE test network. They

focused on optimizing technical, economic, and environmental objectives. ESCA outperformed popular algorithms like GA, PSO, and the Flower Pollination Algorithm, achieving reduced power losses and improved results across cost and emission objectives.

Rao algorithms, introduced by Rao (2020), are sophisticated metaheuristic techniques that eliminate the need for parameter tuning. Gupta et al. (2021c) employed Rao-1, Rao-2, and Rao-3 variants to address OPF problems on IEEE test systems comprising 30, 57, and 118 buses. These algorithms were utilized to optimize a diverse set of objectives, including economic efficiency, technical performance, and environmental impact, under various operating conditions. Rao-3 consistently demonstrated superior optimization results across different scenarios, while Rao-2 excelled specifically in minimizing power losses on the 57-bus system.

Hassan et al. (2021) enhanced the Rao-2 algorithm to create MRao-2, tailored to solve OPF problems in power systems with significant Renewable Energy Source (RES) integration. Improved with quasi-oppositional and Lévy flight techniques, MRao-2 was tested on IEEE 30 and 118-bus networks, addressing objectives related to economic, technical, and environmental performance. Its efficacy was benchmarked against other algorithms like Atom Search Optimization (ASO) and Marine Predator Algorithm (MPA), showing MRao-2's superior convergence capabilities, especially in large-scale applications.

In recent advancements, Alghamdi (2023) introduced the Improved Turbulent Flow Optimization (ITFWO) algorithm to address complex non-linear, non-convex OPF challenges in power systems incorporating renewable sources like solar PV and wind turbines. Evaluated on the IEEE 30-bus system, ITFWO efficiently balances techno-economic and environmental objectives, dynamically adjusting energy generation parameters based on real-time renewable input. Additionally, Alghamdi's study explores the impact of carbon taxes on generator scheduling, demonstrating ITFWO's superior performance in optimizing multiple objectives when compared to other state-of-the-art algorithms. This research highlights a significant shift towards OPF methods that integrate renewable sources and environmental considerations, enhancing system efficiency under variable conditions.

2.3.3 Hybrid and Advanced Techniques

Hybrid methods have become increasingly popular over the past decade as they combine the strengths of individual techniques while addressing their limitations. This hybridization of two or more algorithms produces a new hybrid algorithm, which is more effective and powerful than any of its component methods, yields promising results by exhibiting better and faster convergence characteristics along with covering an expanded area in lesser computational time.

Kumar and Chaturvedi (2013) introduced a hybrid approach that combined fuzzy systems with Genetic Algorithm (GA-Fuzzy) and Particle Swarm Optimization (PSO-Fuzzy) algorithms. This method aimed to optimize control parameters for the SOOPF problem, specifically focusing on cost objective. Applied to a modified IEEE 30-bus network, the PSO-Fuzzy approach achieved a lower fuel cost compared to the GA-Fuzzy method, while GA-Fuzzy demonstrated improved average fitness on the same network. The study found that these integrated approaches were more effective and robust than standalone PSO or GA in solving OPF challenges.

A hybrid algorithm combining modified PSO with the Shuffle Frog Leaping Algorithm (MPSO-SFLA) was proposed by Narimani et al. (2013) to address the MOOPF problem, targeting cost and environmental objectives. To improve PSO's performance, a Self-Adaptive Probabilistic Mutation Operator (SAPMO) was introduced to enhance population diversity. A Pareto-based methodology provided a well-distributed set of solutions, with a fuzzy decision-making model selecting the best compromise solution. MPSO-SFLA was validated on IEEE 30-, 57-, and 118-bus systems, showing superior performance in convergence, computational time, solution quality, and robustness compared to basic SFLA and PSO.

A hybrid PSO and GSA (PSO-GSA) algorithm was proposed by Radosavljević et al. (2015) to solve the OPF problem by combining PSO's global exploration with GSA's local search capabilities. Validated on IEEE 30- and 118-bus networks, the approach addressed single and dual objectives techno-economic objectives. When applied to 30-bus system, the hybrid algorithm demonstrated faster convergence and improved solution quality compared to individual PSO and GSA algorithms, especially for single and dual objective optimization problems. However, some solutions were identified as infeasible due to violations of system constraints, particularly load bus voltage limits. Khunkitti et al. (2018) proposed a hybrid dragonfly-PSO (DA-PSO) algorithm to solve the MO-OPF problem, considering technoeconomic and environmental objectives. The algorithm effectively minimizes fuel cost and transmission losses (techno-economic) and emissions (environmental) on IEEE 30- and 57-bus systems. The hybrid approach combines the exploration capabilities of DA with the exploitation capabilities of PSO, leading to improved performance compared to original DA and PSO algorithms.

Ghasemi et al. (2014) developed a novel hybrid algorithm, MICA-TLA, by integrating a modified imperialist competitive algorithm (MICA) with the teaching-learning algorithm (TLA). This hybrid approach leveraged TLA to boost local search efficiency, particularly near the global optimum. The MICA-TLA was tested on the IEEE 30-bus network for single and complex economic objectives and on the 57-bus IEEE network for economic and technical objectives. The results demonstrated that MICA-TLA outperformed standard population-based algorithms such as ICA, TLA, and MICA, showcasing faster convergence and improved solution quality.

Pulluri et al. (2018) introduced the stud krill herd (SKH) algorithm to solve SOOPF problems. SKH hybridizes KH and SGA to improve exploration and exploitation capabilities. The algorithm was tested on IEEE 14-, 30-, and 57-bus systems, demonstrating superior performance compared to other evolutionary algorithms.

Reddy (2019) introduced a Hybrid DE-HS algorithm, combining DE and Harmony Search (HS) to solve SOOPF and MOOPF problems. The combination of the two algorithms led to the development of a powerful hybrid algorithm that integrated the original DE algorithm with HSA to achieve faster global convergence. This hybrid approach was applied to IEEE 30-, 118-, and 300-bus systems to optimize techno-economic objectives.

El Sehiemy et al. (2020) proposed the PSO-SSO algorithm to address SOOPF and MOOPF problems in IEEE 30, 57, and 118-bus test systems. The algorithm was evaluated across 18 case studies, considering economic, technical, and environmental objectives. Compared to standalone PSO and SSO, PSO-SSO achieved lower power losses, reduced emissions, and minimized fuel costs while converging faster.

Khan et al. (2020) initially implemented the Hybrid Firefly-PSO (HFPSO) method to address SOOPF problems, including economic and technical objectives. The HFPSO algorithm was evaluated on the IEEE 30-bus test system, where it demonstrated significant improvements (lower costs and faster convergence in fewer iterations) over COTs, such as PSO, DE, and BHBO. Later in the same year, Khan et al. (2020) extended the HFPSO method to a multi-objective version (MOHFPSO) for addressing the complex MOOPF problems. This advanced approach integrated non-dominated sorting techniques to generate Pareto optimal fronts and determine optimal solutions across various techno-economic objectives. The MOHFPSO algorithm was tested on IEEE 30- and 57-bus test networks, encompassing five multi-objective

formulations that included three bi-objective and two tri-objective cases, effectively demonstrating its capability to handle multi-dimensional optimization in power systems.

Gupta et al. (2021a) introduced the Jaya-PPS (Jaya-Powell's Pattern Search) hybrid algorithm to solve the OPF problem, integrating Jaya with the derivative-free PPS technique, based on conjugate-direction principles. The algorithm was tested on IEEE 30-, 57-, and 118-bus systems, both with and without distributed generation (DG) sources, considering technoeconomic, environmental, and combined objectives. The Jaya-PPS1 variant consistently outperformed other algorithms by achieving optimal values for various objective combinations on the 30- and 57-bus systems. Additionally, it significantly reduced fuel costs on the 118-bus system. In a subsequent study, Gupta et al. (2021b) introduced a modified Jaya algorithm incorporating a sine-cosine mutation operator (SCM-MJ) to enhance performance in OPF optimization. This modification aimed at maintaining population diversity throughout the search process, resulting in smoother convergence and improved solution accuracy. The SCM-MJ algorithm was evaluated on both the practical 59-bus Algerian system and the IEEE 118-bus network to address technical and cost-based objectives. SCM-MJ consistently achieved superior performance, with a significant reduction in fuel costs on the 118-bus system.

Naderi et al. (2021) proposed the FAHSPSO-DE algorithm, a hybrid approach combining fuzzy adaptive PSO and DE. This algorithm effectively addressed SOOPF and MOOPF problems on IEEE 30-, 57-, and 118-bus systems, focusing on cost, emissions, and power loss minimization. The algorithm's application to the IEEE 57-bus system resulted in significant annual cost savings, highlighting its potential for medium-scale power systems.

Avvari and Vinod Kumar (2022) introduced a hybrid decomposition and local dominance-based multi-objective evolutionary algorithm (MOEA) for tackling the MOOPF problem with conflicting objectives. The algorithm was evaluated on IEEE 57- and 118-bus systems across multiple case studies, considering a combination of techno-economic and environmental objectives. The proposed method exhibited competitive performance compared to established techniques like MOPSO and NSGA-II.

Mallala et al. (2022) developed a hybrid NSHFABC algorithm to solve MOOPF and SOOPF problems on IEEE 30- and 118-bus systems. The algorithm effectively improved the system's techno-economic performance by minimizing fuel cost, power loss, and severity values. NSHFABC demonstrated competitive performance compared to established methods like DE, PSO, and ACO, achieving significant reductions in fuel cost and severity values.

Mohamed et al. (2022) proposed a hybrid GBO-MFO algorithm to optimize OPF considering uncertain load and wind generation. The algorithm was tested on an IEEE 30-bus system with FACT devices. The proposed method effectively reduced fuel cost and power loss compared to standalone GBO, SMA, and MFO algorithms.

Keswani et al. (2023) implemented a hybrid sine cosine—grey wolf optimizer (HSC-GWO) for MOOPF in large power grids, combining the GWO's exploitation strengths with the SCA's exploration capabilities. Applied to IEEE test systems (30, 57, and 118 buses) considering techno-economic aspects, HSC-GWO effectively minimizes fuel costs, enhances voltage profiles, and reduces active power loss. Results showed that it outperformed other metaheuristic methods like DE, TLBO, PSO, BBO, GWO, and others, demonstrating efficiency and robustness in achieving optimal solutions for real-time OPF scenarios.

Upputuri et al. (2023) proposed a hybrid Improved Harris Hawks Optimization and Pattern Search (hIHHO-PS) algorithm to solve OPF problems. The algorithm effectively addresses various objective functions, including techno-economic objectives, social welfare maximization (SWM), and loadability factor maximization (LFM). Additionally, the study investigates the impact of optimally placed multi-line FACTS devices and their control modes on OPF outcomes, demonstrating significant improvements in system performance.

Table 2.1 provides a summary of hybrid approaches for OPF reported in reputable peer-reviewed journals over the past decade.

Table 2.1 Summary of hybrid approaches for OPF in the last decade from reputable peer-reviewed journals

Author(s)	Year	Hybrid approach	Objective Function(s)	MOOPE/		Strength of Hybrid approach
Kumar and Chaturvedi	2013	GA+Fuzzy, PSO+Fuzzy	FCM	SOOPF	IEEE 30- bus (modified)	Improved average fitness and faster convergence
Narimani et al.	2013	Modified PSO+SFLA (HMPSO- SFLA)	FCM, EM	MOOPF	IEEE 30, 57 and 118-bus	Enhanced solution diversity and strong local search capability
Ghasemi et al.	2014	MICA-TLA (Modified ICA + TLA)	FCM, VDM	Both	IEEE 30- and 57-bus	Achieved faster convergence and enhanced solution quality by boosting local search efficiency
Radosavljevića et al.	2015	PSO+GSA (PSOGSA)	FCM, PLM, VDM, VSE	SOOPF and MOOPF (weight	IEEE 30 and 118- bus	Combined exploration and local search strengths

				factor approach)		
Khunkitti et al.	2018	DA-PSO (Dragonfly + PSO)	FCM, EM, PLM	Both	IEEE 30- and 57-bus	DA-PSO combines DA's exploration and PSO's exploitation for better OPF solutions, but its sequential processing slows computation
Pulluri et al.	2018	KH + Stud GA	FCM, PLM, VDM, VSE, EM	SOOPF	IEEE 30- and 118- bus, Algerian 59-bus	Avoids premature convergence and enhances global optimality through SSC operators integrated into KH
S. S. Reddy	2019	DE+HS	FCM, VSE, PLM	Both	IEEE 30, 118 and 300 bus	Balanced exploration-exploitation trade- off
El Sehiemy et al.	2020	PSO+SSO (PSO-SSO)	FCM, VDM, PLM, VSE, EM	Both	IEEE 30, 57 and 118-bus	Mitigated premature convergence, enhanced exploration
Khan et al.	2020	FA+PSO (HFPSO)	FCM, VDM, VSE and PLM (active & reactive)	SOOPF	IEEE 30-bus	HFPSO blends FA's local precision and PSO's quick global exploration, ensuring efficient and balanced convergence
Khan et al.	2020	FA+PSO (MOHFPSO)	FCM, VSE, VDM, PLM	MOOPF	IEEE 30, 57-bus	Balances local and global exploration, superior Pareto solutions
Gupta et al.	2021a	Jaya+PPS	FCM, VDM, EM, PLM	MOOPF (combined SOF)	IEEE 30, 57 and 118 bus	Jaya-PPS enhances local and global search efficiency, achieving a well-balanced exploration and exploitation
Gupta et al.	2021b	SCM+MJ	FCM, VDM, PLM	MOO (MOF turned into SOF)	Algerian 59-bus, IEEE 118- bus	SCM prevents premature convergence, while MJ balances global and local search effectively
Naderi et al.	2021	PSO+DE (FAHSPSO- DE)	FCM, PLM, EM	Both	IEEE 30, 57 and 118-bus	Optimal trade-off with dynamic parameter adjustment
Avvari and Vinod Kumar	2022	(Pareto dominance and decomposition) + EA	FCM, EM, PLM, VDM	MOOPF	IEEE 57 and 118- bus	Improved exploration, exploitation, and uniform Pareto front
Mallala et al.	2022	Fruit fly+ABC (NSHFABC)	FCM, PLM, SVM	Both	IEEE 30 and 118- bus	Enhanced optimal value accuracy, tackles premature convergence
Mohamed et al.	2022	GBO+MFO	FCM, PLM (without and with uncertain load demand)	Both	IEEE 30- bus	Improves convergence using gradient search and local escaping operator (LEO)
Keswani et al.	2023	HSC-GWO	FCM, VDM, PLM	Both	IEEE 30, 57 and 118-bus	Combines GWO's exploitation with SCA's exploration, achieving high efficiency and robustness

			FCM, PLM,		IEEE 30-	Excels	in	cost	reduction	n, loss
Upputuri et al.	2023	IHHO+PS	VDM,	Both	bus	minimizat	tion,	and	system	stability,
			SWM, LFM		ous	enhanced	with	UPFC/	GUPFC	

Figure 2.2 depicts the distribution of Optimization Algorithms (OAs) applied to address OPF problems, offering valuable insights into their percentage-wise adoption in high-impact, peer-reviewed journals over the past decade.

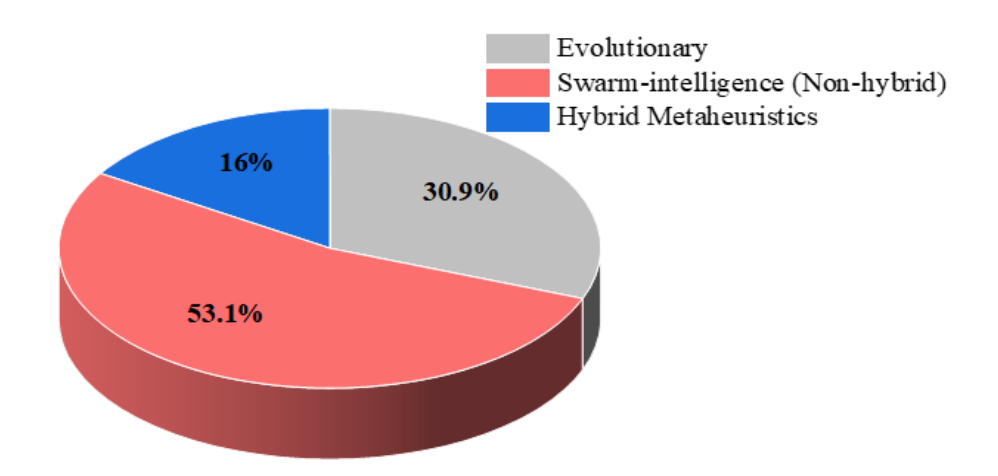


Fig. 2.2 OPF Algorithm Distribution: Evolutionary (30.9%), Swarm Intelligence (53.1%), Hybrid (16%)

2.4 Gaps in Current Research and Opportunities for Further Study

The literature review reveals several research gaps and opportunities for further exploration, as outlined below:

2.4.1 Need for a Robust Optimization Algorithm Capable of Addressing Diverse OPF Scenarios:

Due to the varied formulations and objectives of the OPF problem, no algorithm can be claimed as the best for solving all OPF scenarios. Each algorithm has limitations, especially regarding convergence speed and feasibility in large-scale systems.

• Research Opportunity:

Developing a novel algorithm that is both efficient and reliable remains a critical need. Future research could focus on creating hybrid algorithms that combine strategies from various metaheuristic approaches to effectively address OPF challenges.

2.4.2 Load Growth and Contingency Handling in OPF:

The complex nature of modern power systems, with increased loading and potential for unexpected generator outages, requires robust OPF solutions capable of maintaining stability without resorting to reactive measures like load shedding. While traditional algorithms often struggle to adapt to both single and multi-objective requirements across different loading scenarios, there is a need for optimization techniques that can proactively secure OPF under diverse operational conditions.

• Research Opportunity:

Building on recent advancements in hybrid optimization, future work could explore extending dynamic, hybrid algorithms to tackle even more diverse operational constraints and objectives. For instance, integrating predictive modelling could allow such algorithms to preemptively adjust control variables in response to varying load conditions and potential contingencies, further enhancing system stability and operational flexibility without compromising efficiency.

2.4.3 Integration of Renewable Energy Sources (RES) in OPF:

The integration of RES (e.g., solar, wind, hydro) offers significant benefits, such as reducing greenhouse gas emissions and minimizing transmission losses. By inserting the RES as a negative load, the total load demand is reduced which decreases the fuel cost of the conventional generators and in turn reduces the total objective function. Since most renewable resources are intermittent in nature, it may be advantageous to utilize more than one resource when available.

• Research Opportunity:

Future studies could explore multi-objective OPF optimization that further adapts to renewable energy, emphasizing cost reduction and stability. Additionally, hybrid algorithms that account for multiple renewable sources can enhance the efficiency of OPF solutions.

2.4.4 Incorporation of FACTS Devices:

FACTS devices offer promising potential for improving the steady-state performance of power systems by enhancing voltage regulation and loadability. Their role could be especially impactful under contingency conditions, which aligns with Security Constrained OPF (SC-OPF).

• Research Opportunity:

Incorporating FACTS devices within OPF under both standard and contingency scenarios could be a valuable avenue for future research, potentially advancing system reliability and stability.

2.5 Research Objectives

Based on the literature review and research gaps observed, the following objectives have been identified:

- ➤ Development of a new powerful computational intelligence algorithm or modifications/ improvements in the existing popular algorithms or hybridizing algorithms depending upon the formulation and objectives of the OPF problem (MOOPF) for a given test system.
- ➤ Comparison of the simulation results for validating the superiority and effectiveness of the proposed algorithm over the existing ones for the same test system and objectives reported earlier in literature.
- Examination of load changing effects on the cost and transmission losses.
- Adapting renewable energy resources for further fuel cost reduction.

CHAPTER 3

OPTIMAL POWER FLOW: FUNDAMENTALS AND VARIOUS TEST SYSTEMS

3.1 General Structure of OPF

The OPF problem generally involves a combination of objectives and constraints. Its solution aims to optimize a specific objective function by identifying the best possible values for control variables. The optimized state of the power system is described using a set of state variables.

The operation of the power system must comply with two categories of constraints: **equality constraints** and **inequality constraints**. Equality constraints typically correspond to power balance equations, while inequality constraints set the operational boundaries for system elements like generator limits, voltage levels, and line capacities. Meeting all constraint conditions is essential to ensure a realistic and practical OPF formulation.

3.1.1 Single-Objective OPF

The formulation of single-objective OPF (SOOPF) problems is as follows:

$$Min: Z_{min}(x,u) \tag{3.1}$$

Subject to:
$$g_i(x,u) = 0$$
 $i = 1, 2, 3, ..., m$ (3.2)

and
$$h_i(x,u) \le 0$$
 $j = 1, 2, 3, \dots, n$ (3.3)

The objective function, shown in Equation (3.1), depends on the state variables 'x' and the control variables 'u'. Equation (3.2) outlines the inequality constraints, and Equation (3.3) defines the equality constraints, with 'm' as the number of equality constraints and 'n' as the number of inequality constraints.

3.1.2 Multi-Objective OPF

In the MOOPF problem, a vector of objective functions is optimised rather than a single objective function. Mathematically, MOOPF problem is stated as follows:

Min:
$$Z_{\min}(x,u) = [Z_1(x,u), Z_2(x,u), ..., Z_k(x,u)]^T$$
 (3.4)

Here, 'k' denotes the number of objective functions optimized simultaneously, while ensuring compliance with the constraints in Equations (3.2) and (3.3).

The state vector *i.e.*, the vector of dependent variables is given by Equation (3.5) where P_G is the generator voltage, V_L is the load bus voltage, Q_G is the generated reactive power and S_{line} is the apparent power flow of the transmission line.

$$x^{T} = [P_{G_1}, V_{L_1}, ..., V_{L_{NPQ}}, Q_{G_1}, ..., Q_{G_{NG}}, S_{line_1}, ..., S_{line_{NI}}]$$
(3.5)

Here, P_{G_1} represents the slack bus power. The terms NPQ, NG, and NL denote the counts of load buses, generating units, and transmission lines, respectively. The power system status is represented by the vector of state (or dependent) variables, as defined in Equation (3.6) below;

$$u^{T} = [P_{G_{2}}, ..., P_{G_{NG}}, V_{G_{1}}, ..., V_{G_{NG}}, Q_{C_{1}}, ..., Q_{C_{NC}}, T_{1}, ..., T_{NT}]$$
(3.6)

Here, V_G denotes the voltage at the generator bus, Q_C represents shunt VAR compensation, with NC indicating the number of compensators, and T signifies the tap-changing transformer, with NT representing the number of tap-changing transformers.

3.2 Constraints

For secure and economical grid operation, the state and control variables are subjected to various constraints and limits as described below;

3.2.1 Equality constraints

In the OPF problem, the load flow equations are incorporated as equality constraints. The mathematical formulation is presented below:

$$P_{G_{i}} - P_{D_{i}} = V_{i} \sum_{j=1}^{NL} V_{j} \left(G_{ij} \cos \theta_{ij} + B_{ij} \sin \theta_{ij} \right)$$

$$Q_{G_{i}} - Q_{D_{i}} = V_{i} \sum_{j=1}^{NL} V_{j} \left(G_{ij} \sin \theta_{ij} - B_{ij} \cos \theta_{ij} \right)$$
(3.7)

In Equation (3.7), i = 1, 2, ..., n, where n signifies the total number of buses in the network. Here, G_{ij} signifies the mutual conductance between any bus i and j^{th} load bus, while B_{ij} signifies the mutual susceptance between these buses.

3.2.2 Inequality constraints

The operating bounds of the power system are determined through the following constraints:

a) Generation constraints: For stable operation, the generators must operate within the following ranges of real power, reactive power, and voltages:

$$P_{G_{i}}^{\min} \leq P_{G_{i}} \leq P_{G_{i}}^{\max} \qquad i = 1, 2, ..., NG$$

$$Q_{G_{i}}^{\min} \leq Q_{G_{i}} \leq Q_{G_{i}}^{\max} \qquad i = 1, 2, ..., NG$$

$$V_{G_{i}}^{\min} \leq V_{G_{i}} \leq V_{G_{i}}^{\max} \qquad i = 1, 2, ..., NG$$

$$i = 1, 2, ..., NG$$

$$(3.8)$$

Here, active power generation at i^{th} generator bus (P_{G_i}) is bounded by $P_{G_i}^{\min}$ and $P_{G_i}^{\max}$, while the reactive power generation (Q_{G_i}) is bounded by $Q_{G_i}^{\min}$ and $Q_{G_i}^{\max}$. Additionally, the bus voltage (V_{G_i}) of the i^{th} generator must stay within the limits of $V_{G_i}^{\min}$ and $V_{G_i}^{\max}$.

b) Shunt compensator constraints: Shunt compensation must be maintained within specified lower and upper limits, as shown in Equation (3.9).

$$Q_{C_i}^{\min} \le Q_{C_i} \le Q_{C_i}^{\max}$$
 $i = 1, 2, ..., NC$ (3.9)

c) Transformer constraints: There is a range of tap settings for transformers that must be adhered to. The lower and upper limits are as follows:

$$T_i^{\min} \le T_i \le T_i^{\max}$$
 $i = 1, 2, ..., NT$ (3.10)

d) Security constraints: These constraints involve the maximum MVA limits for line flows and the allowable voltage magnitude ranges at load buses, as represented in Equation (3.11).

$$\begin{vmatrix} S_{line_i} \end{vmatrix} \leq S_{line_i}^{\text{max}} & i = 1, 2, ..., NL \\
V_{L_i}^{\text{min}} \leq V_{L_i} \leq V_{L_i}^{\text{max}} &
\end{vmatrix}$$
(3.11)

3.3 Objective Functions

In OPF, the objective functions define the goals of optimizing power system operations, often balancing technical, economic, and environmental considerations. Below are common objective functions in OPF, detailed with their mathematical formulations:

3.3.1 Fuel cost minimization (FCM)/Total fuel cost minimization (TFCM)

The fuel cost function (\$/h) is a fundamental component of OPF analysis. It represents a primary economic objective, aiming to minimize the cost of power generation. The cost typically exhibits an approximate quadratic relationship with the power generated (MW) (Yuryevich and Wong, 1999). The overall fuel cost function can be expressed mathematically, as shown in Equation (3.12):

$$Z_{FCM}(x,u) = \left(\sum_{i=1}^{NG} a_i + b_i P_{G_i} + c_i P_{G_i}^2\right) \quad (\$/h)$$
(3.12)

Here the $Z_{FCM}(x,u)$ is the overall fuel cost function expressed in h and the fuel cost coefficients of i^{th} generator are a_i , b_i and c_i with P_{G_i} being the active power output of i^{th} generator. The objective is to minimize the total fuel cost function.

a) Fuel cost considering valve-point effect

In practical power systems, the presence of multiple steam turbine valves alters the fuel cost characteristics of generator units, making them non-convex and non-smooth due to ripples introduced in the curve (Walters and Sheble, 1993). This phenomenon, known as the valve-point loading (VPL) effect, adds complexity to the cost function. The modified cost function for the i^{th} generator, incorporating sine components to represent the VPL effect, is expressed in Equation (3.13).

$$Z_{VPL}(x,u) = \left(\sum_{i=1}^{NG} a_i + b_i P_{G_i} + c_i P_{G_i}^2\right) + \left| d_i \sin\left(e_i (P_{G_i}^{\min} - P_{G_i})\right) \right|$$
(3.13)

Here, a_i , b_i , c_i , d_i and e_i are the fuel cost coefficients of i^{th} generating unit, with d_i and e_i particularly representing VPL effect. Additionally, $P_{G_i}^{min}$ represents minimum allowable active-power-generation limit of the i^{th} generator.

In the literature, units 1 and 2 are commonly selected to demonstrate the VPL effect, while the remaining units are modelled using basic quadratic fuel cost (QFC) curves without the inclusion of VPL characteristics.

b) Fuel cost considering multiple fuel sources

Practically, different fuel sources (such as oil, natural gas, etc.) could be used for thermal generators during the operation of the power system. When multiple fuel options are available, the fuel cost function of a generating unit becomes a piecewise polynomial function, with each segment representing a specific type of fuel (Abou El Ela and Abido, 2010) and can be modelled mathematically, for i^{th} generator, for fuel type k, by Equation (3.14).

$$Z_{MFS}(x,u) = \left(\sum_{i=1}^{NG} a_{ik} + b_{ik} P_{G_i} + c_{ik} P_{G_i}^2\right)$$
(3.14)

3.3.2 Voltage deviation minimization (VDM) considering quadratic fuel cost (QFC)

The second most essential objective function of OPF is to minimize load bus voltage deviation (VD) from 1.0 p.u., taken as the reference value. In most cases, the fuel cost function is combined with the voltage profile enhancement to form a combined objective function as given in Equation (3.15).

$$Z_{VDM}(x,u) = \left(\sum_{i=1}^{NG} a_i + b_i P_{G_i} + c_i P_{G_i}^2\right) + K_{vd} \sum_{i=1}^{NPQ} \left| V_{L_i} - 1.0 \right|$$
(3.15)

where, K_{vd} (weighting factor) is assigned an appropriate value depending on the significance of voltage profile objective.

3.3.3 Voltage security index (VSI)

VSI functions as a performance metric to assess a power system's capability to sustain voltage levels within a specified acceptable range, thus reflecting the system's stability and security. VSI is calculated using the formula provided in Equation (3.16):

$$VSI = \sum_{i=1}^{n} \left(\frac{|V_i| - V_{avg}}{dV} \right)^{2n}$$
(3.16)

where, V_{avg} is the average of the maximum and minimum voltages, dV is half the voltage range, and n is set to 1. Minimizing VSI suggests that voltages across the system are closer to the average value, indicating reduced fluctuations and improved stability.

3.3.4 Voltage Stability Improvement (VSI)/voltage stability enhancement (VSE) considering QFC

The stability of an electrical power system network refers to its capacity to keep all bus voltages within acceptable limits under normal conditions and during disturbances. Voltage instability is more likely in systems with high load demands and extensive transmission networks. Improving voltage stability involves reducing the voltage stability index (L-index) across all buses. The L-index, ranging from 0 to 1, is a reliable measure of stability, where 0 represents no load and 1 signifies voltage collapse (Kessel and Glavitsch, 1986). Mathematically, the objective of VSI, *i.e.*, L-index minimization, can be defined using the two-fold objective combining fuel cost with voltage stability as follows in Equation (3.17):

$$Z_{VSI}(x,u) = \left(\sum_{i=1}^{NG} a_i + b_i P_{G_i} + c_i P_{G_i}^2\right) + K_{vs}\left(\max\left(L_j\right)\right)$$
(3.17)

Here, K_{vs} is given an appropriate value according to the priority of the voltage stability objective. The L-index for any j^{th} load bus is denoted as L_j and is determined by Equation (3.18).

$$L_{j} = \left| 1 - \frac{W_{ji} \sum_{i=1}^{NG} V_{i}}{V_{j}} \right| \quad \text{where } j = 1, 2, \dots, NPQ; \quad W_{ji} = -\left[inv(Y_{jj}) \right] * \left[Y_{ji} \right]$$
 (3.18)

Here, Y_{jj} represents the sum of the admittances connected to the j^{th} load bus (self-admittance), while Y_{ji} denotes the mutual admittance of the line connecting the j^{th} and i^{th} buses.

VSE during contingency-

Ensuring voltage stability is vital for power systems, especially when sudden disruptions like line outages or generator breakdowns occur. Improving voltage stability during transmission line issues often requires modelling scenarios where the loss of one line (N-1 contingency) or multiple lines is analysed to evaluate the system's behaviour and identify critical lines. The objective of VSE under these contingency scenarios is a widely studied aspect within OPF-related research.

3.3.5 Active power loss minimization (APLM)

The objective of this OPF is to minimize the total active power losses (total transmission losses), P_{Loss} within the power system. Equation (3.19) represents the overall active power loss as the difference between total generation (P_G) and total demand (P_D).

$$P_{\text{Loss}} = \sum_{i=1}^{NB} P_{i} = \sum_{i=1}^{NB} P_{G_{i}} - \sum_{i=1}^{NB} P_{D_{i}} \qquad \text{MW}$$
(3.19)

The P_{Loss} objective function, which is a nonlinear function of bus voltages, can be expressed by Equation (3.20).

$$Z_{APLM}(x,u) = \min(P_{Loss}) = \sum_{L=1}^{NL} G_L[V_i^2 + V_j^2 - 2V_i V_j Cos \delta_{ij}] \quad MW$$
 (3.20)

Here, G_L is used to designate the conductance of line L between i^{th} and the j^{th} bus. V_i and V_j are the voltages at buses i and j respectively, while δ_{ij} signifies the voltage angle difference between the two buses.

3.3.6 Reactive power loss minimization (RPLM)

This objective focuses on minimizing the total reactive power losses (Q_{Loss}) in the system. These losses, largely due to the reactance of transmission lines, are essential for evaluating system stability and voltage regulation. Reducing Q_{Loss} is vital for the efficient operation of the power system. The calculation Q_{Loss} is given by the following Equation (3.21):

$$Z_{RPLM}(x,u) = \min (Q_{Loss}) = \sum_{l=1}^{NL} B_{L}[V_{i}^{2} + V_{j}^{2} - 2V_{i}V_{j} \sin \delta_{ij}]$$
(3.21)

here, B_L represents the susceptance, which contributes to the reactive power flow between nodes and is crucial for maintaining proper voltage levels and preventing voltage collapse.

3.3.7 Emission minimization (EM)/Emission cost minimization (ECM)

This OPF objective focuses on minimizing emissions by optimizing the system's control variables. This reduces the release of harmful gases, such as SOx and NOx, into the atmosphere. The total emission function, representing the sum of various types of emissions, is directly related to the active power generation in MW. This function is minimized to decrease overall pollution, as expressed in Equation (3.22).

$$Z_{EM}(x,u) = \sum_{i=1}^{NG} (\alpha_i + \beta_i P_{G_i} + \gamma_i P_{G_i}^2 + \omega_i \exp(\mu_i P_{G_i}) \quad \text{(ton/hr)}$$
(3.22)

Here, α_i , β_i , and γ_i represent emission coefficients, while ω_i and μ_i are associated with the exponential term, all corresponding to the same i^{th} generating unit.

Minimizing emissions may be considered alongside other objectives, such as reducing fuel costs, enhancing voltage stability, and minimizing power losses. Achieving a balanced approach to these objectives supports the development of a more sustainable and environmentally friendly power grid.

3.4 Constraints Handling

The penalty factor method addresses constrained optimization problems by converting them into unconstrained ones. This is achieved by augmenting the original objective function with penalty terms. While control variables are inherently subject to constraints, the method incorporates inequality constraints on dependent variables (e.g., slack bus active power, load bus voltages, reactive power generation, line loading) as quadratic penalties within the objective function. This integration ensures that these variables remain within their specified limits, effectively preventing infeasible solutions. The objective function from Equations (3.1) and (3.4) can thus be reformulated as shown in Equation (3.23):

$$Z_{aug} = Z_{\min}(x, u) + penalty \tag{3.23}$$

where,
$$penalty = \lambda_1 (P_{G_1} - P_{G_1}^{\text{lim}})^2 + \lambda_2 \sum_{i=1}^{NPQ} (V_{L_i} - V_{L_i}^{\text{lim}})^2 + \lambda_3 \sum_{i=1}^{NG} (Q_{G_i} - Q_{G_i}^{\text{lim}})^2 + \lambda_4 \sum_{i=1}^{NL} (S_{line_i} - S_{line_i}^{\text{lim}})^2$$

$$(3.24)$$

In Equation (3.24), λ_1 , λ_2 , λ_3 and λ_4 denote penalty factors, all assigned with the same value of 10^5 . If the limit value of dependent variable upon violation is denoted by x^{lim} then it can be conveniently expressed as in Equation (3.25):

$$x^{\text{lim}} = \begin{cases} x^{\text{max}}; (x > x^{\text{max}}) \\ x^{\text{min}}; (x < x^{\text{min}}) \end{cases}$$
(3.25)

3.5 Standard Test Systems for OPF Analysis

Standardized test systems are commonly used in OPF studies to validate and benchmark various optimization models and techniques. These test systems, ranging from simple to complex configurations, provide a controlled environment for researchers to analyze OPF solutions under realistic conditions. Below are the commonly used IEEE systems and standard test systems frequently referenced in the literature:

3.5.1 IEEE 9-bus system

The IEEE 9-bus system is one of the simplest and most commonly used test networks for educational purposes and introductory OPF and stability studies. With 3 generators, 9 buses, and 3 loads, this system offers a basic framework for performing load flow analysis and understanding fundamental OPF principles.

3.5.2 IEEE 14-bus system

The IEEE 14-bus system is a widely used benchmark for testing OPF algorithms, voltage control, and economic dispatch strategies. It consists of 5 generator buses, 14 buses in total, 11 loads, and 20 transmission lines, with a real power demand of 259 MW. The system has 13 control variables, including generator active power settings, generator voltage levels, transformer tap settings, and a shunt capacitor. Voltage magnitudes are maintained between 0.94 and 1.06 p.u., making it suitable for studies on OPF, voltage stability, and realistic power flow analysis.

3.5.3 IEEE 26-bus system

The IEEE 26-bus system offers a mid-sized configuration that provides additional complexity while remaining manageable. With a combination of generators and loads distributed across 26 buses, this system is often utilized for stability, reliability, and control strategy assessments on a scale between the 14-bus and 30-bus systems.

3.5.4 IEEE 30-bus system

The IEEE 30-bus system is a moderately complex network with 6 generators, 30 buses, and 21 loads, featuring both radial and mesh configurations. This setup introduces challenges in OPF analysis, particularly for minimizing power losses and ensuring voltage stability. With generators at buses 1, 2, 5, 8, 11, and 13, along with shunt VAR compensation at nine buses and transformers on lines 11, 12, 15, and 36, this system is ideal for research on power loss optimization, voltage stability, and cost minimization, serving as a standard benchmark for testing OPF algorithms.

3.5.5 IEEE 57-bus system

For more comprehensive testing, the IEEE 57-bus system provides larger and more complex network models. The IEEE 57-bus system features 7 generators, 57 buses, and 42 loads, simulating a real-world grid structure with varied load profiles and multiple voltage levels. This network includes a total load demand of 1250.8 MW and 336.4 MVAR, distributed across 80 transmission lines, 15 branches with load tap-setting transformers, and shunt reactive power sources at buses 18, 25, and 53. Voltage limits for generator buses range from 0.9 to 1.1 p.u., while load bus voltages are maintained between 0.94 and 1.06 p.u. This configuration is widely used in OPF studies to test the efficiency of optimization algorithms in minimizing quadratic cost functions, enhancing voltage stability, and managing reactive power, making it an ideal representation of realistic power system operations.

3.5.6 IEEE 118-bus system

The IEEE 118-bus system is a widely utilized benchmark for detailed OPF and stability studies. It includes 54 generators, 118 buses, 64 loads, 186 transmission lines, 14 shunt VAR compensators, and 9 branches with load tap-setting transformers, forming a highly interconnected network that closely resembles a real-world power grid with diverse operational constraints. This complex configuration, with active and reactive power demands of approximately 4242 MW and 1439 MVAR, respectively, makes the 118-bus system particularly suitable for testing advanced OPF algorithms, multi-objective optimization, and real-time simulation scenarios. It is also valuable in research focused on renewable energy integration, distributed generation, and evaluating the robustness of optimization techniques in complex power system environments.

3.5.7 IEEE 300-bus system

The IEEE 300-bus system is one of the most extensive and complex test networks available, featuring 69 generators, 300 buses, and 411 transmission lines. This system closely mirrors a regional power grid in both size and complexity, with an apparent power demand of 23,525.85 MVA and a reactive power requirement of 7780 MVAR. It includes 259 control variables, such

as generator real power outputs, voltage magnitudes, transformer tap settings, and 14 shunt SVC devices for reactive power management. Voltage magnitudes for PV buses and transformer tap settings are maintained between 0.9 and 1.1 p.u. With an initial total power loss of 408.317 MW, this system is well-suited for rigorous OPF and stability studies, large-scale contingency analysis, and evaluating high-efficiency optimization methods. Due to its complexity, the 300-bus system is commonly utilized in high-performance computing environments to test advanced algorithms and simulate realistic power grid operations.

3.5.8 Indian 75-bus system

The Indian 75-bus system consists of 1 slack bus, 14 generator buses, 60 load buses, and 114 transmission lines. It is a high-stress network model derived from the Uttar Pradesh State Electricity Board's (UPSEB) grid, operating at 400 kV and 220 kV levels. This system is often used for contingency screening and ranking, especially focusing on voltage and line flow security. Various contingency cases, including single line outages, are evaluated under different load conditions, making it suitable for studies on integrated security assessment, voltage stability, and line overload risk.

3.5.9 Algerian 59-bus system

The Algerian 59-bus system includes a network configuration comprising 59 buses, 10 generators, 36 loads with a total demand of 684.10 MW, and 83 branches. In this configuration, generator 5 at bus 13 is not operational. This system is often utilized to examine various OPF scenarios, including generation fuel cost minimization, voltage profile improvement, voltage stability enhancement, and emission reduction, as explored through different case studies.

3.6 Other test systems in OPF literature

3.6.1 Large-Scale Systems

Networks like the 2736-bus and 4000-bus systems are used for high-capacity studies and for testing scalability in OPF solutions, particularly in large regional or national grids.

3.6.2 Regional and Custom Configurations

Regional models, such as the European Transmission Network or custom configurations based on specific countries, like Indian and Algerian grids, provide realistic conditions that reflect unique power flow patterns, load demands, and stability challenges in specific areas.

3.6.3 Specialized Test Networks

Custom test systems are also created to study specific aspects of OPF, such as renewable energy integration, microgrid behaviour, and distributed energy resources (DERs).

3.7 Conclusion

Chapter 3 provides a foundational understanding of OPF, covering its core structure, constraints, and various objective functions that address economic, technical, and environmental considerations in power systems. Both single-objective and multi-objective OPF formulations were discussed, highlighting how these approaches balance operational goals like fuel cost minimization, voltage stability, and power loss reduction. Additionally, standard IEEE and international test systems were introduced, from the simpler IEEE 9-bus and 14-bus systems to complex networks like the 118-bus and 300-bus systems. These systems serve as benchmarks in OPF research, facilitating the evaluation of optimization algorithms under realistic conditions.

The inclusion of regional systems, such as the Indian 75-bus and Algerian 59-bus networks, along with large-scale configurations like the 2736-bus system and custom setups, highlights the need for adaptability in OPF studies to address varying grid structures and operational challenges. These diverse test systems facilitate comprehensive evaluations of OPF algorithms across a wide range of network complexities.

Subsequent chapters will dive deeper into the formulation and application of advanced algorithms for addressing OPF challenges. These sections will examine how such algorithms are designed to achieve diverse objectives, including cost minimization, loss minimization, emission reduction, and system stability enhancement, showcasing improvements achieved in both single and multi-objective scenarios.

CHAPTER 4

LEARNING-BASED SINE-COSINE ALGORITHM (L-SCA) FOR OPF SOLUTIONS

4.1 Motivation for developing L-SCA

The Sine-Cosine Algorithm (SCA) is a widely used optimization method known for its balance between exploration and exploitation in search spaces. Developed by Mirjalili (2016), SCA utilizes trigonometric sine and cosine functions to guide candidate solutions toward optimal solutions, making it efficient for a range of continuous parameter optimization tasks. This SCA optimizer has demonstrated success in a variety of optimization tasks; however, it also has certain limitations, such as slow convergence and restricted local search capabilities, which can impact solution quality in complex problems.

To address these issues, researchers have developed several modified and hybrid variants of SCA, aiming to enhance its performance in real-world applications. Notable adaptations include the Interactive SCA (ISCA) by Mahdad and Srairi (2018), an Improved SCA using Levy Flight by Li et al. (2017), and Enhanced SCA (ESCA) by Raut and Mishra (2021) for optimized network planning, as well as multi-objective versions like the Pareto-based SCA for distributed generation allocation. Despite these advancements, SCA still faces challenges in terms of convergence speed and solution diversity, especially when applied to multi-objective, constrained optimization problems like OPF.

4.2 Introduction to the Proposed Algorithm

4.2.1 Overview of SCA

SCA, a popular swarm intelligence algorithm introduced by Mirjalili in 2016, utilized for optimizing solutions in a wide range of fields and real-world applications. SCA uses sine & cosine functions to generate interdependent candidate solutions and update their positions towards the optimal solution based on trigonometric equations as given in literature by Mirjalili (2016). It offers easy implementation, fast convergence, and efficient execution time. The algorithm balances exploratory & exploitative search patterns to locate the best regions and converge to the global optimum. Position updates are regulated by four parameters, transitioning from a fast random search in the exploration phase to a slow directed search in the exploitation phase. The position of the solutions is updated using following mathematical equations for both phases:

$$x_i^{t+1} = x_i^t + R_1 \times \sin(R_2) \times \left| R_3 P_{best}^{t} - x_i^t \right| \tag{4.1}$$

$$x_i^{t+1} = x_i^t + R_1 \times \cos(R_2) \times \left| R_3 P_{best_i}^t - x_i^t \right|$$
(4.2)

The combination of Equations (4.1) and (4.2) is often represented as Equation (4.3) below:

$$x_{i}^{t+1} = \begin{cases} x_{i}^{t} + R_{1} \times \sin(R_{2}) \times \left| R_{3} P_{best_{i}}^{t} - x_{i}^{t} \right| & ; R_{4} < 0.5 \\ x_{i}^{t} + R_{1} \times \cos(R_{2}) \times \left| R_{3} P_{best_{i}}^{t} - x_{i}^{t} \right| & ; R_{4} \ge 0.5 \end{cases}$$

$$(4.3)$$

Here, R_1 , R_2 , R_3 , R_4 are the random variables, normally distributed according to a Gaussian distribution, and are incorporated to help the algorithm avoid local optima. Here, $|\cdot|$ represents the absolute value. The value of the adaptive parameter R_1 determines whether a solution moves closer to the best solution i.e., $R_1 < 1$ or farther away from it i.e., $R_1 > 1$. Equation (4.4) modifies the range of the sine and cosine functions to achieve a balance between exploitation and exploration, ensuring that the conditions outlined in Equation (4.3) are met.

$$R_1 = a - t \left(\frac{a}{t_{\text{max}}}\right) \tag{4.4}$$

The parameter R_2 dictates whether the next solution moves closer to or farther from the target solution, with a value range of 0 to 2π . Variable R_3 provides random weightage to P_{best_i} with a view to stochastically emphasize $(R_3 > 1)$ or diminish $(R_3 < 1)$ the influence of destination in determining distance. Switching between cosine and sine components of Equation (4.3) is carried out with equal probability using variable R_4 in the range (0-1) (Attia et al. 2018).

4.2.2 Proposed Learning-based SCA (L-SCA)

The SCA algorithm is a valuable optimization tool but can encounter difficulties, such as slow convergence and suboptimal outcomes, particularly with large, complex, and constrained electrical power system problems. The complex tuning parameters of SCA can lead to poor exploitation. To address these issues, a modified variant named L-SCA has been proposed, using a learning strategy inspired by the TLBO learner phase to enhance exploitative features. Furthermore, L-SCA preserves population diversity throughout the search, strengthening its exploratory features and reducing the risk of suboptimal solutions. This balanced approach between exploration and exploitation enables L-SCA to effectively tackle real-world problems, adding an additional phase to address the classical SCA algorithm's limitations. The following mathematical equation has been utilized to modify the population during the learning phase:

$$x_{new_i} = x_{old_i} + rand \times (x_u - x_v); \qquad f(x_u) < f(x_v)$$

$$x_{new_i} = x_{old_i} + rand \times (x_v - x_u); \qquad f(x_v) < f(x_u)$$

$$(4.5)$$

In Equation (4.5), learners u and v interact at random ($u \neq v$) within a population of n, where subscript i refers to an individual in the population ranging from 1 to n, rand corresponds to a random number generated uniformly between 0 and 1. The term ($x_u - x_v$) represents a step in Equation (4.5). The neighbourhood search within the learner phase is typically represented by Equation (4.6) involving the adjustment of learner positions based on P_{best_i} and random selection of another neighbouring search agent, denoted as x_u .

$$x_{new_i} = x_{old_i} + rand \times \left(P_{best_i} - x_{old_i}\right) + rand \times \left(x_u - x_{old_i}\right)$$

$$\tag{4.6}$$

If the fitness corresponding to newly generated solution vector \mathbf{x}_{new_i} is better than that of old solution vector \mathbf{x}_{old_i} then the newly generated solution vector is accepted; otherwise, it is rejected as per Equation (4.7):

$$x_{old_i} = \begin{cases} x_{new_i}; & f\left(x_{new_i}\right) < f\left(x_{old_i}\right) \\ x_{old_i}; & otherwise \end{cases}$$
(4.7)

The proposed L-SCA approach prudently balances exploration and exploitation to effectively handle real-world problems. The flowchart of the proposed L-SCA is shown in Fig. 4.1. The concise computational steps of the proposed L-SCA algorithm for the OPF problem are presented below.

4.3 Computational Steps of the Proposed L-SCA for OPF

The concise computational steps of the proposed L-SCA algorithm for the OPF problem are presented below:

Step 1: Set the population, control variables, load flow data to their initial values. Set the terminating criterion and maximum number of iterations t_{max} .

Step 2: Set iteration count I = 0. Generate an initial population of n individuals (search agents) randomly, uniformly distributed within maximum and minimum values of the control variables. For each individual, run the NRLF (Newton Raphson load flow) program and evaluate the augmented objective function values using Equation (3.23).

- **Step 3:** Evaluate the fitness of each agent, sort the population, and identify the global best position *i.e.*, the position of the target or destination point.
- **Step 4:** Use Equations (4.3) and (4.4) to update the position of individuals in the search space. Update the population by sine function if $R_4 < 0.5$ or cosine function if $R_4 \ge 0.5$. Update and record the global best position.
- **Step 5:** Apply the learning strategy to update the position of search agents from the total population (randomly selected agents) using Equation (4.5) and calculate AOF value for all the search agents using Equation (3.23).
- **Step 6:** Conduct a neighbourhood search using Equation (4.6). If the search agent improves with Equation (4.7), update it. Otherwise, maintain the previous solution to preserve the excellent local search features of the algorithm.
- **Step 7:** If $I < t_{max}$, increase *iteration* count by 1 *i.e.*, I = I + 1, and go to Step 3. Otherwise, proceed to Step 8.
- **Step 8:** Terminate the procedure once the pre-set termination criteria are met. Report the best solution as the final destination point P_{best} .

The flowchart of the proposed L-SCA is shown in Fig. 4.1.

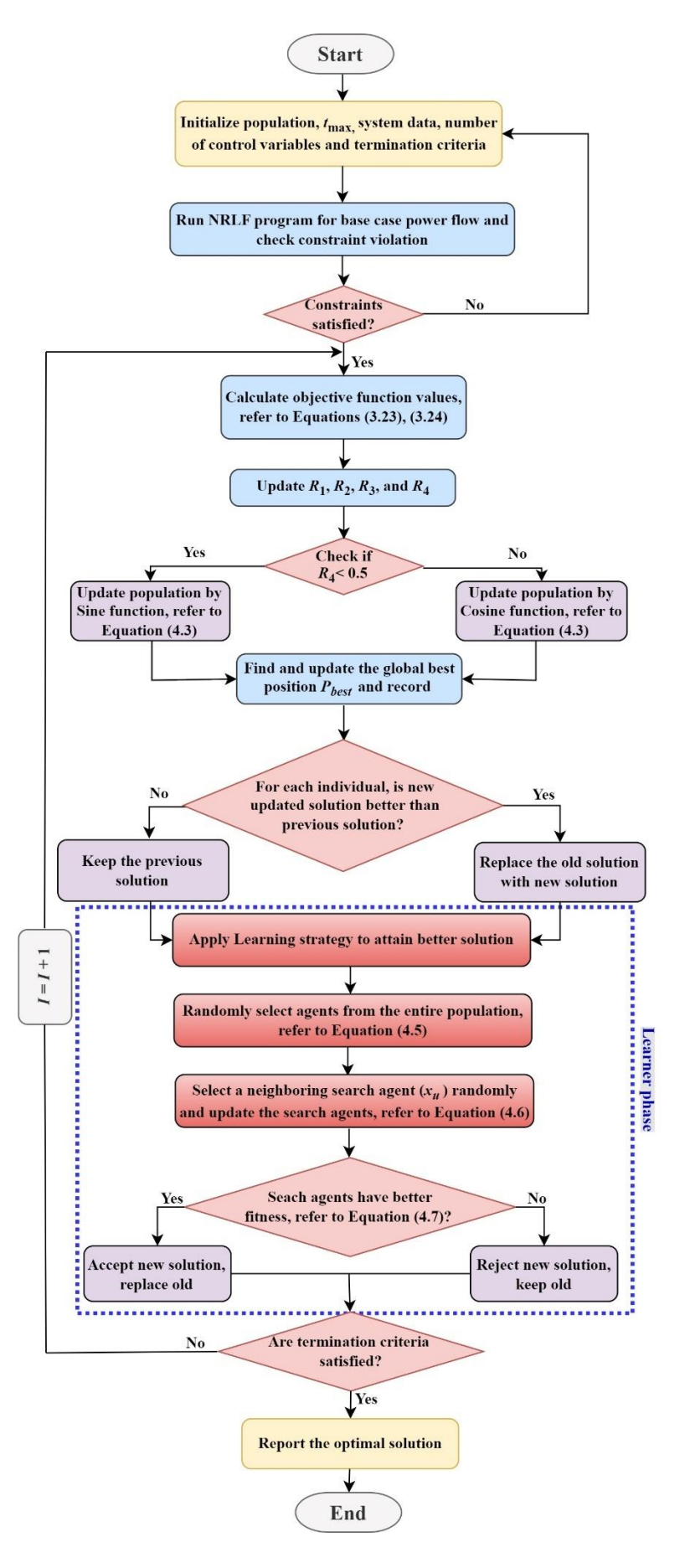


Fig. 4.1 Flowchart of the proposed L-SCA to solve OPF problem

4.4 Case Studies using the Proposed L-SCA for OPF

The effectiveness of the proposed L-SCA algorithm was evaluated through various case studies on practical power systems, addressing challenging and constrained OPF problems. The algorithm was tested and validated on three power system networks: two medium-sized systems (IEEE 57-bus and Algerian 59-bus) and one large-scale system (IEEE 118-bus). A total of 12 different case studies were analyzed, encompassing both single and multiple objectives. Table 4.1 provides a summary of these case studies, highlighting the key objective functions addressed by the proposed L-SCA across various OPF scenarios. These results demonstrate L-SCA's adaptability and effectiveness in achieving multiple OPF goals, consistently outperforming other meta-heuristic algorithms in OPF problem-solving. The simulations were conducted with a maximum iteration count of 150 and a population size of 30, using MATLAB R2018a on a laptop with a 10th Gen Intel Core i7 processor, 8 GB RAM, and a 1.7 GHz clock speed.

Table 4.1 Various cases examined in the present work using L-SCA

Case Name	Objective Function	Test System
Case-1	Total fuel cost minimization (TFCM)	IEEE 57-bus
Case-2	Voltage deviation minimization (VDM) considering QFC	
Case-3	Voltage stability improvement (VSI) considering QFC	
Case-4	Active power loss minimization (APLM)	
Case-5	Total fuel cost minimization (TFCM)	Algerian 59-bus
Case-6	Voltage deviation minimization (VDM) considering QFC	
Case-7	Voltage stability improvement (VSI)	
Case-8	Active power loss minimization (APLM)	
Case-9	Emission minimization (EM)	
Case-10	Total fuel cost minimization (TFCM)	IEEE 118-bus
Case-11	Voltage deviation minimization (VDM)	
Case-12	Active power loss minimization (APLM)	

Figure 4.2 illustrates the graphical framework depicting the implementation of the proposed OPF scheme within the context of the current study.

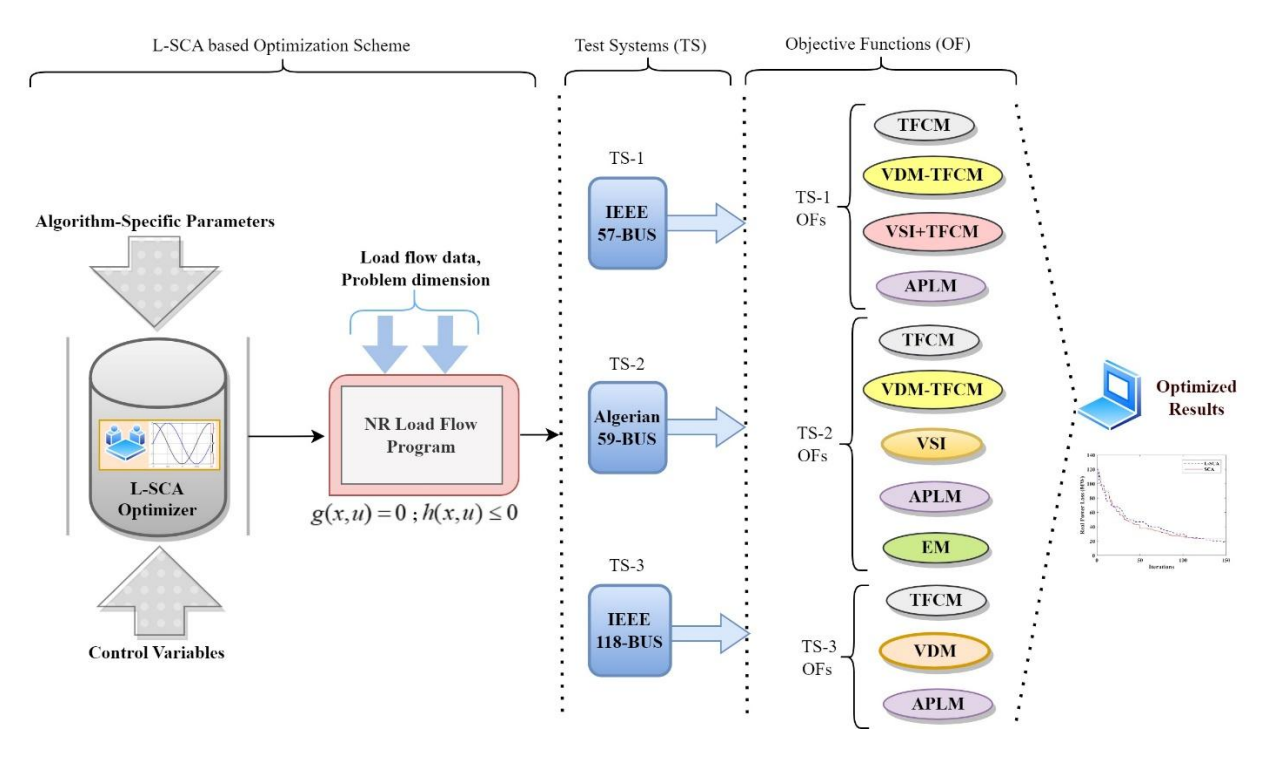


Fig. 4.2 Graphical framework for L-SCA based OPF implementation

4.5 Simulation Results and Analysis

4.5.1 Results for IEEE 57-Bus System

The proposed algorithm was initially tested on the IEEE 57-bus system to evaluate its effectiveness and scalability in addressing both individual and combined OPF cases, covering a total of 4 cases. Detailed system parameters, including upper and lower bounds on control variables, are provided in Zimmerman and Murillo-Sánchez, Matpower 6.0 User's Manual (2016). The network comprises 7 generators (with bus 1 as the swing bus), 80 transmission lines, 17 regulating transformers, and 3 shunt VAR compensators. For the network, $V_{L_i}^{\rm min}$ and $V_{L_i}^{\rm max}$ are 0.94 p.u. and 1.06 p.u., respectively, and $V_{G_i}^{\rm min}$ and $V_{G_i}^{\rm max}$ are restricted within the limits of 0.9 and 1.1 p.u., respectively. On a 100 MVA base, the system's active and reactive power demands have been calculated as 1250.8 MW and 336.4 MVAR, respectively. The algorithm was evaluated by performing 20 independent trials on this test network, and the optimal results for various objective function cases are presented below.

Case-1: OPF for TFCM

The primary objective of OPF is to minimize the generation system's total fuel cost i.e. $Z_{FCM}(x,u)$. The mathematical formulation for TFCM (or simply FCM) is provided by Equation (3.12) with a penalty term in Equation (3.24). Table 4.2 shows that L-SCA outperforms other algorithms yielding best results. Also, compared to SCA (41695.2842 \$/h),

fuel cost gets reduced by 0.09% (41657.6736 \$/h). Figure 4.3 illustrates that L-SCA converges quicker than the basic SCA. Table 4.3 displays the results of L-SCA, including optimal control variable limits and settings.

Table 4.2 Comparison of L-SCA with other popular algorithms reported in literature for Case 1

Algorithm	Fuel cost (\$/h)		
L-SCA	41657.6736		
SCA	41695.2842		
Rao-3 (Gupta et al. 2021c)	41,659.2621		
PSO-SSO (El Sehiemy et al. 2020)	41666.66		
IMFO (Taher et al. 2019a)	41667.1497		
MGOA (Taher et al. 2019b)	41,671.0980		
PSO (Taher et al. 2019a)	41,671.9849		
MSA (Mohamed et al. 2017)	41673.7231		
MICA-TLA (Ghasemi et al. 2014)	41675.0545		
GA (Taher et al. 2019a)	41 676.4786		
SSO (El Sehiemy et al. 2020)	41678.53		
LTLBO (Ghasemi et al. 2015)	41679.5451		
GOA (Saremi et al. 2017)	41,679.6792		
MFO (Taher et al. 2019a)	41679.3749		
MO-DEA (Shaheen et al. 2016)	41683.0000		
DSA (Abaci and Yamacli, 2016)	41686.82		
ABC (Adaryani and Karami, 2013)	41693.9589		
TLBO (Ghasemi et al. 2015)	41695.6626		
GSA (Duman et al. 2012)	41695.8717		
Base case	51345.570		

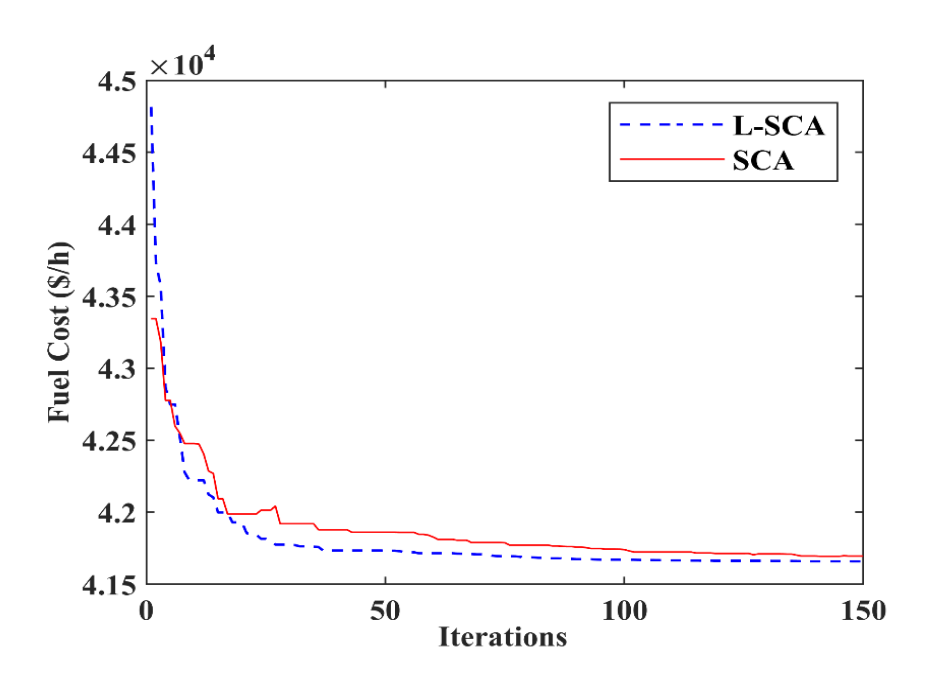


Fig. 4.3. Fuel cost convergence characteristics for Case 1

 Table 4.3 Optimal settings of control variables

C.N.	Control	M:	М	L-SCA for OPF				
S.No.	variables (p.u.)	Min.	Max.	Case 1	Case 2	Case 3	Case 4	
1	P_{G2}	0.0	1.0	0.9005	0.9252	0.9631	0.0792	
2	P_{G3}	0.0	1.4	0.4524	0.4608	0.438	1.3956	
3	P_{G6}	0.0	1.0	0.7064	0.7763	0.7151	0.9999	
4	P_{G8}	0.0	5.5	4.617	4.5429	4.5937	3.0873	
5	P_{G9}	0.0	1.0	0.9472	0.9919	0.9407	0.9999	
6	P_{G12}	0.0	410	3.5956	3.5627	3.5813	4.0999	
7	V_{G1}	0.95	1.10	1.0708	1.0213	1.07	1.0681	
8	V_{G2}	0.95	1.10	1.0733	1.0247	1.0716	1.0673	
9	$V_{\rm G3}$	0.95	1.10	1.0604	1.0133	1.0596	1.065	
10	V_{G6}	0.95	1.10	1.063	1.0175	1.0582	1.061	
11	V_{G8}	0.95	1.10	1.0747	1.037	1.0735	1.0695	
12	V_{G9}	0.95	1.10	1.0705	1.0271	1.0663	1.0609	
13	V_{G12}	0.95	1.10	1.0587	1.0009	1.0577	1.0544	
14	T ₄₋₁₈	0.9	1.10	1.0833	1.0974	1.0994	0.9718	
15	T ₄₋₁₈	0.9	1.10	0.9454	0.9	1.0946	0.9958	
16	T ₂₁₋₂₀	0.9	1.10	1.0269	0.9868	1.0894	1.0253	
17	T ₂₄₋₂₅	0.9	1.10	0.9562	1.096	1.1	1.0955	
18	T ₂₄₋₂₅	0.9	1.10	1.0894	1.0173	1.0996	0.9354	
19	T ₂₄₋₂₆	0.9	1.10	1.0224	1.0033	1.0242	1.0101	
20	T ₇₋₂₉	0.9	1.10	0.9974	1.0161	1.0034	0.9963	
21	T ₃₄₋₃₂	0.9	1.10	0.9619	0.9193	0.9423	0.9607	
22	T ₁₁₋₄₁	0.9	1.10	0.9051	0.9012	0.9075	0.9156	
23	T ₁₅₋₄₅	0.9	1.10	0.9872	0.9419	0.9916	0.988	
24	T ₁₄₋₄₆	0.9	1.10	0.9708	0.9647	0.9732	0.9726	
25	T ₁₀₋₅₁	0.9	1.10	0.992	0.9855	0.9942	0.9825	
26	T ₁₃₋₄₉	0.9	1.10	0.9528	0.9006	0.9448	0.9442	
27	T_{11-43}	0.9	1.10	1.0148	0.9646	0.9827	0.9872	
28	T_{40-56}	0.9	1.10	0.9741	1.0103	1.0992	1.0014	
29	T_{39-57}	0.9	1.10	0.9957	0.9001	0.9701	0.9636	
30	T ₉₋₅₅	0.9	1.10	1.0067	1.024	1.0114	0.9998	
31	$Q_{\rm sh18}$	0.0	20.0	0.1002	0.0627	0.2212	0.0437	
32	Q_{sh25}	0.0	20.0	0.1389	0.1941	0.2547	0.1579	
33	$Q_{\mathrm{sh}53}$	0.0	20.0	0.1109	0.2638	0.12	0.1421	
Fuel cost (\$/h)			41657.6736	41735.3577	41670.2097	44908.9339		
	VDM (p.u.	.)		1.6450	0.5953	1.8902	1.7425	
VSI (L-index)				0.2388	0.241	0.2182	0.2333	
APLM (MW)				14.7021	16.4383	14.9989	9.7299	
Time (sec)				104.2312	107.9262	103.2718	102.3134	

Case-2: OPF for VDM considering QFC

This case focuses on minimizing the deviation of load-bus voltage from 1.0 p.u. and minimizing QFC simultaneously. Equation (3.15) and the penalty term from Equation (3.24)

form the combined bi-objective function with value of K_{vd} chosen as 100. Table 4.3 presents the OPF results and optimal control variable settings. The results of Case 2 demonstrate an improved voltage profile of 0.5953 p.u., a 63.8% improvement over Case 1's voltage deviation of 1.6450 p.u. However, this improvement in voltage stability is accompanied by a slight increase in fuel cost, rising from 41657.6736 \$/h in Case 1 to 41735.3577 \$/h in Case 2.

Table 4.4 provides a comparison of L-SCA results with those obtained from other popular optimization methods in the literature. Additionally, Fig. 4.4 illustrates that the voltage profiles achieved using the proposed L-SCA are closer to unity compared to those from the basic SCA and the base case.

Table 4.4 Comparison of L-SCA with other popular algorithms reported in literature for Case 2

Algorithm	Fuel Cost (\$/h)	VDM (p.u.)		
L-SCA	41735.3577	0.5953		
SCA	41731.8261	0.6896		
Rao-3 (Gupta et al. 2021c)	42,043.2728	0.5725		
MGOA (Taher et al. 2019b)	41,697.9735	0.7381		
GOA (Saremi et al. 2017)	41,715.1396	0.8260		
GA (Taher et al. 2019a)	41,700.4162	0.80517		
PSO (Taher et al. 2019a)	41 684.4009	0.76240		
TLBO (Taher et al. 2019a)	41 694.7778	0.7120		
DSA (Abaci and Yamacli 2016)	41,699.4	0.762		
MSA (Mohamed et al. 2017)	41,714.9851	0.67818		
IMFO (Taher et al. 2019a)	41,692.7178	0.71824		
MFO (Taher et al. 2019a)	41 719.8471	0.75514		
SSO (El Sehiemy et al. 2020)	41705.87	0.6856		
PSO-SSO (El Sehiemy et al. 2020)	41713.72	0.6817		
MICA-TLA (Ghasemi et al. 2014)	41,959.1774	0.539		
Base case	51345.570	1.235		

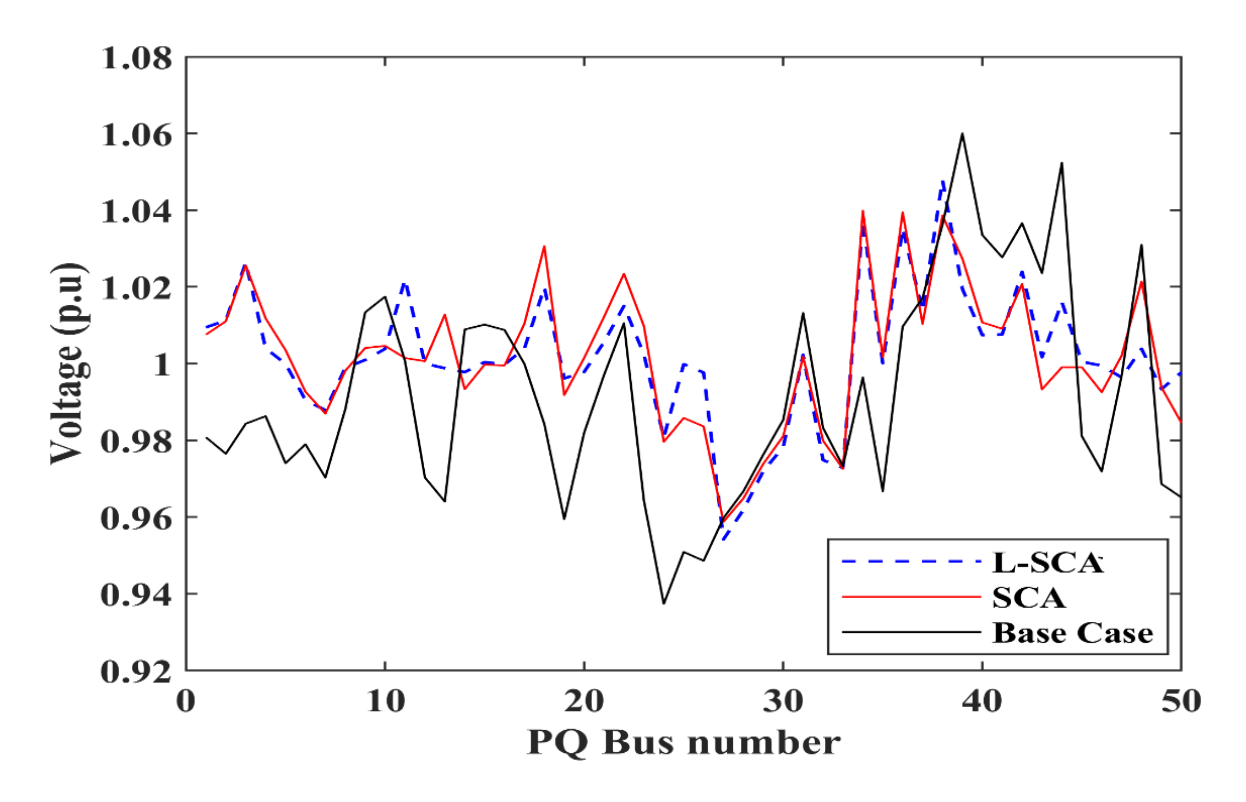


Fig. 4.4. Load bus voltage profile for Case 2

Case-3: OPF for VSI considering QFC

Improving voltage stability requires minimizing the L-index, which ranges from 0 to 1. The aim of this case is to obtain OPF solutions by minimizing both QFC and L-index. The combined objective function is expressed by combining Equations (3.17) and (3.24), with a weight factor K_{vs} assigned a value of 6000 for OPF calculations. The resulting L-index of 0.21820 p.u. represents an improvement over the 0.2388 p.u. achieved in Case 1, though it comes with a slight increase in fuel cost, rising from 41657.6736 \$/h in Case 1 to 41670.2097 \$/h in Case 3. As shown in Table 4.5, L-SCA outperforms other recently published optimization algorithms in achieving these OPF objectives.

Table 4.5 Comparison of L-SCA with other popular algorithms reported in literature for Case 3

Algorithm	Fuel Cost (\$/h)	L-Index
L-SCA	41670.2097	0.2182
SCA	41696.2959	0.224
Rao-3 (Gupta et al. 2021c)	41,692.6149	0.2186
MGOA (Taher et al. 2019b)	41,682.4031	0.2297
IMFO (Taher et al. 2019a)	41 673.6204	0.23525
DSA (Abaci and Yamacli 2016)	41,761.22	0.2383
MFO (Taher et al. 2019a)	41 688.6522	0.2395
GOA (Saremi et al. 2017)	41,698.1175	0.2395
GA (Taher et al. 2019a)	41 670.0872	0.2413

PSO (Taher et al. 2019a)	41 670.1755	0.2420
TLBO (Taher et al. 2019a)	41,685.353	0.24787
SKH (Pulluri et al. 2018)	43,937.1058	0.2721
MSA (Mohamed et al. 2017)	41,675.9948	0.27481
Modified DE (Mohamed et al. 2017)	41689.5878	0.27677
MPSO (Mohamed et al. 2017)	41694.1407	0.27918
Base case	51345.570	0.2953

Case-4: OPF for APLM

The objective function for this case is $Z_{APLM}(x,u)$ described in Equation (3.20) added with penalty term described by Equation (3.24). L-SCA reduces active power losses by 33.8% from 14.7021 MW (Case 1) to 9.7299 MW.

Table 4.3 presents the L-SCA results along with the optimal control variables, while Table 4.6 highlights the superior performance of L-SCA compared to other recent techniques. Figure 4.5 illustrates the smooth convergence of real power loss (showing a steady decline) for Case 4 using L-SCA, demonstrating an improvement over the SCA method.

Table 4.6 Comparison of L-SCA with other popular algorithms reported in literature for Case 4

Algorithm	Power Loss (MW)
L-SCA	9.7299
SCA	10.9059
Rao-3 (Gupta et al. 2021c)	9.7590
SKH (Pulluri et al. 2018)	10.6877
Chaotic KHA (Prasad et al. 2017)	11.1224
HPSO-DE (Naderi et al. 2021)	11.9788
FAHSPSO-DE (Naderi et al. 2021)	11.7328
MOMICA (Naderi et al. 2021)	11.8826
PSO (Naderi et al. 2021)	12.7819
NKEA (Naderi et al. 2021)	12.5053
MSO (Kotb and El-Fergany 2020)	12.7435
MNSGA-II (Naderi et al. 2021)	12.8657
Base case	28.365

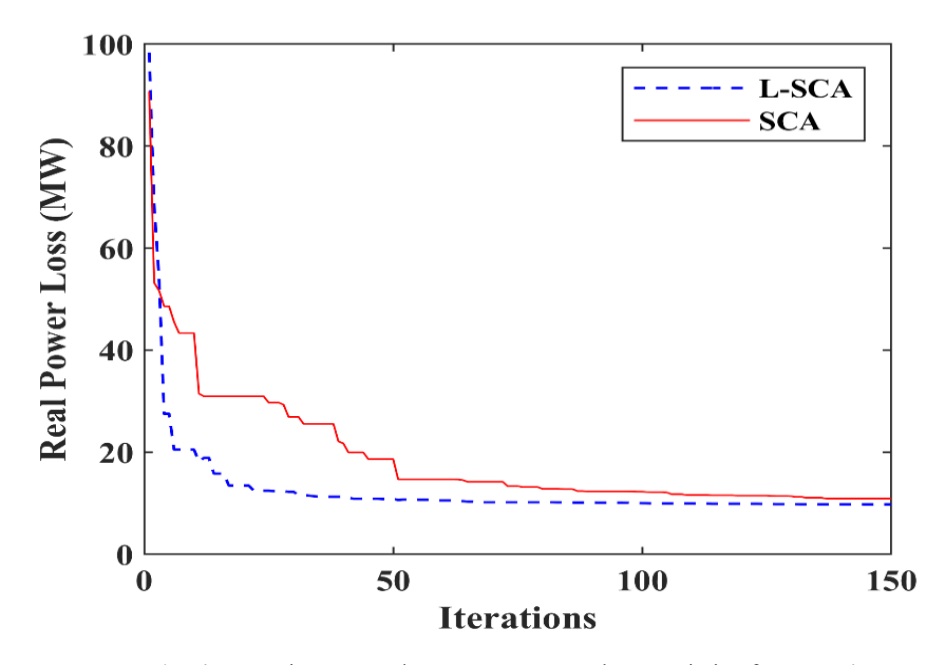


Fig. 4.5 Active power loss convergence characteristics for Case 4

4.5.2 Results for Algerian 59-Bus System

The effectiveness and suitability of the proposed L-SCA approach in solving OPF problems on real-world power systems has been demonstrated on a practical Algerian 59-bus power system network. This network, consisting of 59 buses and 83 branches, has a combined output of 684.10 MW generated by 10 generators. Notably, the generator at bus 13 is currently non-operational.

The performance of the L-SCA algorithm was evaluated through 20 independent runs, with detailed system parameters and bounds on control variables provided in reference (Bouchekara et al. 2014c).

Case-5: OPF for TFCM

This case investigates the objective of minimizing generation fuel cost, usually expressed by a quadratic function. The formulation of the objective function is the same as in Case 1. The performance of the L-SCA algorithm for OPF, including the optimal control variable limits and settings, is detailed in Table 4.7.

The L-SCA approach achieved a 13.13% reduction in total fuel cost, lowering it from 1943.7011 \$/h (base case) to 1688.4653 \$/h. Additionally, it was demonstrated to be superior to other techniques, as evidenced in Table 4.8, and exhibited better convergence than the basic SCA, as shown in Figure 4.6.

 Table 4.7 Optimal settings of control variables

Control]	L-SCA for OPI	7	L-SCA for OPF						
S.N.	variables (p.u.)	Min.	Max.	Initial case	Case 5	Case 6	Case 7	Case 8	Case 9						
1	P_{G2}	0.1	0.7	0.7	0.2356	0.1848	0.1	0.7	0.74						
2	P_{G3}	0.3	5.1	0.7	1.0127	0.9524	0.3	0.5391	0.8965						
3	P_{G4}	0.2	4	1.15	1.1065	1.2341	0.2	1.4981	0.8404						
4	P_{G13}	0.15	1.5	0	0	0	0	0	0						
5	P_{G27}	0.1	1	0.4	0.2587	0.3218	0.1047	1	0.8254						
6	P_{G37}	0.1	1	0.3	0.5107	0.4709	0.3182	0.4092	0.5881						
7	P_{G41}	0.15	1.4	1.1	0.9669	0.5813	0.15	0.4764	0.7199						
8	P_{G42}	0.18	1.75	0.7	1.4081	1.7472	1.745	1.0894	0.9027						
9	P_{G53}	0.3	4.5	2	1.0323	1.228	3.5499	1.0379	0.8527						
10	V_{G1}	0.94	1.1	1.06	1.1	1.0597	1.0996	1.0894	1.0999						
11	V_{G2}	0.94	1.1	1.04	1.0877	1.0725	1.1	1.0984	1.0962						
12	V_{G3}	0.94	1.1	1.05	1.1	1.0998	1.1	1.1	1.1						
13	V_{G4}	0.94	1.1	1.0283	1.0808	1.0413	1.0949	1.1	1.0758						
14	$V_{\rm G13}$	0.94	1.1	1	1.0938	0.9754	1.1	1.1	1.091						
15	$ m V_{G27}$	0.94	1.1	1.0266	1.0803	1.0404	1.0999	1.0992	1.0757						
16	$ m V_{G37}$	0.94	1.1	1.0273	1.1	1.0297	1.1	1.1	1.1						
17	V_{G41}	0.94	1.1	1.0966	1.1	1.0082	0.9887	1.0802	1.1						
18	$ m V_{G42}$	0.94	1.1	1.034	1.1	1.0998	1.1	1.1	1.1						
19	V_{G53}	0.94	1.1	1	1.1	1.1	1.1	1.1	1.1						
	Fuel cost	t (\$/h)		1943.7011	1688.4653	1734.8135	2468.8724	1924.1695	1821.3763						
	VDM (p.u.)		1.5757	2.6206	1.8359	2.6766	3.0488	2.6966							
VSI (L-index)			VSI (L-index)		0.2175	0.219	0.2153	0.2168	0.2177						
APLM (MW)			29.1409	27.6289	26.1014	46.9346	11.8485	23.7158							
	EM (to	n/h)		0.5833	0.525	1.6563	4.3158	0.4583	0.3829						
	Time (sec)		-	92.1921	94.2281	91.0281	96.1921	90.2038						

 Table 4.8 Comparison of L-SCA with other popular algorithms reported in literature for Case 5

Algorithm	Fuel cost (\$/h)
L-SCA	1688.4653
SCA	1689.4053
SKH (Pulluri et al. 2017a)	1688.5742
ESDE-MC (Pulluri et al. 2017b)	1688.5586
SCM-MJ (Gupta et al. 2021b)	1688.5933
M-Jaya (Gupta et al. 2021b)	1689.0281
LCA (Bouchekara et al. 2014c)	1689.0768
KH (Pulluri et al. 2017a)	1690.4697
MFO (Bentouati et al. 2016)	1693.61
ABC (Bouchekara et al. 2014c)	1703.8
BHBO (Bouchekara 2014b)	1710.0859

ACO (Bouchekara et al. 2014c)	1815.7
GA (Bouchekara et al. 2014c)	1937.1
Base case	1943.7011

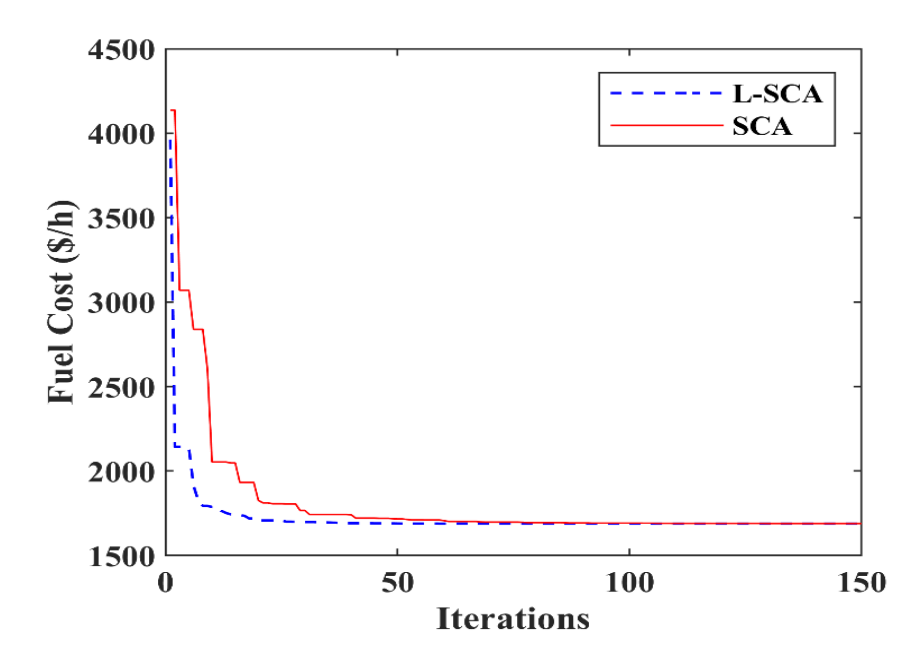


Fig. 4.6 Fuel cost convergence characteristics for Case 5

Case-6: OPF for VDM considering QFC

In Case 5, the voltage profile may not meet acceptable standards, creating a need for a solution that both reduces fuel consumption and improves the voltage profile. In Case 6, the formulation of the objective function remains consistent with Case 2, with the weighting factor set to 100. The optimal control variable settings and results are provided in Table 4.7.

The present Case 6 achieved a 29.94% improvement in the voltage profile, with only a 2.67% increase in fuel cost. Table 4.9 offers a comparison of the results obtained by the proposed L-SCA method against other well-known methods. Figure 4.7 displays the voltage profiles for Case 6, the proposed L-SCA, basic SCA, and the base case, confirming that the voltages at load buses fall within the acceptable limits.

Table 4.9 Comparison of L-SCA with other popular algorithms reported in literature for Case 6

Algorithm	Fuel Cost (\$/h)	VDM (p.u.)
L-SCA	1734.8135	1.8359
SCA	1732.9160	1.8398
MFO (Bentouati et al. 2016)	1732.852	1.435
SCM-MJ (Gupta et al. 2021b)	1718.48938	1.8815
M-Jaya (Gupta et al. 2021b)	1719.8954	1.8842

LCA (Bouchekara et al. 2014c)	1755.5775	1.8404
Base Case	1943.7011	1.5757

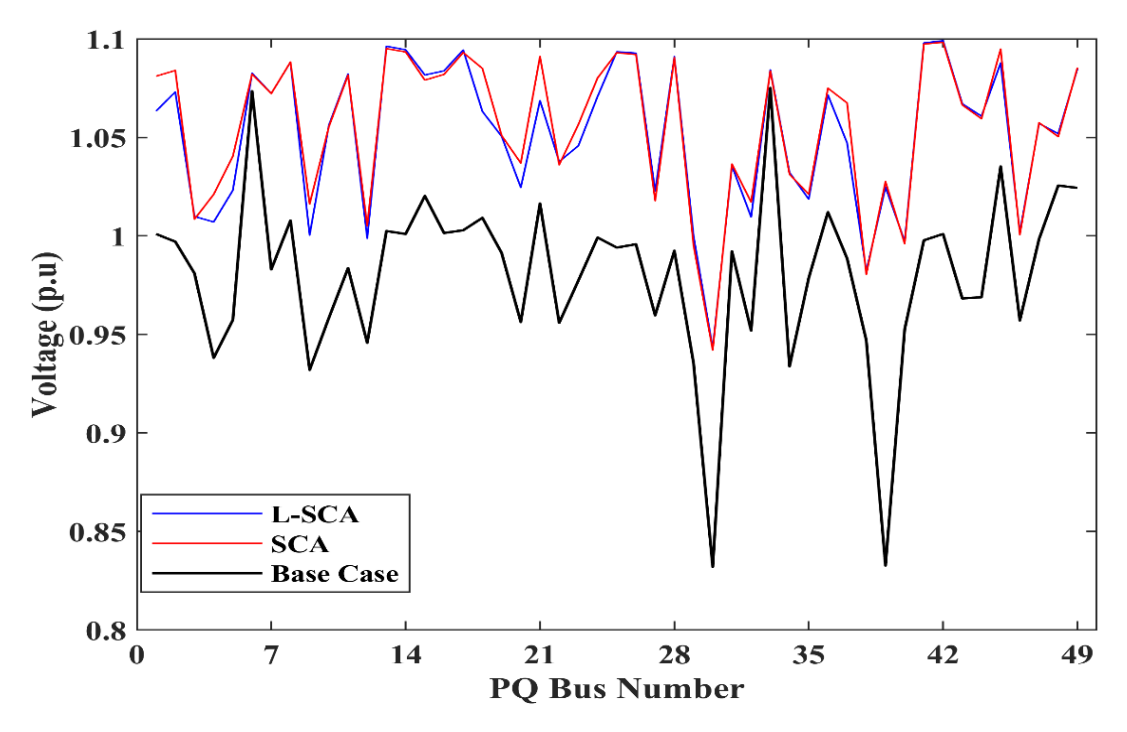


Fig. 4.7 Load bus voltage profile for Case 6

Case-7: OPF for VSI

The L-index (0 to 1) is a measure of voltage stability. It is calculated using Equation (3.18) for any j^{th} load bus (Kessel and Glavitsch, 1986). Minimizing the system voltage stability indicator, as described in Equation (4.8), can significantly improve voltage stability.

$$L = \max(L_j)$$
 where $j = 1, 2, \dots, NPQ;$ (4.8)

The proposed algorithm achieved an L-index of 0.2153 p.u. with an associated cost of 2468.8724 \$/h, marking a 22.2% reduction from the base case value of 0.2767 p.u. The proposed algorithm demonstrated superior reliability and robustness compared to other techniques, as shown in Table 4.10.

Table 4.10 Comparison of L-SCA with other popular algorithms reported in literature for Case 7

Algorithm	L-index (p.u.)
L-SCA	0.2153
SCA	0.2153
SKH (Pulluri et al. 2017a)	0.21519
LCA (Bouchekara et al. 2014c)	0.2152
ESDE-MC (Pulluri et al. 2017b)	0.21519
KH (Pulluri et al. 2017a)	0.21544
Base case	0.2767

Case-8: OPF for APLM

The proposed L-SCA method in this case is shown to be effective in reducing power losses in Algerian system. The objective function used is identical to that of Case 4. The real power loss achieved through proposed L-SCA is 11.8485 MW, lower than the SCA algorithm (12.0012 MW) and the base case (29.14 MW). Table 4.7 includes the results of the OPF for this case, along with the settings of control variables.

While the fuel cost for this case is 1924.1695 \$/h, slightly higher than in Case 5, it remains below the base case fuel cost of 1943.7011 \$/h. The proposed algorithm achieved a real power loss that is lower than those reported in previous studies by SKH (11.9833 MW) and KH (12.2491 MW) (Pulluri et al., 2017a). However, due to limited comparative studies on Algerian power systems, fully evaluating the comparative significance of these results remains challenging. Figure 4.8 illustrates the trend of reducing APLM using both the L-SCA and the conventional SCA.

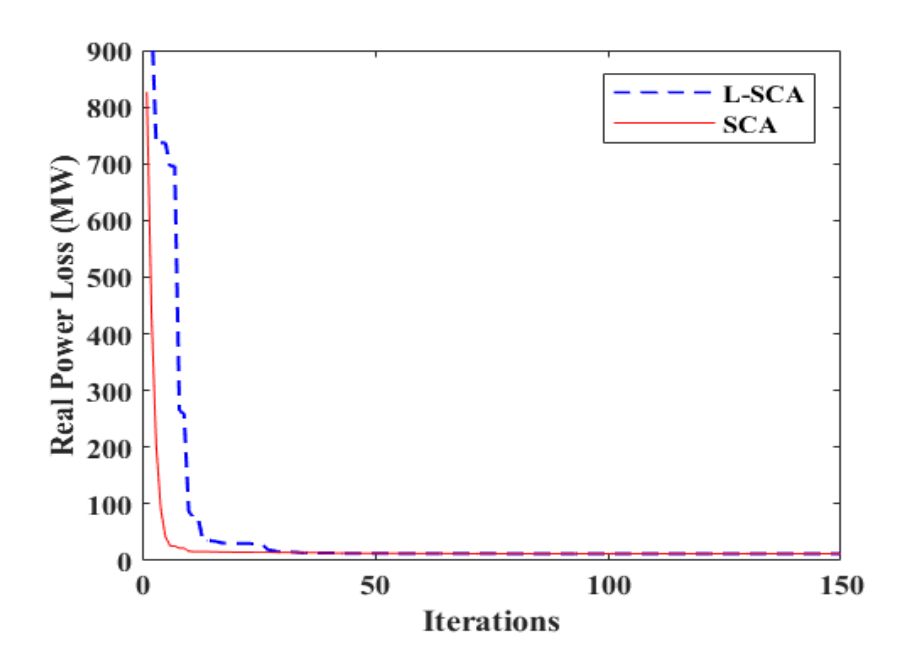


Fig. 4.8 Active power loss convergence characteristics for Case 8

Case-9: OPF for EM

Pollutants like SOx and NOx pose a threat to public health and the environment. With rising concern over environmental issues, the present case holds greater relevance. Equation (3.22) incorporates a penalty factor from Equation (3.24) to formulate the objective function in Case 9. Table 4.7 showcases the optimal control settings and results obtained using L-SCA in the present case. Figure 4.9 illustrates the convergence of emission cost between L-SCA and SCA algorithms, with the emission value dropping dramatically from 0.5833 ton/h in the initial case

to 0.3829 ton/h in Case 9, a 34.35% decrease from the initial case and a 27.07% decrease from Case 5.

However, it's important to note that while emission reduction is a primary focus, other objectives, such as the Total Fuel Cost Minimization (TFCM) objective, may experience slight declines. This trade-off between different objectives highlights the complex nature of power system optimization and the need for careful consideration of various factors.

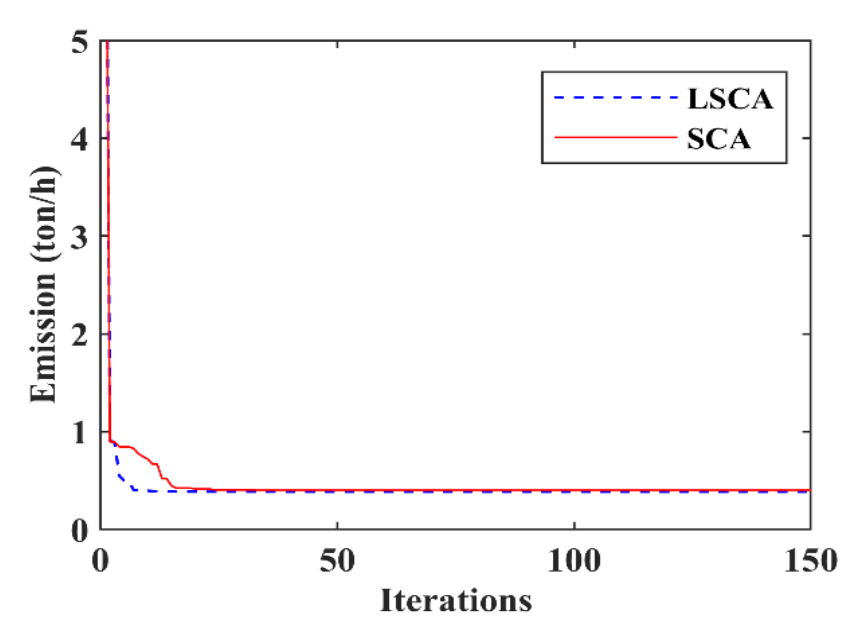


Fig. 4.9 Emission cost convergence characteristics for Case 9

Table 4.11 compares the results using the proposed L-SCA method to previously reported methods, showing its superiority. The proposed algorithm effectively reduces emissions, potentially benefiting public health and the environment in the long run.

Table 4.11 Comparison of L-SCA with other popular algorithms reported in literature for Case 9

Algorithm	Emission Cost (ton/h)
L-SCA	0.3829
SCA	0.3834
MFO (Bentouati et al. 2016)	0.3844
ESDE-MC (Pulluri et al. 2017b)	0.3846
SKH (Pulluri et al. 2017a)	0.3852
KH (Pulluri et al. 2017a)	0.3875
LCA (Bouchekara et al. 2014c)	0.3877
PGA (Mahdad et al. 2009)	0.4213
FSLP (Zehar and Sayah 2008)	0.4329
Base case	0.5833

4.5.3 IEEE 118-bus test network

The proposed L-SCA approach has been tested for scalability and effectiveness on a larger IEEE 118-bus test system. Three objective functions are considered to solve OPF problems in the IEEE 118-bus test system with both SCA and L-SCA. The IEEE 118-bus system comprises 186 transmission lines, 54 generators, 64 load buses, and one slack bus (Bus 69). Additionally, 14 buses have shunt VAR compensators, and 9 branches have tap changers. The active and reactive power demand on a 100 MVA base are 42.4200 p.u. and 14.3800 p.u., respectively. Detailed system data, including upper and lower limits on control variables and their initial values, can be found in the specified references: Zimmerman et al. (2006), Christie (1993), and PSTCA Univ of Washington (2022). To assess the performance of the L-SCA algorithm, 20 independent trials were conducted, and the best results are presented here.

Case-10: OPF for TFCM

In this case, minimizing the Total Fuel Cost (TFCM) was the primary objective for the OPF problem, similar to Cases 1 (57-bus) and 5 (Algerian 59-bus). Table 4.12 presents the OPF results, including initial values and control variables. The L-SCA algorithm achieved the lowest fuel cost of 129256.218 \$/h, outperforming other recent methods as shown in Table 4.13. Figure 4.10 illustrates the smooth convergence of fuel cost for L-SCA, demonstrating its suitability for large-scale systems. The cost coefficients for all generators can be found in Zimmerman et al. (2006).

Table 4.12 Optimal settings of control variables

S.	Control	Initial	L-S	SCA for O	PF	S.	Control	Initial	L-S	CA for OPF	7
No.	variables (p.u.)	value	Case 10	Case 11	Case 12	No.	variables (p.u.)	value	Case 10	Case 10 Case 11 Ca	Case 12
1	$P_{\rm G1}$	0	0.1043	0.577	0.8739	68	$V_{\rm G32}$	0.963	1.0306	1.0148	1.0306
2	P_{G4}	0	0.005	0.0643	0.2988	69	$V_{\rm G34}$	0.984	0.9781	0.9849	1.0296
3	P_{G6}	0	0.0774	0.8198	0.9854	70	$V_{\rm G36}$	0.98	0.9712	1.0033	1.0321
4	P_{G8}	0	0.7783	0.64	0.0097	71	V_{G40}	0.97	1.0318	1.0324	0.9974
5	P_{G10}	4.5	4.0902	0.4835	0.9255	72	V_{G42}	0.985	1.0055	0.9832	0.999
6	P_{G12}	0.85	0.7307	1.3649	1.2713	73	V_{G46}	1.005	0.9486	1.0139	1.017
7	P_{G15}	0	0.0643	0.8598	0.3272	74	V_{G49}	1.025	1.0034	1.0025	1.0032
8	P_{G18}	0	0.0511	0.2266	0.8283	75	V_{G54}	0.955	0.9675	1.017	0.994
9	P_{G19}	0	0.2218	0.667	0.9792	76	V_{G55}	0.952	0.9575	0.9732	0.9942
10	P_{G24}	0	0.1895	0.169	0.5966	77	V_{G56}	0.954	0.9533	1.0079	0.994
11	P_{G25}	2.2	1.7638	0.1555	0.2543	78	V_{G59}	0.985	0.9404	0.9982	0.971
12	P_{G26}	3.14	2.7655	2.0709	0.3178	79	V_{G61}	0.995	0.9587	1.0337	0.9861
13	P_{G27}	0	0	0.8262	0.6952	80	V_{G62}	0.998	0.972	0.9803	0.9913
14	P_{G31}	0.07	0.0801	0.9053	0.4596	81	V_{G65}	1.005	1.06	0.9423	1.0126
15	P_{G32}	0	0.4042	0.0062	0.9115	82	V_{G66}	1.05	1.0565	1.0237	1.0052

1.6	D	0	0.0505	0.5201	0.9772	83	N/	1.025	0.0441	0.0016	0.0772
16	P _{G34}			0.5381			V_{G69}	1.035	0.9441	0.9816	0.9773
17	P _{G36}	0	0.404	0.6492	0.848	84	V_{G70}	0.984	0.9557	0.9743	0.9964
18	P _{G40}	0	0.0269	0.5607	0.986	85	V_{G72}	0.98	0.9856	0.997	0.985
19	P _{G42}		0.6158	0.5057	0.814	86	V_{G73}	0.991	0.9788	1.0246	0.9996
20	P _{G46}	0.19	0.1179	0.7048	1.1549	87	V_{G74}	0.958	0.9512	1.0071	1.0102
21	P _{G49}	2.04	1.7471	2.8053	1.9784	88	V_{G76}	0.943	1.0102	1.0184	0.9902
22	P _{G54}	0.48	0.4956	1.2851	1.4322	89	V_{G77}	1.006	0.9669	0.9912	0.9854
23	P _{G55}	0	0.084	0.0011	0.9499	90	V_{G80}	1.04	0.9906	1.032	0.9945
24	P _{G56}	0	0.1862	0.1318	0.8852	91	V_{G85}	0.985	1.0216	1.0035	0.9919
25	P _{G59}	1.55	1.5056	2.2029	2.2398	92	V_{G87}	1.015	1.0324	1.0228	0.9586
26	P _{G61}	1.6	1.5311	0.303	1.1057	93	V_{G89}	1.005	0.9949	1.0091	1.004
27	P_{G62}	0	0.2966	0.7558	0.87	94	V_{G90}	0.985	0.9766	0.976	1.0209
28	P_{G65}	3.91	3.2599	4.3585	0.701	95	V_{G91}	0.98	0.9627	1.0419	1.0164
29	P_{G66}	3.92	3.357	0.686	0.6269	96	V_{G92}	0.99	0.9631	0.9976	0.9962
30	P_{G70}	0	0.0124	0.2485	0.8329	97	V_{G99}	1.01	0.9531	1.0201	0.9943
31	P_{G72}	0	0.128	0.6637	0.0039	98	V_{G100}	1.017	0.9765	1.0285	1.0065
32	P_{G73}	0	0.3177	0	0.2536	99	V_{G103}	1.01	0.9875	1.0031	1.0222
33	P_{G74}	0	0.0092	0.1828	0.8605	100	V_{G104}	0.971	1.0032	1.018	1.0107
34	P_{G76}	0	0.2613	0.6353	0.9496	101	V_{G105}	0.965	1.0182	1.0111	1.0094
35	P_{G77}	0	0.0069	0	0.8672	102	$V_{\rm G107}$	0.952	1.0465	0.9731	1.0032
36	P_{G80}	4.77	3.8098	1.6419	2.4952	103	V_{G110}	0.973	0.9879	0.9904	1.0147
37	P_{G85}	0	0.1784	0.1276	0.8557	104	V_{G111}	0.98	1.0041	0.9855	1.016
38	P_{G87}	0.04	0.029	0.2334	0.1383	105	V_{G112}	0.975	0.9997	0.9453	0.9975
39	P_{G89}	6.07	4.4034	3.1873	1.3983	106	V_{G113}	0.993	1.028	0.9961	1.0176
40	P_{G90}	0	0.0024	0.6939	0.9963	107	V_{G116}	1.005	1.059	1.0035	1.0104
41	P_{G91}	0	0.0698	0.6053	0.3801	108	T _{5—8}	0.985	0.9024	1.0305	0.961
42	P_{G92}	0	0.0234	0.1809	0.4331	109	T _{26—25}	0.96	0.921	0.9847	1.0915
43	P_{G99}	0	0.0109	0.3573	0.6814	110	T _{30—17}	0.96	0.9557	0.9785	0.9081
44	P_{G100}	2.52	2.3051	1.2205	1.4777	111	T ₃₈ —37	0.935	0.9928	0.9597	0.9413
45	P_{G103}	0.4	0.3541	0.2488	0.1257	112	T _{63—59}	0.96	1.0979	1.0132	1.0006
46	P_{G104}	0	0	0.98	0.5873	113	T _{64—61}	0.985	1.0535	0.9811	1.067
47	P_{G105}	0	0.8987	0.958	0.4629	114	T _{65—66}	0.935	0.9851	1.0243	0.9667
48	$P_{\rm G107}$	0	0.0681	0.3496	0.5067	115	T _{68—69}	0.935	0.9012	1.072	0.9833
49	P_{G110}	0	0.22	0.7612	0.698	116	T _{81—80}	0.935	1.0454	0.9447	0.9991
50	P_{G111}	0.36	0.3408	0.6481	0.0646	117	Q _{C5}	0	0.2997	0.1228	0.2284
51	P_{G112}	0	0	0.4381	0.4671	118	Qc34	0	0.0059	0.0155	0.121
52	P_{G113}	0	0.0569	1	0.4977	119	Qc37	0	0.2582	0.1093	0.176
53	P_{G116}	0	0.0493	0.7561	0.0223	120	Q _{C44}	0	0.0326	0.0535	0.2978
54	V_{G1}	0.995	1.0267	1.0234	0.9635	121	Q _{C45}	0	0.2962	0.2701	0.0979
55	V_{G4}	0.998	1.0335	1.0069	0.9953	122	Q _{C46}	0	0.2801	0.1789	0.276
56	V_{G6}	0.99	1.0447	0.9969	0.9751	123	Q _{C48}	0	0.1804	0.0117	0.1951
57	V_{G8}	1.015	0.967	0.9943	0.9609	124	Q _{C74}	0	0.2549	0.049	0.07
58	V_{G10}	1.05	0.9933	0.9495	0.9761	125	Q _{C79}	0	0.1568	0.2999	0.1323
59	V_{G12}	0.99	1.0598	1.0044	0.9813	126	Q _{C82}	0	0.2761	0.271	0.2019
60	V_{G15}	0.97	1.0402	1.0137	1.0067	127	Q _{C83}	0	0.0403	0.2438	0.2864
61	V_{G18}	0.973	0.9792	0.9487	1.0208	128	Q _{C105}	0	0.0186	0.2942	0.0043

62	V_{G19}	0.962	1.0153	1.0073	1.0138	129	Q _{C107}	0	0.159	0.2907	0.2997
63	$V_{\rm G24}$	0.992	1.0276	1.0052	1.0151	130	Q _{C110}	0	0.1756	0.1542	0.2159
64	$V_{\rm G25}$	1.05	1.06	0.9667	1.0235		el cost (\$/h)	131220 .52	129256.2180	160918.4 300	159445.5 756
65	$V_{\rm G26}$	1.015	1.0366	0.9676	0.9732	VD	M (p.u.)	1.4389	1.9412	0.5395	1.0237
66	$V_{\rm G27}$	0.968	1.0428	1.0076	1.0249		PLM MW)	132.81 01	107.4547	69.4370	17.8810
67	V_{G31}	0.967	1.0107	1.0013	1.0263	Tin	ne (sec)	-	140.0801	139.9871	142.1091

 Table 4.13 Comparison of L-SCA and other popular algorithms for Case 10

Algorithm	Fuel cost (\$/h)
L-SCA	1,29,256.218
SCA	1,29,871.988
SCM-MJ (Gupta et al. 2021b)	1,29,171.960
M-Jaya (Gupta et al. 2021b)	1,29,248.100
CS-GWO (Meng et al. 2021)	1,29,544.010
MSA (Mohamed et al. 2017)	1,29,640.719
TLBO (Bouchekara et al. 2014a)	1,29,682.844
FPA (Mohamed et al. 2017)	1,29,688.721
DSA (Bouchekara et al. 2014a)	1,29,691.615
MFO (Mohamed et al. 2017)	1,29,708.082
SKH (Pulluri et al. 2017a)	1,29,727.625
PSOGSA (Radosavljević et al. 2015)	1,29,733.580
KH (Pulluri et al. 2017a)	1,29,754.813
PSO (Bouchekara et al. 2014a)	1,29,756.228
Base Case (Radosavljević et al. 2015)	1,31,220.520

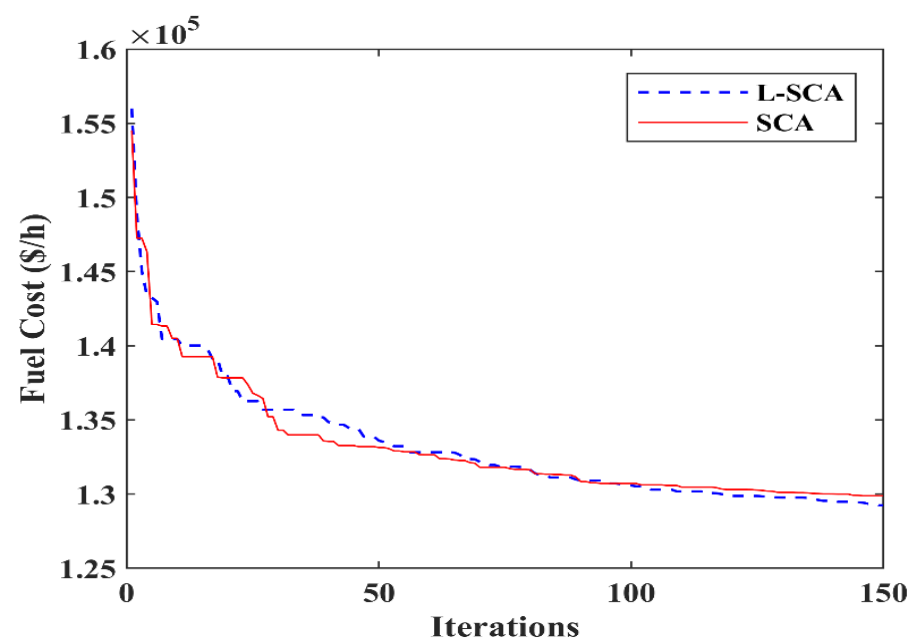


Fig. 4.10 Fuel cost convergence characteristics for Case 10

Case-11: OPF for VDM

In this scenario, the L-SCA algorithm was employed to solve the OPF problem and minimize voltage deviations at load buses to 1.0 p.u. on the 118-bus system. A penalty term was added to the objective function (Equation 3.15) to achieve this. The approach resulted in a significantly improved voltage profile of 0.5395 p.u., as shown in Table 4.14.

Comparative studies are limited, as only a few case studies on improving load bus voltage profiles in IEEE 118-bus systems exist.

Algorithm	VDM (p.u.)
L-SCA	0.5395
SCA	0.6845
M-Jaya (Gupta et al. 2021a)	0.6771
MSCA (Attia et al. 2018)	0.995
Rase Case	1 4389

Table 4.14 Comparison of L-SCA and other reported algorithms for Case 11

Figure 4.11 compares the load bus voltage profiles of the proposed L-SCA, basic SCA, and baseline case. The L-SCA-generated voltage profile ensures that all load bus voltages remain within acceptable limits.

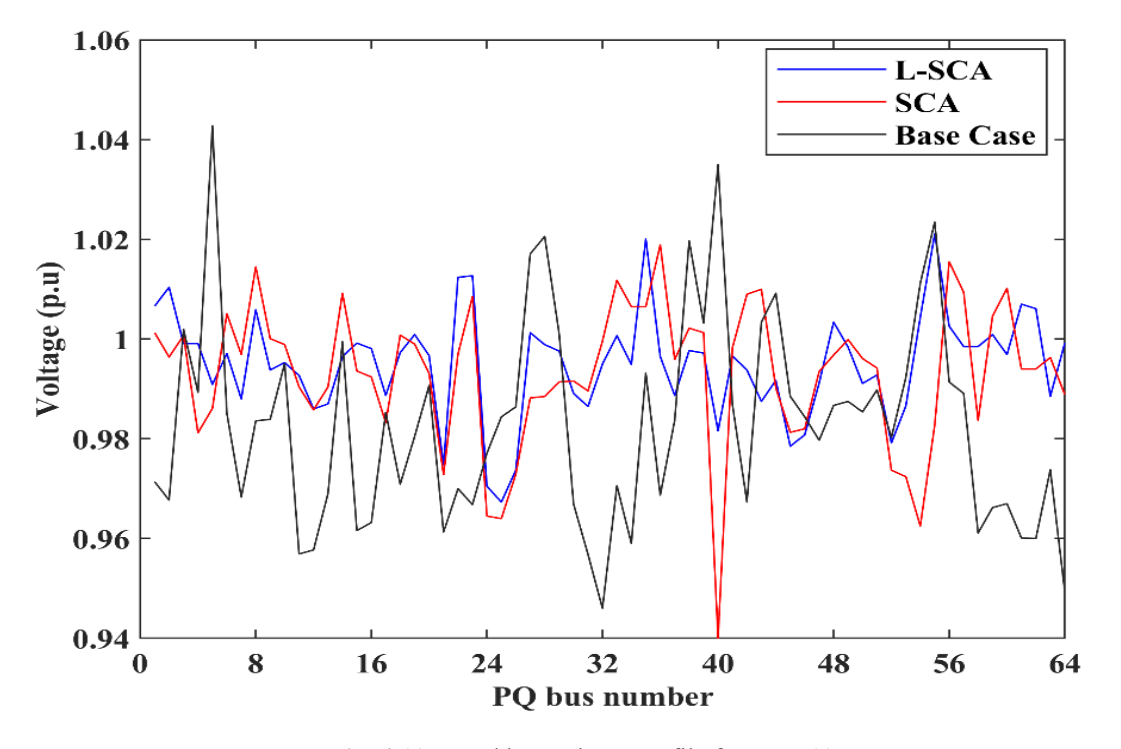


Fig. 4.11 Load bus voltage profile for Case 11

Case-12: OPF for APLM

The objective of this case study is to minimize power loss in the 118-bus network using an independent objective function, identical to that in Cases 4 and 8. The OPF results demonstrate a substantial reduction in power loss, achieving an 86.54% decrease from 132.8101 MW (base case) to 17.881 MW. Table 4.15 provides a comparison of numerical results between the proposed L-SCA and other recent methods. Additionally, power loss has decreased by 83.36% from 107.4547 MW in Case 10. The L-SCA method outperforms the conventional SCA, achieving a smoother convergence curve for power loss and more rapid attainment of the objective function value, as shown in Fig. 4.12.

Table 4.15 Comparison of L-SCA and other popular algorithms for Case 12

Algorithm	APLM (MW)			
L-SCA	17.881			
SCA	22.2156			
SCM-MJ (Gupta et al. 2021b)	19.1525			
M-Jaya (Gupta et al. 2021b)	21.6419			
SKH (Pulluri et al. 2017a)	22.1397			
GWO (Meng et al. 2021)	31.77			
TLBO (Gupta et al. 2021b)	36.8482			
ICBO (Bouchekara et al. 2016b)	62.7315			
MSCA (Attia et al. 2018)	76.22			
Base Case	132.8101			

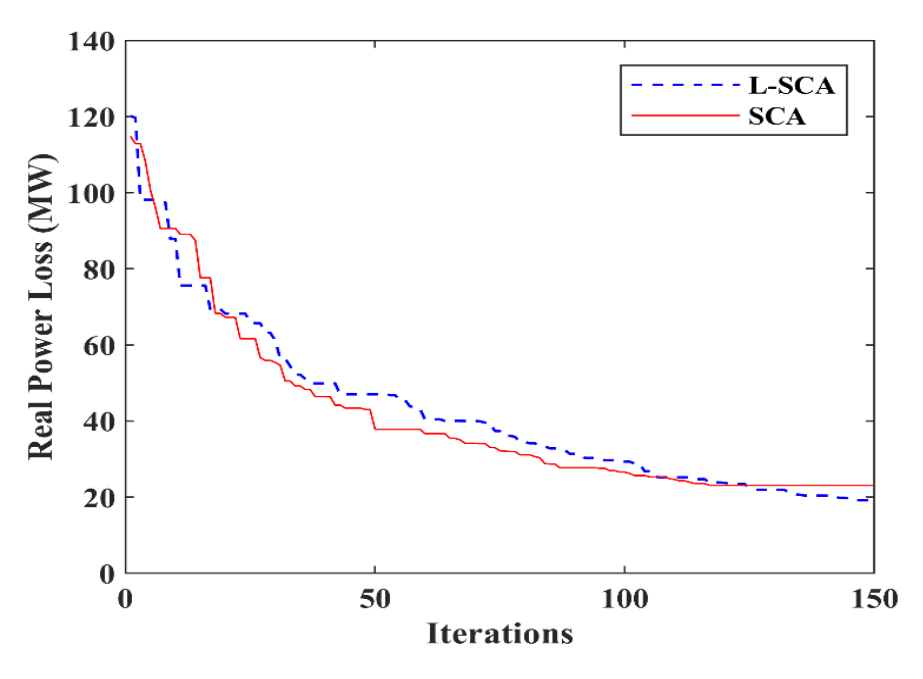


Fig. 4.12 Active power loss convergence characteristics for Case 12

4.6 Discussion of Findings/Statistical Analysis

A statistical analysis was conducted to evaluate the reliability and robustness of the proposed L-SCA technique. Table 4.16 summarizes the statistical results of both the proposed L-SCA and the original SCA for solving the OPF problem. Cases 1, 4, 5, 7, 10, and 12 were evaluated through 20 independent trials, each with identical population size and function evaluations.

The results indicate that for all considered cases (IEEE 57-bus, IEEE 118-bus, and Algerian 59-bus systems), the best, worst, and mean values across the 20 trials are quite close, as evidenced by the low standard deviation (SD) in Table 4.16. This statistical study demonstrates the robustness of the proposed technique, which consistently achieves optimal or near-optimal solutions in all trials.

This capability highlights the suitability of L-SCA for addressing both large-scale, complex optimization problems and practical power system challenges.

	1							
Algorithm	Best	Worst	Mean	SD	Best	Worst	Mean	SD
	Case 1	(Total fuel co	ost)	Case 7 (Voltage stability improvement)				
L-SCA	41657.6736	41663.1653	41659.8873	0.2863	0.2153	0.2155	0.2154	0.3245
SCA	41695.2842	41696.8058	41697.2016	0.3152	0.2154	0.2157	0.2155	0.3406
	Case 4 (Active power	loss)	Case 10 (Total fuel cost)				
L-SCA	9.7299	9.7518	9.7437	0.0368	129256.2180	129276.0972	129263.7314	0.0318
SCA	10.9059	11.5491	10.9912	0.0394	129871.9878	129911.0381	129892.0341	0.0339
	Case 5	(Total fuel co	ost)	Case 12 (Active power loss)				
L-SCA	1688.4653	1693.6109	1690.3216	0.3792	17.8810	21.0853	20.9010	0.3987
SCA	1689.4053	1695.6704	1692.1928	0.4081	22.2156	25.0912	23.3178	0.4056

Table 4.16 Statistical analysis of Cases 1, 4, 5, 7, 10 and 12 using the L-SCA and SCA algorithms

4.7 Conclusion

L-SCA has proven to be a promising solution to OPF problems, outperforming other well-known algorithms across two IEEE test systems (57-bus, 118-bus) and a real-world Algerian network (59-bus). Across these systems, L-SCA consistently achieved reductions in fuel costs, improvements in voltage profiles, enhanced voltage stability, reduced emissions, and minimized power loss through 12 cases. In some cases, bi-objective formulations were transformed into single-objective functions using the weighted sum approach.

This chapter concludes that L-SCA surpasses the original SCA and other meta-heuristic algorithms in performance, demonstrating its superiority across power system networks of varying sizes and complexities. L-SCA's improved performance is attributed to its efficient

utilization of the learner phase of the TLBO algorithm, leading to faster convergence and avoidance of local optima, as illustrated by various convergence curves.

Statistical analysis supports L-SCA's reliability and resilience, as demonstrated by its best, worst, average, and standard deviation outcomes. For instance, L-SCA yielded fuel cost values of 41657.6736 \$/h, 1688.4653 \$/h, and 129256.2180 \$/h for cases 1, 5, and 10, respectively. These values represent a respective reduction of 18.95%, 13.13%, and 1.49% of the base case, with respective standard deviations of 0.2863, 0.3792, and 0.0318.

This research has the potential to be extended to MOOPF problems and OPF challenges in restructured power systems under normal, severe, and contingency conditions. Furthermore, integrating renewable energy sources and storage devices into OPF solutions could offer significant technological, economic, and environmental advantages.

CHAPTER 5

HYBRID RAO-2 SINE COSINE ALGORITHM FOR OPF SOLUTIONS

5.1 Introduction

The past decade has been marked by the increasing popularity of hybrid approaches for OPF. These hybrid methods strategically combine the strengths of individual algorithms, overcoming their limitations. These methods harness natural-inspired actions to deliver robust solutions for complex problems (Blum et al. 2008), specifically in the optimal design of hybrid power systems that combine solar PV and wind-based systems (Gusain et al. 2023). Additionally, such systems benefit from the use of CI-based hybrid machine learning approaches which enhance OPF solutions by improving accuracy and computational efficiency (Syed et al. 2021). Such hybridization leads to stronger algorithms with fast convergence, large search spaces, and computation time reduction, facilitating superior OPF solutions.

Several researchers have contributed innovative hybrid algorithms to the field. Kumar and Chaturvedi (2013) introduced hybrid approaches combining fuzzy systems with Genetic Algorithm (GA-Fuzzy) and Particle Swarm Optimization (PSO-Fuzzy) to optimize control parameter settings. Narimani et al. (2013) proposed a hybrid method combining Modified PSO with the Shuffle Frog Leaping Algorithm (MPSO-SFLA) for Multi-Objective OPF (MOOPF). Mahdad and Srairi (2014) developed a DE-APSO-PS hybrid strategy for solving MOOPF under severe loading conditions. Radosavljević et al. (2015) presented the PSO-GSA hybrid algorithm, merging PSO with the Gravitational Search Algorithm, to address single-objective and MOOPF problems.

Additional hybrid methods have emerged in recent years to tackle diverse OPF challenges. Notable examples include the hybrid DE and Harmony Search (Hybrid DE-HS) algorithm by Reddy (2019), the Hybrid Firefly and PSO (HFPSO) by Khan et al. (2020), and the Jaya-Powell's Pattern Search (Jaya-PPS) by Gupta et al. (2021a). Gupta et al. (2021b) also proposed the Sine-Cosine Mutation-based Modified Jaya (SCM-MJ) algorithm. Other significant contributions include the FAHSPSO-DE algorithm by Naderi et al. (2021), the Hybrid Fruit Fly-based ABC (HFABC) algorithm by Mallala et al. (2022), the Hybrid JAYA Bird Swarm Algorithm (HJBSA) by Aurangzeb et al. (2023), and the Hybrid Sine Cosine-GWO (HSC-GWO) by Keswani et al. (2023).

The success of hybrid approaches in OPF is evident in their ability to solve complex, large-scale optimization problems efficiently. By combining complementary algorithmic strengths, these methods provide advanced tools for tackling the diverse challenges of OPF, including

cost minimization, stability enhancement, and power loss reduction, while adapting seamlessly to evolving system demands.

In emergency scenarios, it is often necessary to shed segments of the load to preserve overall system stability and prevent widespread blackouts caused by voltage instability in stressed power systems. Voltage instability risks are heightened during network topology changes or when transmission lines are overloaded. Studies have revealed that voltage instability is the leading cause of major power blackouts globally, with overloaded transmission systems frequently acting as the catalyst (Alhelou et al. 2019). Over the past decade, numerous blackout reports have identified cascading grid failures stemming from voltage instability as a critical issue.

To mitigate these challenges and augment the capacity of power systems to handle peak demands without overloading, hybrid optimization techniques have emerged as effective solutions to improve system loadability. For example, Gnanambal and Babulal (2012) proposed a hybrid approach that combines DE and PSO (*i.e.* DEPSO) to enhance the loadability limit of power systems. Similarly, Mahdad and Srairi (2015) introduced the Grey Wolf-Pattern Search optimizer (GW-PS), which accounts for load margin stability and generator faults, ensuring system security under critical conditions on the IEEE 30-bus network. In Taher et al. (2021), a method combining Improved MFO (IMFO) with Continuation Power Flow (CPF) was employed to optimize power system loadability and minimize load shedding during emergencies, utilizing shunt FACTS devices. Additionally, Taher et al. (2022) presented an approach for maximizing system loadability by strategically placing and configuring FACTS devices through the IMFO algorithm while simultaneously optimizing multiple OPF objectives.

These advanced hybrid techniques play a pivotal role in improving system loadability, reducing voltage instability risks, and ensuring grid resilience under extreme conditions. By incorporating strategies that enhance stability and optimize power flow, they significantly contribute to minimizing the impact of emergencies on power systems.

This chapter introduces a novel hybrid optimization technique, termed HRSCA, developed to address OPF challenges in power systems, particularly under scenarios of high loading and unforeseen generator outages. The study examines two critical events: the system operating at its load stability limit and contingencies involving generator outages. The simulations were conducted using MATLAB R2018a, enabling a comprehensive evaluation of the proposed algorithm. Extensive testing and validation on various power system networks highlight the effectiveness of HRSCA in enhancing security-oriented OPF solutions. The algorithm

demonstrates robust performance in optimizing power flow schemes (OPFS) across networks of different sizes and under diverse operational conditions.

5.2 Mathematical Formulation of the OPF Problem

The OPF problem formulation fundamentally involves defining specific objectives within a set of constraints. Solving the OPF problem requires adjusting certain power system parameters, known as control variables (CVs), to achieve an optimal system configuration that meets a predefined objective function. The optimized state of the power system is governed by the state variables (SVs). Power system operation must adhere to two types of constraints: equality constraints, represented by power balance equations, and inequality constraints, which define the limits on controllable quantities and the operating boundaries of the power system. The standard objective function is described in Equation (5.1), while the operating constraints of the OPF problem chosen for this work are described in Equations (5.2–5.3) (Bouchekara et al. 2014a).

$$Min: Z_{min}(x,u)$$
 (5.1)

Subject to the constraints

$$g_i(x,u) = 0$$
 ; $i = 1, 2, 3, \dots, N_e$ (5.2)

and,
$$h_j(x,u) \le 0$$
 ; $j = 1, 2, 3, \dots, N_{ie}$ (5.3)

The objective function, Z_{\min} , is intricately linked to both the SVs, denoted by x, and the CVs, represented by u. As shown above, g_i represents the ith equality constraints imposed by non-linear load flow equations and h_j denotes jth inequality constraints that pertain to the operational limits of the physical components within the system. Here, N_e denotes the total number of equality constraints, while N_{ie} denotes the total count of inequality constraints. The state vector, i.e., the vector of dependent variables, is given by Equation (5.4) as follows:

$$x^{T} = [P_{G_1}, V_{L_1}, ..., V_{L_{NPQ}}, Q_{G_1}, ..., Q_{G_{NG}}, S_{line_1}, ..., S_{line_{NL}}]$$
(5.4)

Similarly, Equation (5.5) specifies the control variables vector, consisting of adjustable variables optimized for the power flow scheme:

$$u^{T} = [P_{G_{2}}...P_{G_{NG}}, V_{G_{1}}...V_{G_{NG}}, Q_{C_{1}}....Q_{C_{NG}}, T_{1}....T_{NT}]$$
(5.5)

5.2.1 Objectives Functions

The objective functions addressed in the present work encompass five distinct objectives, each mathematically represented as follows:

a) Fuel cost minimization (FCM)

The fuel cost function is the most fundamental function of OPF and has been extensively studied in the literature. Fuel cost (\$/h) and the power generated (MW) have an approximate quadratic relationship as follows (Yuryevich and Wong, 1999):

$$Z_{FCM}(x,u) = \left(\sum_{i=1}^{NG} a_i + b_i P_{G_i} + c_i P_{G_i}^2\right) \quad (\$/h)$$
 (5.6)

here the $Z_{FCM}(x,u)$ is the overall fuel cost function expressed in \$/h.

b) Minimization of a Combined Voltage Deviation and Cost

The second most essential objective function of OPF aims at reducing load bus voltage deviation (VD) from the standard reference of 1.0 per unit (p.u.). This is essential for maintaining power system stability and ensuring the quality of power supply to consumers. In most cases, the fuel cost function is combined with the voltage profile enhancement to form a combined objective function as given in Equation (5.7).

$$Z_{VDM}(x,u) = \left(\sum_{i=1}^{NG} a_i + b_i P_{G_i} + c_i P_{G_i}^2\right) + K_{vd} \sum_{i=1}^{NPQ} \left| V_{L_i} - 1.0 \right|$$
(5.7)

where, K_{vd} is assigned an appropriate value based on user experience and depending on the relative importance of minimizing voltage deviation compared to minimizing fuel cost.

c) Minimization of a Combined Voltage Stability Index (VSI) and Cost

The stability of an electrical power system network is characterized by ensuring that all bus voltages remain within permissible ranges both during normal operation and in the event of a disturbance. Power systems with high load demands and extensive transmission networks are particularly vulnerable to voltage instability.

Improving voltage stability requires lowering the L-index of all buses. The L-index, defined within a bounded interval of [0, 1], serves as a reliable stability indicator. A value of '0' indicates an unloaded condition, while a value of '1' signifies voltage collapse (Kessel and Glavitsch, 1986).

Mathematically, the objective of VSI, i.e., L-index minimization, can be defined using the two-fold objective combining fuel cost with voltage stability as follows in Equation (5.8):

$$Z_{VSI}(x,u) = \left(\sum_{i=1}^{NG} a_i + b_i P_{G_i} + c_i P_{G_i}^2\right) + K_{vs}\left(\max\left(L_j\right)\right)$$
(5.8)

where, K_{vs} is assigned an appropriate value based on user experience and depending on the relative importance of voltage stability compared to fuel cost. The L-index of any *j*th load bus is denoted by L_j and is defined by Equation (5.9).

$$L_{j} = \left| 1 - \frac{W_{ji} \sum_{i=1}^{NG} V_{i}}{V_{j}} \right| \quad \text{where } j = 1, 2, \dots, NPQ; \qquad W_{ji} = -\left[inv(Y_{jj}) \right] * \left[Y_{ji} \right] \quad (5.9)$$

d) Power Loss Minimization (PLM)

The objective here is to minimize the total active power loss P_{losses} in the power system. Equation (5.10) calculates the difference between the total power generated by all the generators in the system and the total power consumed by all the loads. A positive value indicates a power loss in the system, which is undesirable.

$$P_{losses} = \sum_{i=1}^{NB} P_{i} = \sum_{i=1}^{NB} P_{G_{i}} - \sum_{i=1}^{NB} P_{D_{i}}$$
 MW (5.10)

Equation (5.11) typically represents the function for minimization of transmission loss in a power system which is a nonlinear function of bus voltage magnitudes:

$$Z_{PLM}(x,u) = \min(P_{losses}) = \sum_{L=1}^{NL} G_{L_{i-j}} [V_i^2 + V_j^2 - 2V_i V_j Cos \delta_{ij}] \quad MW$$
 (5.11)

e) Emission Cost Minimization (ECM)

Minimizing the emission of harmful gases from thermal power plants is an important objective in OPF, as it reduces environmental impact. The emission cost is generally associated with the active power output of the generators.

Equation (5.12) defines the emission cost as a function of the active power output of the *i*th generator measured in MW:

$$Z_{ECM}(x,u) = \text{Emission} = \sum_{i=1}^{NG} (\alpha_i + \beta_i P_{G_i} + \gamma_i P_{G_i}^2 + \omega_i \exp(\mu_i P_{G_i}) \quad (\text{ton } / h)$$
 (5.12)

where α_i , β_i , γ_i , ω_i and μ_i are the emission coefficient of *i*th generator.

5.2.2 Constraints:

a) Equality constraints

The equality constraints represent the conventional power flow equations that ensure the balance between active and reactive power flows in the system. These constraints are mathematically described by Equations (5.13) and (5.14) as follows:

$$P_{losses} = \sum_{i=1}^{NB} P_{G_i} - \sum_{i=1}^{NB} P_{D_i}$$
 (5.13)

$$Q_{losses} = \sum_{i=1}^{NB} Q_{G_i} - \sum_{i=1}^{NB} Q_{D_i}$$
 (5.14)

b) Inequality constraints

The inequality constraints set the limits for adjustable variables and operational thresholds in the power system. These thresholds cover voltage levels at generator and load buses, active and reactive power outputs from generators, transformer tap changer settings, and restrictions on compensating reactive power. The inequality constraints are detailed in Equations (5.15-5.21):

Each generator unit's active power, reactive power, and voltage magnitude are constrained by upper and lower bounds as follows:

$$P_{G_i}^{\min} \le P_{G_i} \le P_{G_i}^{\max} \qquad i = 1, 2,, NG$$
 (5.15)

$$V_{G_i}^{\min} \le V_{G_i} \le V_{G_i}^{\max} \qquad i = 1, 2,, NG$$
 (5.16)

$$Q_{G_i}^{\min} \le Q_{G_i} \le Q_{G_i}^{\max} \quad i = 1, 2,, NG$$
 (5.17)

Every regulating transformer tap has lower and upper limits for discrete tap settings as:

$$T_i^{\min} \le T_i \le T_i^{\max}$$
 $i = 1, 2, ..., NT$ (5.18)

Every reactive power compensator injects reactive power (*i.e.*, shunt VAR compensation) within discrete lower and upper limits as:

$$Q_{C_i}^{\min} \le Q_{C_i} \le Q_{C_i}^{\max} \quad i = 1, 2,, NC$$
 (5.19)

The transmission line power flow capacity (upper limit), and the upper and lower limits of load bus voltage are categorized under system security constraints and are described as follows:

$$S_{line_i} \le S_{line_i}^{max}$$
 $i = 1, 2,, NL$ (5.20)

$$V_{L_i}^{\text{min}} \le V_{L_i} \le V_{L_i}^{\text{max}} \qquad i = 1, 2, ..., NPQ$$
 (5.21)

By carefully considering and incorporating these constraints into the OPF problem, we can ensure the safe, reliable, and efficient operation of the power system. These constraints are typically imposed through quadratic penalty terms in the objective function, utilizing a penalty factor approach. Therefore, the Equation (5.1) can be augmented as;

$$Z_{aug} = Z_{\min}(x, u) + penalty \tag{5.22}$$

where,
$$penalty = \lambda_1 (P_{G_1} - P_{G_1}^{\lim})^2 + \lambda_2 \sum_{i=1}^{NPQ} (V_{L_i} - V_{L_i}^{\lim})^2 + \lambda_3 \sum_{i=1}^{NG} (Q_{G_i} - Q_{G_i}^{\lim})^2 + \lambda_4 \sum_{i=1}^{NL} (S_{line_i} - S_{line_i}^{\lim})^2$$

$$(5.23)$$

In Equation (5.23), λ_1 , λ_2 , λ_3 and λ_4 denote penalty factors. If the limit value of dependent variable upon violation is denoted by x^{lim} then it can be conveniently expressed as per Equation (5.24):

$$x^{\text{lim}} = \begin{cases} x^{\text{max}}; (x > x^{\text{max}}) \\ x^{\text{min}}; (x < x^{\text{max}}) \end{cases}$$
 (5.24)

5.3 Proposed Hybrid Rao-2 Sine Cosine Algorithm (HRSCA) Methodology

The *Hybrid Rao-2 Sine Cosine Algorithm (HRSCA)* is introduced as a novel optimization technique designed to address critical OPF challenges in power systems, particularly under conditions of high loading and unforeseen generator outages. The algorithm is tailored to handle two key scenarios: systems reaching their load stability limits and generator outage contingencies. By integrating the strengths of the Sine Cosine Algorithm (SCA) and Rao-2, HRSCA provides a robust solution that enhances both exploration and exploitation capabilities, ensuring efficient and secure power system operation.

The hybridization of SCA and Rao-2 allows HRSCA to utilize SCA's strong global exploration ability, which prevents getting trapped in local optima, while employing Rao-2's rapid convergence and refined local search capabilities. This combination dynamically balances exploration and exploitation, enabling diverse and optimal solutions that meet OPF problem constraints effectively and efficiently.

HRSCA has demonstrated exceptional performance in both SOOPF and MOOPF scenarios. Extensive testing and validation on the IEEE 30-bus and IEEE 118-bus standard test systems reveal that the algorithm consistently delivers superior or comparable results to existing optimization methods documented in the literature. Key objectives addressed by HRSCA include FCM, VDM, PLM, ECM, and VSI, within both single and bi-objective frameworks.

5.3.1 Overview of Sine Cosine Algorithm (SCA)

The introduction of SCA by Mirjalili has generated significant interest among researchers, leading to its extensive application across various fields to tackle optimization problems

(Mirjalili, 2016). SCA and its variants have been widely used in diverse applications, including feature selection for machine learning (Sindhu et al. 2017; Belazzoug et al. 2020), solving global engineering optimization problems (Abd Elaziz et al. 2017), sizing distributed generators to meet load demands in AC distribution systems (Montoya et al. 2020), addressing single and multi-objective OPF problems (Attia et al. 2018; Gupta et al. 2021b; Karimulla and Ravi, 2021), and enhancing loading margin stability in security OPF during contingencies.

A comprehensive overview of SCA is provided in Chapter 4, Section 4.2.1. As discussed therein, SCA employs sine and cosine functions through a movement mechanism to reposition search agents within the solution space. Each agent's position update is influenced by the best solution found thus far and is determined by specific mathematical expressions, detailed in Equation (5.25):

$$x_{j,k}^{t+1} = \begin{cases} x_{j,k}^{t} + R_{1} \times \sin(R_{2}) \times \left| R_{3} P_{best_{j}}^{t} - x_{j,k}^{t} \right| & ; R_{4} < 0.5 \\ x_{j,k}^{t} + R_{1} \times \cos(R_{2}) \times \left| R_{3} P_{best_{j}}^{t} - x_{j,k}^{t} \right| & ; R_{4} \ge 0.5 \end{cases}$$

$$(5.25)$$

where, $x_{j,k}^t$ represents the position of the current solution at t^{th} iteration in jth dimension (j = 1,2...,n), with "n" being the number of design variables and $P_{best_j}^t$ is the position of the best solution (target point) at t^{th} iteration in jth dimension. Additionally, the variables R_1, R_2, R_3 , and R_4 are Gaussian-distributed random variables used in the algorithm to prevent getting stuck in local optima. In the updating process, R_1 dynamically guides solution movement, initiating with a higher influence for broad search and gradually reducing for targeted exploitation as optimization progresses. The fine tuning of R_1 during search process is carried out using Equation (5.26) as:

$$R_1 = a - t \times a / t_{\text{max}} \tag{5.26}$$

where, t represents the current iteration number, t_{\max} denotes the maximum number of iterations, and 'a' is a user defined constant. The parameter $R_2 \in [0, 2\pi]$ determines the step size for exploring the search space, and parameter $R_3 \in [0, 1]$ provides random weight to P_{best_j} . The algorithm alternates between the cosine and sine components of Equation (5.25) with equal probability, which is controlled by the variable R_4 that ranges from [0-1].

Despite its success in various optimization tasks, SCA suffers from drawbacks such as slow convergence rates and restricted local search abilities. Researchers have responded to these

challenges by creating modified and hybrid versions of SCA tailored for real-world applications, as previously mentioned. Expanding on these enhancements, the authors of this study propose a new hybrid approach that combines SCA with another strategically selected algorithm. The goal is to overcome existing limitations and improve overall performance.

5.3.2 Overview of Rao-2 Algorithm

In 2020, a new set of algorithms known as Rao-1, Rao-2, and Rao-3 was introduced and evaluated using 23 benchmark functions, as detailed in Rao (2020). One major advantage of these advanced Rao variants is their metaphor-free design, which frees them from the complexities of problem-dependent control parameters. This eliminates the need for parameter tuning, requiring only basic parameters such as population size and iteration count. Additionally, these algorithms demonstrate a notably fast convergence rate. The Rao algorithms operate by identifying the best and worst solutions found during the optimization process and enabling random interactions among potential solutions. The Rao algorithms and their various adaptations have been widely used to tackle a variety of optimization problems, including the optimal design of mechanical components (Rao and Pawar, 2020), determining the optimal parameters of renewable energy systems by Rao et al. 2023, optimal load frequency regulation in hybrid power grids by Khamies et al. 2021, solving the traveling salesman problem (TSP) by Nikum (2021), and addressing OPF problems (Gupta et al. 2021c; Hassan et al. 2021). In our OPF study, we integrated the *Rao-2* algorithm within a hybrid approach, selecting it for its strong feature of high convergence rate and lack of reliance on any solverspecific parameters, thus enhancing the efficiency of the optimization process.

The Rao-2 algorithm employs a search strategy that explores the solution space by utilizing both the best and worst solutions and incorporates stochastic interactions among the population's elements, as outlined in the model presented in Equation (5.27):

$$x_{j,k}^{t+1} = x_{j,k}^{t} + r_{1j}^{t} \times \left| P_{best_{j}}^{t} - P_{worst_{j}}^{t} \right| + r_{2j}^{t} \times \left(\left| x_{j,k}^{t} \ or \ x_{j,d}^{t} \right| - \left| x_{j,d}^{t} \ or \ x_{j,k}^{t} \right| \right)$$
(5.27)

where $x_{j,k}^t$ denotes the *j*th variable value (where j = 1,2,...,n) for the *k*th candidate solution (where k = 1,2,...,m) after the t^{th} iteration, with "n" being the number of design variables and "m" being the population size. $x_{j,k}^{t+1}$ denotes the updated value of the *j*th variable in the next iteration. The best and worst candidate solutions at t^{th} iteration are represented by $P_{best_j}^t$ and $P_{worst_j}^t$ respectively. Here, r_{1j}^t and r_{2j}^t are the random numbers within [0, 1], generated for the *j*th variable during the t^{th} iteration. In Equation (5.27), the second term on the right-hand side

guides the candidate solution based on the interaction between the best and worst solutions, ensuring convergence toward promising regions of the solution space. The third term is indicative of random interaction between the presently considered kth solution and a randomly picked dth solution. The term " $x_{j,k}^t$ or $x_{j,d}^t$ " in Equation (5.27) compares fitness values of the current solution and randomly selected search agent. If the fitness value of the kth candidate solution is better than that of the dth candidate, the term " $x_{j,k}^t$ or $x_{j,d}^t$ " evaluates to $x_{j,k}^t$, and in that case, " $x_{j,d}^t$ or $x_{j,k}^t$ " becomes $x_{j,d}^t$. Similarly, if the fitness value of the dth candidate solution is better than that of the kth candidate solution, the term " $x_{j,k}^t$ or $x_{j,d}^t$ " evaluates to $x_{j,d}^t$, and in such condition, " $x_{j,d}^t$ or $x_{j,d}^t$ " evaluates to $x_{j,k}^t$.

While Rao-2's interaction term promotes both exploration (diversifying search capability) and exploitation (local search capability), the algorithm may still fall into local optima due to limited knowledge exchange, weak exploration ability, and minimal use of valuable information gained during the search process. These shortcomings have led to hybridizing Rao-2 with another algorithm to improve both its exploration and exploitation capabilities.

5.3.3 Hybrid Rao-2 Sine Cosine Algorithm (HRSCA)

The Hybrid Rao-2 Sine Cosine Algorithm (HRSCA) is an innovative straightforward approach that merges the strengths of the SCA and Rao-2 algorithms to optimize their performance and address their limitations. The SCA provides extensive exploration capabilities to prevent early convergence to local optima, while the Rao-2 algorithm boosts convergence speed and improves the effectiveness of local searches.

In this hybrid approach, each search agent can choose between SCA movements or Rao-2 update procedures to update its position, based on conditions specified in Equation (5.28).

$$\begin{cases} x_{j}^{t+1} = x_{j}^{t} + R_{1} \times \sin\left(R_{2}\right) \times \left| R_{3} P_{best_{j}}^{t} - x_{j}^{t} \right| & ; 0 \leq R_{4} \leq 0.35 \\ x_{j}^{t+1} = x_{j}^{t} + R_{1} \times \cos\left(R_{2}\right) \times \left| R_{3} P_{best_{j}}^{t} - x_{j}^{t} \right| & ; 0.35 < R_{4} \leq 0.7 \\ x_{j,k}^{t+1} = x_{j,k}^{t} + r_{1,j}^{t} \times \left| P_{best_{j}}^{t} - P_{worst_{j}}^{t} \right| + r_{2,j}^{t} \times \left(\left| x_{j,k}^{t} \text{ or } x_{j,d}^{t} \right| - \left| x_{j,d}^{t} \text{ or } x_{j,k}^{t} \right| \right) & ; 0.7 < R_{4} \leq 1 \end{cases}$$

The equation set indicates that the proposed hybrid strategy follows a straightforward structure by adjusting its search strategy based on the value of R_4 . For lower values of R_4 (0 $\leq R_4 \leq 0.35$), the algorithm explores a broader range of potential solutions by utilizing the sine-based update mechanism. For moderate values (0.35 $< R_4 \leq 0.7$), the cosine-based update

mechanism is activated. Cosine-based updates maintain exploratory behaviour while gradually introducing exploitation characteristics, targeting promising regions of the search space with a balanced approach. Higher values $(0.7 < R_4 \le 1.0)$ signify intensified exploitation, where the Rao-2 mechanism takes over to refine the already-discovered promising areas through intensified search, thereby improving convergence speed. HRSCA iteratively evaluates and updates solutions based on best and worst candidates, reducing the risk of suboptimal convergence and sustaining an effective exploration-exploitation balance throughout the optimization process. Figure 5.1 presents a graphical framework that demonstrates the application and process flow of the proposed HRSCA-based scheme in this study.

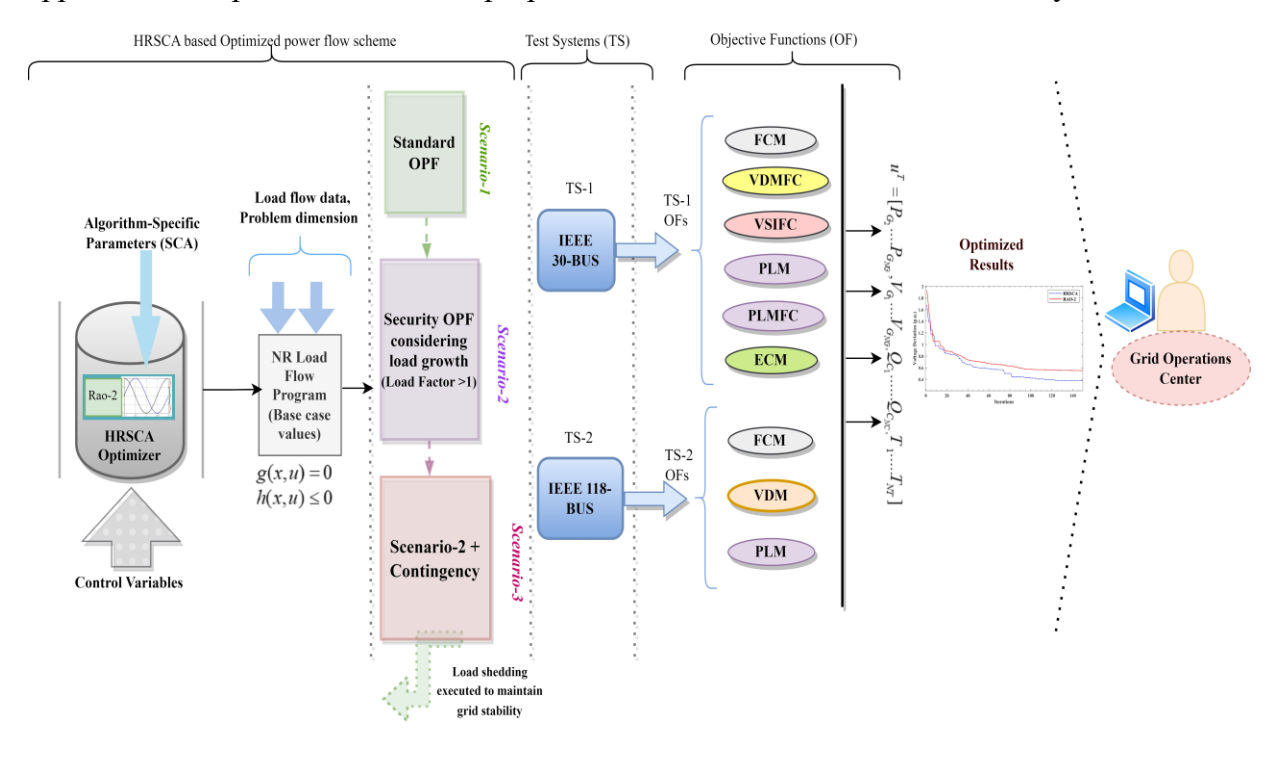


Fig. 5.1 Graphical framework for HRSCA based OPF scheme for diverse scenarios

5.3.4 Computation Steps for HRSCA and Flowchart

Table 5.1 provides a clear and structured presentation of the implementation steps involved in the proposed HRSCA approach, outlining the detailed computational procedure for solving the OPF problem.

Table 5.1 Steps in HRSCA **HRSCA INPUT** • Problem dimension, n • Population size, m • Stopping criteria: Maximum number of iterations, t_{max} • Upper and lower bounds of decision variables, $[x_{\min}, x_{\max}]$. **INITIALIZATION** • Set iteration counter, t = 0. • Randomly initialize the population of m search agents within bounds $[x_{\min}, x_{\max}]$. ullet Identify the best (P_{best}) and worst (P_{worst}) solutions in the initial population based on the objective function. **EVALUATION** • Compute the fitness value for each search agent using the objective function specified in Equation (5.22). • Fitness evaluation integrates sine-cosine updates for global adjustments and Rao-2's stochastic interactions for refined local search. • Update P_{best} and P_{worst} solutions in the population. • Check constraint satisfaction and handle violations, if applicable. ALGORITHM LOOP: STEP-1 • Generate a random number $R_4 \in [0,1]$, which serves as the random switching parameter. • Update each search agent's position using R₄ to determine the transition between exploration and exploitation phases. STEP-2 • The hybrid mechanism uses R₄ to decide whether to follow SCA or Rao-2 for position updates: • If $0 \le R_4 \le 0.35$: Apply the sine-based update, $x_{i,k}^{t+1} = x_{i,k}^{t} + R_1 \times \sin(R_2) \times \left| R_3 P_{best}^{t} - x_{i,k}^{t} \right|$ (Sine-based update prevents premature convergence to local optima) • If $0.35 < R_4 \le 0.7$: Apply the cosine-based update, $x_{i,k}^{t+1} = x_{i,k}^{t} + R_1 \times \cos(R_2) \times |R_3 P_{best}^{t} - x_{i,k}^{t}|$ (Cosine-based update targets promising areas of search space while maintaining diversity) • If $0.7 < R_4 \le 1.0$: Use Rao-2-based stochastic updates for refining local search, $x_{i,k}^{t+1} = x_{i,k}^{t} + r_{i,k}^{t} \times \left| P_{best}^{t} - P_{worst}^{t} \right| + r_{2,i}^{t} \times \left(\left| x_{i,k}^{t} \text{ or } x_{i,d}^{t} \right| - \left| x_{i,d}^{t} \text{ or } x_{i,d}^{t} \right| \right)$ (Rao-2 update intensifies local search by refining solutions near the best-known candidates) STEP-3 • Compute the objective function value for each updated solution. • Compare the kth candidate solution with a randomly chosen dth candidate: • If: $Z(x_k^t) < Z(x_d^t)$, $(x_{i,k}^t \ or \ x_{i,d}^t) \to x_{i,k}^t$ • Otherwise: $(x_{i,k}^t \text{ or } x_{i,d}^t) \rightarrow x_{i,d}^t$ • Compare the updated solution $x_{j,k}^{t+1}$ with its current solution $x_{j,k}^{t}$: • If: $Z(x_{i,k}^{t+1}) < Z(x_{i,k}^{t})$: Update the solution by replacing the current one.

• Otherwise: Retain the existing solution.

• If $t \ge t_{\text{max}}$: Stop the algorithm and return the best solution.

• If $t < t_{\text{max}}$: Increment the iteration counter (t = t + 1) and return to STEP-1.

• Check the termination condition:

STEP-4

With this hybrid approach, search agents dynamically switch between two optimization algorithms, guided by a stochastic process. This strategy utilizes the SCA's extensive exploration capabilities, helping to avoid early convergence to local optima. At the same time, the Rao-2 algorithm, with its efficient local search abilities, enhances convergence speed toward the best solutions. This hybrid mechanism balances exploring the search space through SCA movements and refining the best solutions identified by the population via the focused exploitation of the Rao-2 algorithm.

The flowchart illustrating the proposed HRSCA is shown in Fig. 5.2.

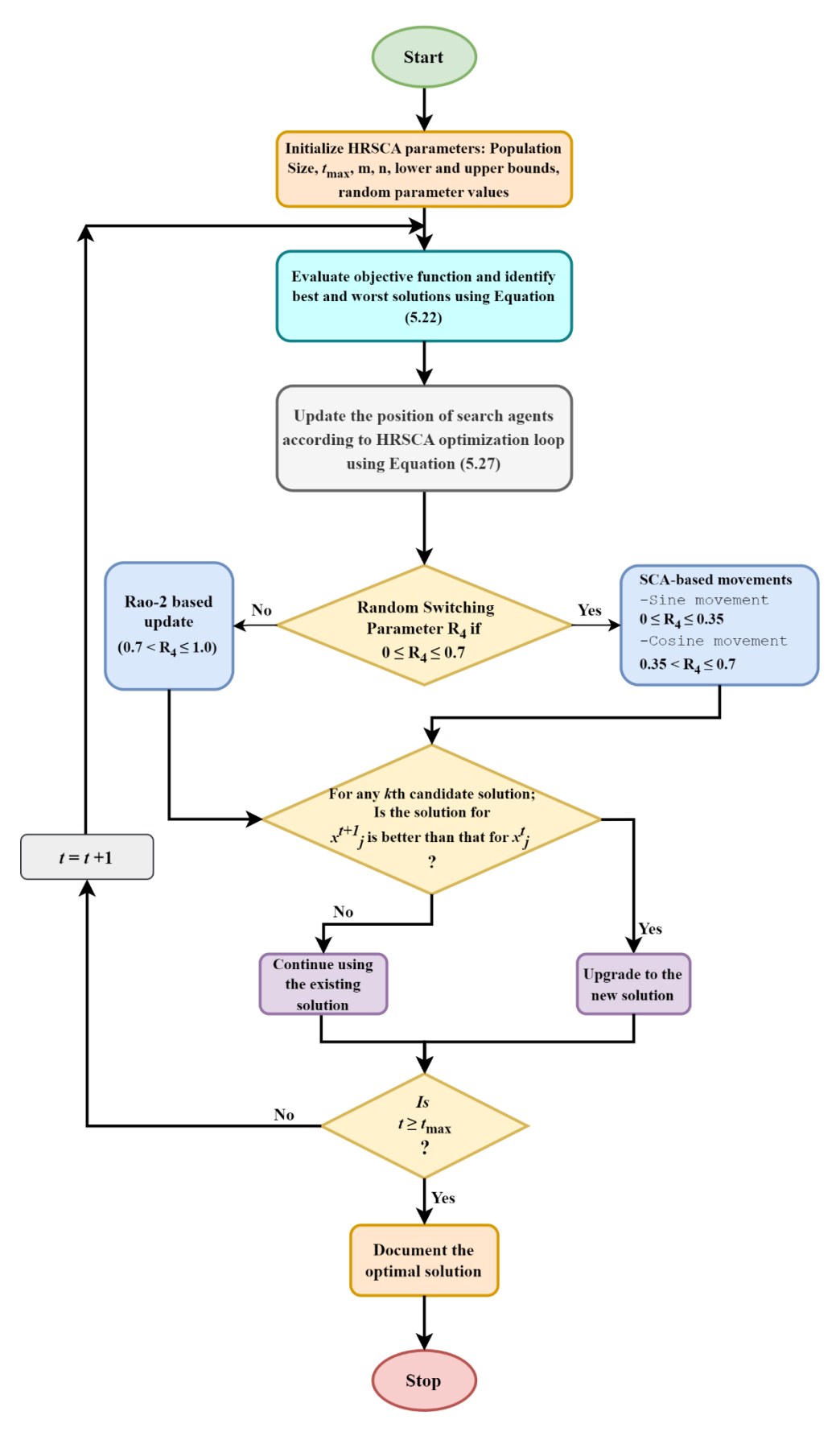


Fig. 5.2 Proposed HRSCA algorithm flow chart

The implementation of this hybridized approach enables search agents to dynamically switch between the two optimization algorithms, guided by a stochastic process. The SCA enhances exploration, preventing premature convergence, while Rao-2 improves local search efficiency, accelerating convergence to optimal solutions. This synergy balances exploration via SCA and exploitation through Rao-2, refining the search process. The proposed HRSCA operates with parameters detailed in Table 5.2. The "No Free Lunch" theorem, established by Wolpert and Macready (1997), highlights the limitations of any single optimization method and the importance of tailored algorithms for specific challenges. This makes the hybrid SCA-Rao-2 approach a valuable tool for addressing the OPF problem effectively.

 Table 5.2 Parameter settings for HRSCA in the current study

Parameter	Value	Component	Description
Population size (<i>m</i>)	30	Shared	Number of candidate solutions in the population.
Maximum iterations (t_{max})	100 (30-bus), 150 (118-bus)	Shared	Maximum number of optimization steps.
Random coefficients (r_1, r_2)	[0, 1]	Rao-2	Random numbers for diversity in solution updates.
Switching parameter (R_4)	[0, 1]	SCA	Switches transition between sine and cosine components.
Control parameter (R_1)	$R_1 = a - t \times a / t_{\text{max}}$	SCA	Dynamically guides solution movement based on iteration progress, with $a = 2$ (user defined)
Step size (R_2)	$[0, 2\pi]$	SCA	Parameter for exploring the search space.
Weight coefficient (R_3)	[0, 1]	SCA	Random weight assigned to the best solution.

5.4 Simulation Results and Analysis

The HRSCA was rigorously tested through power system simulations, validating its effectiveness in security OPF across different network sizes and operating scenarios. Two electrical grids were analysed: the IEEE 30-bus network (cases 1-8) and the 118-bus network (cases 9-12), with key characteristics summarized in Table A.1 (Appendix). For both the 30-bus and 118-bus networks, the best results were achieved using a population size (m) of 30, setting the iteration limits (t_{max}) to 100 and 150, respectively (Table 5.2). The simulations were carried out using MATLAB R2018a on a system equipped with a 10th Gen Intel Core i7 processor, 8.0 GB RAM, and a clock speed of 1.7 GHz. Each case study involved 30 successful trials for both test systems, ensuring the robustness of results across multiple trials. The best results from these 30 trials are presented here. Simulations have revealed that HRSCA

consistently outperforms contemporary OPF algorithms, proving its reliability in handling load growth and unforeseen disruptions in real-world power system operations

5.4.1 Performance on IEEE 30-Bus Test System

The initial standard test system selected for this study has the following features: it consists of six thermal generating units located at buses 1, 2, 5, 8, 11, and 13, with an active power demand of 283.4 MW and reactive loading of 126.2 MVAR. Additionally, the system includes four transformers with a $\pm 10\%$ tapping range located on lines 6-9, 6-10, 4-12, and 28-27. Furthermore, nine shunt VAR compensators are positioned at buses 10, 12, 15, 17, 20, 21, 23, 24, and 29 (Lee and Park, 1985). Table 5.3 provides the minimum and maximum permissible values for generator unit parameters, along with their respective fuel cost coefficients.

Bus No.	P _{min} (MW)	P _{max} (MW)	Q _{min} (MVAR)	Q _{max} (MVAR)	a (\$/h)	b (\$/h-MW)	c (\$/h-MW ²)
1	50	200	-20	200	0	2	0.00375
2	20	80	-20	100	0	1.75	0.01750
5	15	50	-15	80	0	1	0.06250
8	10	35	-15	60	0	3.25	0.00830
11	10	30	-10	50	0	3	0.02500
13	12	40	-15	60	0	3	0.02500

Table 5.3 Allowable generator unit parameters and fuel cost coefficients for IEEE 30-bus test system

Additionally, load data, line data, and bus data for the 30-bus system on a 100 MVA base are available in (Abou El Ela et al. 2010). The lower and upper bounds of the control variables (CVs) are depicted in Table 5.4 for Cases 1-5.

5.4.1.1 Scenario-1: Standard OPF

This scenario involves a standard OPF analysis on a 30-bus power system test case. For this scenario, five distinct single and multi-objective cases have been analyzed. These cases aim to minimize parameters including total fuel cost, total voltage deviation, total active power losses, emissions, and the stability index (L-index). The primary intent of this scenario is to contrast the outcomes derived from the proposed strategy under standard operational conditions with the outcomes yielded by recently developed optimization techniques. The five cases considered are:

Case 1: Fuel Cost Minimization (FCM)

- Case 2: Voltage Deviation Minimization considering Fuel Cost (VDMFC)
- Case 3: Voltage Stability Improvement considering Fuel Cost (VSIFC)
- Case 4: (a) Power Loss Minimization (PLM)
 - (b) Power Loss Minimization considering Fuel Cost (PLMFC)
- Case 5: Emission Cost Minimization (ECM)

Case-1 FCM

The proposed HRSCA technique was applied to Case 1, which focuses on minimizing basic fuel cost (FCM objective). Table 5.4 displays the optimal settings and their associated objective function values. The decision variables (P_G , V_G , Q_C and T) are defined as per Equation (5.5). The basic FCM objective is given by Equation (5.6).

The total fuel cost (FC) was reduced to 799.1617 \$/h, reflecting a significant 11.4% reduction compared to the base case (initial case). Additionally, the voltage deviation (VD) and active power loss P_{losses} were minimized to 1.7309 p.u. and 8.6451 MW, respectively. These results surpass the performance of several algorithms reported in the literature, including SCA (800.1018 \$/h) by Attia et al. (2018), MSCA (799.31 \$/h) by Attia et al. (2018), MGOA (800.4744 \$/h) by Taher et al. (2019b), GOA (800.7806 \$/h) by Taher et al. (2019b), TLBO (800.6108 \$/h) by Taher et al. (2019b), PSO (800.5912 \$/h) by Taher et al. (2019b), CS-GWO (799.9978 \$/h) by Meng et al. (2021), AMTPG-Jaya (800.1946 \$/h) by Warid (2020), Chaotic Rao-2 (800.1537 \$/h) by Warid (2022), and Partitioned ALO *i.e.* PALO (799.9160 \$/h) by Mahdad (2020).

While the Jaya optimizer in El-Sattar et al. (2019) achieved a slightly better FC value (798.9386 \$/h), it required 200 iterations to do so, with a less favourable VD value of 2.01 p.u. Similarly, other competitive algorithms, such as MSCA, required more than 400 iterations, and PALO needed 200 iterations to achieve their respective optimized values. In contrast, the proposed method achieved rapid convergence within 100 iterations in approximately 92 s. Figure 5.3 illustrates the trend of reducing the total fuel cost using the proposed hybrid approach compared to Rao-2 and SCA.

 Table 5.4 Optimized control variables obtained by HRSCA for IEEE 30-bus test system

CV- ()	M:	Max	Base case	Case 1	Case 2	Case 3	Case 4		Coso 5
CVs (p.u.)	Min	Max	Dase case			Case 3	(a)	(b)	Case 5
P _{G2}	20	80	80	0.4869	0.4892	0.4874	0.6626	0.5539	0.6637
P _{G5}	15	50	50	0.2136	0.2164	0.2182	0.5	0.3788	0.5
P _{G8}	10	35	20	0.2105	0.2208	0.2373	0.35	0.35	0.35
P _{G11}	10	30	20	0.1193	0.124	0.1338	0.3	0.2999	0.3
P _{G13}	12	40	20	0.12	0.12	0.12	0.4	0.2604	0.4
V_{G1}	0.95	1.1	1.05	1.1	1.0434	1.1	1.1	1.0799	1.1
V_{G2}	0.95	1.1	1.04	1.088	1.0287	1.1	1.0959	1.0687	1.1
V_{G5}	0.95	1.1	1.01	1.0624	1.0168	1.1	1.079	1.0451	1.0821
V_{G8}	0.95	1.1	1.01	1.0703	1.0779	1.1	1.085	1.054	1.0906
V_{G11}	0.95	1.1	1.05	1.1	0.9999	1.1	1.1	1.0999	1.1
V_{G13}	0.95	1.1	1.05	1.1	0.9955	1.0996	1.098	1.0591	1.0999
TS ₁₁	0.9	1.1	1.078	1.0664	1.0161	0.9827	1.05	1.0773	1.0999
TS ₁₂	0.9	1.1	1.069	0.9	0.9	1.0873	0.95	0.9028	0.9
TS ₁₅	0.9	1.1	1.032	1.0001	0.9379	1.09	1.02	0.9859	1.02
TS ₃₆	0.9	1.1	1.068	0.9735	0.9685	0.981	1.003	0.9763	0.9943
Qc10	0	5	0	0.05	0.05	0.05	0.05	0.0075	0
Qc12	0	5	0	0.05	0	0.05	0.05	0.0453	0.0471
Qc15	0	5	0	0.05	0.05	0.05	0.05	0.0492	0.0485
Qc17	0	5	0	0.05	0	0.05	0.05	0.05	0
Qc20	0	5	0	0.05	0.05	0.05	0.05	0.0428	0.05
Qc21	0	5	0	0.05	0.05	0.05	0.05	0.0499	0.0497
Qc23	0	5	0	0.0392	0.05	0.05	0.0415	0.0301	0.05
Qc24	0	5	0	0.05	0.05	0.05	0.05	0.0499	0.05
Qc29	0	5	0	0.0333	0.0264	0.05	0.0305	0.0288	0.0253
FCM (\$/h)	-	-	902.0046	799.1617	803.4166	800.8527	941.8419	857.2174	942.0814
VDM (p.u.)	-	-	1.1601	1.7309	0.0959	1.7544	1.6891	1.1502	1.6734
VSI (p.u.)			0.1772	0.121	0.1412	0.118	0.1234	0.1282	0.1242
PLM (MW)	-	-	5.8423	8.6451	10.0268	8.7055	3.0589	4.5259	3.0852
ECM (ton/h)	-	-	0.2359	0.3347	0.3332	0.3258	0.2037	0.2263	0.2036
Total Load			202.4	202.4	202.4	202.4	202.4	202.4	202.4
(MW)			283.4	283.4	283.4	283.4	283.4	283.4	283.4
Load Factor			1	1	1	1	1	1	1
(LMS) p.u.			1	1	1	1	1	1	1

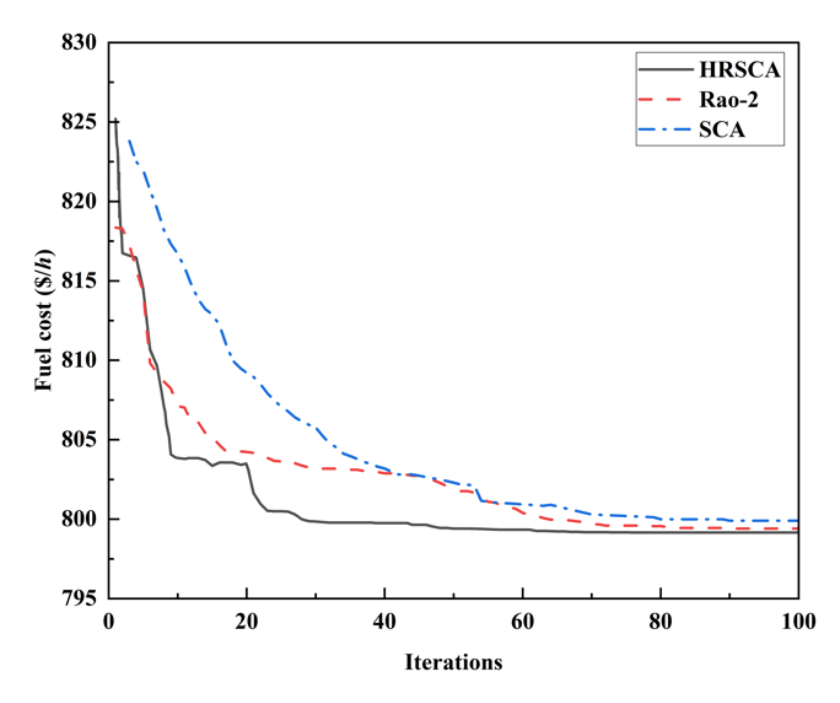


Fig. 5.3 Convergence curves in Case 1 with HRSCA, Rao-2, and SCA

Case 2: VDMFC

This case focuses on minimizing the total voltage deviation (VDM) while simultaneously optimizing the fuel cost (FC), as defined by Equation (5.7). The weighted sum method was employed to combine these objectives. The proposed HRSCA achieves a VD of 0.0959 p.u., representing a substantial reduction of 91.7% compared to the initial case (1.1601 p.u.). The corresponding fuel cost was 803.4166 \$/h, with an associated power loss of 10.0268 MW.

When compared to Case 1, the fuel cost increased slightly by 0.53%, while the VD value decreased significantly by 94.45%, demonstrating a strong trade-off between cost and voltage profile improvement. The proposed technique outperformed results from recent literature, including methods such as SCA (0.1082 p.u., 843.604 \$/h) in Attia et al. (2018), GA (0.1257 p.u., 803.9156 \$/h) in Taher et al. (2019b), TLBO (0.1087 p.u., 804.5827 \$/h) in Taher et al. (2019b), PALO (0.1117 p.u., 850.2739 \$/h) in Mahdad (2020), and various Rao variants by Gupta et al. (2021c).

Although IAOA by Akdag (2022) achieved a marginally better VD value (0.0953 p.u.), it yielded a higher FC value (803.57 \$/h) and required 400 iterations, leading to increased computational burden. Similarly, methods like ISCA by Mahdad and Srairi (2018) and IMOMRFO by in Kahraman et al. (2022) achieved slightly better FC values than HRSCA (802.3510 \$/h and 801.3908 \$/h, respectively); however, their VD values were significantly higher, highlighting their limitations in maintaining an optimal voltage profile.

Figure 5.4 illustrates the voltage profile, showing the distribution of voltage magnitudes at all load buses. The proposed HRSCA demonstrates consistently stable voltage magnitudes close to 1.0 p.u., outperforming the Rao-2 algorithm in maintaining an improved voltage profile. The CV settings are presented in Table 5.4.

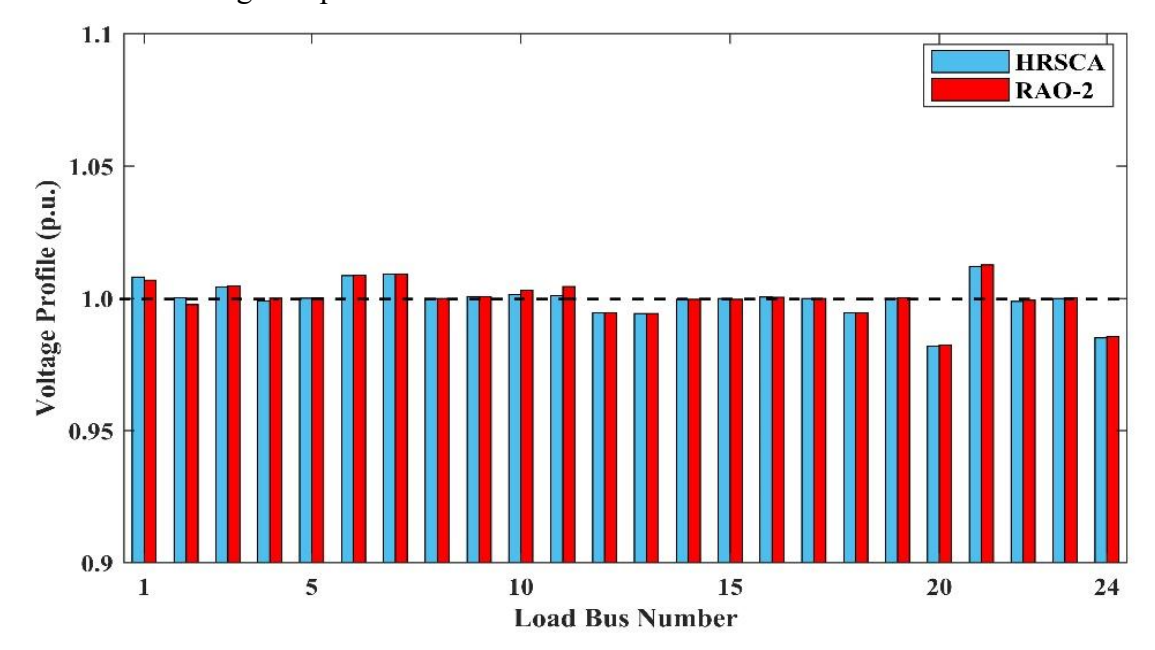


Fig. 5.4 Comparison of voltage profiles in Case 2 using HRSCA and Rao-2 algorithms

Case 3: VSIFC

This case focuses on minimizing the voltage stability index (L-index), as defined by Equation (5.8), while simultaneously addressing FCM and VSI objectives to form a bi-objective function. The proposed HRSCA approach was applied, and the results, along with the CV settings, are presented in Table 5.4.

The achieved L-index value of 0.118 p.u. represents a significant 33.4% reduction compared to the base case (0.1772 p.u.). The corresponding fuel cost is 800.8527 \$/h, reflecting an improvement of 11.2% over the base case. These results outperform those achieved by various optimization methods documented in the literature, including MSA by Mohamed et al. (2017), and MFO, PSO, and TLBO reported by Taher et al. (2019b), along with other recent approaches. Although Rao algorithm variants in Gupta et al. (2021c) achieved slightly better fuel cost values, the proposed hybrid approach delivers a superior L-index, demonstrating its effectiveness in enhancing voltage stability while maintaining competitive fuel cost performance.

Case 4:

(a) PLM

In this case, the objective is to minimize the total real power loss (P_{losses}) as defined by Equation (5.11). Using the proposed HRSCA technique, P_{losses} is reduced to a competitive value of 3.0589 MW, representing a significant 47.64% reduction compared to the initial case (5.8423 MW). The corresponding VD and FC values are 1.6891 p.u. and 941.8419 \$/h, respectively. While the VD experiences a slight increase, the substantial reduction in real power loss highlights the effectiveness of the hybrid approach.

These results outperform several optimization methods documented in the literature, including MSA by Mohamed et al. (2017), MFO by Taher et al. (2019a), PSO by Taher et al. (2019b), Rao-1 by Gupta et al. (2021c), Rao-2 by Gupta et al. (2021c), Rao-3 by Gupta et al. (2021c), and various other widely used approaches. However, MGOA by Taher et al. (2019b) achieves better power loss reduction, but it is associated with higher fuel and emission costs.

Figure 5.5 illustrates the convergence trends for P_{losses} in Case 4(a), comparing the proposed HRSCA with Rao-2 and SCA. The superior performance of HRSCA in minimizing real power loss (PLM) is further validated by its ability to satisfy all operational constraints within their permissible limits.

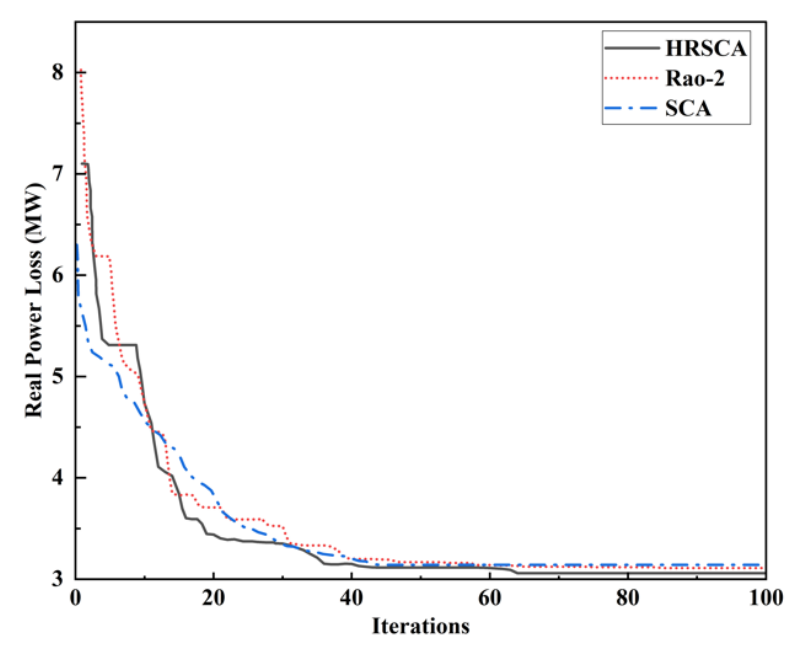


Fig. 5.5 Convergence curve in Case 4 (a) with HRSCA, Rao-2 and SCA algorithms

(b) PLMFC

This case aims to evaluate the effectiveness of the proposed HRSCA in simultaneously minimizing real power loss (P_{losses}) and fuel cost (FC) through a bi-objective formulation defined by Equation (5.29):

$$F_{PLMFC}(x,u) = F_{FCM}(x,u) + K_{pl}F_{PLM}(x,u) + penalty$$
(5.29)

here, K_{pl} represents a weighting factor determined based on the importance assigned to the PLM objective.

The HRSCA results demonstrate an FC value of 857.2174 \$/h and an optimized P_{losses} of 4.5259 MW. These results surpass those obtained by several advanced algorithms, such as ISCA by Mahdad and Srairi (2018), MPSO by Mohamed et al. (2017), MFO by Mohamed et al. (2017), MGOA by Taher et al. (2019b), GOA by Taher et al. (2019b), PSO by Taher et al. (2019b), TLBO by Taher et al. (2019b), and MSA by Taher et al. (2019b). This highlights the capability of HRSCA in handling complex OPF problems with bi-objective formulations.

In comparison, CS-GWO by Meng et al. (2021) achieved an FC of 854.9948 \$/h and P_{losses} of 4.3427 MW, slightly outperforming HRSCA in power loss reduction but requiring more iterations (250 iterations compared to just 100 for HRSCA), leading to increased computational burden. Similarly, the Jaya optimizer by El-Sattar et al. (2019) attained an FC of 817.13 \$/h, but with a significantly higher P_{losses} of 6.04 MW. MOHFPSO by Khan et al. (2020) also achieved lower fuel cost but incurred significantly higher power losses, reflecting a less balanced optimization. Furthermore, MOHFPSO lacked explicit details on optimal population size and iteration count, while the Jaya optimizer utilized 200 iterations. In contrast, the proposed HRSCA effectively balanced both objectives, achieving competitive results within just 100 iterations and with a reduced computational burden. Detailed optimal configurations of control variables for this case are provided in Table 5.4.

Case 5: ECM

In this case, the HRSCA approach focuses on minimizing emissions, as defined by the objective function in Equation (5.12). The algorithm achieves a significant 13.7% reduction in emissions compared to the base case (0.2359 ton/h), lowering the value to 0.2036 ton/h. This performance surpasses several established optimization techniques reported in the literature, including conventional GOA by Taher et al. (2019b), ABC by Adaryani and Karami (2013), PSO, TLBO, MFO (all references from Taher et al. (2019b)), and Rao variants by Gupta et al. (2021c)

Although MGOA by Taher et al. (2019b) exhibited marginally lower emission values, it achieved this at the expense of increased power loss and fuel cost. Additionally, MGOA required a larger population size of 50, compared to 30 in HRSCA, potentially increasing

computational demands. Other leading algorithms, such as IAOA by Akdag (2022) (400 iterations), and IMFO by Taher et al. (2019a) (500 iterations), also required higher computational resources to achieve comparable emission levels. These results demonstrate the effectiveness of HRSCA in achieving a balance between emission reduction and computational efficiency. Figure 5.6 illustrates the convergence curves for emission costs, comparing the performance of HRSCA with Rao-2 and SCA. The proposed method exhibits a superior convergence rate, further affirming its efficiency and stability in minimizing emissions. The CV settings obtained using HRSCA are detailed in Table 5.4.

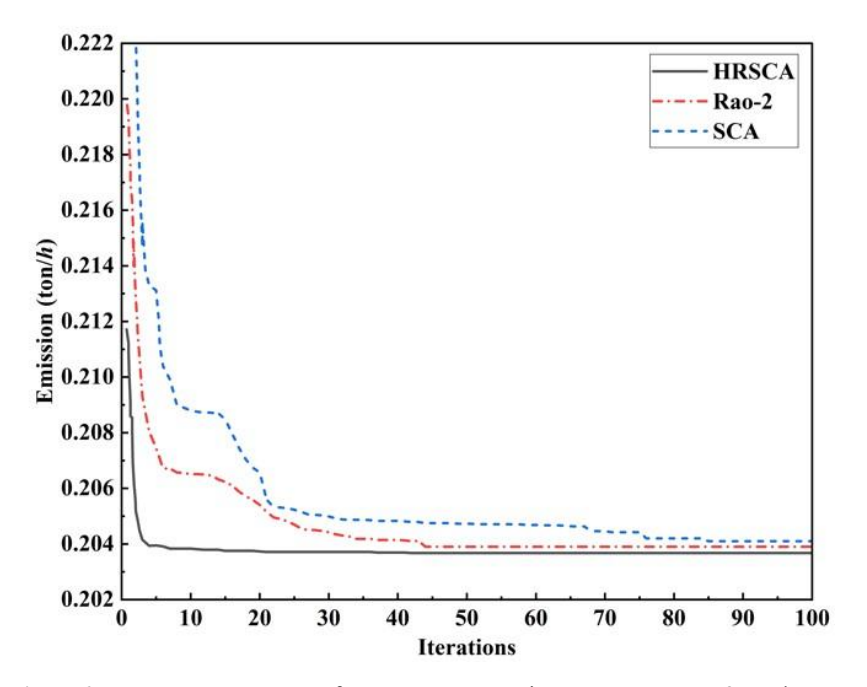


Fig. 5.6 Convergence curves for Case 5 comparing HRSCA, Rao-2, and SCA

5.4.1.2 Scenario-2: OPF Considering Load Growth

Case 6: Optimizing OPF Objectives: Maximizing Loading Factor

This case evaluates the effectiveness of the proposed HRSCA approach in addressing security-constrained OPF under challenging scenarios, such as load growth. Loading Margin Stability (LMS), the technical term for the loading factor, serves as a crucial parameter for evaluating a power system's resilience to increasing load demands. Examining LMS involves gradually increasing the load, which essentially governs the power system's ability to handle load expansion without instability or voltage collapse.

In this case, the load demand (P_D) was elevated to 421.6014 MW, resulting in a corresponding LMS value of 1.487655 p.u. (Mahdad and Srairi, 2015). The proposed HRSCA optimized decision variables within their permissible limits, including generator active powers, generator bus voltages, transformer taps, and shunt compensations. At the specified LMS

value, the proposed approach achieved competitive fuel costs of 1404.716 \$/h, with remarkably low total power loss (13.3886 MW), minimal voltage deviation (1.0072 p.u.), and a significantly reduced L-index (0.1964 p.u.). Furthermore, the HRSCA demonstrated minimal environmental impact with emission levels of 0.3666 ton/h, underscoring its capability to handle load growth while ensuring system stability, operational efficiency, and environmental sustainability.

Table 5.5 provides the optimized CV settings along with the corresponding objective function values, highlighting the effectiveness of the OPFS achieved using the proposed HRSCA approach. System security is maintained by ensuring compliance with the specified maximum apparent power limits ($S_{Line}^{\rm max}$) across 41 branches (detailed in the Appendix A.2). The optimized control vector eliminates the need for load shedding, enabling the seamless delivery of the full 421.6014 MW load to consumers, ensuring a reliable and uninterrupted power supply.

Furthermore, by integrating constraints directly into the OPF formulation, the HRSCA method proactively identifies solutions that minimize the risk of voltage collapse during load growth scenarios. This demonstrates the algorithm's capability to optimize power flow while maintaining system stability and meeting increased electricity demand.

Table 5.5 Optimized control variables obtained for Case 6

CVs	Min	Max	Case 6
P _{G1} (Slack) (MW)	50	200	199.99
P_{G2}	20	80	80
P_{G5}	15	50	50
P_{G8}	10	35	35
P _{G11}	10	30	30
P _{G13}	12	40	40
V _{Gl} (p.u.)	0.95	1.1	1.1
$V_{\rm G2}$	0.95	1.1	1.0881
V_{G5}	0.95	1.1	1.06
V_{G8}	0.95	1.1	1.0662
V_{G11}	0.95	1.1	1.1
V_{G13}	0.95	1.1	1.0999
TS ₆₋₉ (p.u.)	0.9	1.1	1.092
TS ₆₋₁₀	0.9	1.1	0.9
TS ₄₋₁₂	0.9	1.1	1.0509
TS ₂₈₋₂₇	0.9	1.1	0.97
Qc10 (MVAR)	0	5	5
Qc12	0	5	4.91

Qc15	0	5	4.88
Qc17	0	5	5
Qc20	0	5	4.94
Qc21	0	5	4.83
Qc23	0	5	5
Qc24	0	5	4.97
Qc29	0	5	4.98
FCM (\$/h)	-	-	1404.716
VDM (p.u.)	-	-	1.0072
VSI (p.u.)	-	-	0.1964
PLM (MW)	-	-	13.3886
ECM (ton/h)	-	-	0.3666
Total Load Demand, PD in MW	-	-	421.6014
Load Factor (LMS) in p.u.			1.487655

5.4.1.3 Scenario-3: Security OPF Considering Load Growth and Unexpected Outages at Generating Units

The current scenario examines two significant unforeseen events: the system being pushed to its load stability limit and the contingency of generator outage. This scenario assesses the proficiency of the HRSCA method suggested in improving the quality of energy supplied to consumers under critical conditions. The primary objective is to ensure system resilience against blackouts, maintaining continuous service amidst load growth and addressing faults at two specified generating units.

The HRSCA approach has been shown to be an effective strategy for minimizing critical load shedding during key events, ensuring that essential services remain operational. It successfully meets multiple objectives spanning economic (FCM), technical (VDM, VSI, and PLM), and environmental (ECM) domains. These outcomes are achieved through the strategic optimization of control variables while maintaining the stability and security of the system under severe contingencies.

To safeguard the system's operational security, load shedding measures were strategically implemented at buses 5 and 8, reducing the stress on critical components and ensuring a balanced power flow across the network. This also facilitates secure transmission of power in branches, preventing overloading and reducing the risk of voltage collapse. Furthermore, this approach enables a comparative study with previously reported methods in the literature, highlighting the advantages of HRSCA in maintaining system stability, minimizing disruptions, and achieving superior performance metrics in critical scenarios.

Case 7: Faults Occurred Simultaneously at G2 and G11

This case examines the impact of simultaneous faults at generators G2 and G11. To mitigate the consequences of these contingencies, the proposed HRSCA approach optimizes CVs to minimize disruptions in power delivery to consumers. An optimized power flow scheme (OPFS) was achieved, with the details of CV settings provided in Table 5.6 (Case 7).

In this critical scenario, the load demand (P_D) was adjusted to 309.7998 MW, corresponding to a load factor of 1.0932 relative to P_D as reported by Mahdad and Srairi. At bus 5, the optimized active and reactive power demands were 46.7124 MW and 9.4218 MVAR, respectively. Similarly, at bus 8, the active and reactive power requirements were optimized to 26.2527 MW and 26.2527 MVAR, respectively. By maintaining the load factor of 1.0932, the proposed HRSCA approach successfully upheld the economic (FCM) objective at 1021.6998 \$/h and achieved a power loss minimization (PLM) value of 9.8845 MW. The environmental objective (ECM) was also optimized, reaching a value of 0.3726 ton/h.

Table 5.6 further presents the optimized values for other technical objectives, including VDM and VSI. The performance of the proposed approach was compared to that of the grey wolf optimizer with pattern search (GWO-PS) strategy under the same generation contingency scenario, as described by Mahdad and Srairi. The comparison revealed that while maintaining the identical load factor, the proposed HRSCA method achieved a slight improvement of 0.03% in the FCM objective and a 1.06% enhancement in the PLM objective. However, GWO-PS demonstrated a marginally better voltage deviation value of 0.4794 p.u. It is worth mentioning that GWO-PS required twice the number of iterations compared to HRSCA, and its population size was not explicitly reported.

 Table 5.6
 Optimized control variables for Case 7 and Case 8 for IEEE 30-bus test system (Scenario-3)

CVs	Case 7	Case 8
P _{G1} (Slack) (MW)	194.6843	196.8214
P_{G2}	0	0
P _{G5}	50	50
P_{G8}	35	35
PG11	0	30
P_{G13}	40	0
V _{G1} (p.u.)	1.1	1.1
V_{G2}	0.99	1.08
V_{G5}	1.09	1.08
V_{G8}	1.1	1.07
V _{G11}	1.1	1.08

V _{G13}	1.0996	1.09
TS ₆₋₉ (p.u.)	1.1	1.06
TS ₆₋₁₀	0.92	0.99
TS4-12	1.1	1.01
TS ₂₈₋₂₇	1.04	1.02
Qc10 (p.u.)	0.05	0.05
Qc12	0.05	0.05
Qc15	0.049	0.05
Qc17	0.05	0.05
Qc20	0.05	0.05
Qc21	0.05	0.05
Qc23	0.05	0.05
Qc24	0.05	0.05
Qc29	0.04	0.05
FCM (\$/h)	1021.6998	982.8172
VDM (p.u.)	0.6377	0.7239
VSI (p.u.)	0.2187	0.2091
PLM (MW)	9.8845	9.4336
ECM (ton/h)	0.3726	0.3802
Total Load Demand, PD in MW	309.7998	302.3878
Load Factor (LMS) in p.u.	1.0932	1.067

Case 8: Faults Occurred Simultaneously at G2 and G13

This case examines the occurrence of simultaneous faults at generators G2 and G13. To mitigate disruptions to consumer power delivery, an OPFS was achieved by adjusting the CVs while maintaining the same load demand ($P_D = 302.3878$ MW) as reported in by Mahdad and Srairi, corresponding to an LMS value of 1.067 p.u.

At bus 5, the active power demand was set at 40.0392 MW, with the corresponding reactive power demand set at 8.0758 MVAR. Similarly, at bus 8, the active power requirement was fixed at 25.5027 MW, and the corresponding reactive power demand was fixed at 25.5027 MVAR. The FCM objective attained a competitive value of 982.8172 \$/h, demonstrating the algorithm's efficiency in economic optimization.

The proposed HRSCA approach achieves a 3.46% improvement in PLM, compared to the 9.772 MW reported by Mahdad and Srairi, under identical fault and loading conditions. Furthermore, Table 5.6 presents optimized results for other technical objectives, including VDM and VSI, as well as the environmental objective (ECM).

Strict adherence to security constraints has been a priority throughout this scenario, ensuring reliable and secure power system operation even in the face of concurrent generator faults.

These results underscore the robustness and reliability of the proposed HRSCA approach in handling challenging contingencies while achieving a balanced optimization of economic, technical, and environmental objectives.

5.4.2 Performance on IEEE 118-Bus Test System

The scalability of the proposed HRSCA approach is evaluated using the IEEE 118-bus standard test system. This network includes 54 generating units, an active power demand of 4242 MW, and a reactive power loading of 1438 MVAR. The system comprises 186 branches and 64 load buses, with an acceptable voltage range at load buses between 0.94 p.u and 1.06 p.u.

The network features 9 transformers strategically positioned along lines 8-5, 26-25, 30-17, 38-37, 63-59, 64-61, 65-66, 68-69, and 81-80. Additionally, 14 buses are equipped with shunt VAR compensators to enhance voltage regulation and stability. Detailed load data, line data, bus data, and control variable bounds for the IEEE 118-bus system, based on a 100 MVA base, can be found in Christie (1993). Additionally, cost coefficients and generation limits for the system can be found in Appendix A, Table A.3.

5.4.2.1 Scenario-1: Standard OPF

This scenario involves conducting a standard OPF analysis on the IEEE 118-bus test system. Three distinct single-objective cases are evaluated. These cases These cases aim to minimize total FC, VD, and P_{losses} . The objective of this scenario is to benchmark the outcomes of the proposed HRSCA approach under normal operating conditions against those obtained using recently developed optimization techniques.

The three cases considered in this scenario are as follows:

Case 9: Fuel Cost Minimization (FCM)

Case 10: Voltage Deviation Minimization (VDM)

Case 11: Power Loss Minimization (PLM)

Case 9: FCM

In this case, the total fuel cost (FC) is minimized under normal operating conditions of the power grid. The OPF results obtained using the proposed HRSCA approach, including initial values and optimized control variables (CVs), are presented in Table 5.7. The HRSCA achieved the lowest FC value of 129,088.6331 \$/h, exhibiting a significant 1.62% enhancement over the base case (131,220.52 \$/h) and a 0.13% improvement over the results obtained using the

standalone Rao-2 algorithm (129,256.5242 \$/h). Furthermore, the HRSCA outperformed other recent methods documented in the literature, as illustrated in Table 5.8.

The proposed HRSCA approach exhibits smooth and rapid convergence, achieving optimal results in just 150 iterations, which underscores its stability and suitability for larger systems. This superior performance is illustrated using convergence curves in Fig. 5.7. The cost coefficients for all generators are available in reference Zimmerman et al. (2006).

 Table 5.7 Optimized control variables obtained by HRSCA for IEEE 118-bus test system

S.	CVs	Base	Н	RSCA for (OPF	S.	CVs	Base	Н	HRSCA for OPF		
No.	(p.u.)	p.u.) case value	Case 9	Case 10	Case 11	No.	(p.u.)	case value	Case 9	Case 10	Case 11	
1	P_{G1}	0	0.0887	0.6338	0.3336	69	$V_{\rm G34}$	0.984	0.9601	1.0154	1.0333	
2	P_{G4}	0	0.006	0.363	0.4876	70	V_{G36}	0.98	0.9608	0.9991	1.0285	
3	P_{G6}	0	0.0481	0.2907	0.3583	71	V_{G40}	0.97	0.9415	1.0108	1.0152	
4	P_{G8}	0	0.4327	0.7127	0.7986	72	V_{G42}	0.985	0.9912	0.9896	1.0243	
5	P_{G10}	4.5	4.0618	2.8383	0.6452	73	V_{G46}	1.005	0.9781	0.953	1.0223	
6	P_{G12}	0.85	0.8109	0.1203	1.846	74	V_{G49}	1.025	1.0285	1.0216	1.0157	
7	P_{G15}	0	0.111	0.082	0.9879	75	V_{G54}	0.955	1.0595	1.0117	1.0073	
8	P_{G18}	0	0.0575	0.207	0.077	76	V_{G55}	0.952	1.059	1.0426	1.009	
9	P_{G19}	0	0.0055	0.8547	0.7804	77	V_{G56}	0.954	1.0599	1.0011	1.0084	
10	P_{G24}	0	0.056	0.5375	0.0198	78	V_{G59}	0.985	1.0555	0.9608	1.014	
11	P_{G25}	2.2	2.127	2.004	0.2455	79	V_{G61}	0.995	1.0396	1.0117	1.0158	
12	P_{G26}	3.14	2.6122	3.543	0.09	80	V_{G62}	0.998	1.0589	0.9922	1.011	
13	P_{G27}	0	0.0542	0.6096	0.9738	81	V_{G65}	1.005	0.94	0.9479	1.0463	
14	P_{G31}	0.07	0.0352	0.4846	0.9215	82	V_{G66}	1.05	1.0361	1.0072	1.015	
15	P_{G32}	0	0.8643	0.5266	0.4844	83	V_{G69}	1.035	1.0442	1.0317	1.0162	
16	P_{G34}	0	0.2089	0.9619	0.7468	84	V_{G70}	0.984	1.0358	0.989	1.0225	
17	P_{G36}	0	0	0.8679	0.8009	85	V_{G72}	0.98	0.9793	1.0053	1.0028	
18	P_{G40}	0	0.454	0.566	0.528	86	V_{G73}	0.991	0.944	1.0144	1.0085	
19	P_{G42}	0	0.3999	0.9878	0.9771	87	V_{G74}	0.958	1.0253	0.9976	1.0222	
20	P_{G46}	0.19	0.209	0.1769	1.0097	88	V_{G76}	0.943	1.0345	1.0087	1.0068	
21	P_{G49}	2.04	1.7846	1.2358	2.1007	89	V_{G77}	1.006	1.0326	1.0086	1.0005	
22	P_{G54}	0.48	0.481	0.8783	1.1985	90	V_{G80}	1.04	1.0479	1.0177	0.9891	
23	P_{G55}	0	0.0172	0.7102	0.9444	91	V_{G85}	0.985	0.9532	1.0113	1.0172	
24	P_{G56}	0	0.1751	0.6521	0.6943	92	V_{G87}	1.015	0.945	0.9898	1.0585	
25	P_{G59}	1.55	1.6021	1.8801	2.5281	93	V_{G89}	1.005	1.0392	1.0053	1.0227	
26	P_{G61}	1.6	1.5558	2.4447	1.0179	94	V_{G90}	0.985	1.0192	1.0013	1.0123	
27	P_{G62}	0	0.007	0.3421	0.4286	95	V_{G91}	0.98	1.034	1.059	1.0082	
28	P_{G65}	3.91	3.9943	2.9204	1.5621	96	V_{G92}	0.99	1.0599	1.0154	1.0201	
29	P_{G66}	3.92	3.547	0.8149	0.7446	97	V_{G99}	1.01	1.026	1.0564	0.9839	
30	P_{G70}	0	0.0215	0.036	0.4266	98	V_{G100}	1.017	1.0397	1.0001	0.9892	
31	P_{G72}	0	0.0096	0.0475	0.0333	99	V_{G103}	1.01	1.0082	1.0491	0.9937	
32	P_{G73}	0	0.094	0.3391	0.4116	100	V_{G104}	0.971	1.0498	0.9794	0.9741	
33	P_{G74}	0	0.059	0.0036	0.9526	101	V_{G105}	0.965	1.0481	1.0028	0.9851	
34	P_{G76}	0	0.2163	0.4545	0.9344	102	V_{G107}	0.952	1.0583	1.0178	0.9979	
35	P_{G77}	0	0.0004	0.1098	0.9426	103	V_{G110}	0.973	1.0065	0.9984	1.0012	
36	P_{G80}	4.77	4.0965	0.7462	2.6551	104	V_{G111}	0.98	0.9401	0.9422	1.0048	
37	P_{G85}	0	0.068	0.1934	0.6619	105	V_{G112}	0.975	0.9939	0.9976	0.9991	
38	P_{G87}	0.04	0.0213	0.5328	0.2136	106	V_{G113}	0.993	1.0064	1.0046	1.0443	
39	P_{G89}	6.07	4.4969	1.1472	1.8227	107	V_{G116}	1.005	0.95	0.999	1.0581	
40	P_{G90}	0	0.0064	0.6778	0.9731	108	T _{5—8}	0.985	0.9006	0.9939	0.9673	
41	P_{G91}	0	0.0219	0.013	0.16	109	T ₂₆₋₂₅	0.96	1.1	0.9871	1.0066	
42	P_{G92}	0	0.0185	0.572	0.7758	110	T _{30—17}	0.96	0.9241	0.9814	0.9512	
43	P_{G99}	0	0.0035	0.7987	0.5345	111	T _{38—37}	0.935	0.9002	0.9615	0.9704	
44	P_{G100}	2.52	1.9039	1.7001	1.2773	112	T _{63—59}	0.96	1.1	1.0458	0.9648	
45	P_{G103}	0.4	0.3708	0.395	0.5924	113	T ₆₄₋₆₁	0.985	1.0444	1.0115	0.9944	

$ \begin{array}{c ccccccccccccccccccccccccccccccccccc$	46	I -	1.0	0.0045	0.6065	0.500		T	0.025		0.0001	1.0551
$ \begin{array}{c ccccccccccccccccccccccccccccccccccc$	46	P_{G104}	0	0.0045	0.6965	0.509	114	T _{65—66}	0.935	1.1	0.9921	1.0771
$ \begin{array}{c ccccccccccccccccccccccccccccccccccc$	47	P_{G105}	0	0.698	0.0082	0.2089	115	T _{68—69}	0.935	0.9035	1.0398	1.0247
$ \begin{array}{c ccccccccccccccccccccccccccccccccccc$	48	$P_{\rm G107}$	0	0.0135	0.8418	0.4539	116	T _{81—80}	0.935	1.0933	0.9629	1.0166
$ \begin{array}{c ccccccccccccccccccccccccccccccccccc$	49	P_{G110}	0	0.3242	0.1637	0.188	117	Q_{C5}	0	0.0409	0.2987	0.1822
$ \begin{array}{c ccccccccccccccccccccccccccccccccccc$	50	P_{G111}	0.36	0.1726	0.6973	0.2619	118	Q _{C34}	0	0.2517	0.0767	0.2939
$ \begin{array}{c ccccccccccccccccccccccccccccccccccc$	51		0	0.0077	0.6912	0.6553	119	Q _{C37}	0	0.2963	0.0062	0.1119
$ \begin{array}{c ccccccccccccccccccccccccccccccccccc$	52	P_{G113}	0	0	0.5889	0.9863	120	Q _{C44}	0	0.0024	0.2481	0.0815
$ \begin{array}{c ccccccccccccccccccccccccccccccccccc$	53	P_{G116}	0	0.0412	0.927	0.6019	121	Q _{C45}	0	0.0902	0.0949	0.2804
$ \begin{array}{c ccccccccccccccccccccccccccccccccccc$	54		0.995	0.9461	0.9925	1.0237	122	Q_{C46}	0	0.0028	0.1842	0.2498
$\begin{array}{c ccccccccccccccccccccccccccccccccccc$	55	V_{G4}	0.998	1.0078	1.0038	1.0019	123	Q _{C48}	0	0.0052	0.0345	0.2216
$\begin{array}{c ccccccccccccccccccccccccccccccccccc$	56	V_{G6}	0.99	1	0.9946	0.9982	124	Q _{C74}	0	0.2978	0.004	0.2883
59 V _{G12} 0.99 0.9765 1.0103 1.0186 127 Q _{C83} 0 0.2899 0.175 0.0663 60 V _{G15} 0.97 0.991 0.98 1.0241 128 Q _{C105} 0 0.0045 0.1243 0.1578 61 V _{G18} 0.973 0.9899 0.9588 1.0293 129 Q _{C107} 0 0.192 0.2035 0.296 62 V _{G19} 0.962 0.9855 1.0171 1.028 130 Q _{C110} 0 0.0646 0.2983 0.0965 63 V _{G24} 0.992 0.9761 0.9837 1.0344 FCM (\$/h) 131220.52 129088.6331 154690.85 165878.7 64 V _{G25} 1.05 1.0589 1.0112 1.0307 VDM (p.u.) 1.4389 1.8975 0.4720 1.133 65 V _{G26} 1.015 1.0475 0.978 1.0028 PLM (MW) 132.8101 112.2514 101.1812 19.2766	57	V_{G8}	1.015	0.9898	0.9799	0.9948	125	Qc79	0	0.2995	0.1412	0.2868
60 V _{G15} 0.97 0.991 0.98 1.0241 128 Q _{C105} 0 0.0045 0.1243 0.1578 61 V _{G18} 0.973 0.9899 0.9588 1.0293 129 Q _{C107} 0 0.192 0.2035 0.296 62 V _{G19} 0.962 0.9855 1.0171 1.028 130 Q _{C110} 0 0.0646 0.2983 0.0965 63 V _{G24} 0.992 0.9761 0.9837 1.0344 FCM (\$/h) 131220.52 129088.6331 154690.85 165878.7 64 V _{G25} 1.05 1.0589 1.0112 1.0307 VDM (p.u.) 1.4389 1.8975 0.4720 1.133 65 V _{G26} 1.015 1.0475 0.978 1.0028 PLM (MW) 132.8101 112.2514 101.1812 19.2766 66 V _{G27} 0.968 1.0141 0.9956 1.0387 Load Factor (p.u.) 1 1 1 1 1 1	58	V_{G10}	1.05	1.0073	0.9541	1.0047	126	Q_{C82}	0	0.2995	0.0291	0.0977
$\begin{array}{c ccccccccccccccccccccccccccccccccccc$	59	V_{G12}	0.99	0.9765	1.0103	1.0186	127	Q _{C83}	0	0.2899	0.175	0.0663
62 V_{G19} 0.962 0.9855 1.0171 1.028 130 Q_{C110} 0 0.0646 0.2983 0.0965 63 V_{G24} 0.992 0.9761 0.9837 1.0344 FCM (\$/h) 131220.52 129088.6331 154690.85 165878.7 64 V_{G25} 1.05 1.0589 1.0112 1.0307 VDM (p.u.) 1.4389 1.8975 0.4720 1.133 65 V_{G26} 1.015 1.0475 0.978 1.0028 PLM (MW) 132.8101 112.2514 101.1812 19.2766 66 V_{G27} 0.968 1.0141 0.9956 1.0387 Load Factor (p.u.) 1	60	V_{G15}	0.97	0.991	0.98	1.0241	128	Q _{C105}	0	0.0045	0.1243	0.1578
62 V_{G19} 0.962 0.9855 1.0171 1.028 130 Q_{C110} 0 0.0646 0.2983 0.0965 63 V_{G24} 0.992 0.9761 0.9837 1.0344 FCM (\$/h) 131220.52 129088.6331 154690.85 165878.7 64 V_{G25} 1.05 1.0589 1.0112 1.0307 VDM (p.u.) 1.4389 1.8975 0.4720 1.133 65 V_{G26} 1.015 1.0475 0.978 1.0028 PLM (MW) 132.8101 112.2514 101.1812 19.2766 66 V_{G27} 0.968 1.0141 0.9956 1.0387 Load Factor (p.u.) 1	61	V_{G18}	0.973	0.9899	0.9588	1.0293	129	Q _{C107}	0	0.192	0.2035	0.296
64 V _{G25} 1.05 1.0589 1.0112 1.0307 VDM (p.u.) 1.4389 1.8975 0.4720 1.133 65 V _{G26} 1.015 1.0475 0.978 1.0028 PLM (MW) 132.8101 112.2514 101.1812 19.2766 66 V _{G27} 0.968 1.0141 0.9956 1.0387 Load Factor (p.u.) 1 1 1 1 1 1 1 1 1 1 1 1 1 1 1 1 1 1 1	62	V_{G19}	0.962	0.9855	1.0171	1.028	130	Q _{C110}	0	0.0646	0.2983	0.0965
65 V _{G26} 1.015 1.0475 0.978 1.0028 PLM (MW) 132.8101 112.2514 101.1812 19.2766 66 V _{G27} 0.968 1.0141 0.9956 1.0387 Load Factor (p.u.) 1 1 1 1 1 1 1 1 67 V _{G31} 0.967 1.028 1.0139 1.0586 Slack Power 513.8101 502.5673 1.77.6589 107.5023	63	$V_{\rm G24}$	0.992	0.9761	0.9837	1.0344	FCM ((\$/h)	131220.52	129088.6331	154690.85	165878.7
66 V _{G27} 0.968 1.0141 0.9956 1.0387 Load Factor (p.u.) 1 1 1 1 1 1 67 V _{G31} 0.967 1.028 1.0139 1.0586 Slack Power 513 8101 502 5673 177 6589 107 5023	64	V_{G25}	1.05	1.0589	1.0112	1.0307	VDM	(p.u.)	1.4389	1.8975	0.4720	1.133
66 V _{G27} 0.968 1.0141 0.9956 1.0387 (p.u.) 1 1 1 1 1 1 1 1 1 1 1 1 1 1 1 1 1 1 1	65	$V_{\rm G26}$	1.015	1.0475	0.978	1.0028	PLM (MW)	132.8101	112.2514	101.1812	19.2766
513.8101 502.5673 177.6589 107.5023	66	V_{G27}	0.968	1.0141	0.9956	1.0387		Factor	1	1	1	1
68 V _{G32} 0.963 1.0108 1.0125 1.0453 (P _{G69}) (MW) 313.8101 302.3673 177.6389 107.3023	67	V_{G31}	0.967	1.028	1.0139	1.0586	Slack	Power	512 9101	502 5672	177 6590	107 5022
	68	V_{G32}	0.963	1.0108	1.0125	1.0453	(P_{G69}) ((MW)	313.6101	302.3073	1//.0389	107.3023

 Table 5.8 Comparison of HRSCA, Rao-2, SCA, and other algorithms for FCM in Case 9

Algorithm	Case 9: FCM (\$/h)	Algorithm	Case 9: FCM (\$/h)	Algorithm	Case 9: FCM (\$/h)
HRSCA	129088.6331	CS-GWO (Meng et al. 2021)	129544.01	SKH (Pulluri et al. 2017a)	129727.6248
Rao-2	129256.5242	SSA (Jebaraj and Sakthivel, 2022)	129561.0305	KH (Pulluri et al. 2017a)	129754.8130
Chaotic Rao-2 (Warid, 2022)	129385.643	MSCA (Attia et al. 2018)	129620.22	PSOGSA (Reddy, 2019)	129733.58
SCM-MJ (Gupta et al. 2021b)	129171.96	SCA (Attia et al. 2018)	129622.6500	PSO (Bouchekara et al. 2014a)	129756.2275
Jaya-PPS1 (Gupta et al. 2021a)	129221.889	MSA (Mohamed et al. 2017)	129640.7191	GSA (Reddy, 2019)	129873.89
Rao-1 (Gupta et al. 2021c)	129241.1787	TLBO (Bouchekara et al. 2014a)	129682.844	NISSO (Nguyen, 2019)	129879.4536
Rao-2 (Gupta et al. 2021c)	129256.5242	DSA (Bouchekara et al. 2014a)	129691.6152	MPSO (Mohamed et al. 2017)	132039.212
Rao-3 (Gupta et al. 2021c)	129220.6794	FPA (Mohamed et al. 2017)	129688.7209	GA (Bouchekara et al. 2014a)	132746.3517
M-Jaya (Gupta et al., 2021b)	129248.10	MFO (Mohamed et al. 2017)	129708.0821		

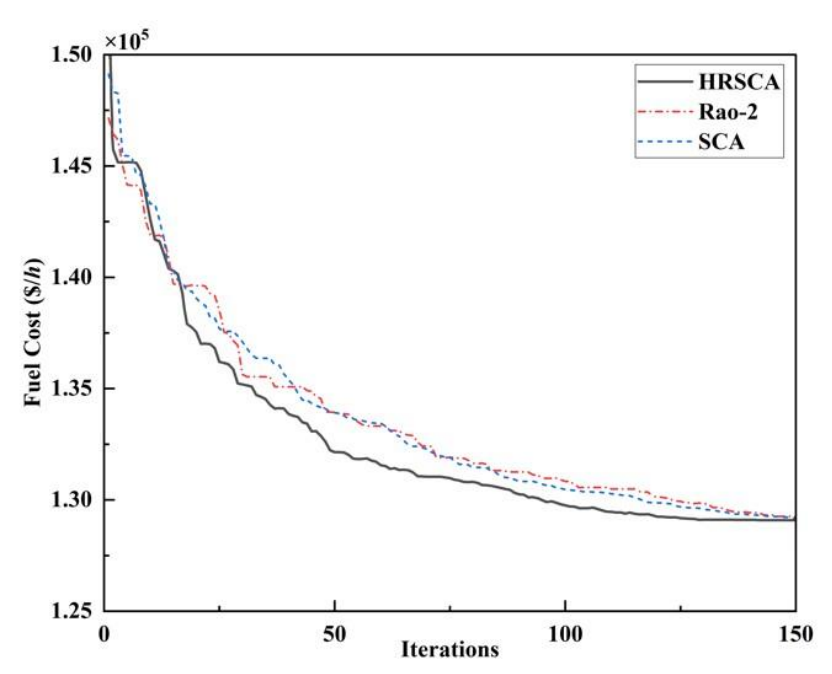


Fig. 5.7 Convergence curve in Case 9 with HRSCA, Rao-2 and SCA

Case 10: VDM

The primary objective in this case is to minimize voltage deviation (VD) in the large-scale 118-bus system under normal operating conditions. The proposed HRSCA approach achieves a minimum VD value of 0.4720 p.u., significantly improving upon both the base case (1.4389 p.u.) and the results of Case 9 (1.8975 p.u.). The corresponding power loss is measured at 101.1812 MW. Detailed optimized CV settings and objective function values are provided in Table 5.7.

The performance of HRSCA surpasses that of several algorithms reported in the literature, including MSCA (0.995 p.u.) (Attia et al. 2018), SCA (1.32 p.u.) (Attia et al. 2018), M-Jaya (0.6771 p.u.) (Gupta et al. 2021b), and SSA (0.6078 p.u.) (Jebaraj and Sakthivel, 2022). It is also competitive with DE-APSO-PS (0.4364 p.u.) (Mahdad and Srairi, 2014), SCM-MJ (0.4366 p.u.) (Gupta et al. 2021b), and ISCA (0.454 p.u. with t_{max} =200) (Mahdad and Srairi, 2018). Furthermore, while the DE-APSO-PS algorithm exhibits competitive performance, key control parameters such as population size and the maximum number of iterations (t_{max}) are not explicitly reported in the study, limiting direct comparability.

It's important to mention here that only a few metaheuristic approaches have been explored in the literature for optimizing this specific objective function withing the 118-bus system, underscoring the significance of HRSCA's results. Figure 5.8(a) provides a visual representation of the voltage profiles across all load buses, while Fig. 5.8(b) illustrates the

convergence characteristics of voltage deviation for the proposed HRSCA in comparison to Rao-2 and SCA algorithm.

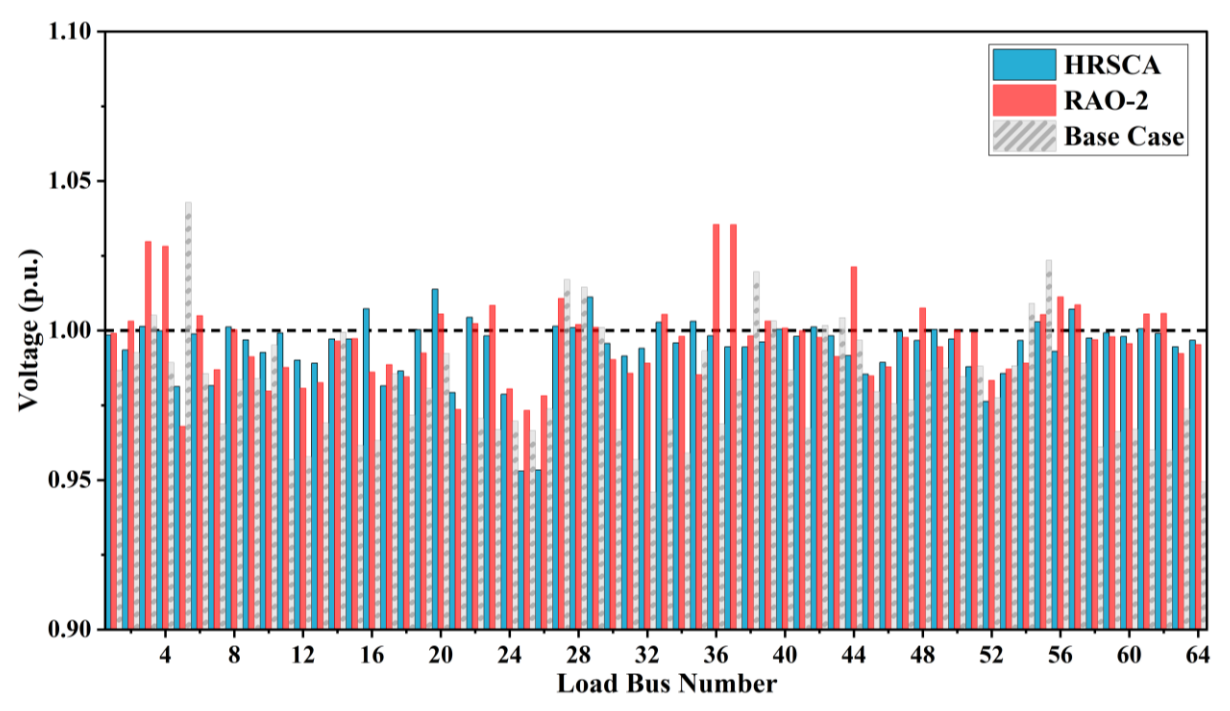


Fig. 5.8(a) Comparison of voltage profiles in Case 10 using HRSCA, Rao-2, and the base case

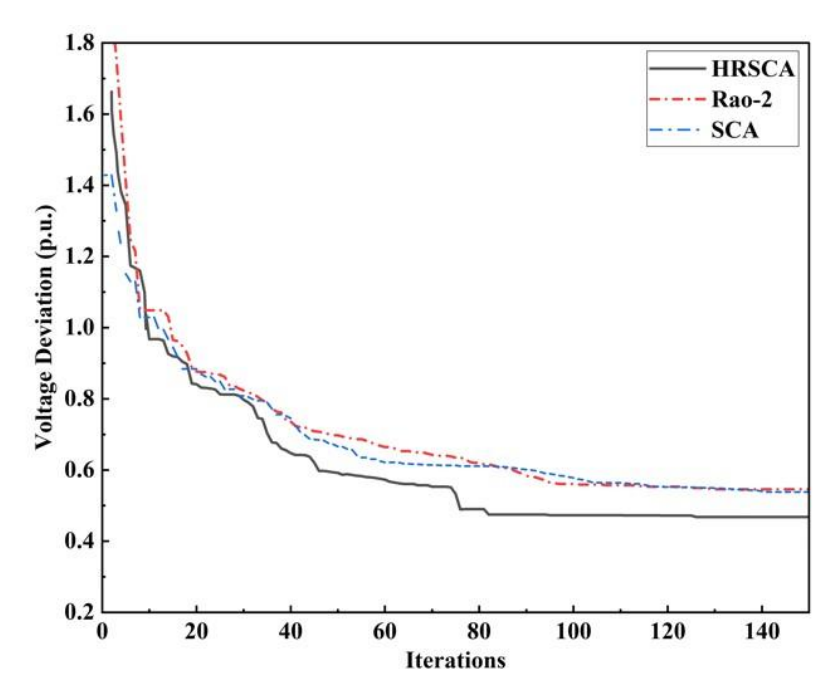


Fig. 5.8(b) Convergence curves for Case 10 comparing HRSCA, Rao-2, and SCA

Case 11: PLM

In Case 11, the primary objective is the independent minimization of power loss (P_{losses}), as described in Case 4 part (a). Under normal operating conditions, the optimized CV settings

obtained using the proposed HRSCA approach are detailed in Table 5.7. The P_{losses} achieved by HRSCA is 19.2766 MW, representing a substantial 85.4% reduction compared to the base case power loss of 132.8101 MW. Additionally, the corresponding voltage deviation of 1.133 p.u. reflects a 21.2% improvement over the base case. To further validate the effectiveness of HRSCA, Table 5.9 provides a comparative analysis with Rao-2 algorithm, SCA, and other state-of-the-art optimization algorithms documented in the literature. Figure 5.9 illustrates the convergence characteristics of the proposed HRSCA in comparison to Rao-2 and SCA, highlighting the efficiency and rapid convergence of the hybrid approach.

Table 5.9 Comparing HRSCA with Rao-2 and other leading algorithms for PLM in Case 11

Algorithm	Case 11: PLM (MW)
HRSCA	19.2766
Rao-2	25.1265
Chaotic Rao-2 (Warid, 2022)	36.483
SCM-MJ (Gupta et al. 2021b)	19.1525
M-Jaya (Gupta et al. 2021b)	21.6419
SKH (Pulluri et al. 2017a)	22.1397
KH (Pulluri et al. 2017a)	23.3212
SSA (Jebaraj and Sakthivel, 2022)	30.7826
QOTLBO (Mandal and Roy, 2014)	35.3191
TLBO (Mandal and Roy, 2014)	36.8482
MSCA (Attia et al. 2018)	77.0873
SCA (Attia et al. 2018)	77.1113
BBO (Roy et al. 2010)	128.9700
PSO (Roy et al. 2010)	131.9146

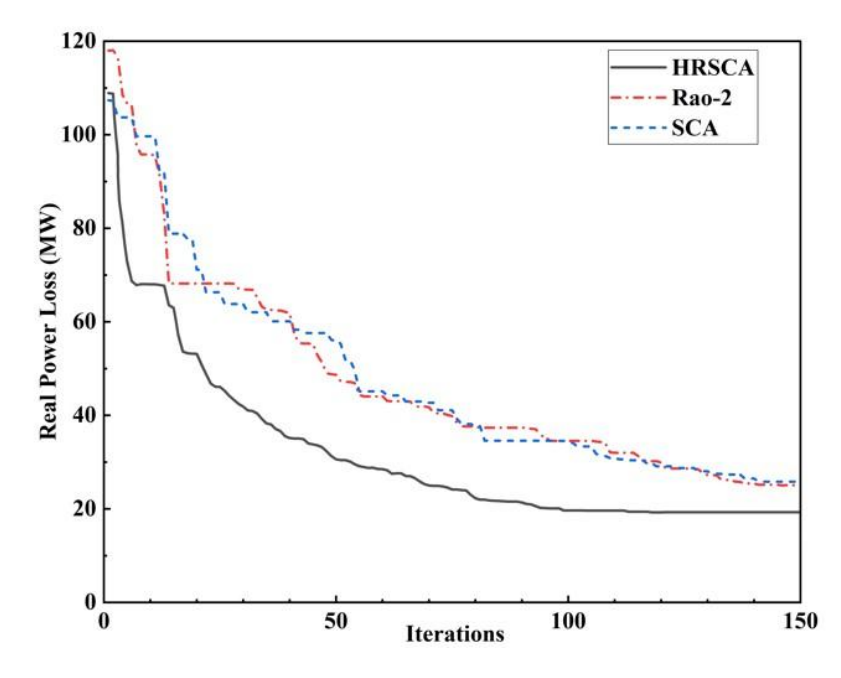


Fig. 5.9 Convergence curves for Case 11 comparing HRSCA, Rao-2, and SCA

5.4.2.2 Scenario-2: Security OPF considering load growth

Case 12: Optimizing OPF Objectives: Minimizing Power Loss under Maximum Specified Load Factor

In this scenario, the IEEE 118-bus system experiences load growth while maintaining the specified load demand ($P_D = 7033.236$ MW) as outlined in Mahdad and Srairi (2014). This results in an LMS value of 1.658 p.u., with the primary objective being the minimization of power loss (P_{losses}) under the PLM objective.

The proposed HRSCA approach achieves an optimized power flow by adjusting CVs, as detailed in Table 5.10, which also presents the corresponding objective function values. The P_{losses} obtained by HRSCA is 81.8483 MW at the given loadability value, while the achieved VD is 1.1412 p.u., ensuring all bus voltages remain within prescribed limits. For comparison, the same scenario reported by Mahdad and Srairi (2014) resulted in P_{losses} = 82.8415MW. The proposed HRSCA strategy achieves a 1.19% improvement over the earlier technique (DE-APSO-PS technique by Mahdad and Srairi), demonstrating its robustness and effectiveness in addressing complex OPF problems under high-load conditions.

Table 5.10 Optimized control variables in Case 12 with PLM Objective at LF = 1.658 p.u.

S. No.	CVs (p.u.)	Optimized value (Case 12)	S. No.	CVs (p.u.)	Optimized value (Case 12)	S. No.	CVs (p.u.)	Optimized value (Case 12)
1	P_{G1}	0.9895	46	P _{G104}	0.2499	91	V_{G85}	1.0472
2	P_{G4}	0.9785	47	P _{G105}	0.9222	92	V_{G87}	1.0092
3	P_{G6}	0.0795	48	P_{G107}	0.6787	93	V_{G89}	1.0359
4	P_{G8}	0.9565	49	P _{G110}	0.7547	94	V_{G90}	0.9845
5	P_{G10}	1.9652	50	P _{G111}	0.0098	95	V_{G91}	0.9425
6	P_{G12}	1.8497	51	P _{G112}	0.9945	96	V_{G92}	1.0103
7	P _{G15}	0.9359	52	P _{G113}	1	97	V_{G99}	1.0107
8	P_{G18}	1	53	P _{G116}	0.9292	98	V_{G100}	1.0319
9	P _{G19}	0.9878	54	V_{G1}	1.0129	99	V_{G103}	1.0207
10	P _{G24}	0.9853	55	V_{G4}	1.0396	100	V_{G104}	1.0597
11	P _{G25}	0.0336	56	V_{G6}	1.029	101	V_{G105}	1.0361
12	P _{G26}	2.9963	57	V_{G8}	0.9993	102	$V_{\rm G107}$	0.9971
13	P_{G27}	0.9839	58	V_{G10}	1.0091	103	V_{G110}	1.0072
14	P_{G31}	0.9082	59	V_{G12}	1.028	104	V_{G111}	1.0109
15	P_{G32}	0.9811	60	V_{G15}	0.9867	105	V_{G112}	1.012
16	P _{G34}	0.9019	61	V_{G18}	0.9829	106	V _{G113}	0.9798
17	P _{G36}	0.934	62	V_{G19}	0.9929	107	V_{G116}	1.0022
18	P _{G40}	0.998	63	V_{G24}	1.0022	108	T ₅ —8	0.906
19	P _{G42}	0.9979	64	$V_{\rm G25}$	0.944	109	T ₂₆ —25	1.0992
20	P _{G46}	1.0746	65	$V_{\rm G26}$	0.9759	110	T30—17	1.0541
21	P _{G49}	3.0129	66	$V_{\rm G27}$	0.9408	111	T38—37	0.9021
22	P _{G54}	1.4634	67	V_{G31}	0.9802	112	T63—59	1.097
23	P _{G55}	0.9987	68	$V_{\rm G32}$	0.9704	113	T ₆₄ — ₆₁	0.9337

45	P_{G103}	0.4976	90	V_{G80}	1.017	(p.u.)		1.658
44	P _{G100}	3.4861	89	$V_{\rm G77}$	1.0053	Load Factor		1 (50
43	P_{G99}	0.9038	88	$V_{\rm G76}$	1.0034	PLM (MW)		81.8483
42	P_{G92}	0.1914	87	$V_{\rm G74}$	0.9857	VDM (p.u.)		1.1412
41	P _{G91}	0.8912	86	V _{G73}	0.9741	FCM (269521.7117
40	P_{G90}	1	85	V_{G72}	1.0207	130	Q _{C110}	0.3
39	P _{G89}	3.4807	84	V_{G70}	0.9867	129	QC107	0.2998
38	P _{G87}	0.2559	83	V_{G69}	1.0301	128	QC105	0.0019
37	P _{G85}	0.6997	82	V_{G66}	1.0448	127	QC83	0.1935
36	P_{G80}	5.6483	81	V_{G65}	0.9857	126	QC82	0.2995
35	P _{G77}	0.9935	80	V _{G62}	0.9985	125	Qc79	0.0911
34	P _{G76}	0.9481	79	V _{G61}	0.9972	124	Qc74	0.1264
33	P _{G74}	0.8616	78	V _{G59}	1.0074	123	QC48	0.1419
32	P _{G73}	0.3921	77	V _{G56}	1.0009	122	QC46	0.2978
31	P _{G72}	0.2651	76	V _{G55}	1.0046	121	Qc45	0.3
30	P _{G70}	0.8225	75	V_{G54}	0.9968	120	QC44	0.014
29	P _{G66}	3.5307	74	V_{G49}	1.0235	119	QC34 QC37	0.0033
28	P _{G65}	4.5953	73	V_{G42}	0.9823	118	Qc5 Qc34	0.0035
27	P _{G62}	0.9623	72	V _{G40}	0.9823	117	T ₈₁ —80	0.9002
25	P _{G59}	2.52 2.5646	70	V_{G36} V_{G40}	0.9921	115 116	T68—69	0.9122 0.9602
24	P _{G56}	1	69	V _{G34}	0.9889	114	T65—66	0.9507

5.5 Discussion of Findings

The study in this chapter introduces a novel hybrid optimization technique, the Hybrid Rao-2 Sine Cosine Algorithm (HRSCA), developed to enhance security-oriented power flow optimization across diverse operational scenarios. The algorithm is specifically tailored to address challenges posed by load growth, unexpected contingencies such as generator outages, and the increasing complexity of modern power systems. An innovative aspect of HRSCA is its integration of the SCA for effective global exploration and the Rao-2 algorithm for enhanced local exploitation, enabling faster convergence and improved solution quality. The SCA employs simple and efficient parameters for exploration, while the parameter-free Rao-2 algorithm excels in local search, making the combination both robust and efficient. This hybrid approach effectively addresses global and local optimization challenges, which are crucial for managing the increasing complexity and variability of modern power systems influenced by the integration of RES, EVs, and other emerging technologies.

The proposed HRSCA-based OPF scheme has been rigorously validated through simulations on a range of test networks, from small-sized (30-bus) to relatively large-sized (118-bus) systems, ensuring its scalability and robustness across diverse scenarios. For instance, in the IEEE 30-bus system under the standard OPF scenario, HRSCA achieved fuel cost savings of 11.39% compared to the base case, amounting to \$102.84 per hour or an annual savings of \$900,884.81. In generator outage scenarios for the same system, it achieved a

modest savings of 0.03%, equivalent to \$0.308 per hour or \$2,698.08 annually, alongside a significant 3.46% reduction in power loss, bringing it down to 9.4336 MW, outperforming previously reported results in the literature. Demonstrating its scalability for large-scale OPF problems, HRSCA effectively minimized the fuel cost on the IEEE 118-bus system to 129,088.63 \$/h, representing a 1.62% reduction over the base case. This translates to savings of 2,131.89 \$/h or an annual savings of \$18,676,358.40.

These findings highlight the capability of HRSCA to provide cost-effective and reliable solutions for power system operations, offering valuable insights for policymakers and power system planners.

5.6 Conclusion

This study presented a novel Hybrid Rao-2 Sine Cosine Algorithm (HRSCA), designed to enhance the security and efficiency of OPF solutions under various operational conditions. By balancing global exploration and local exploitation strategies, HRSCA ensures fast convergence and high-quality solutions, making it a robust tool for modern power system optimization.

The algorithm's effectiveness was validated on IEEE 30-bus and 118-bus systems, demonstrating its scalability, cost minimization, emission reduction, and improvement in voltage stability and loading margins. It effectively handled both normal and contingency scenarios, ensuring reliable power system operations.

Future research can expand the application of HRSCA to optimize distributed energy resources (DERs) and demand response programs. Additionally, incorporating machine learning into the HRSCA framework could enhance its efficiency by predicting system behavior and dynamically adjusting its parameters. These advancements would enable the algorithm to adapt to real-time conditions more effectively and further reduce the risk of blackouts. The proven ability of HRSCA to handle complex and critical power system challenges, coupled with its capacity to mitigate risks such as blackouts, positions it as a leading tool for next-generation power system applications. Its robust performance under normal and critical scenarios highlights its potential to ensure a sustainable, reliable, and secure energy future.

CHAPTER 6

APPLICATION OF THE COOT OPTIMIZATION ALGORITHM FOR OPF

6.1 Introduction to the Coot Optimization Algorithm (COA)

The Coot Optimization Algorithm (COA) is a nature-inspired metaheuristic technique modelled on the unique behaviour of coot birds. These birds exhibit collective movement, exploration, and exploitation abilities while foraging, which serve as an analogy for solving complex optimization problems. COA has been developed to address real-world optimization challenges, including those in power systems, by efficiently balancing exploration (global search) and exploitation (local search).

The OPF is a fundamental optimization problem in power system operations, aimed at optimizing objectives such as fuel cost minimization, emission reduction, and power loss minimization while adhering to system constraints. The increasing integration of renewable energy resources, dynamic load profiles, and environmental concerns necessitate advanced optimization algorithms capable of handling the multi-dimensional and non-linear nature of OPF problems.

The COA algorithm introduces an effective approach to solving OPF problems, ensuring high-quality solutions with improved convergence and computational efficiency. Its adaptability to complex problem landscapes and ability to maintain a balance between exploration (global search) and exploitation (local refinement) make it well-suited for modern power system requirements. The algorithm operates through a series of computational steps that mimic the collective foraging behavior of coots. The exploration phase involves the search for potential solutions across the entire solution space, ensuring that the algorithm does not prematurely converge to suboptimal solutions. This is followed by the exploitation phase, where the algorithm refines the identified potential solutions to find the optimal or near-optimal solutions.

This chapter explores the application of COA to OPF, providing a comprehensive analysis of its methodology, simulation results, and comparative performance with other state-of-the-art optimization techniques. The specific parameter settings employed for COA, including population size, number of leaders, maximum iterations, and random value ranges, are discussed in the context of the IEEE 30-bus system.

6.2 Problem Formulation for OPF

OPF is a fundamental optimization problem in power system operations that aims to determine the optimal settings of control variables while satisfying a set of equality and inequality constraints. The primary goal of OPF is to achieve various operational objectives, such as minimizing fuel cost, reducing power losses, maintaining voltage stability, and minimizing emissions, all while ensuring the secure and reliable operation of the power system.

6.2.1 Objectives of OPF

This study involves solving three diverse single-objective OPF formulations, yielding three different cases.

Fuel cost minimization (FCM)

The cost-related objective is a fundamental component of OPF and has been thoroughly investigated in literature. There exists an approximate quadratic correlation between the fuel cost (h) and $P_G(MW)$, as described by Equation (6.1) (Abaci and Yamacli, 2016).

FCM
$$(P_G) = \left(\sum_{i=1}^{NG} A_i P_{G_i}^2 + B_i P_{G_i} + C_i\right) (\$/h)$$
 (6.1)

For the i^{th} generator, the fuel cost coefficients are denoted by A_i , B_i and C_i with active power output of P_{G_i}

Emission minimization (EM)

Emission minimization is a crucial objective of OPF, seeking to optimize the system control variables that can lead to a reduction of noxious gases into the atmosphere. The quantity of these gases present in the atmosphere is directly correlated with the generated active power (in MW), as expressed in Equation (6.2) (Elattar 2018).

$$EM = \sum_{i=1}^{NG} \left[(\alpha_i + \beta_i P_{G_i} + \gamma_i P_{G_i}^2 + \omega_i \exp(\mu_i P_{G_i})) \right] \quad \text{(fon/h)}$$

here, α_i , β_i , γ_i , ω_i and μ_i represent the emission coefficients for i^{th} generating unit.

Active power loss minimization (PLM)

The PLM objective focuses on reducing the cumulative active power losses (P_{Loss}) in the system, calculated as the difference between total generation and demand, as expressed in Equation (6.3). P_{Loss} in transmission lines is calculated using Equation (6.4) as outlined in Abaci and Yamacli (2016).

$$P_{\text{Loss}} = \sum_{i=1}^{NB} P_{i} = \sum_{i=1}^{NB} P_{G_{i}} - \sum_{i=1}^{NB} P_{D_{i}}$$
(6.3)

$$P_{Loss} = \sum_{I=1}^{NL} G_L [V_i^2 + V_j^2 - 2V_i V_j Cos \delta_{ij}]$$
(6.4)

here, G_L is used to designate the conductance of line L between nodes i and j. V_i and V_j are the voltages at nodes i and j respectively, while δ_{ij} signifies the angle difference between voltage phasors at these nodes. Here, NB stands for the total count of network buses.

6.2.2 Constraints in OPF

In OPF, there are two key constraint types: equality constraints governing power balance (active and reactive) and inequality constraints establishing operating limits for power system components, including limits to ensure system security. Consequently, voltage magnitude constraints apply to both generator and load buses. Furthermore, there are limits on P_G and Q_G from generators, tap changer settings (T), shunt compensator reactive power (Q_C), and line flows (S_{line}) (Abd El-sattar et al. 2021). The objective function accounts for inequality constraints by including quadratic penalty terms.

6.2.3 OPF Problem Formulation for COA

The COA addresses the OPF problem by formulating it as a non-linear, constrained optimization problem. The objective functions, as defined above, are optimized while ensuring that all equality and inequality constraints are satisfied. The algorithm dynamically explores the solution space to identify optimal configurations that balance operational costs, technical performance, and environmental impact.

6.3 Implementation of the Coot Optimization Algorithm

6.3.1 Overview of COA

COA is a novel metaheuristic algorithm pioneered by Naruei and Keynia (2021), making it a relatively recent addition to the field of metaheuristic algorithms. The Coot algorithm takes inspiration from collective behaviours and movements of a swarm of birds, known as coots, observed on the surface of water as shown in Fig. 6.1. The algorithm simulates the intricate behaviors observed in colonies of American coots (Fulica americana) while they move in the sea. The Coot algorithm mimics two distinct bird movement patterns on the water surface, which can be categorized into primary and secondary phases. The primary phase is distinguished by low density and irregularly fluctuating body orientations. The second phase, on the other hand, is more synchronised with uniform body orientation, surface swimming speed, and a clearly-defined high-density pattern.



Fig. 6.1 Coots gliding in a synchronised manner across the water surface

The transition from the primary disordered phase to the secondary synchronised phase is driven by two factors. The first is that as individuals within the flock gain speed, they are drawn closer to slower moving coots (coot followers) and they are enabled to align their orientation with accelerating coots (coot leaders) as they gain speed. The movement of group leaders is the second factor that triggers the transition between the two phases. When coot leaders alter their orientations and speeds, it prompts the rest of the coots to trail behind them.

6.3.2 Steps in COA for OPF

The Coot algorithm is a simple population-based OA, involving following basic steps to be carried out:

Step 1 Population initialization and population size

The Coot algorithm begins by randomly generating an initial population of coots (N_{POP}), encompassing the entire range of potential solutions within the search space, in accordance with Equation (6.5).

$$CP(i) = rand (1,D).*(upb-lwb) + lwb$$
(6.5)

Where, CP(i) indicates the coot position of i^{th} coot, and D denotes the problem dimension, determined by the count of involved decision variables. The variables involved in the problem have upper and lower bounds, represented as upb and lwb, respectively.

Step 2 Fitness evaluation and designation of Coot leaders

Using positions of each agent from Equation (6.5), the fitness function is evaluated for every set of solutions. The number of leaders can be drawn at random from the total population and termed as coot leaders (N_{Leader}). The rest of the coots can be termed as coot followers (N_{COOT}) *i.e.* ($N_{\text{COOT}} = N_{\text{POP}} - N_{\text{Leader}}$).

Step 3 Coot position update

This step involves simulating four diverse movement behaviors of coots, resembling their movement on water.

1) Random movement: Using random coot movement, the algorithm investigates multiple areas of the solution space, thereby avoiding trapping in local optima. The new position of coot is ascertained through Equation (6.6).

$$CP(i) = CP(i) + T \times r2 \times \left[\left\{ rand(1, D) \cdot *(upb - lwb) + lwb \right\} - CP(i) \right]$$
(6.6)

Here, r2 is an arbitrarily chosen number spanning 0 to 1. The value of T is determined using Equation (6.7).

$$T = 1 - (it / it_{\text{max}}) \tag{6.7}$$

Where, it represents current iteration number and it_{max} represents the maximum iteration count.

2) Chain movement: The mathematical approximation of chain movement involves computing the distance vector between a pair of coots and moving one coot halfway towards the other as per Equation (6.8).

$$CP(i) = 0.5 \times [CP(i-1) + CP(i)]$$
(6.8)

Where, CP(i-1) denotes second coot's position.

3) Position adjustment through coot leaders: In the group, coot leaders take the lead position and guide the movement, while the remaining coots adjust their positions to follow and align with the leaders. Each coot follower is associated with a coot leader and their locations are updated accordingly. The mechanism adopted for leader selection relies on the average position among them, as indicated in Equation (6.9).

$$k = 1 + MOD (i, N_{\text{Leader}}) \tag{6.9}$$

Here, i designates the index of the current coot, and k denotes the index of the coot leader. N_{Leader} is the aggregate count of coot leaders. Each coot (i) in the group is required to align its position with the leader (k) and subsequently adjust its position accordingly. As a result, the next coot position with respect to its associated leader is given in Equation (6.10).

$$CP(i) = LP(k) + 2 \times r1 \times \cos(2\pi r) \times \left[LP(k) - CP(i)\right]$$
(6.10)

Here, CP(i) is current position of the i^{th} coot and LP(k) is the leader position of the k^{th} leader chosen. Random number r1 ranges from 0 to 1, while random number r ranges from -1 to 1.

4) Leaders position update towards the global best position: Leaders must update their position in relation to the global best which then guides the entire flock of coot birds towards global optima (food source location). The leader's position is updated using Equation (6.11) to get closer to the optimal position.

$$LP(i) = \begin{cases} U \times r3 \times \cos(2\pi r) \times (g_{best} - LP(i)) + g_{best} & ; r4 < 0.5 \\ U \times r3 \times \cos(2\pi r) \times (g_{best} - LP(i)) - g_{best} & ; r4 \ge 0.5 \end{cases}$$

$$(6.11)$$

Here, g_{best} refers to the global best position, while r3 and r4 take on random values within the interval of 0 to 1. The value of U is given by Equation (6.12).

$$U = 2 - (it/it_{\text{max}}) \tag{6.12}$$

Figure 6.2 presents a flowchart illustrating the utilization of the Coot algorithm in implementing an OPF solution.

6.3.3 Simulation Setup and Test System

This research article utilizes the Coot algorithm to conduct optimization of fuel cost (FCM), emissions (EM), and real power loss (PLM) as individual objectives. Remarkably, the Coot algorithm has been implemented for the first time to address OPF problems. To assess its performance, the standard IEEE test system comprising 30 buses is chosen as the benchmark test network. The algorithm was implemented using MATLAB 2018a and run on a laptop featuring an Intel Core i5 processor and 8 GB of system memory.

a) IEEE 30-bus Test System

The IEEE 30-bus network, with its limited size and manageable complexity, falls into the category of a small-scale electrical network. At the 100 MVA base, the combined demand for active power amounts to 283.4 MW, and for reactive power, it amounts to 126.2 MVAR. The system comprises six generating units located at buses 1, 2, 5, 8, 11, and 13, with bus 1 designated as the slack bus. The loads are distributed across 24 load buses. PV bus voltage magnitudes are restricted to values between 0.95 and 1.1 p.u. The load buses must operate within the acceptable operating limits of 0.95 to 1.05 p.u. Detailed system data and operating conditions for the IEEE 30-bus system are available in the Power Systems Test Case Archive (Christie, 1993).

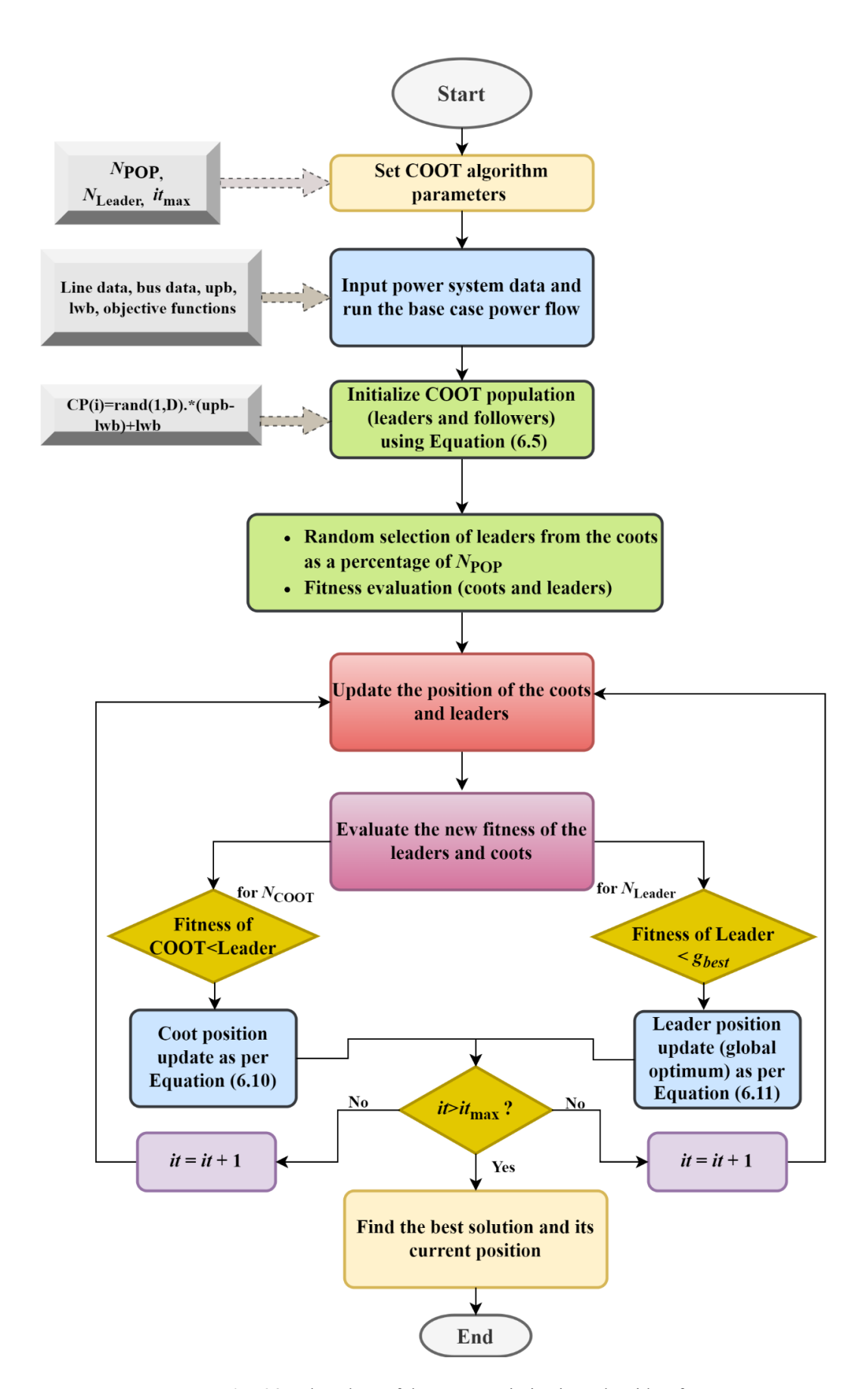


Fig. 6.2 Flowchart of the Coot Optimization Algorithm for OPF

b) Algorithm Parameters

To solve the OPF problem using the COA, a fixed population size of 40 and a maximum iteration count of 100 were employed. These algorithmic parameters were determined through extensive testing and evaluation. Table 6.1 presents the optimal parameter settings used for the Coot algorithm in this case study.

 Parameter
 Value

 N_{POP} 40

 N_{Leader} $0.1 * N_{POP} = 4$
 it_{max} 100

 D 24

 r1, r2 [0, 1]

 r3, r4 [0, 1]

[-1, 1]

 Table 6.1
 Algorithm Parameters assigned for COOT Algorithm on IEEE 30-bus System

6.4 Case Studies, Results, and Discussion

6.4.1 Case 1- OPF for FCM

The aim of this case involves the reduction of fuel expenses using the Coot algorithm, and the corresponding objective function is formulated in Equation (6.1). In Case 1, the Coot algorithm significantly reduces the total system fuel cost from 902.02 \$/h (base case) to 799.2125 \$/h, resulting in a substantial reduction of 11.39%. The obtained total cost is compared with other algorithms implemented to solve the given case under the same conditions, as shown in Table 6.2.

Table 6.2 Comparison of the outcomes achieved through various optimization algorithms for Case 1

Method	Total fuel cost (\$/h)	P _{Loss} (MW)	Emission (ton/h)	Method Description
ISSA (Abd El-sattar et al. 2021)	800.4752	9.1044	NR*	Improved Salp Swarm Algorithm
MGOA (Taher et al. 2019b)	800.4744	8.9882	0.3649	Modified Grasshopper OA
GOA (Taher et al. 2019b)	800.7806	8.9882	0.3678	Grasshopper OA
Jaya (Warid 2020)	800.4794	9.0648	NR	Jaya Algorithm
TLBO (Taher et al. 2019b)	800.6108	8.9899	0.3653	Teaching-Learning based OA
PSO (Khan et al. 2020)	799.5433	8.7158	NR	Particle Swarm Optimization
HFPSO (Khan et al. 2020)	799.123	8.6375	NR	Hybrid Firefly PSO
Rao-2 (Warid et al. 2022)	800.3865	9.0535	NR	Rao-2 Algorithm
SCA (Attia et al. 2018)	800.1018	9.0633	NR	Sine-Cosine Algorithm

ABC (Mohamed et al. 2017)	800.66	9.0328	0.3651	Artificial Bee Color Algorithm	ıy
Coot	799.2125	8.7353	0.3645	Coot Algorithm	

Additionally, Fig. 6.3 shows the convergence traits of the Coot algorithm alongside those of alternative competing algorithms. The COOT algorithm demonstrates superior performance over ISSA, MGOA, GOA, TLBO, SSO, Jaya, PSO, Rao-2, SCA, and ABC in both convergence rate and solution quality. The Coot algorithm demonstrates its remarkable convergence speed by reaching the best value for Case 1 in just 74 iterations, especially when dealing with small-scale OPF problems.

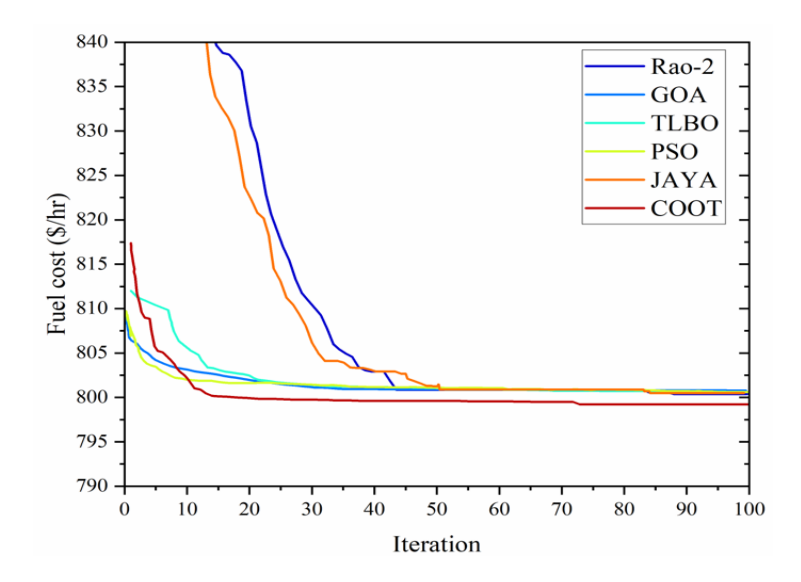


Fig. 6.3 Convergence characteristics comparison of Case 1 using the Coot algorithm and other recent algorithms

6.4.2 Case 2- OPF for EM

The objective of this case is to lower emission levels resulting from the fossil-fuel fired power plants. The corresponding objective function is defined in Equation (6.2), and the optimal solution is presented in Table 6.3. Utilizing the Coot algorithm, the generation fuel emission is reduced to 0.20423 ton/h, leading to a reduction of approximately 44% compared to the emission results of cost-based OPF (Case 1). Moreover, the fuel cost increases from 799.2125 \$/h (Case 1) to 943.1206 \$/h, signifying a percentage increase of just 18%. It is noteworthy that this achievement surpasses the results obtained from other OAs (*i.e.*, TLBO, DE, IDE, GA, PSO, and GOA), as reported in Table 6.3, while still adhering to the imposed constraints for the identical system data. Here, MGOA achieves the best solution for minimising emissions, though it involves trade-offs with other objectives, while IDE initially shows a faster convergence rate but fails to attain an optimal solution.

Table 6.3 Comparison of the outcomes achieved through various optimization algorithms for Case 2

Method	Emission (ton/h)	P _{Loss} (MW)	Total fuel cost (\$/h)	Method Description
TLBO (Taher et al. 2019b)	0.20486	3.3608	944.7442	Teaching-Learning based OA
DE (Al-Bahrani et al. 2022)	0.20488	3.2793	943.4304	Differential Evolution
IDE (Al-Bahrani et al. 2022)	0.20476	3.0120	943.7258	Improved DE
GA (Taher et al. 2019b)	0.20487	3.3776	945.0166	Genetic Algorithm
PSO (Taher et al. 2019b)	0.2049	3.4950	944.7462	Particle Swarm OA
GOA (Taher et al. 2019b)	0.20503	3.8265	946.4789	Grasshopper OA
MGOA (Taher et al. 2019b)	0.20259	3.6325	955.3623	Modified GOA
Coot	0.20423	3.4162	943.1206	Coot Algorithm

The convergence behaviors of the Coot algorithm and competing techniques are depicted in Fig. 6.4. Remarkably, the Coot algorithm demonstrates its superiority by achieving convergence in just 50 iterations, outperforming other recent techniques in terms of convergence speed and effectiveness.

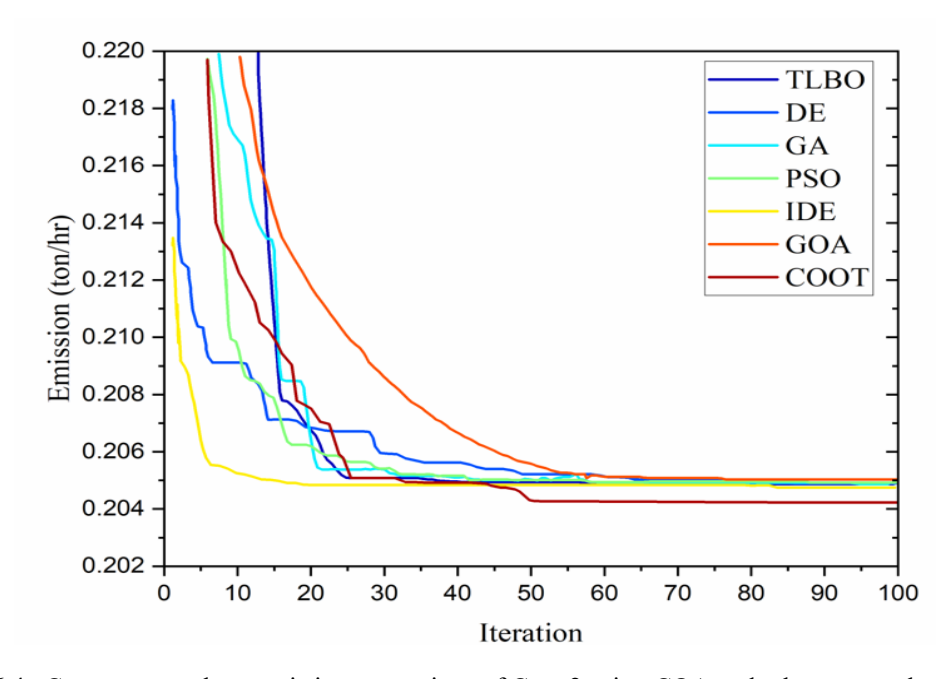


Fig. 6.4 Convergence characteristics comparison of Case 2 using COA and other recent algorithms

6.4.3 Case 3- OPF for PLM

The goal here is the reduction of actual power loss (P_{Loss}) within transmission lines. P_{Loss} can be calculated using Equation (6.4) for any given network. Table 6.4 clearly demonstrates the superiority of the Coot algorithm when contrasted with previously reported population-based OAs implemented to solve the given case under identical system data, while still adhering to the imposed constraints.

The Coot algorithm achieves an impressive value of 3.0628 MW, which is the lowest among techniques like SSO, DE, GOA, Rao-2, TLBO, and others, except for MGOA. This noteworthy result represents a reduction of approximately 47.66% compared to the base case value of 5.8482 MW. The Coot algorithm exhibits rapid convergence to the optimal solution within just 38 iterations, showcasing its highly efficient convergence capabilities.

Table 6.4 Comparison of the outcomes achieved through various optimization algorithms for Case 3

Method	P _{Loss} (MW)	Total fuel cost (\$/h)	Emission (ton/h)	Method Description
SSO (Nguyen 2019)	3.8239	NR	NR	Social Spider OA
DE (Mohamed et al. 2017)	3.38	968.23	NR	Differential Evolution
GOA (Taher et al. 2019b)	3.3141	963.099	0.2083	Grasshopper OA
MGOA (Taher et al. 2019b)	3.0039	966.1892	0.2039	Modified GOA
AMTPG-Jaya (Warid 2020)	3.0802	967.6830	NR	Adaptive Multiple Teams Perturbation-Guiding Jaya
Rao-2 (Warid et al. 2022)	3.0975	967.6599	NR	Rao-2 Algorithm
TLBO (Taher et al. 2019b)	3.1202	967.2312	0.2072	Teaching-Learning based OA
MSA (Mohamed et al. 2017)	3.1005	967.6636	0.20727	Moth Swarm Algorithm
Jaya (Warid et al. 2016)	3.1035	967.6827	NR	Jaya Algorithm
ABC (Mohamed et al. 2017)	3.1078	967.6810	0.207268	Artificial Bee Colony Algorithm
PSO (Taher et al. 2019b)	3.1079	967.2312	0.2072	Particle Swarm OA
Coot	3.0628	966.8212	0.2071	Coot Algorithm

Figure 6.5 vividly portrays the trend for minimizing real power losses through the implementation of the Coot algorithm. These outcomes evidently showcase the excellence of the Coot approach in achieving the optimal solution while demonstrating a smooth convergence characteristic curve with highest convergence speed. In this case the MGOA offers the optimal solution to minimize the power loss. In the meantime, the Coot algorithm achieves the second-most optimal solution, displaying a higher convergence rate as evident from the convergence curve in Fig. 6.5. In this case, though, additional system objective functions, like total fuel cost, exhibited less favourable performance.

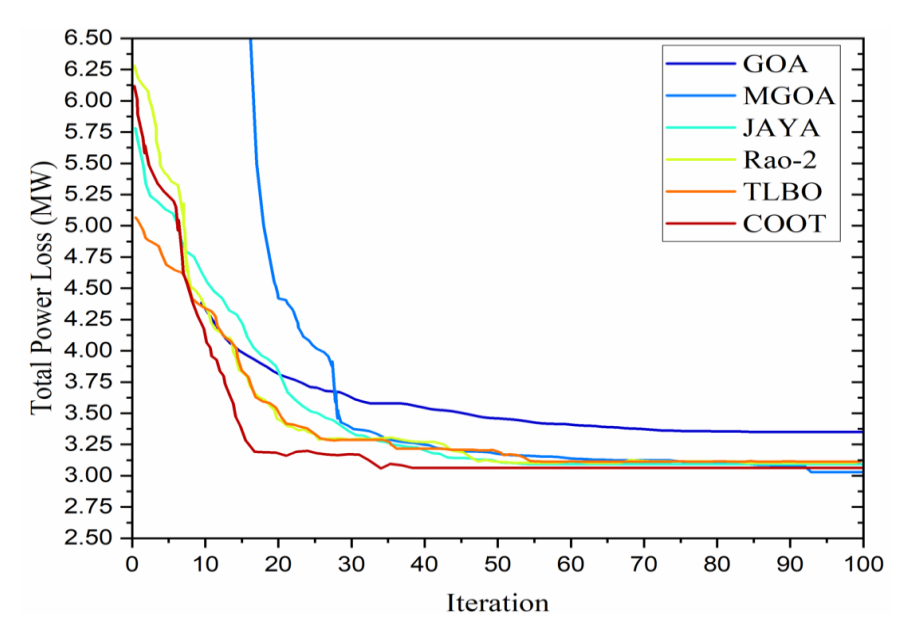


Fig. 6.5 Convergence characteristics comparison of Case 3 with Coot algorithm and other recent algorithms

6.5 Conclusion

In this study, the recently introduced metaheuristic OA, known as the Coot optimization algorithm, has been thoroughly examined and has successfully demonstrated its reliability and effectiveness in solving single-objective frameworks of the OPF problem. The successful testing of the Coot approach on IEEE 30-bus network illustrates its capability to achieve nearly global optimal adjustments of control variables. The simulation outcomes for all test scenarios attained using the Coot algorithm were contrasted with the outcomes achieved by competitive algorithms like DE, GOA, TLBO, Jaya, ABC, PSO, GA, as well as other enhanced variants proposed in existing literature. The comparison vividly accentuates the remarkable performance and robustness of the Coot algorithm in contrast to these previously reported techniques.

However, while the basic COA enhances the convergence rate, it may encounter difficulties in addressing complex, larger-scale problems, often getting trapped in local optima. The selection of parameters can also significantly affect algorithm performance. Nevertheless, an improved version with superior global search capabilities and local optima avoidance can effectively handle large-scale electrical grid OPF problems. To address these challenges, it is recommended to integrate the COA with other metaheuristic algorithms or AI-based approaches, coupled with parameter tuning and the development of specialized adaptations.

Future work can expand on making the COA suitable for addressing multi-objective OPF issues, particularly in large-scale power systems that incorporate non-conventional energy sources alongside thermal generators. This advancement would enhance the algorithm's adaptability and effectiveness in more complex and varied power system environments.

CHAPTER 7

OPF WITH DISTRIBUTED GENERATION: APPLICATION OF THE EEFO ALGORITHM

7.1 Introduction

The growing demand for electricity, along with the urgent need to curb greenhouse gas emissions, has spurred a rapid shift towards renewable energy sources (RES) over the past two decades. Distributed Generation (DG) refers to decentralized, small-scale electricity generation systems located close to the point of consumption, often utilizing RES. Factors like market deregulation and government incentives for green energy have further accelerated this shift. Among various DG options, renewable energy-based systems have emerged as the most promising alternatives to fossil fuels for electricity generation. Technological advancements in these systems have led to significant reductions in installation costs while enhancing their reliability and standardization. Current trends and reports indicate that electricity generated from RES is poised to become more cost-effective than traditional fossil fuel-based energy production in the near future.

Despite these advancements, the intermittent nature of RES poses significant challenges to power system optimization. The OPF problem plays a crucial role in addressing these challenges by ensuring the economic and stable operation of the power grid. OPF focuses on determining the optimal settings for control variables (CVs), such as generator outputs, voltage levels, and transformer tap positions, to achieve key objectives like cost minimization and loss reduction. Simultaneously, it ensures system stability and adheres to operational constraints, making it an essential tool in modern power system management. (Alghamdi, 2023)

The rapid advancements in computational power over recent years have led to a growing trend of employing nature-inspired optimization techniques to solve OPF problems. Numerous stochastic optimization methods have been proposed and effectively utilized, including GA (Lai et al. 1997; Kumari and Maheswarapu 2010), PSO (Abido 2002; Vlachogiannis and Lee 2006, Niknam et al. 2012a), DE (Abou El Ela et al. 2010), HS (Pandiarajan and Babulal 2016; Reddy 2019; Elattar 2018), ABC (Adaryani and Karami 2013; Khorsandi et al. 2013), GSA (Duman et al. 2012; Bhattacharya and Roy 2012), TLBO algorithm (Bouchekara et al. 2014; Ghasemi et al. 2015), BBO (Bhattacharya and Chattopadhyay 2009; Kumar et al. 2015), and Jaya algorithm (Warid et al. 2016; Warid 2020). These approaches are particularly well-suited for handling the nonlinear and non-convex nature of OPF problems, as detailed in various studies. However, the

"No Free Lunch" theorem emphasizes that no single optimization method can universally solve all complex engineering problems, underlining the importance of developing new algorithms tailored to specific challenges (Wolpert and Macready 1997).

In this context, the present study explores the application of the Electric Eel Foraging Optimization (EEFO) algorithm - a recently developed nature-inspired, population-based optimization method - for solving the OPF problem in DG-integrated power systems. The EEFO algorithm showcases significant potential for achieving optimal solutions, especially in scenarios involving the integration of RES into power systems. By providing cost-effective and stable grid operations, EEFO emerges as a promising and innovative tool for modern power system optimization.

7.2 Problem Formulation

7.2.1 General Structure of OPF

The OPF framework typically encompasses objectives and constraints. An OPF solution fine-tunes power system variables, referred to as control variables (CVs), for optimizing a chosen objective function. The optimized state of the system is governed through the state variables. The power system must operate under two sorts of constraints: equality constraints and inequality constraints. All conditions of constraint satisfaction have to be followed to formulate a realistic problem. A SOOPF problem involves only one objective function and is formulated as:

$$Min: f(x,u) \tag{7.1}$$

$$g_i(x,u) = 0$$
 $i = 1, 2, 3, \dots, m$ (7.2)

and,
$$h_j(x,u) \le 0$$
 $j = 1, 2, 3, \dots, n$ (7.3)

Equation (7.1) represents the objective function, which is dependent on both the state variables 'x' and the control variables 'u'. Equation (7.2) exhibits the equality constraints, while the inequality constraints are denoted by Equation (7.3). Here, m indicates the count of equality constraints, while n signifies the count of inequality constraints. Equation (7.4) presents the state vector, which is the vector of dependent variables, wherein P_G corresponds to the active power output of generator, V_L is the load bus voltage, Q_G is the reactive power output of generator, and S_{line} is the loading of the power line, which must not surpass the specified upper loading limit for any given line.

$$x^{T} = [P_{G_1}, V_{L_1}, \dots, V_{L_{NDO}}, Q_{G_1}, \dots, Q_{G_{NG}}, S_{line_1}, \dots, S_{line_{NI}}]$$
(7.4)

Here, P_{G_1} represents slack bus power. The notations NPQ, NG, and NL represent the count of load buses, generator units, and power lines, respectively. The control vector, given in Equation (7.5), encompasses the adjustable variables used to govern the power flow scheme.

$$u^{T} = [P_{G_{2}} P_{G_{NG}}, V_{G_{1}} V_{G_{NG}}, Q_{C_{1}} Q_{C_{NC}}, T_{1} T_{NT}]$$
(7.5)

Here, V_G refers to the voltage at generation bus, Q_C represents shunt VAR compensation and T represents the tap changing transformer with NT representing the count of tap changing transformers.

7.2.2 OPF Objective Functions

This study involves solving two diverse single-objective OPF (SOOPF) formulations, yielding two different cases:

a) Fuel cost minimization (FCM)

The cost-related objective is a core component within OPF and has been thoroughly investigated in various literature. There exists an approximate quadratic correlation between the fuel cost (\$/h) and $P_G(MW)$ as expressed in the following equation (Abaci and Yamacli, 2016).

$$f_{FCM}(x,u) = \left(\sum_{i=1}^{NG} A_i P_{G_i}^2 + B_i P_{G_i} + C_i\right) (\$/h)$$
(7.6)

For the i^{th} generator, the fuel cost coefficients are denoted by A_i , B_i and C_i with active power output of \mathbf{P}_{G_i}

b) Active power loss minimization (PLM)

The PLM objective strives to reduce the cumulative active power losses (P_{Loss}) in the system, calculated as the difference between total generation and demand. P_{Loss} can be defined as follows (Abaci and Yamacli, 2016):

$$f_{PLM}(x,u) = P_{Loss} = \sum_{i=1}^{NB} P_{i} = \sum_{i=1}^{NB} P_{G_{i}} - \sum_{i=1}^{NB} P_{D_{i}} = \sum_{I=1}^{NL} G_{L} [V_{i}^{2} + V_{j}^{2} - 2V_{i}V_{j}Cos\delta_{ij}]$$
(7.7)

7.2.3 Constraints

OPF problem consists of two types of constraints namely, equality and inequality. The equality constraints, g(x,u), consist of power flow equations. The power flow equations are as follows:

$$\sum_{i=1}^{NB} (P_{G_i} + P_{DG_i}) = \sum_{i=1}^{NB} P_{D_i} + P_{Loss}$$
(7.8)

$$\sum_{i=1}^{NB} (Q_{G_i} + Q_{DG_i}) = \sum_{i=1}^{NB} Q_{D_i} + Q_{Loss}$$
(7.9)

Where P_{DG_i} and Q_{DG_i} are the active and reactive power output of i^{th} DG unit and NB is the number of buses.

The inequality constraints, h(x,u), define the boundaries for adjustable variables and the operational thresholds within the power system. These operational thresholds include voltage levels at generator and load buses, active and reactive power outputs from generators, settings of transformer tap changers, and limits on compensating reactive power. Additionally, constraints on active and reactive power outputs of distributed generation must also be taken into account.

7.3 Overview of Electric Eel Foraging Optimization (EEFO) algorithm

7.3.1 Inspiration

Electric eels, native to South America and part of the Gymnotidae family, are remarkable predators known for their ability to generate powerful electrical discharges of up to 800 V to stun and capture prey effectively. These High-voltage discharges serve as a defense mechanism against predators and as an attack tool to incapacitate prey. This unique adaptation, often likened to "high voltage wires" within freshwater ecosystems, is facilitated by specialized organs composed of thousands of electrogenic cells known as electrocytes. These electrocytes function as biological batteries, storing and releasing energy to support the eel's predatory and defensive behaviours. Additionally, eels use low-voltage discharges, typically around 10 V, for navigation and prey detection, compensating for their poor vision and enabling them to efficiently locate fast-moving targets.

Electric eels also exhibit advanced swarm behaviours similar to social predation strategies observed in mammals. These behaviours include *interacting*, *migrating*, *resting*, and *hunting* in coordinated groups to locate and capture prey. For instance, when hunting in groups, eels often

cluster together, encircle prey, and drive them into a concentrated "prey ball" before delivering a synchronized high-voltage attack. This group hunting strategy not only increases the chances of success but also enables eels to target larger quantities of prey in areas with abundant fish populations.

Inspired by these sophisticated foraging and behavioural patterns, Zhao et al. (2024) developed the Electric Eel Foraging Optimization (EEFO) algorithm. By mimicking the dynamic and adaptive strategies of electric eels, this algorithm provides an innovative approach to solving complex optimization problems.

7.3.2 Interacting behaviour in EEFO

The Interaction Phase in EEFO algorithm emulates the natural behaviour of eels when they encounter a school of fish. The eels form electrified circular formations to trap smaller fish at the centre. In the optimization context, each eel represents a candidate solution, and the best solution found so far acts as the target prey. During this phase, eels cooperate by exchanging positional information to enhance the search process, akin to the *global exploration* phase in optimization algorithms. This enables a broader search of the solution space. Each eel's position is updated by evaluating the difference between a randomly selected eel's position and the search space's centre. This update mechanism ensures effective exploration of the search space and prevents premature convergence. The mathematical model for this phase is given by Equation (7.10):

$$X_{i}(t+1) = X_{i}(t) + r_{1} \times (X_{rand} - X_{c})$$
(7.10)

where, r_1 is a random number constrained to the interval [0, 1]. $X_i(t+1)$ is the updated position of the i^{th} eel. $X_i(t)$ is the current position of the i^{th} eel. X_{rand} is the position of a randomly selected eel. X_i is the centre of the search space, calculated as per Equation (7.11):

$$X_{c} = \frac{1}{N} \sum_{i=1}^{N} X_{i}(t)$$
 (7.11)

Additionally, eels may interact with multiple randomly selected eels to incorporate local search information. This interaction includes the concept of "churn", which introduces randomness into the movement of eels, ensuring diverse exploration patterns (Zhao et al., 2024). The updated position of the eel considering churn is defined as:

$$X_{i}(t+1) = X_{i}(t) + r_{2} \times (X_{rand1} - X_{rand2})$$
(7.12)

where, X_{rand1} and X_{rand2} are the positions of two randomly selected eels. r_2 is another random number within the range [0,1]. This interaction mechanism mimics the dynamic and adaptive foraging strategy of electric eels, combining global exploration with local search information to identify promising areas in the solution space effectively.

7.3.3 Resting Behavior in EEFO

In the EEFO algorithm, resting behavior represents a crucial phase that enhances the search efficiency by allowing electric eels to converge toward promising areas in the solution space (Zhao et al. 2024). The resting area for the eels is determined through the normalization of the search space and the positional information of each eel. This involves projecting the position vector of an eel onto the main diagonal of the search space to establish a reference point. A normalized position is calculated based on the eel's random placement, ensuring positions remain within bounds for effective exploration and optimization. The resting position of the eel within the resting area is then obtained as:

$$R_i(t+1) = Z(t) + \alpha \times \left| Z(t) - x_{prey}(t) \right| \tag{7.13}$$

where α , also known as the resting factor, is the scale of the resting area and controls the size of the resting area. α can be defined as;

$$\alpha = \alpha_0 \times \sin(2\pi r_2) \tag{7.14}$$

where, r_2 is a random number constrained to the interval [0, 1]. Once the resting position is determined, the eel moves toward it. The resting behavior is expressed as:

$$v_i(t+1) = R_i(t+1) + v_2 \times \left[R_i(t+1) \cdot round(rand) \cdot x_i(t)\right]$$
(7.15)

where v_2 is a random value sampled from a standard normal distribution. This mechanism allows the eels to focus their search within a defined area while narrowing exploration over iterations. This balance of exploration and exploitation enhances the algorithm's ability to converge on optimal solutions.

7.3.4 Hunting Behavior in EEFO

In the EEFO algorithm, the hunting behavior mimics the cooperative strategy of electric eels when they locate prey. Eels interact by forming an electrified circle around the prey, effectively trapping it within the hunting area. This coordinated behavior involves low electric discharges, enabling the eels to communicate and reduce the hunting area's size as their interaction

intensifies. The algorithm models this behavior by defining a dynamic hunting area centered around the prey's position, with its range determined by the initial scale of the hunting area (β_0) and the distance from the prey. Once the hunting area is defined, a new prey position is generated as:

$$H_{prey}(t+1) = x_{prey}(t) + \beta \times |\overline{x}(t) - x_{prey}(t)|$$
(7.16)

where x(t) is the mean position of all eels at the current iteration t and $x_{prey}(t)$ is the position of the prey. Here β is the scale of hunting area defined as;

$$\beta = \beta_0 \times \sin(2\pi r_3) \tag{7.17}$$

here, r_3 is a random number within interval [0,1]. This mechanism ensures gradual shrinkage of the hunting area, facilitating a transition from global exploration to focused exploitation.

Additionally, the eels exhibit curling behavior, where their positions are updated relative to the prey's new position. This behavior is represented as:

$$v_i(t+1) = H_{prey}(t+1) + \eta \times \left[H_{prey}(t+1) - round(rand) \cdot x_i(t) \right]$$
(7.18)

The curling factor η , which decreases over time, is defined as:

$$\eta = e^{\frac{r_4(1-t)}{T_{\text{max}}}} \times \cos(2\pi r_4) \tag{7.19}$$

where r_4 is a random number within the range [0,1], t is current iteration number and t_{max} is the maximum number of iterations. The algorithm adjusts t_{max} dynamically using Equation (7.19) as iterations progress. At the start, a moderate value of t_{max} must be chosen to encourage diverse movement (exploration) across the search space. This curling behaviour allows the algorithm to refine the search and maintain diversity within the population, thereby ensuring an effective balance between exploration and exploitation throughout the optimization process.

7.3.5 Migration behaviour in EEFO

In the migrating phase of the EEFO algorithm, eels transition from their resting areas to designated hunting zones. This behaviour models the natural movement of eels as they relocate towards more promising regions in their search for prey. Each eel assesses its position relative to a defined hunting area, which is determined by the position of the prey and the surrounding region. The mathematical model governing this phase begins with determining the new position of an eel within the hunting area, represented as:

$$v_i(t+1) = -r_5 \times R_i(t+1) + r_6 \times H_r(t+1) - L \times (H_r(t+1) - x_i(t))$$
(7.20)

here r_5 and r_6 are random numbers in [0,1]. The term $(H_r(t+1)-x_i(t))$ directs the eel toward the hunting area. The variable L represents a Lévy flight function, which ensures that the algorithm explores the search space broadly while avoiding local optima (Zhao et al. 2024). The hunting area position is determined using Equation (7.21):

$$H_r(t+1) = x_{prey}(t) + \beta \times |\bar{x}(t) - x_{prey}(t)|$$
 (7.21)

where $H_r(t)$ is any position within the hunting area and β , also known as the hunting factor, defines the scale of the hunting area, as specified in Equation (7.17).

After the new position is determined, the fitness of $v_i(t+1)$ is evaluated. If the new position improves the fitness value, it is retained; otherwise, the eel remains at its current position:

$$x_i(t+1) = \begin{cases} v_i(t+1) & \text{; if fitness } (v_i(t+1)) < \text{fitness } (x_i(t)), \\ x_i(t) & \text{; otherwise.} \end{cases}$$
 (7.22)

The social hunting behaviours of electric eels serve as the foundation for the EEFO algorithm. The algorithm's exploitation and exploration phases are modelled after these behaviours, drawing inspiration from the dynamic and cooperative strategies electric eels employ during foraging.

Figure 7.1 shows the representation of electric eels using their electric pulses to locate and capture prey in an underwater environment.



Fig. 7.1. Electric Eels: Utilizing Electric Pulses for Prey Capture

7.3.6 Transition from Exploration to Exploitation

The Transition from Exploration to Exploitation in the EEFO algorithm is driven by an energy factor E(t), which facilitates a smooth shift between global exploration and local

exploitation. This transition is critical for maintaining an effective balance between searching new regions of the solution space and refining solutions in promising areas. The energy factor E is defined in Equation (7.23):

$$E(t) = 4 \times \sin\left(1 - \frac{t}{T_{\text{max}}}\right) \ln\left(\frac{1}{r_7}\right) \tag{7.23}$$

where 't' is the current iteration, T_{max} is the total iterations, and r_7 is a random value in [0,1].

When E(t) > 1, the eels engage in global exploration by interacting with other individuals across the entire solution space. Conversely, when $E(t) \le 1$, the algorithm prioritizes local exploitation through behaviors like resting, hunting, or migrating to fine-tune solutions in promising subregions. The probability of E > 0 being approximately 50% during optimization ensures a dynamic balance between exploration and exploitation. This balance prevents premature convergence and promotes robust search capabilities. The behavior of E(t) during iterations highlights its significance in improving the algorithm's adaptability and efficiency in solving complex optimization problems (Zhao et al. 2024).

To provide further clarification, Figure 7.2 presents a flowchart illustrating the utilization of the EEFO algorithm in implementing an OPF solution.

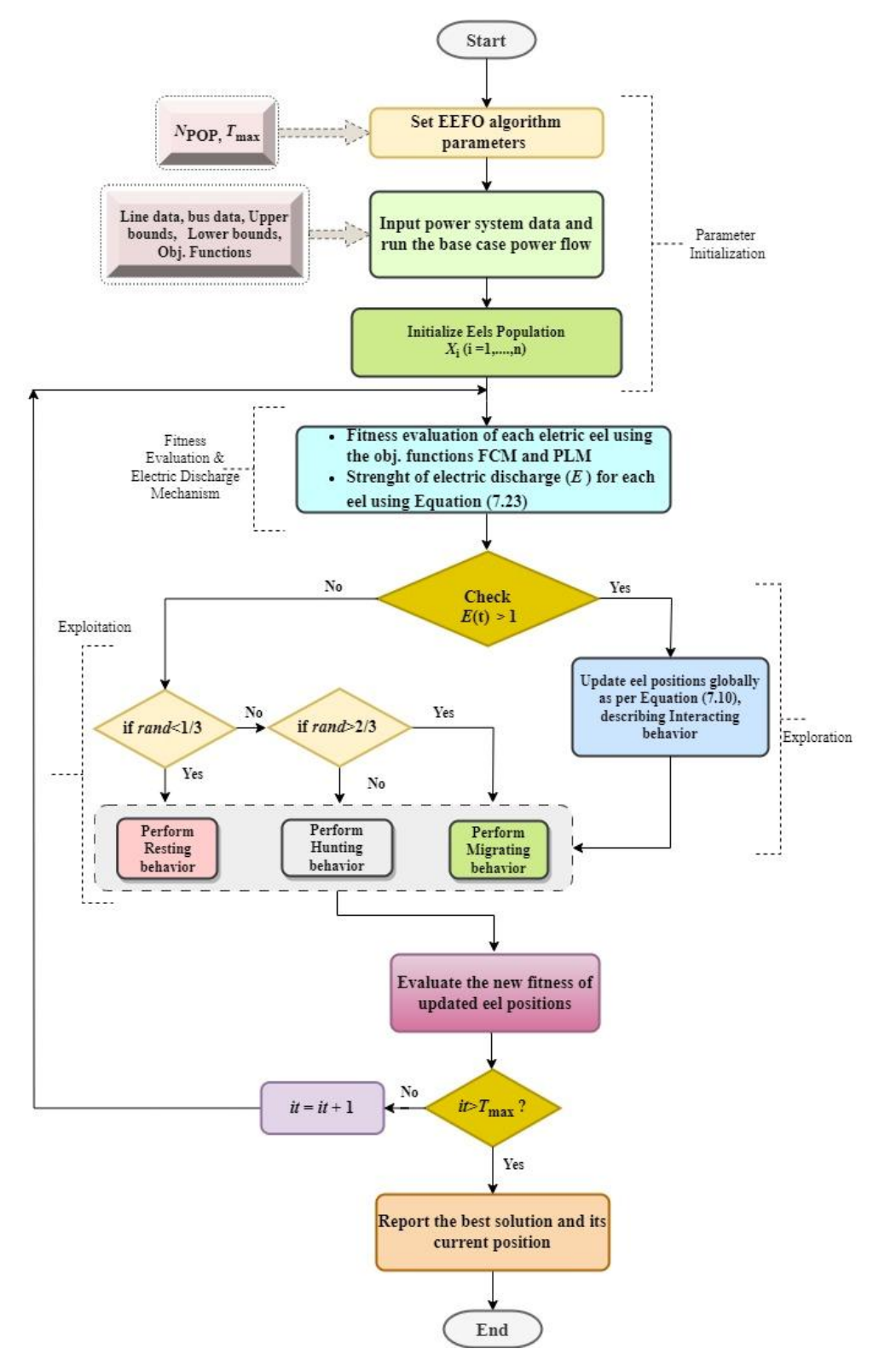


Fig. 7.2. Flowchart of the Electric Eel Foraging Optimizer for OPF

7.4 Simulation Results and Analysis

The effectiveness of the EEFO algorithm was validated by solving SOOPF problems with FCM and PLM as objectives on the IEEE 30-bus network, both with and without distributed generation (DG). DG was incorporated into the OPF formulation to evaluate its impact on

optimization. The computational setup involved a population size (N_{POP}) of 40 and a maximum iteration count (T_{max}) of 100. Simulations were conducted using MATLAB R2018a on a 10th Gen Intel Core i5 laptop (8 GB RAM, 1.19 GHz base speed), ensuring accurate and efficient evaluations. The results demonstrated that EEFO consistently outperformed other algorithms, highlighting its effectiveness in solving real-world OPF challenges.

7.4.1 Test System: IEEE 30-Bus

The IEEE 30-bus standard test system utilized in this study includes six thermal generating units located at buses 1, 2, 5, 8, 11, and 13, with an active power demand of 283.4 MW and a reactive power load of 126.2 MVAR. Additionally, the system features four transformers with a ±10% tapping range situated on lines 6-9, 6-10, 4-12, and 28-27. The system also incorporates nine shunt VAR compensators at buses 10, 12, 15, 17, 20, 21, 23, 24, and 29, as described by Lee et al. (1985). The CV limits (lower and upper bounds), such as line data, bus data, and their initial settings for the IEEE 30-bus system on a 100 MVA base, were also taken from Lee et al. (1985) and Abou El Ela et al. (2010). Table 7.1 outlines the minimum and maximum permissible values for generator unit parameters along with their respective fuel cost coefficients.

Table 7.1 Allowable generator unit parameters and fuel cost coefficients for IEEE 30-bus test system

Bus No.	$P_{ m min}$	P _{max}	$oldsymbol{Q}_{ ext{min}}$	$oldsymbol{Q}_{ ext{max}}$	a (\$/h)	<i>b</i> (\$/ <i>h</i> - MW)	c (\$/h- MW)
1	50	200	-20	200	0.00375	2	0
2	20	80	-20	100	0.0175	1.75	0
5	15	50	-15	80	0.0625	1	0
8	10	35	-15	60	0.0083	3.25	0
11	10	30	-10	50	0.025	3	0
13	12	40	-15	60	0.025	3	0

The considered IEEE 30-bus system is modified by integrating a constant power DG model at bus 30, identified as the optimal location for DG placement by Warid et al. (2016). Their sensitivity analysis identified bus 30 as the most suitable location for DG integration to minimize active power losses and generation costs. The integrated DG unit is a Type 1 unit capable of supplying both active and reactive power. It has a generation capacity of **9.1478 MW** and operates at a **0.85 power factor**, providing **5.6692 MVAR** of reactive power. The EEFO algorithm is applied to further optimize the system, focusing on minimizing power losses and reducing generation costs. This Type-1 DG is, therefore, modelled as a PQ node, injecting both active and reactive power, in line with current operational practices and grid code requirements.

The best results reported in this paper were achieved using the EEFO method with a fixed population size of $N_{\text{POP}} = 40$ and a maximum iteration count of $T_{\text{max}} = 100$ to solve the OPF problem. Table 7.2 contains the optimum parameter setting for the EEFO algorithm, identified through various trials.

 Table 7.2
 Algorithm Parameters

Parameter	Value
$N_{ m POP}$	40
$T_{ m max}$	100
Resting factor, α	0.5
Hunting factor, β	0.5
Curling factor, η	0.55

7.4.2 Case Studies

In this study, the DG unit with a capacity of **9.1478 MW** is modelled as a **constant power source** to simplify the analysis. Although RES like wind and solar are inherently intermittent, a fixed output is assumed to focus on evaluating the impact of DG integration on key OPF objectives, such as FCM and PLM. This simplification allows for a focused assessment of the effectiveness of the EEFO algorithm in achieving optimized solutions.

a) Case 1- OPF for FCM

Scenario (i): OPF with no DG in IEEE 30-bus system

The recently developed EEFO algorithm was applied to solve the OPF problem with the fuel cost as the objective function. The results obtained using this method, along with the optimal CV settings, are presented in the Table 7.3 below. Without incorporating DG, the EEFO algorithm successfully reduced the fuel cost from 902.0046 \$/h to 800.0252 \$/h within 100 iterations, showcasing its efficient convergence capabilities as shown in Figure 7.3 (dashed line). Additionally, the voltage stability index was improved to 0.1301 p.u., representing an enhancement of approximately 24.45% over the base case. However, this improvement in voltage stability was accompanied by a marginal increase in power loss compared to the base case. To validate the effectiveness of EEFO, the results for Case 1 (Scenario (i)) were compared with the Jaya algorithm proposed by Warid et al. The EEFO algorithm achieved a lower fuel cost of 800.0252 \$/h, compared to 800.479 \$/h obtained by Jaya. Additionally, the power loss was reduced to 8.8634 MW with EEFO, compared to 9.0648 MW achieved by the Jaya algorithm.

Table 7.3 OPF solution with optimal CV settings for the IEEE 30-bus test system (Cases 1 & 2)

CVs (n u)	Min	Max	Base case	Ca	se-1	Case-2		
CVs (p.u.)	IVIIII			Scenario (i)	Scenario (ii)	Scenario (i)	Scenario (ii)	
P _{G1} (slack) (MW)	50	200	99.24	1.7677	1.7337	0.5149	0.4227	
P _{G2} (MW)	20	80	80	0.48717	0.4725	0.8	0.79559	
P _{G5} (MW)	15	50	50	0.21521	0.21247	0.49993	0.5	
P _{G8} (MW)	10	35	20	0.21497	0.17392	0.3499	0.35	
P _{G11} (MW)	10	30	20	0.11754	0.11169	0.3	0.3	
P _{G13} (MW)	12	40	20	0.12001	0.12191	0.39998	0.39999	
V _{G1}	0.95	1.1	1.05	1.0953	1.09183	1.07095	1.06755	
$V_{\rm G2}$	0.95	1.1	1.04	1.07677	1.07223	1.06658	1.06444	
V_{G5}	0.95	1.1	1.01	1.04836	1.04147	1.04613	1.04204	
V_{G8}	0.95	1.1	1.01	1.04891	1.0485	1.0537	1.05447	
V _{G11}	0.95	1.1	1.05	1.09981	1.09387	1.07954	1.1	
V _{G13}	0.95	1.1	1.05	1.05212	1.0666	1.06751	1.07513	
TS ₁₁	0.9	1.1	1.078	1.03816	1.05142	1.0854	1.03065	
TS ₁₂	0.9	1.1	1.069	0.95606	0.9022 0.9		0.95282	
TS ₁₅	0.9	1.1	1.032	0.96917	0.98702	1.00436	1.00489	
TS ₃₆	0.9	1.1	1.068	0.97861	0.987	0.9824	0.98292	
Qc10	0	5	0	0.03216	0.00017	0.04804	0.05	
Qc12	0	5	0	0.04406	0.04965	0.04997	0.00265	
Qc15	0	5	0	0.01274	0.00334	0.04993	0	
Qc17	0	5	0	0.05	0.02917	0.04787	0.04285	
Qc20	0	5	0	0.03741	0.04995	0.04735	0	
Qc21	0	5	0	0.04906	0.05	0.04944	0.05	
Qc23	0	5	0	0.02748	0.04999	0.03269	0.04995	
Qc24	0	5	0	0.04969	0.04932	0.05	0	
Qc29	0	5	0	0.02431	0.04964	0.02969	0.04831	
FCM (\$/h)	-	-	902.0046	800.0252	766.6201	967.5437	943.9521	
VDM (p.u.)	-	-	1.1601	1.0525	1.1135	1.0923	0.9938	
VSI (p.u.)	-	-	0.1772	0.1301	0.0885	0.1285	0.0923	
PLM (MW)	-	-	5.8423	8.8634	8.3625	3.0728	2.5773	
ECM (ton/h)	-	-	0.2359	0.3343	0.3293	0.2066	0.2059	
Total Load (MW)	-	-	283.4	283.4	274.2522	283.4	274.2522	

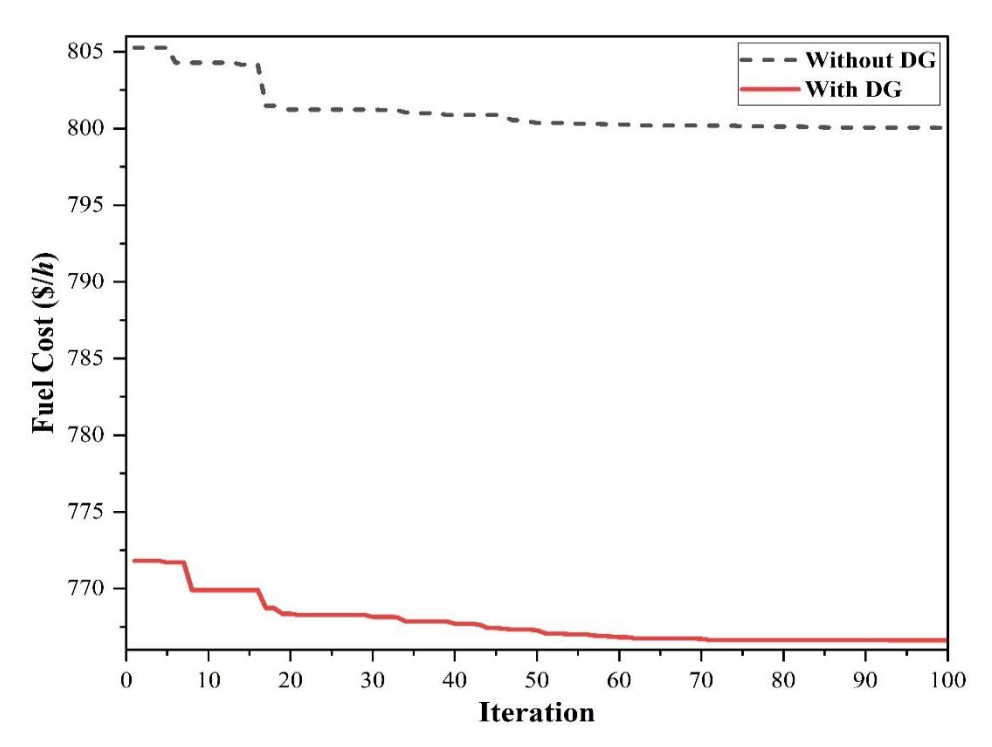


Fig. 7.3. Convergence characteristics comparison of Case 1 using the EEFO - without DG and with DG scenarios

Scenario (ii): OPF with DG unit in IEEE 30-bus system

In this scenario, the EEFO algorithm was applied to solve the OPF problem incorporating one type 1 DG with the same FCM objective. As anticipated, placing the DG strategically at bus 30 enabled the algorithm to reduce the fuel cost further to 766.6201 \$/h, marking a significant improvement of approximately 4.18% compared to the scenario without DG and about 15% improvement from the base case. The convergence characteristics of the EEFO algorithm for both scenarios are illustrated in Fig. 7.3, with the curve (solid line) for the DG-integrated case achieving its optimized value in within 75 iterations, highlighting the algorithm's rapid convergence capabilities. The smooth convergence curves and reduced fuel costs demonstrate the effectiveness of DG integration in enhancing the performance of the EEFO algorithm. Additionally, the incorporation of the DG unit significantly improved system stability. The Lindex decreased to 0.0885 p.u., marking a 31.94% improvement compared to the scenario without DG (0.1301 p.u.). Concurrently, power losses were reduced to 8.3625 MW, representing a 5.65% improvement over the scenario without DG. Moreover, the emission cost decreased from 0.3343 ton/h in the case without DG to 0.3293 ton/h with DG. This inclusion of DG contributed to a marginal but meaningful reduction in emissions, further demonstrating the effectiveness of the algorithm.

When compared with the Jaya algorithm by Warid et al. for DG placement at bus 30, the EEFO algorithm demonstrated superior performance. The fuel cost achieved by Jaya was 768.039 \$/h, whereas EEFO reduced it further to 766.6201 \$/h. Similarly, the power loss was reduced from 8.4983 MW with Jaya to 8.3625 MW with EEFO.

Figure 7.4 depicts the voltage profile provided by the proposed EEFO for Case 1, showing that voltage magnitudes at all buses remain within the specified limits in both the scenarios.

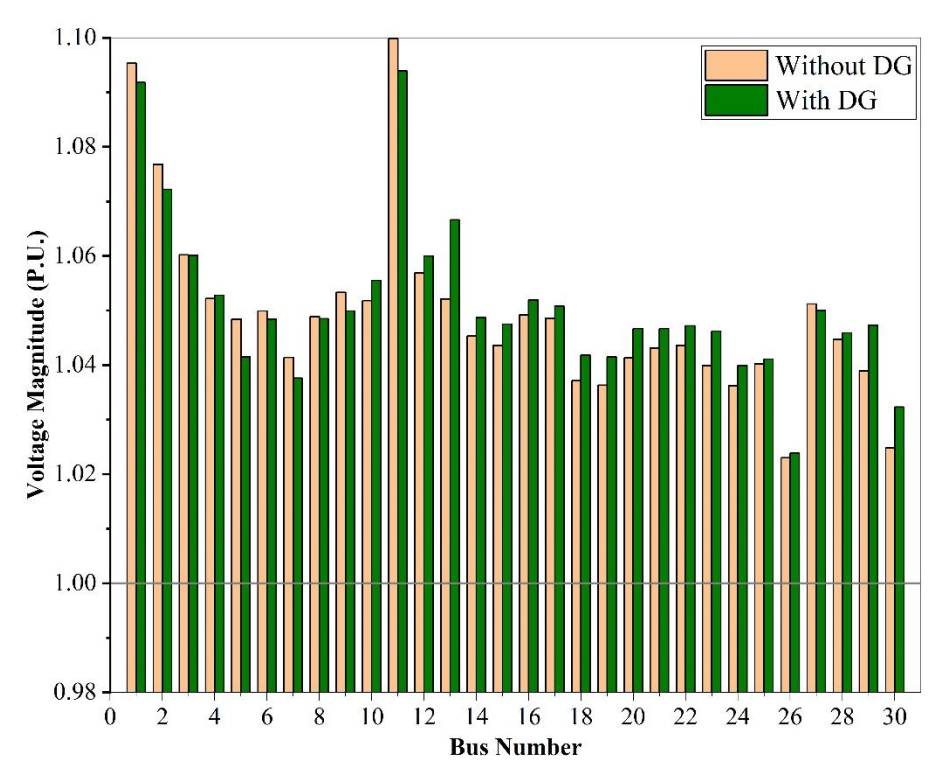


Fig. 7.4. Voltage profile for Case 1 - without DG and with DG scenarios

b) Case 2: OPF for PLM

Scenario (i): OPF with no DG in IEEE 30-bus system

The primary objective in this case was to minimize active power losses (P_{Loss}). The EEFO algorithm was applied to achieve the optimal solution, with the results summarized in Table 7.3. The EEFO algorithm proved to be highly effective in determining the optimal CV settings to minimize system losses. As a result, the real power losses were significantly reduced from 5.8423 MW (base case) to 3.0728 MW, representing an improvement of approximately 47.40% without incorporating DG. The smooth convergence characteristics of the EEFO algorithm, as illustrated in Fig. 7.5 (dashed line), further highlight its efficiency in finding the optimal solution.

Scenario (ii): OPF with DG in IEEE 30-bus system

In this case, the EEFO algorithm was utilized to solve the OPF problem considering PLM objective, incorporating one Type 1 DG unit. Placing the DG strategically at bus 30 resulted in a reduction of real power losses to 2.5773 MW, a generation fuel cost saving of approximately 23.6 \$/h, along with an impressive voltage stability index value of 0.0923 p.u. Figure 7.5 (solid line) demonstrates the rapid convergence of the EEFO algorithm towards the optimal solution within 100 iterations, showcasing its effectiveness in minimizing power losses with DG integration.

In comparison to the Jaya algorithm proposed by Warid et al. for DG placement at bus 30, the EEFO algorithm achieved a 3.65% reduction in power losses, recording a value of 2.5773 MW compared to Jaya's 2.67504 MW. Although, in this scenario, the Jaya algorithm demonstrated a slight advantage in minimizing fuel costs, the EEFO algorithm's superior capability in reducing power losses highlights its effectiveness in optimizing system operation.

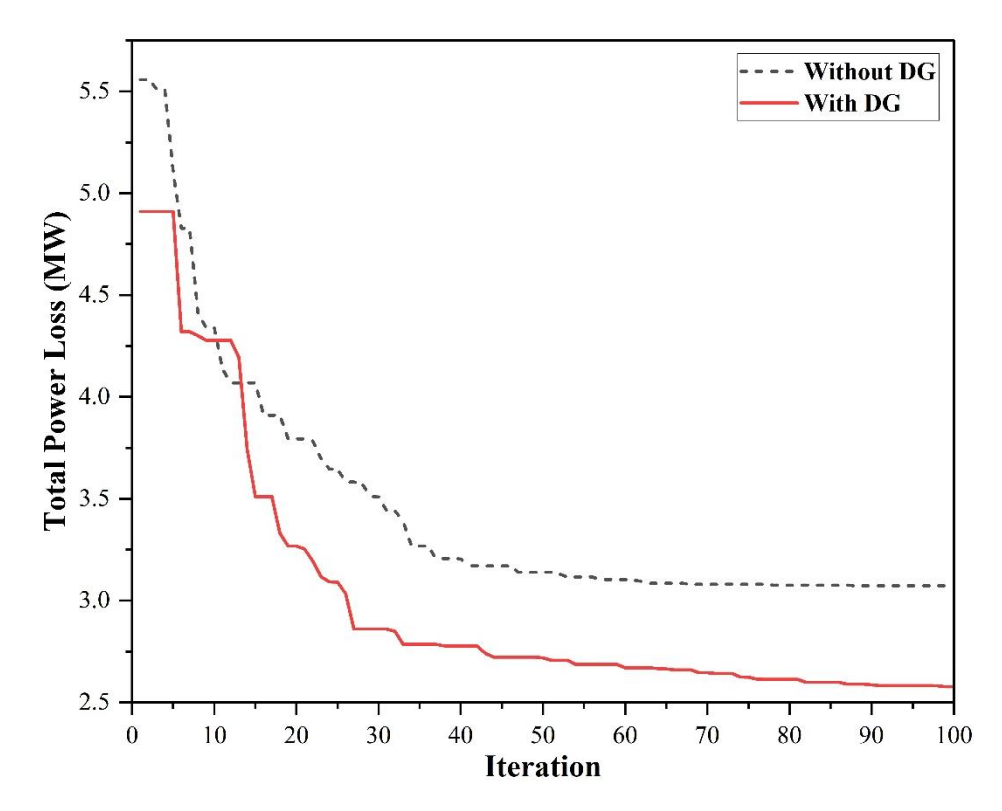


Fig. 7.5. Convergence characteristics comparison of Case 1 using the EEFO - without DG and with DG scenarios

Figure 7.6 depicts the voltage profile provided by the proposed EEFO for Case 2, showing that voltage magnitudes at all buses remain within the specified limits. In the with DG scenario, voltage magnitudes are predominantly closer to the reference value of 1.0 p.u. The addition of

DG results in a more uniform and stable voltage distribution across the network while adhering to operational constraints.

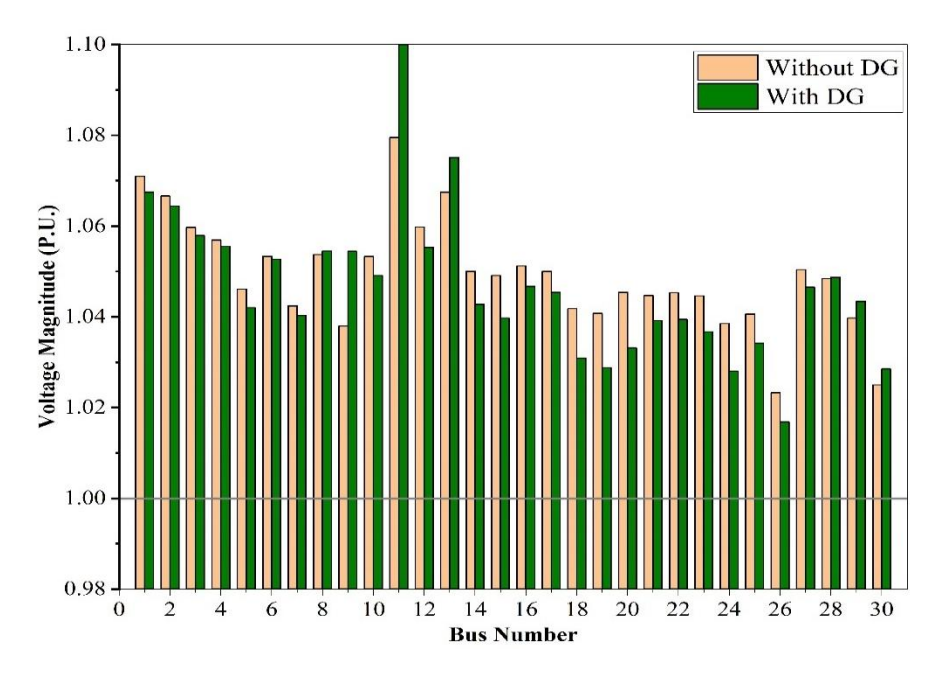


Fig. 7.6. Voltage profile for Case 2 - without DG and with DG scenarios

7.5 Conclusion

In this paper, the EEFO algorithm is successfully applied to solve the OPF problem in electrical power networks. The algorithm is tested both without and with the incorporation of DG in single-objective optimization cases. The primary objectives considered are generation cost reduction and active power loss minimization. The performance of the EEFO algorithm was validated using standard IEEE 30-bus test system.

The results demonstrated that the EEFO algorithm effectively minimized fuel cost and power loss while adhering to system constraints, including generator limits, voltage profiles, and line flow limits. Compared with literature values, EEFO showcased competitive performance in achieving optimal solutions with fast convergence and enhanced system stability, especially with optimally integrated DG.

These findings suggest that EEFO is a promising optimization technique for solving OPF problems in small-scale power systems. Its simplicity, solution quality, and computational efficiency make it a promising approach for practical power system applications. Future work could extend EEFO to multi-objective OPF (MOOPF) problems, large-scale systems, and probabilistic models to address uncertainties associated with RES, enhancing its practical applicability.

CHAPTER 8

CONCLUSION, FUTURE SCOPE AND SOCIAL IMPACT

8.1 Conclusion

This research presents innovative optimization techniques tailored to address the complex and multi-faceted challenges of OPF in modern power systems. Among the algorithms introduced and evaluated are the Hybrid Rao-2 Sine Cosine Algorithm (HRSCA), the Learning-based Sine Cosine Algorithm (L-SCA), the Coot Optimization Algorithm (COA), and the Electric Eel Foraging Optimization (EEFO) Algorithm. Each of these methods has demonstrated its effectiveness in solving key OPF objectives, such as fuel cost minimization (FCM), voltage deviation minimization (VDM), voltage stability enhancement (VSE) power loss minimization (PLM), and emission minimization (EM). The algorithms were rigorously tested on diverse power system networks, including IEEE 30-bus, 57-bus, 118-bus systems, and the Algerian 59-bus network, under various operating scenarios, including load growth and contingency events.

The L-SCA addresses the limitations of the standard SCA by introducing a learner phase inspired by TLBO. This enhancement improves the algorithm's exploitation capabilities while maintaining population diversity. L-SCA has demonstrated significant improvements in solution quality, convergence speed, and scalability, making it highly effective for solving complex OPF problems across small-, medium-, and large-scale networks.

Similarly, the Hybrid Rao-2 Sine Cosine Algorithm (HRSCA) demonstrates exceptional performance by effectively balancing exploration and exploitation dynamics. By integrating the global exploration capability of the SCA with the convergence efficiency of the Rao-2 Algorithm, HRSCA achieves faster convergence and delivers high-quality solutions. This hybrid approach proves effective in both single-objective and multi-objective optimization scenarios. Extensive case studies, including scenarios involving load growth and contingency conditions, underline the algorithm's robustness and adaptability.

Additionally, the COA, inspired by the cooperative foraging behaviour of coot birds, has proven to be a robust and adaptive solution for OPF problems. The COA successfully handles the non-linear, non-convex nature of OPF by maintaining population diversity and preventing premature convergence. Its effectiveness has been demonstrated specifically on the 30-bus system.

The EEFO algorithm, inspired by the unique electrical behaviour of eels, stands out for its capability to adapt dynamically to complex and constrained optimization landscapes. By mimicking the electrical discharges and movement strategies of eels, this algorithm efficiently balances exploration and exploitation, ensuring robust convergence to high-quality solutions. The electric eel algorithm, specifically, was applied to the IEEE 30-bus system with two key objective functions: generation cost minimization (FCM objective) and real power loss reduction (PLM objective). By optimizing control variables and incorporating the impact of DG, the algorithm demonstrated significant improvements in operational efficiency. The results highlight reduced fuel costs and lower power losses making the Electric EEL algorithm a promising tool for modern OPF challenges with RER integration.

The ability of the algorithms like L-SCA and HRSCA to optimize multiple objectives while satisfying system constraints positions them as valuable tools for power system optimization. The results obtained from this research highlight the practicality and scalability of the proposed algorithms in addressing real-world challenges in power systems. Collectively, these approaches offer reliable and efficient solutions for modern power system challenges, demonstrating significant improvements over conventional methods. Significant improvements were observed in reducing fuel costs, emissions, and power losses while maintaining voltage stability and ensuring operational security under normal and critical conditions.

8.2 Future Scope

The field of OPF continues to evolve with the introduction of advanced computational algorithms and the integration of renewable energy resources. The promising results obtained in this research open up exciting avenues for future exploration and development:

8.2.1 Incorporation of Renewable Energy Sources (RES)

The integration of RES into OPF formulations offers opportunities to enhance the sustainability and resilience of power systems. Future research can focus on developing methods to better incorporate RES, considering their intermittent and variable nature. Additionally, the impact of uncertainties in RES generation on the performance of the proposed algorithms can be investigated to improve their robustness and reliability while ensuring grid stability. Such studies will contribute to the development of more adaptive and sustainable power system operations.

8.2.2 Real-time Applications

Real-time implementation of OPF can play a key role in improving the dynamic control and optimization of power systems. Future work can focus on developing algorithms that can quickly provide solutions to meet the requirements of real-time operations. Additionally, advanced communication technologies can be explored to ensure smooth and efficient data exchange between control centres and distributed energy resources (DERs). This will help in better coordination, faster decision-making, and improved use of resources in modern, decentralized power systems

8.2.3 Multi-Objective Optimization

The application of multi-objective optimization techniques offers significant potential for addressing conflicting objectives in power system operation, such as minimizing operational costs while maximizing renewable energy penetration. Future work can focus on developing and implementing advanced optimization frameworks capable of balancing economic, environmental, and social considerations particularly with RER integration. These frameworks should incorporate strategies to address trade-offs between cost-effectiveness, environmental sustainability, and grid reliability.

8.2.4. Hybrid Approaches

This thesis has demonstrated the effectiveness of a hybrid approach in specific OPF scenarios, but further research is needed to unlock their full potential. Future directions may include:

Advanced Hybrid Frameworks

Developing more advanced hybrid frameworks that effectively combine the strengths of multiple algorithms, such as integrating metaheuristics with traditional optimization techniques. Additionally, ML-based methods can be explored to adaptively select and combine algorithms based on the characteristics of specific OPF problems, improving performance and flexibility.

Real-Time Applications

Extending hybrid approaches for real-time OPF to handle dynamic power system conditions, such as load variations and fluctuating renewable energy generation. The focus can be on designing efficient algorithms capable of adapting quickly to real-time changes and providing optimal solutions within limited time frames.

• Large-Scale Systems

Investigating the scalability of hybrid approaches for application in large-scale power systems. Future work can include developing parallel and distributed implementations to enhance computational efficiency and address the complexities of larger optimization problems effectively.

8.2.5. Advanced Power System Models

Incorporating more detailed power system models into OPF formulations can enhance the accuracy and reliability of solutions. Future research can focus on integrating dynamic models and performing transient stability analysis to better capture the real-world behaviour of power systems.

Additionally, the influence of emerging technologies, such as Flexible AC Transmission Systems (FACTS) and energy storage systems, on OPF should be explored. FACTS devices provide greater flexibility and control over power flows, voltage levels, and system stability, enabling more precise management of the power grid. Energy storage systems, on the other hand, offer the ability to store excess energy and dispatch it during peak demand periods, improving overall system efficiency and reliability. These technologies can provide greater flexibility and control in system operations, and their integration into OPF models can further optimize performance under diverse operating conditions.

8.2.6. Exploration of Novel Objective Functions

While traditional OPF objectives like cost minimization, emission reduction, and power loss minimization are crucial, there is a growing need to address more customer-centric metrics. Future research can shift towards including reliability indices, which measure the consistency and dependability of the power supply, ensuring that customers experience fewer interruptions and better service quality. Additionally, power quality metrics, such as frequency stability, transient response, harmonic distortion, etc., can be incorporated to ensure that the electricity delivered is not only reliable but also meets high standards of quality, preventing equipment damage and improving overall customer satisfaction.

Furthermore, real-time pricing optimization can be explored to better align electricity prices with supply and demand fluctuations, encouraging more efficient energy use. By integrating these metrics into OPF formulations, the focus can move towards enhancing the end-user experience, promoting smarter energy consumption patterns, and supporting the grid's stability through dynamic pricing strategies.

Integrating social and environmental factors, such as public health benefits and sustainability, can lead to more holistic power system management. This approach ensures that

power systems are not only efficient and reliable but also aligned with societal and environmental goals.

8.3 Social Impact

The optimization techniques developed in this research have profound implications for societal well-being and contribute significantly to addressing key challenges in the energy sector.

8.3.1 Economic Impact

The implementation of the L-SCA and HRSCA demonstrates significant reductions in fuel costs and power losses. These cost efficiencies translate into substantial operational savings for utilities, which can ultimately lower energy prices for consumers. By making energy more affordable, this research contributes to the vital goal of ensuring reliable and accessible power for a growing population.

8.3.2 Environmental Sustainability

From a social perspective, the proposed algorithms contribute to global sustainability efforts by minimizing emissions and facilitating the integration of renewable energy sources into the power systems. These advancements align with international efforts to combat climate change and achieve carbon neutrality. By reducing the reliance on traditional, carbon-intensive energy generation methods, the research contributes to preserving the environment for future generations.

8.3.3 Grid Stability and Resilience

The proposed optimization techniques enhance grid stability by improving voltage stability, loading margin stability, and overall system security. These improvements make the power grid more resilient to blackouts and voltage collapses, especially under high-load conditions or contingency scenarios. This ensures a reliable energy supply, which is crucial for maintaining societal functions and economic activities, thereby bolstering community resilience against energy-related challenges.

8.3.4 Advancing Smart Grids

The research is highly relevant to next-generation power systems, particularly smart grids. The optimization strategies introduced in this study facilitate the efficient operation of advanced technologies, including electric vehicles, energy storage systems, and distributed energy resources. These advancements are critical for modernizing the energy sector and fostering the growth of more adaptive and intelligent grids.

8.3.5 Global Energy Transition

On a global scale, the methodologies developed and discussed in this thesis offer a practical framework for addressing the dual challenges of rising energy demand and environmental conservation. This framework facilitates a transition towards low-carbon energy solutions, supporting international sustainability goals and contributing to a healthier, more sustainable society.

The adaptive strategies implemented in L-SCA, along with the hybridization techniques introduced in HRSCA, offer substantial potential for advancing optimization methodologies. L-SCA, as an enhanced version of the SCA, and HRSCA, a hybrid approach combining the strengths of SCA and the Rao-2 algorithm, demonstrate exceptional capability in addressing complex optimization challenges. While primarily applied to power systems in this research, these methodologies hold promise for broader applications across various engineering and industrial domains. By providing scalable and robust solutions, they open up new possibilities for addressing complex optimization challenges in diverse fields.

In conclusion, the optimization techniques developed in this research not only tackle the current challenges in power system management but also lay the groundwork for a sustainable, efficient, and socially responsible energy future. These contributions play a key role in the development of smarter, greener, and more adaptive energy systems, supporting the global transition toward a sustainable and low-carbon energy landscape.

REFERENCES

- 1. Abaci, K. and Yamacli, V., 2016. Differential search algorithm for solving multi-objective optimal power flow problem. *International Journal of Electrical Power & Energy Systems*, Vol. 79, pp. 1–10. https://doi.org/10.1016/j.ijepes.2015.12.021
- 2. Abd El-sattar, S., Kamel, S., Ebeed, M. and Jurado, F., 2021. An improved version of salp swarm algorithm for solving optimal power flow problem. *Soft Computing*, Vol. 25, pp. 4027–4052. https://doi.org/10.1007/s00500-020-05431-4
- 3. Abd Elaziz, D., Oliva, D. and Xiong, S., 2017. An improved opposition-based sine cosine algorithm for global optimization. *Expert Systems with Applications*, Vol. 90, pp. 484–500. https://doi.org/10.1016/j.eswa.2017.07.043
- 4. Abido, M. A., 2003. Environmental/economic power dispatch using multi-objective evolutionary algorithms. *IEEE Transactions on Power Systems*, Vol. 18, No. 4, pp. 1529–1537. https://doi.org/10.1109/TPWRS.2003.818693
- 5. Abido, M. A., 2002. Optimal power flow using particle swarm optimization. *International Journal of Electrical Power & Energy Systems*, Vol. 24, No. 7, pp. 563–571.
- 6. Abou El Ela, A. A., Abido, M. A. and Spea, S. R., 2010. Optimal power flow using differential evolution algorithm. *Electric Power Systems Research*, Vol. 80, No. 7, pp. 878–885. https://doi.org/10.1016/j.epsr.2009.12.018
- 7. Abou El Ela, A. A., El-Sehiemy, R. A. A., Mouwafi, M. T. and Salman, D. A. F., 2018. Multi-objective fruit fly optimization algorithm for OPF solution in power system. *Proceedings of the 2018 Twentieth International Middle East Power Systems Conference (MEPCON)*, pp. 254–259. https://doi.org/10.1109/MEPCON.2018.8635232
- 8. Adaryani, M. R. and Karami, A., 2013. Artificial bee colony algorithm for solving multi-objective optimal power flow problem. *International Journal of Electrical Power & Energy Systems*, Vol. 53, pp. 219–230. https://doi.org/10.1016/j.ijepes.2013.04.021
- 9. Akbari, E., Ghasemi, M., Gil, M., Rahimnejad, A., and Andrew Gadsden, S., 2022. Optimal power flow via teaching-learning-studying-based optimization algorithm. *Electric Power Components and Systems*, Vol. 49, Nos. 6–7, pp. 584–601. https://doi.org/10.1080/15325008.2021.1971331
- 10. Akdag, O., 2022. An improved Archimedes optimization algorithm for multi/single-objective optimal power flow. *Electric Power Systems Research*, Vol. 206, p.107796. https://doi.org/10.1016/j.epsr.2022.107796
- 11. Al-Bahrani, L., Al-Kaabi, M., and Al Hasheme, J., 2022. Solving optimal power flow problem using improved differential evolution algorithm. *International Journal of Electrical and Electronic Engineering & Telecommunications*, Vol. 11, No. 2, pp. 146–155. https://doi.org/10.18178/ijeetc.11.2.146-155
- 12. Al-Kaabi, M., Dumbrava, V., and Eremia, M., 2022. A slime mould algorithm programming for solving single and multi-objective optimal power flow problems with Pareto front approach: A case study of the Iraqi super grid high voltage. *Energies*, Vol. 15, No. 20, Article 7473. https://doi.org/10.3390/en15207473
- 13. Alghamdi, A. S., 2022. Optimal power flow of renewable-integrated power systems using a Gaussian bare-bones Levy-flight firefly algorithm. *Frontiers in Energy Research*, Vol. 10, p.921936. https://doi.org/10.3389/fenrg.2022.921936
- 14. Alghamdi, A.S., 2023. Optimal power flow of hybrid wind/solar/thermal energy integrated power systems considering costs and emissions via a novel and efficient search optimization algorithm. *Applied Sciences*, Vol. 13, No. 8, p.4760. https://doi.org/10.3390/app13084760

- 15. Alhelou, H. H., Hamedani-Golshan, M. E., Njenda, T. C., and Siano, P., 2019. A survey on power system blackout and cascading events: Research motivations and challenges. *Energies*, Vol. 12, No. 4, p.682. https://doi.org/10.3390/en12040682
- 16. AlRashidi, M., and El-Hawary, M., 2009. Applications of computational intelligence techniques for solving the revived optimal power flow problem. *Electric Power Systems Research*, Vol. 79, No. 4, pp. 694–702. https://doi.org/10.1016/j.epsr.2008.10.004
- 17. Amjady, N., Fatemi, H., and Zareipour, H., 2012. Solution of optimal power flow subject to security constraints by a new improved bacterial foraging method. *IEEE Transactions on Power Systems*, Vol. 27, No. 3, pp. 1311–1323. https://doi.org/10.1109/TPWRS.2011.2175455
- 18. Athari, M. H. and Wang, Z., 2018. Impacts of wind power uncertainty on grid vulnerability to cascading overload failures. *IEEE Transactions on Sustainable Energy*, Vol. 9, No. 1, pp. 128–137. https://doi.org/10.1109/TSTE.2017.2718518
- 19. Attia, A. F., Al-Turki, Y. A., and Abusorrah, A. M., 2012. Optimal power flow using adapted genetic algorithm with adjusting population size. *Electric Power Components and Systems*, Vol. 40, No. 11, pp. 1285–1299. https://doi.org/10.1080/15325008.2012.689417
- 20. Attia, A.F., El Sehiemy, R.A. and Hasanien, H.M., 2018. Optimal power flow solution in power systems using a novel Sine-Cosine algorithm. *International Journal of Electrical Power & Energy Systems*, Vol. 99, pp.331-343. https://doi.org/10.1016/j.ijepes.2018.01.024
- 21. Aurangzeb, K., Shafiq, S., Pamir, P., Javaid, N., Alhussein, M. and Imran, M., 2023. An effective solution to the optimal power flow problem using meta-heuristic algorithms. *Frontiers in Energy Research*, Vol. 11, p.1170570. https://doi.org/10.3389/fenrg.2023.1170570
- 22. Avvari, R. K., and Vinod Kumar, D., 2022. Multi-objective optimal power flow with efficient constraint handling using hybrid decomposition and local dominance method. *Journal of The Institution of Engineers (India): Series B*, Vol. 103, No. 5, pp. 1643–1658. https://doi.org/10.1007/s40031-022-00748-0
- 23. Bai, W., Eke, I., and Lee, K. Y., 2017. An improved artificial bee colony optimization algorithm based on orthogonal learning for optimal power flow problem. *Control Engineering Practice*, Vol. 61, pp. 163–172. https://doi.org/10.1016/j.conengprac.2017.02.010
- 24. Bakirtzis, A. G., Biskas, P. N., Zoumas, C. E., and Petridis, V., 2002. Optimal power flow by enhanced genetic algorithm. *IEEE Transactions on Power Systems*, Vol. 17, No. 2, pp. 229–236. https://doi.org/10.1109/TPWRS.2002.1007886
- 25. Basu, M., 2016. Group search optimization for solution of different optimal power flow problems. *Electric Power Components and Systems*, Vol. 44, No. 6, pp. 606–615. https://doi.org/10.1080/15325008.2015.1122109
- 26. Belazzoug, M., Touahria, M., Nouioua, F. and Brahimi, M., 2020. An improved sine cosine algorithm to select features for text categorization. *Journal of King Saud University Computer and Information Sciences*, Vol. 32, No. 4, pp. 454–464. https://doi.org/10.1016/j.jksuci.2019.07.003
- 27. Bentouati, B., Khelifi, A., Shaheen, A. M., and El-Sehiemy, R. A., 2021. An enhanced moth-swarm algorithm for efficient energy management-based multi-dimensions OPF problem. *Journal of Ambient Intelligence and Humanized Computing*, Vol. 12, pp. 9499–9519. https://doi.org/10.1007/s12652-020-02692-7
- 28. Bhattacharya, A., and Chattopadhyay, P. K., 2009. Biogeography-based optimization for different economic load dispatch problems. *IEEE Transactions on Power Systems*, Vol. 25, No. 2, pp. 1064–1077. https://doi.org/10.1109/TPWRS.2009.2034525

- 29. Bhattacharya, A., and Roy, P., 2012. Solution of multi-objective optimal power flow using gravitational search algorithm. *IET Generation, Transmission & Distribution*, Vol. 6, No. 8, pp. 751–763. https://doi.org/10.1049/iet-gtd.2011.0593
- 30. Blum, C., Blesa Aguilera, M. J., Roli, A. and Sampels, M., 2008. *Hybrid Metaheuristics: An Emerging Approach to Optimization. Studies in Computational Intelligence*, Vol. 114. Springer.
- 31. Bouchekara, H. R. E. H. and Abido, M. A., 2014. Optimal power flow using differential search algorithm. *Electric Power Components and Systems*, Vol. 42, No. 15, pp. 1683–1699. https://doi.org/10.1080/15325008.2014.949912
- 32. Bouchekara, H. R. E. H., Abido, M. A. and Boucherma, M., 2014a. Optimal power flow using teaching-learning-based optimization technique. *Electric Power Systems Research*, Vol. 114, pp. 49–59. https://doi.org/10.1016/j.epsr.2014.03.032
- 33. Bouchekara, H.R.E.H., 2014b. Optimal power flow using black-hole-based optimization approach. *Applied Soft Computing*, Vol. 24, pp.879-888. https://doi.org/10.1016/j.asoc.2014.08.056
- 34. Bouchekara, H. R. E. H., Abido, M. A., Chaib, A. E. and Mehasni, R., 2014c. Optimal power flow using the league championship algorithm: A case study of the Algerian power system. *Energy Conversion and Management*, Vol. 87, pp. 58–70. https://doi.org/10.1016/j.enconman.2014.06.088
- 35. Bouchekara, H. R. E. H., Chaib, A. E. and Abido, M. A., 2016a. Multiobjective optimal power flow using a fuzzy-based grenade explosion method. *Energy Systems*, Vol. 7, pp. 699–721. https://doi.org/10.1007/s12667-016-0206-8
- 36. Bouchekara, H. R., Chaib, A. E., Abido, M. A. and El-Sehiemy, R. A., 2016b. Optimal power flow using an improved colliding bodies optimization algorithm. *Applied Soft Computing*, Vol. 42, pp. 119–131. https://doi.org/10.1016/j.asoc.2016.01.041
- 37. Boussaïd, I., Lepagnot, J., and Siarry, P., 2013. A survey on optimization metaheuristics. *Information Sciences*, Vol. 237, pp. 82–117. https://doi.org/10.1016/j.ins.2013.02.041
- 38. Buch, H., Trivedi, I. N., and Jangir, P., 2017. Moth flame optimization to solve optimal power flow with non-parametric statistical evaluation validation. *Cogent Engineering*, Vol. 4, No. 1, p.1286731. https://doi.org/10.1080/23311916.2017.1286731
- 39. Buch, H., and Trivedi, I. N., 2019. An efficient adaptive moth flame optimization algorithm for solving large-scale optimal power flow problem with POZ, multifuel, and valve-point loading effect. *Iranian Journal of Science and Technology, Transactions of Electrical Engineering*, Vol. 43, pp. 1031–1051. https://doi.org/10.1007/s40998-019-00211-9
- 40. Carpentier, J., 1962. Contribution à l'étude du dispatching économique. *Bulletin de la Société Française des Électriciens*, Vol. 3, No. 1, pp. 431–447.
- 41. Chaib, A., Bouchekara, H., Mehasni, R., and Abido, M. A., 2016. Optimal power flow with emission and non-smooth cost functions using backtracking search optimization algorithm. *International Journal of Electrical Power & Energy Systems*, Vol. 81, pp. 64–77. https://doi.org/10.1016/j.ijepes.2016.02.004
- 42. Chen, H., Bo, M. L., and Zhu, Y., 2014. Multi-hive bee foraging algorithm for multi-objective optimal power flow considering the cost, loss, and emission. *International Journal of Electrical Power & Energy Systems*, Vol. 60, pp. 203–220. https://doi.org/10.1016/j.ijepes.2014.02.017
- 43. Christie, R., 1993. Power Systems Test Case Archive. University of Washington. [Online]. Available: http://www.ee.washington.edu/research/pstca/pf118/pg_tca118bus.htm. Accessed: 4 Sept 2023.

- 44. Daqaq, F., Ouassaid, M., and Ellaia, R., 2021. A new meta-heuristic programming for multi-objective optimal power flow. *Electrical Engineering*, Vol. 103, pp. 1217–1237. https://doi.org/10.1007/s00202-020-01173-6
- 45. Daryani, N., Hagh, M. T., and Teimourzadeh, S., 2016. Adaptive group search optimization algorithm for multi-objective optimal power flow problem. *Applied Soft Computing*, Vol. 38, pp. 1012–1024. https://doi.org/10.1016/j.asoc.2015.10.057
- 46. Dash, S. P., Subhashini, K., and Chinta, P., 2022. Development of a boundary assigned animal migration optimization algorithm and its application to optimal power flow study. *Expert Systems with Applications*, Vol. 200, p.116776. https://doi.org/10.1016/j.eswa.2022.116776
- 47. Dommel, H. W. and Tinney, T. F., 1968. Optimal power flow solutions. *IEEE Transactions on Power Apparatus and Systems*, Vol. 87, No. 5, pp. 1866–1876. https://doi.org/10.1109/TPAS.1968.292150
- 48. Duman, S., Güvenç, U., Sönmez, Y., and Yörükeren, N., 2012. Optimal power flow using gravitational search algorithm. *Energy Conversion and Management*, Vol. 59, pp. 86–95. https://doi.org/10.1016/j.enconman.2012.02.024
- 49. El-Dabah, M., Ebrahim, M. A., El-Sehiemy, R. A., Alaas, Z., and Ramadan, M. M., 2022. A modified whale optimizer for single- and multi-objective OPF frameworks. Energies, Vol. 15, No. 7, p.2378. https://doi.org/10.3390/en15072378
- 50. El-Fergany, A. A., and Hasanien, H. M., 2015. Single and multi-objective optimal power flow using grey wolf optimizer and differential evolution algorithms. *Electric Power Components and Systems*, Vol. 43, No. 13, pp. 1548–1559. https://doi.org/10.1080/15325008.2015.1041625
- 51. El-Fergany, A. A. and Hasanien, H. M., 2020. Salp swarm optimizer to solve optimal power flow comprising voltage stability analysis. *Neural Computing and Applications*, Vol. 32, No. 9, pp. 5267–5283. https://doi.org/10.1007/s00521-019
- 52. El-Hana Bouchekara, H. R., Abido, M. A., and Chaib, A. E., 2016. Optimal power flow using an improved electromagnetism-like mechanism method. *Electric Power Components and Systems*, Vol. 44, No. 4, pp. 434–449. https://doi.org/10.1080/15325008.2015.1115919
- 53. El Sehiemy, R. A., Selim, F., Bentouati, B., and Abido, M. A., 2020. A novel multi-objective hybrid particle swarm and salp optimization algorithm for technical-economical-environmental operation in power systems. *Energy*, Vol. 193, Article 116817. https://doi.org/10.1016/j.energy.2019.116817
- 54. Elattar, E. E., 2018. Modified harmony search algorithm for combined economic emission dispatch of microgrid incorporating renewable sources. *Energy*, Vol. 159, pp. 496–507. https://doi.org/10.1016/j.energy.2018.06.137
- 55. El-Sattar, S. A., Kamel, S., El Sehiemy, R. A., Jurado, F. and Yu, J., 2019. Single- and multi-objective optimal power flow frameworks using Jaya optimization technique. *Neural Computing and Applications*, Vol. 31, pp. 8787–8806. https://doi.org/10.1007/s00521-019-04194-w
- 56. Elattar, E. E. and ElSayed, S. K., 2019. Modified JAYA algorithm for optimal power flow incorporating renewable energy sources considering the cost, emission, power loss, and voltage profile improvement. *Energy*, Vol. 178, pp. 598–609. https://doi.org/10.1016/j.energy.2019.04.159
- 57. Farhat, M., Kamel, S., Atallah, A. M. and Khan, B., 2021. Optimal power flow solution based on jellyfish search optimization considering uncertainty of renewable energy sources. *IEEE Access*, Vol. 9, pp. 100911–100933. https://doi.org/10.1109/ACCESS.2021.3097006
- 58. Frank, S., Steponavice, I. and Rebennack, S., 2012a. Optimal power flow: A bibliographic survey I: Formulations and deterministic methods. *Int J Energy Systems*, Vol. 3, pp. 221–258. https://doi.org/10.1007/s12667-012-0056-y

- 59. Frank, S., Steponavice, I. and Rebennack, S., 2012b. Optimal power flow: A bibliographic survey II: Non-deterministic and hybrid methods. *Energy Systems*, Vol. 3, pp. 259–289. https://doi.org/10.1007/s12667-012-0057-x
- 60. Gabis, A. B., Meraihi, Y., Mirjalili, S. and Ramdane-Cherif, A., 2021. A comprehensive survey of sine cosine algorithm: Variants and applications. *Artificial Intelligence Review*, Vol. 54, No. 7, pp. 5469–5540. https://doi.org/10.1007/s10462-021-10026-y
- 61. Ghasemi, M., Ghavidel, S., Rahmani, S., Roosta, A., and Falah, H., 2014. A novel hybrid algorithm of imperialist competitive algorithm and teaching-learning algorithm for optimal power flow problem with non-smooth cost functions. *Engineering Applications of Artificial Intelligence*, Vol. 29, pp. 54–69. https://doi.org/10.1016/j.engappai.2013.11.003
- 62. Ghasemi, M., Ghavidel, S., Gitizadeh, M. and Akbari, E., 2015. An improved teaching-learning-based optimization algorithm using Lévy mutation strategy for non-smooth optimal power flow. *International Journal of Electrical Power & Energy Systems*, Vol. 65, pp. 375–384. https://doi.org/10.1016/j.ijepes.2014.10.027
- 63. Gnanambal, K. and Babulal, C. K., 2012. Maximum loadability limit of power system using hybrid differential evolution with particle swarm optimization. *International Journal of Electrical Power & Energy Systems*, Vol. 43, pp. 150–155. https://doi.org/10.1016/j.ijepes.2012.04.033
- 64. Gouda, E. A., Kotb, M. F., Ghoneim, S. S., Al-Harthi, M. M. and El-Fergany, A. A., 2021. Performance assessment of solar generating units based on coot bird metaheuristic optimizer. *IEEE Access*, Vol. 9, pp. 111616–111632. https://doi.org/10.1109/ACCESS.2021.3072605
- 65. Gupta, S., Kumar, N. and Srivastava, L., 2021a. An efficient Jaya algorithm with Powell's Pattern Search for optimal power flow incorporating distributed generation. *Energy Sources, Part B: Economics, Planning, and Policy*, Vol. 16, No. 8, pp. 759–786. https://doi.org/10.1080/15567249.2021.1942595
- 66. Gupta, S., Kumar, N. and Srivastava, L., 2021b. Solution of optimal power flow problem using sine-cosine mutation based modified Jaya algorithm: A case study. *Energy Sources, Part A: Recovery, Utilization, and Environmental Effects*, pp. 1–24. https://doi.org/10.1080/15567036.2021.1957043
- 67. Gupta, S., Kumar, N., Srivastava, L., Malik, H., Anvari-Moghaddam, A. and García Márquez, F. P., 2021c. A robust optimization approach for optimal power flow solutions using Rao algorithms. *Energies*, Vol. 14, No. 17, p.5449. https://doi.org/10.3390/en14175449
- 68. Gusain, C., Tripathi, M. M. and Nangia, U., 2023. Study of meta-heuristic optimization methodologies for design of hybrid renewable energy systems. *Thermal Science and Engineering Progress*, Vol. 39, Article 101711. https://doi.org/10.1016/j.tsep.2023.101711
- 69. Hassan, M. H., Kamel, S., Selim, A., Khurshaid, T. and Domínguez-García, J. L., 2021. A modified Rao-2 algorithm for optimal power flow incorporating renewable energy sources. *Mathematics*, Vol. 9, No. 13, p.1532. https://doi.org/10.3390/math9131532
- 70. Hazra, J., and Sinha, A. K., 2011. A multi-objective optimal power flow using particle swarm optimization. *European Transactions on Electrical Power*, Vol. 21, No. 1, pp. 1028–1045. https://doi.org/10.1002/etep.494
- 71. He, S., Wu, Q. H., Saunders, J. R. and Paton, R. C., 2004. A particle swarm optimizer with passive congregation. *Biosystems*, Vol. 78, No. 1–3, pp. 135–147. https://doi.org/10.1016/j.biosystems.2004.08.003
- 72. He, X., Wang, W., Jiang, J. and Xu, L., 2015. An improved artificial bee colony algorithm and its application to multi-objective optimal power flow. *Energies*, 8(4), pp.2412-2437. https://doi.org/10.3390/en8042412

- 73. Islam, M. Z., Othman, M. L., Abdul Wahab, N. I., Veerasamy, V., Opu, S. R., Inbamani, A., and Annamalai, V., 2021. Marine predators algorithm for solving single-objective optimal power flow. *PLOS ONE*, Vol. 16, No. 8, p.e0256050. https://doi.org/10.1371/journal.pone.0256050
- 74. Jadhav, H., and Bamane, P., 2016. Temperature dependent optimal power flow using g-best guided artificial bee colony algorithm. *International Journal of Electrical Power & Energy Systems*, Vol. 77, pp. 77–90. https://doi.org/10.1016/j.ijepes.2015.11.026
- 75. Jebaraj, L. and Sakthivel, S., 2022. A new swarm intelligence optimization approach to solve power flow optimization problem incorporating conflicting and fuel cost-based objective functions. *e-Prime Advances in Electrical Engineering, Electronics and Energy*, Vol. 2, p.100031. https://doi.org/10.1016/j.prime.2022.100031
- 76. Kahourzade, S., Mahmoudi, A., and Mokhlis, H. B., 2015. A comparative study of multi-objective optimal power flow based on particle swarm, evolutionary programming, and genetic algorithm. *Electrical Engineering*, Vol. 97, No. 1, pp. 1–12. https://doi.org/10.1007/s00202-014-0307-0
- 77. Kahraman, H. T., Akbel, M. and Duman, S., 2022. Optimization of optimal power flow problem using multi-objective manta ray foraging optimizer. *Applied Soft Computing*, Vol. 116, Article 108334. https://doi.org/10.1016/j.asoc.2021.108334
- 78. Karimulla, S. and Ravi, K., 2021. Solving multi-objective power flow problem using enhanced sine cosine algorithm. *Ain Shams Engineering Journal*, Vol. 12, No. 4, pp. 3803–3817. https://doi.org/10.1016/j.asej.2021.02.037
- 79. Kaveh, A., and Mahdavi, V. R., 2014. Colliding bodies optimization: A novel meta-heuristic method. *Computers & Structures*, Vol. 139, pp. 18–27. https://doi.org/10.1016/j.compstruc.2014.04.005
- 80. Kaveh, A., and Ghazaan, M. I., 2014. Enhanced colliding bodies optimization for design problems with continuous and discrete variables. *Advances in Engineering Software*, Vol. 77, pp. 66–75. https://doi.org/10.1016/j.advengsoft.2014.08.003
- 81. Kessel, P. and Glavitsch, H., 1986. Estimating the voltage stability of a power system. *IEEE Transactions on Power Delivery*, Vol. 1, No. 3, pp. 346–354. https://doi.org/10.1109/TPWRD.1986.4308013
- 82. Keswani, R., Verma, H. K. and Sharma, S. K., 2023. Multi-objective optimal power flow employing a hybrid sine cosine–grey wolf optimizer. *Iranian Journal of Science and Technology, Transactions of Electrical Engineering*, Vol. 47, pp. 1365–1388. https://doi.org/10.1007/s40998-023-00631-8
- 83. Khamies, G., Magdy, A., Selim, S. and Kamel, S., 2021. An improved Rao algorithm for frequency stability enhancement of nonlinear power system interconnected by AC/DC links with high renewables penetration. *Neural Computing and Applications*, Vol. 34, pp. 2883–2911. https://doi.org/10.1007/s00521-021-06545-y
- 84. Khan, A., Hizam, H., bin Abdul Wahab, N. I., and Lutfi Othman, M., 2020. Optimal power flow using hybrid firefly and particle swarm optimization algorithm. *PLOS ONE*, Vol. 15, No. 8, p.e0235668. https://doi.org/10.1371/journal.pone.0235668
- 85. Khan, A., Hizam, H., Abdul-Wahab, N. I., and Othman, M. L., 2020. Solution of optimal power flow using non-dominated sorting multi-objective-based hybrid firefly and particle swarm optimization algorithm. *Energies*, Vol. 13, No. 16, p.4265. https://doi.org/10.3390/en13164265
- 86. Khorsandi, A., Hosseinian, S. H., and Ghazanfari, A., 2013. Modified artificial bee colony algorithm based on fuzzy multi-objective technique for optimal power flow problem. *Electric Power Systems Research*, Vol. 95, No. 2, pp. 206–213. https://doi.org/10.1016/j.epsr.2012.09.002

- 87. Khunkitti, S., Siritaratiwat, A., Premrudeepreechacharn, S., Chatthaworn, R., and Watson, N. R., 2018. A hybrid DA-PSO optimization algorithm for multiobjective optimal power flow problems. *Energies*, Vol. 11, No. 9, p.2270. https://doi.org/10.3390/en11092270
- 88. Khunkitti, S., Siritaratiwat, A., and Premrudeepreechacharn, S., 2021. Multi-objective optimal power flow problems based on slime mould algorithm. *Sustainability*, Vol. 13, No. 13, p.7448. https://doi.org/10.3390/su13137448
- 89. Kılıç, U., 2015. Backtracking search algorithm-based optimal power flow with valve point effect and prohibited zones. *Electrical Engineering*, Vol. 97, pp. 101–110. https://doi.org/10.1007/s00202-014-0315-0
- 90. Kotb, M. F., and El-Fergany, A. A., 2020. Optimal power flow solution using moth swarm optimizer considering generating units' prohibited zones and valve ripples. *Journal of Electrical Engineering & Technology*, Vol. 15, pp. 179–192. https://doi.org/10.1007/s42835-019-00144-7
- 91. Kumari, M. S. and Maheswarapu, S., 2010. Enhanced Genetic Algorithm-based computation technique for multi-objective optimal power flow solution. *International Journal of Electrical Power & Energy Systems*, Vol. 32, pp. 736–742. http://dx.doi.org/10.1016/j.ijepes.2010.01.010
- 92. Kumar, S. and Chaturvedi, D., 2013. Optimal power flow solution using fuzzy evolutionary and swarm optimization. *International Journal of Electrical Power & Energy Systems*, Vol. 47, pp. 416–423. https://doi.org/10.1016/j.ijepes.2012.11.019
- 93. Laghari, J. A., Mokhlis, H., Bakar, A. H. A. and Mohamad, H., 2013. Application of computational intelligence techniques for load shedding in power systems: A review. *Energy Conversion and Management*, Vol. 75, pp. 130–140. https://doi.org/10.1016/j.enconman.2013.06.010
- 94. Lai, L. L., Ma, J. T., Yokoyama, R. and Zhao, M., 1997. Improved genetic algorithms for optimal power flow under both normal and contingent operation states. *International Journal of Electrical Power & Energy Systems*, Vol. 19, pp. 287–292. https://doi.org/10.1016/S0142-0615(96)00051-8
- 95. Lee, K. Y., Park, Y. M. and Ortiz, J. L., 1985. A united approach to optimal real and reactive power dispatch. *IEEE Transactions on Power Apparatus and Systems*, Vol. 104, No. 5, pp. 1147–1153. https://doi.org/10.1109/TPAS.1985.323466
- 96. Li, N., Li, G., and Deng, Z., 2017. An improved sine cosine algorithm based on levy flight. In: *Ninth International Conference on Digital Image Processing (ICDIP 2017)*, Vol. 10420, pp. 1032–1037. SPIE. https://doi.org/10.1117/12.2282076
- 97. Liang, X., Chai, H. and Ravishankar, J., 2022. Analytical methods of voltage stability in renewable-dominated power systems: A review. *Electricity*, Vol. 31, pp. 75–107. https://doi.org/10.3390/electricity3010006
- 98. Lin, W.-M., Chen, S.-J., and Su, Y.-S., 2000. An application of interior-point based OPF for system expansion with FACTS devices in a deregulated environment. *Proceedings of PowerCon International Conference on Power System Technology*, Vol. 3, pp. 1407–1412. https://doi.org/10.1109/ICPST.2000.898175
- 99. Mahdad, B., Bouktir, T., and Srairi, K., 2009. OPF with environmental constraints with multi-shunt dynamic controllers using decomposed parallel GA: application to the Algerian network. *Journal of Electrical Engineering and Technology*, Vol. 4, No. 1, pp. 55–65. https://doi.org/10.5370/jeet.2009.4.1.055
- 100. Mahdad, B. and Srairi, K., 2014. Multi-objective large power system planning under severe loading condition using learning DE-APSO-PS strategy. *Energy Conversion and Management*, Vol. 87, pp. 338–350. https://doi.org/10.1016/j.enconman.2014.06.090

- 101. Mahdad, B. and Srairi, K., 2015. Blackout risk prevention in a smart grid based flexible optimal strategy using Grey Wolf-pattern search algorithms. *Energy Conversion and Management*, Vol. 98, pp. 411–429. https://doi.org/10.1016/j.enconman.2015.04.005
- 102. Mahdad, B. and Srairi, K., 2018. A new interactive sine cosine algorithm for loading margin stability improvement under contingency. *Electrical Engineering*, Vol. 100, No. 2, pp. 913–933. https://doi.org/10.1007/s00202-017-0539-x
- 103. Mahdad, B., 2020. Improvement of optimal power flow solution considering SVC and TCSC controllers using new partitioned ant lion algorithm. *Electrical Engineering*, Vol. 102, No. 4, pp. 2655–2672. https://doi.org/10.1007/s00202-020-01033-3
- 104. Mahdy, A., Hasanien, H. M., Helmy, W., Turky, R. A. and Abdel Aleem, S. H. E., 2022. Transient stability improvement of wave energy conversion systems connected to power grid using anti-windup-coot optimization strategy. *Energy*, Vol. 245, Article 123249. https://doi.org/10.1016/j.energy.2022.123321
- 105. Mallala, B., Papana, V. P., Sangu, R., Palle, K. and Chinthalacheruvu, V. K. R., 2022. Multi-objective optimal power flow solution using a non-dominated sorting hybrid fruit fly-based artificial bee colony. *Energies*, Vol. 15, No. 11, p.4063. https://doi.org/10.3390/en15114063
- 106. Mandal, B. and Roy, P. K., 2014. Multi-objective optimal power flow using quasi-oppositional teaching-learning-based optimization. *Applied Soft Computing*, Vol. 21, pp. 590–606. https://doi.org/10.1016/j.asoc.2014.04.010
- 107. Maskar, M. B., Thorat, A., and Korachgaon, I., 2017. A review on optimal power flow problem and solution methodologies. In: 2017 International Conference on Data Management, Analytics and Innovation (ICDMAI), Pune, India, pp. 64–70. https://doi.org/10.1109/ICDMAI.2017.8073487
- 108. Memarzadeh, G., Keynia, F., 2021. A new optimal energy storage system model for wind power producers based on long short-term memory and coot bird search algorithm. *Journal of Energy Storage*, Vol. 44, p.103401. https://doi.org/10.1016/j.est.2021.103401
- 109. Meng, C., Zeng, C., Wang, P., Chen, D., Zhou, T., Zheng, X. and Yin, H., 2021. A high-performance crisscross search-based grey wolf optimizer for solving optimal power flow problem. *Energy*, Vol. 225, p.120211. https://doi.org/10.1016/j.energy.2021.120211
- 110. Mirjalili, S., 2015. Moth-flame optimization algorithm: A novel nature-inspired heuristic paradigm. *Knowledge-Based Systems*, Vol. 89, pp. 228–249. https://doi.org/10.1016/j.knosys.2015.07.006
- 111. Mirjalili, S., 2016. SCA: A sine cosine algorithm for solving optimization problems. *Knowledge-Based Systems*, Vol. 96, pp. 120–133. https://doi.org/10.1016/j.knosys.2015.12.022
- 112. Mittal, U., Nangia, U. and Jain, N. K., 2022. Computational intelligence-based optimal power flow methods A review. *Proceedings of the 2022 IEEE Delhi Section Conference (DELCON)*, pp. 1–8. https://doi.org/10.1109/DELCON54057.2022.9753276
- 113. Mittal, U., Nangia, U. and Jain, N. K., 2023. Application of the coot optimization algorithm for optimal power flow solution. *2023 International Conference on Computing, Communication, and Intelligent Systems (ICCCIS)*, Greater Noida, India, pp. 362–368. 10.1109/ICCCIS60361.2023.10425729
- 114. Mittal, U., Nangia, U. and Jain, N. K., 2024. An in-depth examination of artificial intelligence-based methods for optimal power flow solutions. *Neural Computing and Applications*, Vol. 36, pp. 17881–17929. https://doi.org/10.1007/s00521-024-10312-0

- 115. Mohamed, A.-A., Mohamed, Y. S., El-Gaafary, A. A. M. and Hemeida, A. M., 2017. Optimal power flow using moth swarm algorithm. *Electric Power Systems Research*, Vol. 142, pp. 190–206. https://doi.org/10.1016/j.epsr.2016.09.025
- 116. Mohamed, A. A., Kamel, S., Hassan, M. H., Mosaad, M. I., and Aljohani, M., 2022. Optimal power flow analysis based on hybrid gradient-based optimizer with moth–flame optimization algorithm considering optimal placement and sizing of FACTS/wind power. *Mathematics*, Vol. 10, No. 3, p.361. https://doi.org/10.3390/math10030361
- 117. Momoh, J. A., El-Hawary, M. E., Adapa, R., 1999a. A review of selected optimal power flow literature to 1993: Part I: Nonlinear and quadratic programming approaches. *IEEE Transactions on Power Systems*, Vol. 14, No. 1, pp. 96–104. https://doi.org/10.1109/59.744492
- 118. Momoh, J. A., El-Hawary, M. E., Adapa, R., 1999b. A review of selected optimal power flow literature to 1993: Part II: Newton, linear programming, and interior point methods. *IEEE Transactions on Power Systems*, Vol. 14, No. 1, pp. 105–111. https://doi.org/10.1109/59.744495
- 119. Montoya, O. D., Molina-Cabrera, A., Chamorro, H. R., Alvarado-Barrios, L., and Rivas-Trujillo, E., 2020. A hybrid approach based on SOCP and the discrete version of the SCA for optimal placement and sizing of DGs in AC distribution networks. *Electronics*, Vol. 10, p.26. https://doi.org/10.3390/electronics10010026
- 120. Mukherjee, A., and Mukherjee, V., 2015. Solution of optimal power flow using chaotic krill herd algorithm. *Chaos, Solitons & Fractals*, Vol. 78, pp. 10–21. https://doi.org/10.1016/j.chaos.2015.06.020
- 121. Naderi, E., Pourakbari-Kasmaei, M., Cerna, F. V., Lehtonen, M., 2021. A novel hybrid self-adaptive heuristic algorithm to handle single- and multi-objective optimal power flow problems. *International Journal of Electrical Power & Energy Systems*, Vol. 125, Article 106492. https://doi.org/10.1016/j.ijepes.2020.106492
- 122. Narimani, M. R., Azizipanah-Abarghooee, R., Zoghdar-Moghadam-Shahrekohne, B. and Gholami, K., 2013. A novel approach to multi-objective optimal power flow by a new hybrid optimization algorithm considering generator constraints and multi-fuel type. *Energy*, Vol. 49, pp. 119–136. https://doi.org/10.1016/j.energy.2012.09.031
- 123. Naruei, I. and Keynia, F., 2021. A new optimization method based on coot bird natural life model. *Expert Systems with Applications*, Vol. 183, No. 30, p.115352. https://doi.org/10.1016/j.eswa.2021.115352
- 124. Narikmulla, S. K. and Ravi, K., 2021. Solving multi-objective power flow problem using enhanced sine cosine algorithm. *Ain Shams Engineering Journal*, Vol. 12, No. 4, pp. 3803–3817. https://doi.org/10.1016/j.asej.2021.02.037
- 125. Nguyen, T. T., 2019. A high-performance social spider optimization algorithm for optimal power flow solution with single-objective optimization. *Energy*, Vol. 171, pp. 218–240. https://doi.org/10.1016/j.energy.2019.01.021
- 126. Niknam, T., Narimani, M. R., Aghaei, J., and Azizipanah-Abarghooee, R., 2012. Improved particle swarm optimisation for multi-objective optimal power flow considering the cost, loss, emission, and voltage stability index. *IET Generation, Transmission & Distribution*, Vol. 6, No. 6, pp. 515–527. https://doi.org/10.1049/iet-gtd.2011.0851
- 127. Niknam, T., Narimani, M.R. and Azizipanah-Abarghooee, R., 2012. A new hybrid algorithm for optimal power flow considering prohibited zones and valve point effect. *Energy Conversion and Management*, 58, pp.197-206. https://doi.org/10.1016/j.enconman.2012.01.017
- 128. Nikum, A. K., 2021. Novel discrete Rao algorithms for solving the travelling salesman problem. *International Journal of Applied Evolutionary Computation*, Vol. 12, No. 3, pp. 44–61. https://doi.org/10.4018/IJAEC.2021070104

- 129. Niu, M., Wan, C., and Xu, Z., 2014. A review on applications of heuristic optimization algorithms for optimal power flow in modern power systems. *Journal of Modern Power Systems and Clean Energy*, Vol. 2, No. 4, pp. 289–297. https://doi.org/10.1007/s40565-014-0089-4
- 130. Nocedal, J. and Wright, S., 2006. *Numerical Optimization (2nd ed.)*. Springer Science & Business Media.
- 131. Pandya, K. A., 2008. A survey of optimal power flow methods. *Journal of Theoretical and Applied Information Technology*, Vol. 4, No. 5, pp. 450–458
- 132. Pandiarajan, K. and Babulal, C.K., 2016. Fuzzy harmony search algorithm-based optimal power flow for power system security enhancement. *International Journal of Electrical Power & Energy Systems*, Vol. 78, pp. 72–79. https://doi.org/10.1016/j.ijepes.2015.11.053
- 133. Power Systems Test Case Archive: University of Washington. [Online]. Available: http://www.ee.washington.edu/research/pstca/. Accessed: 10 Sept 2022.
- 134. Pulluri, H., Naresh, R., and Sharma, V., 2017a. Application of stud krill herd algorithm for solution of optimal power flow problems. *International Transactions on Electrical Energy Systems*, Vol. 27, No. 6, Article 2316. https://doi.org/10.1002/etep.2316
- 135. Pulluri, H., Naresh, R., and Sharma, V., 2017b. An enhanced self-adaptive differential evolution-based solution methodology for multi-objective optimal power flow. *Applied Soft Computing*, Vol. 54, pp. 229–245. https://doi.org/10.1016/j.asoc.2017.01.030
- 136. Pulluri, H., Naresh, R. and Sharma, V., 2018. A solution network based on stud krill herd algorithm for optimal power flow problems. *Soft Computing*, Vol. 22, pp. 159–176. https://doi.org/10.1007/s00500-016-2319-3
- 137. Radosavljević, J., Klimenta, D., Jevtić, M. and Arsić, N., 2015. Optimal power flow using a hybrid optimization algorithm of particle swarm optimization and gravitational search algorithm. *Electric Power Components and Systems*, Vol. 43, No. 17, pp. 1958–1970. https://doi.org/10.1080/15325008.2015.1061620
- 138. Ramesh Kumar, A., and Premalatha, L., 2015. Optimal power flow for a deregulated power system using adaptive real coded biogeography-based optimization. *International Journal of Electrical Power & Energy Systems*, Vol. 73, pp. 393–399. https://doi.org/10.1016/j.ijepes.2015.05.011
- 139. Rao, R. V., Savsani, V. J., and Vakharia, D. P., 2011. Teaching–learning-based optimization: A novel method for constrained mechanical design optimization problems. *Computer-Aided Design*, Vol. 43, No. 3, pp. 303–315. https://doi.org/10.1016/j.cad.2010.12.015
- 140. Rao, R. V., 2020. Rao algorithms: Three metaphor-less simple algorithms for solving optimization problems. *International Journal of Industrial Engineering Computations*, Vol. 11, pp. 107–130. https://doi.org/10.5267/j.ijiec.2019.6.002
- 141. Rao, R. V. and Pawar, R. B., 2020. Constrained design optimization of selected mechanical system components using Rao algorithms. *Applied Soft Computing*, Vol. 89, Article No. 106141. https://doi.org/10.1016/j.asoc.2020.106141
- 142. Rao, R. V., Keesari, H. S., Taler, J., Oclon, P. and Taler, D., 2023. Elitist Rao algorithms and R-method for optimization of energy systems. *Heat Transfer Engineering*, Vol. 44, pp. 926–950. https://doi.org/10.1080/01457632.2022.2113448
- 143. Raut, U., and Mishra, S., 2021. Enhanced sine—cosine algorithm for optimal planning of distribution network by incorporating network reconfiguration and distributed generation. *Arab Journal of Science and Engineering*, Vol. 46, pp. 1029–1051. https://doi.org/10.1007/s13369-020-04808-9

- 144. Reddy, S. S., and Rathnam, C. S., 2016. Optimal power flow using glowworm swarm optimization. *International Journal of Electrical Power & Energy Systems*, Vol. 80, pp. 128–139. https://doi.org/10.1016/j.ijepes.2016.01.036
- 145. Reddy, S. S., 2018. Solution of multi-objective optimal power flow using efficient meta-heuristic algorithm. *Electrical Engineering*, Vol. 100, pp. 401–413. https://doi.org/10.1007/s00202-017-0518-2
- 146. Reddy, S. S., 2019. Optimal power flow using hybrid differential evolution and harmony search algorithm. *International Journal of Machine Learning and Cybernetics*, Vol. 10, pp. 1077–1091. https://doi.org/10.1007/s13042-018-0786-9
- 147.Reid, G. F. and Hasdorf, L., 1973. Economic dispatch using quadratic programming. *IEEE Transactions on Power Apparatus and Systems*, Vol. 92, pp. 2015–2023. https://doi.org/10.1109/TPAS.1973.293582
- 148. Roy, P. K., Ghoshal, S. P. and Thakur, S. S., 2010. Biogeography-based optimization for multi-constraint optimal power flow with emission and non-smooth cost function. *Expert Systems with Applications*, Vol. 37, No. 12, pp. 8221–8228. https://doi.org/10.1016/j.eswa.2010.05.064
- 149. Roy, P. K., and Paul, C., 2015. Optimal power flow using krill herd algorithm. *International Transactions on Electrical Energy Systems*, Vol. 25, No. 8, pp. 1397–1419. https://doi.org/10.1002/etep.1888
- 150. Saha, A., Das, P., and Chakraborty, A. K., 2017. Water evaporation algorithm: A new metaheuristic algorithm towards the solution of optimal power flow. *Engineering Science and Technology, an International Journal*, Vol. 20, No. 6, pp. 1540–1552. https://doi.org/10.1016/j.jestch.2017.12.009
- 151. Samuel, I., Katende, J., Daramola, A., and Awelewa, A., 2014. Review of system collapse incidences on the 330-kV Nigerian national grid. *International Journal of Engineering Science Invention*, Vol. 3, No. 4, pp. 55–59.
- 152. Saremi, S., Mirjalili, S., and Lewis, A., 2017. Grasshopper optimisation algorithm: theory and application. *Advances in Engineering Software*, Vol. 105, pp. 30–47. https://doi.org/10.1016/j.advengsoft.2017.01.004
- 153. Shabanpour-Haghighi, A., Seifi, A. R., and Niknam, T., 2014. A modified teaching–learning-based optimization for multi-objective optimal power flow problem. *Energy Conversion and Management*, Vol. 77, pp. 597–607. https://doi.org/10.1016/j.enconman.2013.09.028
- 154. Shaheen, A. M., El-Sehiemy, R. A., and Farrag, S. M., 2016. Solving multi-objective optimal power flow problem via forced initialized differential evolution algorithm. *IET Generation, Transmission & Distribution*, Vol. 10, No. 7, pp. 1634–1647. https://doi.org/10.1049/iet-gtd.2015.0892
- 155. Shaheen, A. M., Farrag, S. M., and El-Sehiemy, R. A., 2017. MOPF solution methodology. *IET Generation, Transmission & Distribution*, Vol. 11, No. 2, pp. 570–581. https://doi.org/10.1049/iet-gtd.2016.1379
- 156. Shaheen, A. M., El-Sehiemy, R. A., Hasanien, H. M. and Ginidi, A. R., 2022. An improved heap optimization algorithm for efficient energy management based optimal power flow model. *Energy*, Vol. 250, p.123795. https://doi.org/10.1016/j.energy.2022.123795
- 157. Shaheen, M. A. M., Hasanien, H. M. and Al-Durra, A., 2021. Solving of optimal power flow problem including renewable energy resources using HEAP optimization algorithm. *IEEE Access*, Vol. 9, pp. 35846–35863. https://doi.org/10.1109/ACCESS.2021.3059665
- 158. Shiraki, H., Ashina, S., Kameyama, Y., Hashimoto, S. and Fujita, T., 2016. Analysis of optimal locations for power stations and their impact on industrial symbiosis planning under transition

- toward low-carbon power sector in Japan. *Journal of Cleaner Production*, Vol. 114, pp. 81–94. https://doi.org/10.1016/j.jclepro.2015.09.079
- 159. Sindhu, R., Ngadiran, R., Yacob, Y. M., Zahri, N. A. H. and Hariharan, M., 2017. Sine—cosine algorithm for feature selection with elitism strategy and new updating mechanism. *Neural Computing and Applications*, Vol. 28, pp. 2947–2958. https://doi.org/10.1007/s00521-017-2837-7
- 160. Sun, D.I., Ashley, B., Brewer, B., Hughes, A. and Tinney, W.F., 1984. Optimal power flow by Newton approach. *IEEE Transactions on Power Apparatus and systems*, Vol. PAS-103, No. 10, pp.2864-2880. https://10.1109/TPAS.1984.318284
- 161. Syed, M. S., Chintalapudi, S. V. and Sirigiri, S., 2021. Optimal power flow solution in the presence of renewable energy sources. *Iranian Journal of Science and Technology, Transactions of Electrical Engineering*, Vol. 45, pp. 61–79. https://doi.org/10.1007/s40998-020-00339-z
- 162. Taher, M. A., Kamel, S., Jurado, F. and Ebeed, M., 2019a. An improved moth-flame optimization algorithm for solving optimal power flow problem. *International Transactions on Electrical Energy Systems*, Vol. 29, No. 3, pp. e2743. https://doi.org/10.1002/etep.2743
- 163. Taher, M. A., Kamel, S., Jurado, F. and Ebeed, M., 2019b. Modified grasshopper optimization framework for optimal power flow solution. *Electrical Engineering*, Vol. 101, No. 1, pp. 121–148. https://doi.org/10.1007/s00202-019-00762-4
- 164. Taher, M. A., Kamel, S., Sayed, F., Khurshaid, T., and Jurado, F., 2021. Load shedding reduction and loadability enhancement of power system using shunt FACTS devices. *Journal of Electrical Systems*, Vol. 17, No. 1, pp. 121–140.
- 165. Taher, M. A., Kamel, S., Jurado, F. and Yu, J., 2022. Optimal locations and sizes of shunt FACT devices for enhancing power system loadability using improved moth flame optimization. *Electric Power Components and Systems*, Vol. 49, No. 20, pp. 1536–1554. https://doi.org/10.1080/15325008.2022.2134512
- 166. Tinney, W. G. and Hart, C. E., 1967. Power flow solutions by Newton's method. *IEEE Transactions on Power Apparatus and Systems*, Vol. 86, No. 11, pp. 1449–1460. https://doi.org/10.1109/TPAS.1967.291823
- 167. Upputuri, R., Kumar, N., and Suresh, C. V., 2024. Optimal power flow using a hybrid improved Harris Hawks optimization algorithm-pattern search method. *IETE Journal of Research*, Vol. 70, No. 3, pp. 2684–2704. https://doi.org/10.1080/03772063.2023.2194253
- 168. Vlachogiannis, J. G., and Lee, K. Y., 2006. A comparative study on particle swarm optimization for optimal steady-state performance of power systems. *IEEE Transactions on Power Systems*, Vol. 21, No. 4, pp. 1718–1728. https://doi.org/10.1109/TPWRS.2006.883687
- 169. Walters, D. C., and Sheble, G. B., 1993. Genetic algorithm solution of economic dispatch with valve point loading. *IEEE Transactions on Power Systems*, Vol. 8, No. 3, pp. 1325–1332. https://doi.org/10.1109/59.260861
- 170. Warid, W., Hizam, H., Mariun, N. and Abdul-Wahab, N.I., 2016. Optimal power flow using the Jaya algorithm. *Energies*, Vol.9, No.9, p.678. https://doi.org/10.3390/en9090678
- 171. Warid, W., 2020. Optimal power flow using the AMTPG-Jaya algorithm. *Applied Soft Computing*, Vol. 91, Article No. 106252. https://doi.org/10.1016/j.asoc.2020.106252
- 172. Warid, W., 2022. A novel chaotic Rao-2 algorithm for optimal power flow solution. *International Journal of Electrical and Computer Engineering*, p.7694026. https://doi.org/10.1155/2022/7694026

- 173. Wang, Z., Pei, Y., Li, J., 2023. A survey on search strategy of evolutionary multi-objective optimization algorithms. *Applied Sciences*, Vol. 13, No. 7, p.4643. https://doi.org/10.3390/app13074643
- 174. Wei, H., Sasaki, H., Kubakawa, J., and Yokoyama, R., 1998. An interior point nonlinear programming for optimal power flow problems with a novel data structure. *IEEE Transactions on Power Systems*, Vol. 13, No. 3, pp. 870–877. https://doi.org/10.1109/59.708745
- 175. Wolpert, D. H. and Macready, W. G., 1997. No free lunch theorems for optimization. *IEEE Transactions on Evolutionary Computation*, Vol. 1, No. 1, pp. 67–82. https://doi.org/10.1109/4235.585893
- 176. Wu, Q. H., Cao, Y. J., Wen, J. Y., 1998. Optimal reactive power dispatch using an adaptive genetic algorithm. *International Journal of Electrical Power & Energy Systems*, Vol. 20, pp. 563–569. https://doi.org/10.1016/S0142-0615(98)00016-7
- 177. Yuryevich, J., Wong, K. P., 1999. Evolutionary programming-based optimal power flow algorithm. *IEEE Transactions on Power Systems*, Vol. 14, No. 4, pp. 1245–1250. https://doi.org/10.1109/59.801880
- 178. Zehar, K. and Sayah, S., 2008. Optimal power flow with environmental constraint using a fast successive linear programming algorithm: Application to the Algerian power system. *Energy Conversion and Management*, Vol. 49, No. 11, pp. 3362–3366. https://doi.org/10.1016/j.enconman.2007.10.033
- 179. Zhao, W., Wang, L., Zhang, Z., Fan, H., Zhang, J., Mirjalili, S., Khodadadi, N. and Cao, Q., 2024. Electric eel foraging optimization: A new bio-inspired optimizer for engineering applications. *Expert Systems with Applications*, Vol. 238, p.122200. https://doi.org/10.1016/j.eswa.2023.122200
- 180. Zimmerman, R. D., Murillo-Sanchez, C. E., Gan, D., 2006. MATLAB power system simulation package (Version 3.1b2).
- 181. Zimmerman, R. D., and Murillo-Sánchez, C. E., 2016. MATPOWER 6.0 User's Manual.

Appendix

 Table A.1
 Summary of systems under study

Characteristics	IEEE 30		IEEE 118				
Characteristics	Quantity	Details	Quantity	Details			
Buses	30	[59]	118	[65]			
Branches	41	[59]	186	[65]			
Generators	6	Buses:1 (swing), 2, 5, 8, 11 and 13	54	Buses: 1, 4, 6, 8, 10, 12, 15, 18, 19, 24, 25, 26, 27, 31, 32, 34, 36, 40, 42, 46, 49, 54, 55, 56, 59, 61, 62, 65, 66, 69 (swing), 70, 72, 73, 74, 76, 77, 80, 85, 87, 89, 90, 91, 92, 99, 100, 103, 104, 105, 107, 110, 111, 112, 113 and 116			
Shunt VAR compensators	9	Buses: 10, 12, 15, 17, 20, 21, 23, 24 and 29	14	Buses: 5, 34, 37, 44, 45, 46, 48, 74, 79, 82, 83, 105, 107 and 110			
Transformers	4	Branches: 11, 12, 15 and 36	9	Branches: 8, 32, 36, 51, 93, 95, 102, 107 and 127			
Control variables	24		130				
Load volt. limits	[0.95-1.05] p.u		[0.94-1.06] p.u.				
Gen. volt. limits	[0.95-1.1] p.u.		[0.94-1.06] p.u.				
Tap-setting limits	[0.9-1.1] p.u.		[0.9-1.1] p.u.				
Connected load	283.4 MW	, 126.2 MVAR	4242 MW,	4242 MW, 1438 MVAR			

Table A.2 Branch power flow in Case 6 with $P_D = 421.6014$ MW

Branch No. (NL)	From ith bus To jth bus	PQ sent	PQ received	$S_{Line}^{ m max}$ (MVA)	Branch No. (NL)	From ith bus To jth bus	PQ sent	PQ received	S_{Line}^{\max} (MVA)
1	1-2	1.2987 - 0.1828i	-1.2893 + 0.2350i	130	22	15-18	0.0967 + 0.0122i	-0.0957 - 0.0103i	16
2	1-3	0.6836 - 0.0012i	-0.6662 + 0.0486i	130	23	18-19	0.0481 - 0.0031i	-0.0480 + 0.0034i	16
3	2-4	0.4121 - 0.0256i	-0.4039 + 0.0291i	65	24	19-20	-0.0933 - 0.0540i	0.0937 + 0.0547i	32
4	3-4	0.6305 - 0.0665i	-0.6259 + 0.0748i	130	25	10-20	0.1279 + 0.0189i	-0.1264 - 0.0157i	32
5	2-5	0.8018 + 0.0059i	-0.7761 + 0.0777i	130	26	10-17	0.0642 + 0.0469i	-0.0640 - 0.0464i	32
6	2-6	0.5526 - 0.0161i	-0.5376 + 0.0399i	65	27	10-21	0.2347 + 0.0902i	-0.2327 - 0.0859i	32
7	4-6	0.6230 + 0.0249i	-0.6190 - 0.0160i	90	28	10-22	0.1127 + 0.0375i	-0.1118 - 0.0356i	32
8	5-7	-0.1252 + 0.1384i	0.1267 - 0.1460i	70	29	21-22	-0.0277 - 0.0324i	0.0277 + 0.0325i	32
9	6-7	0.4712 + 0.0228i	-0.4659 - 0.0162i	130	30	15-23	0.0861 - 0.0070i	-0.0854 + 0.0084i	16
10	6-8	0.1177 - 0.1114i	-0.1174 + 0.1073i	32	31	22-24	0.0841 + 0.0031i	-0.0834 - 0.0019i	16
11	6-9	0.1538 - 0.3123i	-0.1538 + 0.3389i	65	32	23-24	0.0378 + 0.0178i	-0.0375 - 0.0174i	16
12	6-10	0.1720 + 0.2913i	-0.1720 - 0.2457i	32	33	24-25	-0.0085 - 0.0307i	0.0087 + 0.0310i	16
13	9-11	-0.3000 - 0.2877i	0.3000 + 0.3208i	65	34	25-26	0.0530 + 0.0357i	-0.0521 - 0.0342i	16
14	9-10	0.4538 - 0.0512i	-0.4538 + 0.0724i	65	35	25-27	-0.0617 - 0.0667i	0.0626 + 0.0683i	16
15	4-12	0.2938 - 0.1526i	-0.2938 + 0.1797i	65	36	28-27	0.2618 + 0.0972i	-0.2618 - 0.0711i	65
16	12-13	-0.4000 - 0.2927i	0.4000 + 0.3233i	65	37	27-29	0.0932 - 0.0097i	-0.0915 + 0.0130i	16
17	12-14	0.1178 + 0.0140i	-0.1163 - 0.0108i	32	38	27-30	0.1060 + 0.0125i	-0.1027 - 0.0064i	16
18	12-15	0.2856 + 0.0163i	-0.2808 - 0.0068i	32	39	29-30	0.0558 + 0.0234i	-0.0550 - 0.0219i	16
19	12-16	0.1237 + 0.0203i	-0.1224 - 0.0175i	32	40	8-28	0.0211 - 0.0162i	-0.0208 - 0.0077i	32
20	14-15	0.0241 - 0.0130i	-0.0239 + 0.0132i	16	41	6-28	0.2419 + 0.0858i	-0.2409 - 0.0895i	32
21	16-17	0.0703 - 0.0093i	-0.0699 + 0.0102i	16					

 Table A.3
 Allowable generator unit parameters and fuel cost coefficients for IEEE 118-bus test system

Generators (G)	Bus No.	P _{min} (MW)	P _{max} (MW)	Q _{min} (MVAR)	Q _{max} (MVAR)	a (\$/h)	<i>b</i> (\$/ <i>h</i> -MW)	c (\$/h-MW ²)
G ₁	10	50	500	-147	200	0	1.818	0.0018
G_2	12	10	90	-35	120	0	5.405	0.0054
G_3	25	30	300	-47	140	0	3.215	0.0032
G_4	26	40	400	-1000	1000	0	2.415	0.0024
G 5	31	0	10	-300	300	0	9.346	0.0093
G_6	46	0	23	-100	100	0	3.743	0.0031
G_7	49	30	240	-85	210	0	3.589	0.0033
G_8	69	20	200	-60	180	0	2.612	0.0024
G ₉	61	20	200	-60	180	0	2.453	0.0023
G_{10}	65	90	600	-67	200	0	2.21	0.002
G_{11}	66	90	600	-67	200	0	2.21	0.002
G_{12}	69	100	900	-300	300	0	1.242	0.0014
G_{13}	80	50	600	-165	280	0	9.95	0.0096
G ₁₄	87	0	5	-100	1000	0	1.951	0.0019
G ₁₅	89	50	700	-210	300	0	2.841	0.0028
G_{16}	100	50	300	-210	300	0	2.841	0.0028
G ₁₇	103	0	50	-15	40	0	2.841	0.0028
G_{18}	111	0	40	-100	100	0	7.353	0.0074
G ₁₉	111	0	40	-100	100	0	7.353	0.0074

LIST OF PUBLICATIONS

• List of papers (s) published in Peer Reviewed Referred International Journals

- 1. Mittal, U., Nangia, U., Jain, N.K. et al., 2024. Optimal power flow solution using a learning-based sine—cosine algorithm. *The Journal of Supercomputing*. Vol. 80, pp. 15974–16012. https://doi.org/10.1007/s11227-024-06043-7
- 2. Mittal, U., Nangia, U., and Jain, N. K., 2024. An in-depth examination of artificial intelligence-based methods for optimal power flow solutions. *Neural Computing and Applications*, Vol. 36, pp. 17881–17929. https://doi.org/10.1007/s00521-024-10312-0
- 3. Mittal, U., Nangia, U., Jain, N. K., & Gupta, S., 2025. Optimal power flow solutions for normal and critical loading scenarios using hybrid Rao-2 sine cosine algorithm. Computers and Electrical Engineering, Vol. 123, p.110230. https://doi.org/10.1016/j.compeleceng.2025.110230

• List of paper(s) published in Peer Reviewed International Conference

- Mittal, U., Nangia, U., and Jain, N. K., 2022. Computational intelligence-based optimal power flow methods - A review. 2022 IEEE Delhi Section Conference (DELCON), New Delhi, India, pp. 1–8. https://doi.org/10.1109/DELCON54057.2022.9753276
- 2. Mittal, U., Nangia, U., and Jain, N. K., 2024. An Improved Coot Optimization Algorithm for Optimal Power Flow in Small-Scale Power System, 2024 International Conference on Distributed Computing and Optimization Techniques (ICDCOT), Bengaluru, India, pp. 1-7. https://doi:10.1109/ICDCOT61034.2024.10515827
- **3.** Mittal, U., Nangia, U., and Jain, N. K., 2023. Application of the Coot Optimization Algorithm for Optimal Power Flow Solution, *2023 International Conference on Computing, Communication, and Intelligent Systems (ICCCIS)*, Greater Noida, India, pp. 362-368. https://doi:10.1109/ICCCIS60361.2023.10425729.
- **4.** Mittal, U., Nangia, U. and Jain, N. K., 2025. Optimal Power Flow Using Electric Eel Foraging Algorithm with Distributed Generation. Paper presented at the *1st International Conference on Power and Intelligent Control Systems (PICS-2025)*, NIT Hamirpur, India. (**to be published online**)



DELHI TECHNOLOGICAL UNIVERSITY

(Formerly Delhi College of Engineering) Shahbad Daulatpur, Main Bawana Road, Delhi-42

PLAGIARISM VERIFICATION

APPLICATIONS OF COMPUTATIONAL INTELLIGENCE TECHNIQUES FOR SOLVING THE OPTIMAL POWER FLOW PROBLEM IN MODERN POWER Title of the Thesis SYSTEMS Total Pages Name of the Scholar UDIT MITTAL Supervisor (s) Prof. Uma Nangia (2)Prof. N. K. Jain (3) Department ELECTRICAL ENGINEERING This is to report that the above thesis was scanned for similarity detection. Process and outcome is given below: Software used: ___ Similarity Index: _____, Total Word Count: _____ Date: 08/05/2025 Signature of Supervisor(s) Candidate's Signature

PLAGIARISM REPORT

UDIT MITTAL

PhD Thesis (udit mittal).pdf

Delhi Technological University

Document Details

Submission ID

trn:oid:::27535:94928724

Submission Date

May 8, 2025, 7:31 PM GMT+5:30

Download Date

May 8, 2025, 7:35 PM GMT+5:30

File Name

PhD Thesis (udit mittal).pdf

File Size

4.9 MB

174 Pages

56,911 Words

301,441 Characters



Submission ID trn:oid:::27535:94928724



Page 2 of 182 - Integrity Overview

Submission ID trn:oid:::27535:94928724

8% Overall Similarity

The combined total of all matches, including overlapping sources, for each database.

Filtered from the Report

- Bibliography
- Ouoted Text
- Small Matches (less than 10 words)
- Crossref database

Match Groups

255Not Cited or Quoted 7%

Matches with neither in-text citation nor quotation marks

38 Missing Quotations 1%

Matches that are still very similar to source material

 Missing Citation 0% Matches that have quotation marks, but no in-text citation

O Cited and Quoted 0% Matches with in-text citation present, but no quotation marks

Top Sources

1% Publications

4% La Submitted works (Student Papers)

Integrity Flags

0 Integrity Flags for Review

No suspicious text manipulations found.

Our system's algorithms look deeply at a document for any inconsistencies that would set it apart from a normal submission. If we notice something strange, we flag it for you to review.

A Flag is not necessarily an indicator of a problem. However, we'd recommend you focus your attention there for further review.

BRIEF PROFILE

I, Udit Mittal, completed my B.E. (Honors) in Electrical Engineering from Aligarh Muslim University (AMU), Aligarh, India, followed by an M.Tech. in Power System & Drives from the same university. Currently, I am working as an Assistant Professor in the Department of Electrical Engineering at JSS Academy of Technical Education, Noida, since August 2010.

I pursued my Ph.D. in the Department of Electrical Engineering at Delhi Technological University (DTU), Delhi, India, under the supervision of Prof. Uma Nangia and Prof. N.K. Jain.

My research primarily focuses on advanced optimization techniques for power system optimization, specifically Optimal Power Flow (OPF). I am also a Senior Member of IEEE and actively engage in research, teaching, and academic activities.